Abrikosov Center for Theoretical Physics

Conference Proceedings

The International Summer Conference on Theoretical Physics 2023

3rd-7th July 2023

Moscow
2023

Metastable states in the J_1-J_2 Ising model

V.A. Abalmasov

Institute of Automation and Electrometry SB RAS, 630090 Novosibirsk, Russia

abalmasov@iae.nsc.ru

Abstract

We study the J_1-J_2 Ising model on the square lattice using the random local field approximation (RLFA) and Monte Carlo (MC) simulations for various values of the ratio $p = J_2/|J_1|$ with antiferromagnetic coupling J_2, ensuring spin frustration. RLFA predicts metastable states with zero order parameter (polarization) at low temperature for $p \in (0, 1)$. MC simulations show that the system relaxes into metastable states with not only zero, but also with arbitrary polarization, depending on its initial value, external field, and temperature. We support our findings by calculating the energy barriers of these states at the level of individual spin flips relevant to the MC calculation.

Key words: J_1-J_2 Ising model, ferroelectrics, ferromagnetics, supercondutors

Introduction

In recent years, many compounds have been discovered in which electron spins form a two-dimensional square lattice and interact with their nearest and diagonal next-nearest neighbors via isotropic exchange interaction with the coupling constants J_1 and J_2, respectively. This also includes the parent compound of cuprate high-temperature superconductors La_2CuO_4 and is likely relevant to iron-based superconductors. The corresponding quantum Heisenberg model has been studied extensively by a variety of methods. Although its implementations seem less common in nature, the easier to study J_1-J_2 Ising model nonetheless is interesting in its own right, and can also shed light on some properties of its more complex quantum Heisenberg counterpart.

Main text

First, we use the random local field approximation (RLFA) [1] to study the J_1-J_2 Ising model on a square lattice. The solution of the RLFA equation for uniform (at $p < p_0$) and striped (at $p > p_0$) polarization is shown in Fig. 1. Three solutions at low temperatures correspond to a stable state with polarization $m \approx 1$, an unstable state ($m \approx 0.29$ for $p \in (0, p_0)$ and $m \approx 0.65$ for $p \in (p_0, 1)$), and a metastable state with $m = 0$. In an external field, unstable and metastable states exist only within a certain temperature window.

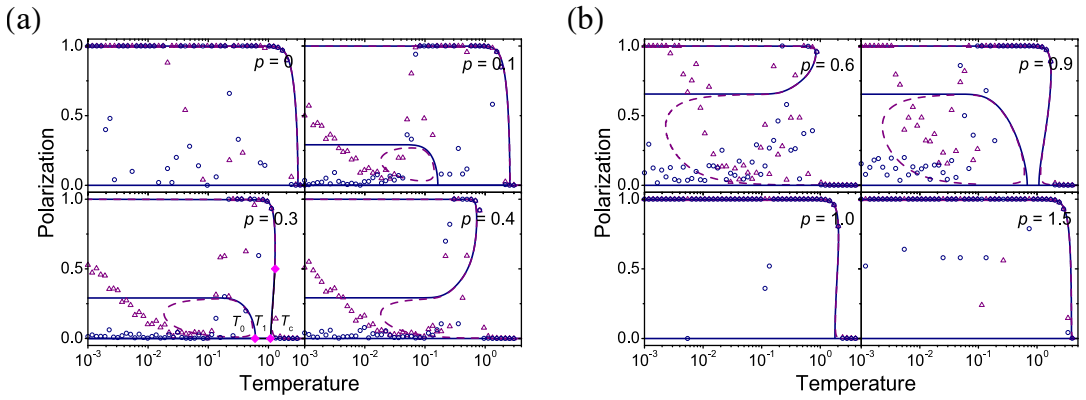

Figure 1: Polarization as a function of temperature obtained using the RLFA analytical approach and MC simulations. (a), Solution of the RLFA equation (lines) and MC results (markers) for uniform polarization in a uniform field at $p < p_0$, and (b), for striped polarization in a striped field at $p > p_0$. The magnitude of the field is $h = 0.001$ (purple dashed line and triangles) and $h = 0$ (blue solid line and circles).

To further explore the metastable states, we perform MC simulations with single-spin-flip dynamics, making a deep quench from a (high-temperature) random spin configuration (Fig. 1). Metastable spin configurations depend on the initial polarization, external field, and temperature. For $p \in (0, p_0)$, where the ground state is ferromagnetic, metastable states consist of rectangles with at least two spins on each side, surrounded by spins with the opposite direction [2]. For $p \in (p_0, 1)$, the elementary excitation is more complicated [3].

Similar phase diagrams of the J_1-J_2 Ising and quantum Heisenberg models allow us to expect some features of the discussed metastable states in the latter case as well. At least RLFA predicts metastable states for the J_1-J_2 Ising model in a sufficiently small external transverse field [3].

References

1. B. E. Vugmeister and V. A. Stephanovich, New random field theory for the concentrational phase transitions with appearance of long-range order. Application to the impurity dipole systems, Solid State Commun. **63**, 323 (1987).

2. J. D. Shore and J. P. Sethna, Prediction of logarithmic growth in a quenched Ising model, Physical Review B **43**, 3782 (1991).

3. V. A. Abalmasov and B. E. Vugmeister, Metastable states in the J_1-J_2 Ising model, Physical Review E **107**, 034124 (2023).

Title: Parabolic accelerating relativistic jets from active galactic nuclei

Author: Dr. Elena Nokhrina

Abstract:

We review the most recent results on the connection a plasma acceleration and relativistic jets physics. Latest wave of discoveries of AGN jets with their shapes changing from quasi-parabolic to quasi-conical suggests that the underlying physics may be universal.

We discuss the connection of a jet shape break with a plasma acceleration within a Bondi sphere. We relate a position and a width at the jet shape break to the key parameters: black hole spin, ambient medium pressure amplitude, terminal plasma Lorentz factor and magnetic flux, which defines the jet power and the dick state: MAD or SANE (Kovalev et al. 2020, Nokhrina et al. 2020). This allows us to develop an instrument to assess the AGN properties through observations of jet shape break. We show that 11 distant sources with jets, unresolved at the expected jet shape break, demonstrate the parabolic jet shape at the scales of 8-15 GHz radio cores (Nokhrina et al. 2022). The expected terminal Lorentz factor for them may be as large as a hundred, which is consistent with the kinematics Lorentz factor measurements (Lister et al. 2019).

We discuss the impact of a jet shape and an ongoing acceleration on the core shift dependence on the observational frequency (k_r index). For parabolic jets (observed at high frequencies 8-15 GHz and higher) we predict different k_r indices for different observational angles, with typical values of 0.5-1.0. For all these cases, a magnetic field can be estimated by measuring core shift in a parabolic jet.

Multielectronic QED effects in the g-factor of multicharged ions

E. V. Tryapitsyna [1,2], D. A. Glazov [1,2], A. V. Volotka [2]

[1]Saint-Petersburg University

[2]ITMO University

Abstract

Key words: Theoretical physics, two-electron self energy, quantum electrodynamics, gauge invariance, g-factor, Li-like ions, hyperfine structure

Introduction

In recent years, the g-factor of ions with a small number of electrons has been of great interest. For example, high-precision measurements of the g factor [1-3] in combination with theoretical developments [4-6] provided the most accurate determination of the electron mass [2] and the most rigorous verification of the effects of QED and recoil of the nucleus in the presence of a magnetic field [7,8]. Promising areas of research include independent determination of the fine structure constant, precise measurements of nuclear magnetic moments and much more.

Modern theoretical calculations of the g-factor of electrons in the bound state include a rigorous calculation of first- and second-order QED diagrams. In particular, the contribution of two-electron self-energy diagrams is currently being considered as a possible reason for the discrepancy between the theoretical values of the coefficient g [10,11] and experimental [9, 12]. One of a possible test for such calculations is the gauge invariance of the total contribution of certain sets of diagrams. The method of corresponding analytical consideration is presented in [13] for two-photon exchange diagrams, the results are confirmed by numerical calculation.

Main text

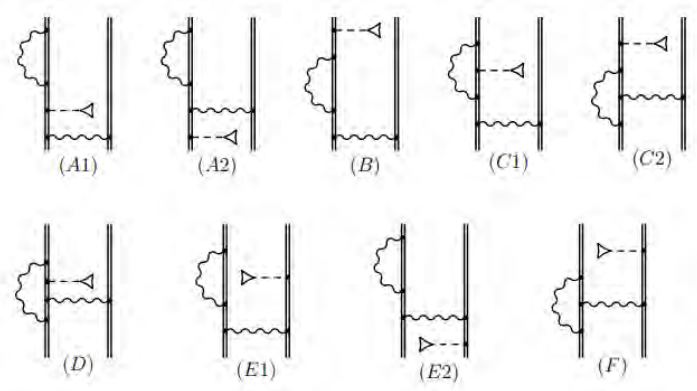

Figure 1: Feynman diagrams corresponding to two-electron self-energy in presence of an external magnetic field.

It is known that all observable quantities in quantum electrodynamics do not depend on the choice of gauge of the electromagnetic field. The choice of gauge sometimes allows you to achieve certain advantages when calculating specific diagrams [14]. At the same time, it is possible to distinguish sets of diagrams in each order of perturbation theory, the total contribution of which has gauge invariance. This property can serve as one of the ways to check the correctness of the calculation of complex diagrams. In the second and even more so in the third order of perturbation theory in quantum electrodynamics for bound states, even the derivation of formulas is a difficult task [15,16]. In such a situation, the gauge invariance can be used to verify the formulas obtained. It is especially important that the so-called irreducible and reducible contributions are not invariant separately. This makes it possible to check the coefficients in the reduced contributions, which may not be obvious, since these contributions do not always have an analogue in quantum mechanical perturbation theory.

In this paper, the Feynman and Coulomb calibrations for first- and second-order interelectronic interaction diagrams are considered. Analytically, it is shown that the difference between the results in the two gauges is zero. In the course of consideration, it becomes clear which minimal gauge-invariant sets of diagrams can be distinguished. Gauge-invariant sets of diagrams are identified analytically, then these results are confirmed by numerical calculation.

References

1. S. Sturm, A. Wagner, M. Kretzschmar, W. Quint, G. Werth, and K. Blaum, Phys. Rev. A 87, 030501(R) (2013)

2. S. Sturm, F. K ohler, J. Zatorski, A. Wagner, Z. Harman, G. Werth, W. Quint, C. H. Keitel, and K. Blaum, Nature 506, 467 (2014)

3. T. Sailer, V. Debierre, Z. Harman, F. Heiße, C. Konig, J. Morgner, B. Tu, A. V. Volotka, C. H. Keitel, K. Blaum, and S. Sturm, Nature 606, 479 (2022).

4. U. D. Jentschura, Phys. Rev. A 79, 044501 (2009)

5. V. A. Yerokhin and Z. Harman, Phys. Rev. A 88, 042502 (2013)

6. V. A. Yerokhin, C. H. Keitel, and Z. Harman, J. Phys. B 46, 245002 (2013).

7. V. M. Shabaev, D. A. Glazov, A. M. Ryzhkov, C. Brandau, G. Plunien, W. Quint, A. M. Volchkova, and D. V. Zinenko, Phys. Rev. Lett. 128, 043001 (2022)

8. V. Debierre, N. S. Oreshkina, I. A. Valuev, Z. Harman, and C. H. Keitel, Phys. Rev. A 106, 062801 (2022)

9 D. A. Glazov, F. Kohler-Langes, A. V. Volotka, K. Blaum, F. Heiße, G. Plunien, W. Quint, S. Rau, V. M. Shabaev, S. Sturm, and G. Werth, Phys. Rev. Lett. 123, 173001 (2019).

10. V. A. Yerokhin, K. Pachucki, M. Puchalski, C. H. Keitel, and Z. Harman, Phys. Rev. A 102, 022815 (2020)

11. V. A. Yerokhin, C. H. Keitel, and Z. Harman, Phys. Rev. A 104, 022814 (2021).

12. F. Kohler, K. Blaum, M. Block, S. Chenmarev, S. Eliseev, D. A. Glazov, M. Goncharov, J. Hou, A. Kracke, D. A. Nesterenko, Yu. N. Novikov, W. Quint, E. Minaya Ramirez, V. M. Shabaev, S. Sturm, A. V. Volotka, and G. Werth, Nat. Commun. 7, 10246 (2016)

13. R. N. Soguel, A. V. Volotka, E. V. Tryapitsyna, D. A. Glazov, V. P. Kosheleva, and S. Fritzsche, Phys. Rev. A 103, 042818 (2021).

14. D. Hedendahl and J. Holmberg, Phys. Rev. A 85, 012514 (2012).

15. V. M. Shabaev, and G. Fokeeva, Phys. Rev. A 49, 4489 (1994)

16. V. M. Shabaev, Phys. Rep. 356, 119 (2002).

Tests of pairing symmetry in multiterminal superconducting junctions

A. A. Golubov [1,2], T.H. Kokkeler[1,3], Y. Tanaka[4]

[1] *Faculty of Science and Technology, University of Twente, The Netherlands*
[2] *Moscow Institute of Physics and Technology, Dolgoprudny, Russia*
[3] *Donostia International Physics Center (DIPC), 20018 Donostia-San Sebastian, Spain*
[4] *Department of Applied Physics, Nagoya University, Nagoya 464-8603, Japan*

We present the results of theoretical study of the influence of superconducting pairing symmetry on charge transport in multiterminal junctions. We derive a boundary condition for the Nambu-Keldysh Green's function in diffusive normal metal - unconventional superconductor junctions applicable for mixed parity pairing [1]. Applying this theory to an of s + p-wave superconductor, we calculate local density of states (LDOS) in the diffusive normal metal (N) and charge conductance of a junction between N and s + p-wave superconductor. When the s-wave component of the pair potential is dominant, LDOS has a gap like structure at zero energy and the dominant pairing in N is even-frequency spin-singlet s-wave. On the other hand, when the p-wave component is dominant, the resulting LDOS has a zero energy peak and the dominant pairing in N is odd-frequency spin-triplet s-wave. The results show the robustness of the anomalous proximity effect specific to spin-triplet superconductor junctions.

Using the developed approach, multi-terminal (SNN) junctions are investigated where the superconducting potential is a mixture between s-wave and p-wave potentials [2]. The ways are proposed to determine whether S has a mixed pair potential and to distinguish between s + chiral and s + helical p-wave superconductors. It is found that a difference in conductance for electrons with opposite spins arises if both an s-wave and a p-wave components are present, even in the absence of a magnetic field. It is shown that a setup containing two SN junctions provides a clear difference in spin conductance between the s + chiral p-wave and s + helical p-wave symmetries.

Further, we propose new approach to distinguish p-wave from s-wave symmetry by measuring conductance a four terminal junction consisting of S and N terminals [3]. The N-terminals are used to manipulate the energy distribution functions of electrons in the junction in order to control the charge transport. It is shown that the differential conductance of junctions containing p-wave and s-wave superconductors is distinctly different, thus providing experimental test to detect potential p-wave superconductivity.

References

1. Y. Tanaka, T.H. Kokkeler, and A.A. Golubov, Phys. Rev. B **10**5, 214512 (2022).
2. T.H. Kokkeler, Y. Tanaka, and A.A. Golubov, Phys. Rev. Research **5**, L012022 (2023)

3. T.H. Kokkeler, A.A. Golubov, and B.J. Geurts, Supercond. Sci. Technol. 35, 084005 (2022).

Optical probing of collective modes in low-dimensional unconventional superconductors.

In conventional BCS s-wave superconductors there exist two distinct collective modes corresponding to the perturbation of amplitude and phase of the order parameter, Higgs and Goldstone modes. However, as is known from the pioneering works of Leggett, in multiband superconductors, additional collective modes may appear with resonant frequencies lying in the bulk of the superconducting gap. In my talk I will discuss, how these modes may be probed by means of AC electromagnetic field in low dimensional superconductors, discuss how the spectroscopy of these modes may be used to extract the information on the pairing symmetry, and speculate on the perspective of these materials as a novel polaritonic platform.

In this talk we plan to discuss the distinctive features of photogalvanic phenomena in superconducting systems in comparison with the normal metals. We analyze several theoretical models which allow to describe the mechanisms of generation of photoinduced dc currents, magnetic moment and Abrikosov vortices in superconductors and switching between the superconducting current states under the influence of electromagnetic wave of different polarization. We also discuss the relation between the photogalvanic phenomena and the Hall effect in superconductors, peculiarities of the nonequilibrium dynamics of condensate and potential of charge imbalance arising in the field of incident electromagnetic wave.

2D magnetic monolayers for excitonics and polaritonics

I.A. Shelykh
[a] *Science Institute, University of Iceland, Dunhagi 3, IS-107, Reykjavik, Iceland and Abrikosov Center for Theoretical Physics, MIPT, Dolgoprudny, Moscow Region 141701, Russia*
* Corresponding author: shelykh@hi.is

Cromium trihalides (CrI3, CrBr3 and CrCl3) is a family of 2D materials which combine the presence of ferromagnetic ordering of the Ising type with robust excitonic response up to room temperature.

The interaction between excitons and magnetic lattice of these materials can lead to a set of remarkable optomagnetic effects, which include polarization-sensitive resonant magnetization switching and excitonic anomalous Hall effect.

Moreover, huge binding energies (up to 1 eV) and optical oscillator strengths of bright excitons in CrI_3 make this material an attractive candidate for polaritonics, with characteristic Rabi splitting of several tens of meV. The presence of lattice ferromagnetism also leads to record-high values of polariton Zeeman splitting up to 15 meV, which can be of importance for spinoptronic applications.

In our talk we will present the theory of aforementioned effects.

References

[1] A. Kudlis, I. Iorsh, and I. A. Shelykh, All-optical resonant magnetization switching in CrI3 monolayers, Phys. Rev. B 104, L020412 (2021).
[2] M. Kazemi, V. A. Shahnazaryan, Y. V. Zhumagulov, P. F. Bessarab and I. A. Shelykh, Interaction of excitons with magnetic topological defects in 2D magnetic monolayers: localization and anomalous Hall effect, 2D Mater. 10, 015003 (2023).
[3] Y. V. Zhumagulov, S. Chiavazzo, I. A. Shelykh, O. Kyriienko, Robust polaritons in magnetic monolayers of CrI3, arXiv:2208.12228 (2022).
[4] A. Kudlis, M. Kazemi, Y. Zhumagulov, H. Schrautzer, P. F. Bessarab, I. V. Iorsh, I. A. Shelykh, All-optical magnetization control in CrI3 monolayers: a microscopic theory, arXiv:2304.00331 (2023)

Schwinger mechanism of pair production in rapidly-varying electric fields

I. A. Aleksandrov

Saint Petersburg State University, Saint Peterburg, Russia

Ioffe Institute, Saint Peterburg, Russia

i.aleksandrov@spbu.ru

Abstract

In this talk, we consider a nonperturbative process of electron-positron pair production in strong electric fields (Schwinger mechanism). We discuss two approaches to shaping the temporal profile of the external background that can be used to enhance the total particle yield and, thus, lower the pair-production threshold. First, one can superimpose a weak high-frequency pulse on a slowly varying strong background, so that the former efficiently stimulates pair production (dynamically assisted Schwinger effect). Second, the external field can be rapidly switched off in the vicinity of its maximum, which also substantially increases the particle yield. Here we perform nonperturbative calculations, discuss how the two mechanisms are related, and assess their experimental feasibility.

Key words: quantum electrodynamics, strong fields, pair production, nonperturbative methods

Introduction

Electron-positron pair production from vacuum in the presence of strong external fields is one of the striking phenomena predicted by quantum electrodynamics (QED) [1, 2, 3]. In the nonperturbative regime of a strong quasistatic external background, this process (Schwinger effect) has never been observed experimentally. According to the estimates obtained decades ago [1, 2, 3], the pair-production probability in an electric field is strongly suppressed by the exponential factor $\exp(-\pi E_\mathrm{c}/E)$ unless the field strength E is close to the (Schwinger) critical value $E_\mathrm{c} \approx 1.3 \times 10^{16}$ V/cm. Nevertheless, it turns out that temporal oscillations of the external field enhance the particle yield. From the experimental viewpoint, the corresponding field setups can be formed, e.g., by a combination of two counterpropagating high-intensity laser pulses. Such fields can be considered classical and also preserve the nonperturbative nature of the pair-production process. Moreover, one should also take into account a large preexponential factor involving the interaction volume. However, the pair-production threshold still clearly exceeds $0.01E_\mathrm{c}$, so the corresponding peak intensity is at least 2–3 orders of magnitude higher than the values that are currently available in the experiment [4]. In this talk, we will discuss two approaches to optimizing the temporal profile of the external field in order to maximize the number of particles produced.

Dynamically assisted Schwinger effect versus fast switch off

As was demonstrated in Ref. [5], the (tunneling) pair-production mechanism in the nonperturbative regime can be efficiently assisted if one provides an additional weak rapidly-varying pulse. A combination of this high-frequency component and the strong background field may increase the pair-production probabilities by several orders of magnitude. Note that in this case, whereas the volume factor is not affected, the weak pulse alters the exponential itself, but the nonperturbative part $\exp(-\pi E_{\rm c}/E)$ remains. This scenario appears to be very promising from the viewpoint of possible experimental investigations of the Schwinger mechanism.

The second approach is based on the following idea. Theoretical methods for calculating the momentum distributions of particles created usually imply that one has to evolve the *adiabatic* electron (or positron) number density in time. At intermediate time instants, the adiabatic number of pairs cannot be clearly interpreted as it depends on the one-particle basis set employed within the corresponding calculations. However, when the field is switched off the equilibrium momentum distribution can be obtained unambiguously. It turns out that the adiabatic number of e^+e^- pairs within numerical computations may drastically exceed the final (asymptotic) number. In Ref. [6] it was argued that a large adiabatic particle number can be turned to a large *final* particle yield by properly shaping the switch-off profile of the external field. It was shown that a sufficiently rapid (but smooth) switching function can make the intermediate (non-equilibrium) values of the particle number experimentally observable.

In this talk, we examine the two mechanisms described above and identify the relation between them [7]. By performing numerical computations based on the quantum kinetic equations [8], we inspect the onset of the enhancement effects and compare the domains of the field parameters where the particle yield is notably increased. Within this analysis, we also utilize a semiclassical approach in the form of the worldline instanton technique (see, e.g., Ref. [9]). Finally, we discuss the experimental prospects of the two mechanisms.

References

1. F. Sauter, Über das Verhalten eines Elektrons im homogenen elektrischen Feld nach der relativistischen Theorie Diracs, Z. Phys. **69**, 742 (1931).

2. W. Heisenberg and H. Euler, Folgerungen aus der Diracschen Theorie des Positrons, Z. Phys. **98**, 714 (1936).

3. J. Schwinger, On gauge invariance and vacuum polarization, Phys. Rev. **82**, 664 (1951).

4. J. W. Yoon *et al.*, Realization of laser intensity over 10^{23} W/cm^2, Optica **8**, 630 (2021).

5. R. Schützhold, H. Gies, and G. Dunne, Dynamically assisted Schwinger mechanism, Phys. Rev. Lett. **101**, 130404 (2008).

6. A. Ilderton, Physics of adiabatic particle number in the Schwinger effect, Phys. Rev. D **105**, 016021 (2022).

7. I. A. Aleksandrov, D. G. Sevostyanov, and V. M. Shabaev, Schwinger particle production: rapid switch off of the external field versus dynamical assistance, arXiv:2210.15626.

8. I. A. Aleksandrov, V. V. Dmitriev, D. G. Sevostyanov, and S. A. Smolyansky, Kinetic description of vacuum e^+e^- production in strong electric fields of arbitrary polarization, Eur. Phys. J. ST **229**, 3469 (2020).

9. G. V. Dunne and C. Schubert, Worldline instantons and pair production in inhomogenous fields, Phys. Rev. D **72**, 105004 (2005).

Superconductor-polariton non-dissipative drag in optical microcavity

Azat F. Aminov[1,*], Alexey A. Sokolik[2,1,†], Yurii E. Lozovik [2,1,‡]

[1]National Research University Higher School of Economics, Moscow, Russia

[2]Institute for Spectroscopy, Russian Academy of Sciences, Troitsk, Moscow, Russia

[*]afaminov@hse.ru, [†]asokolik@hse.ru, [‡] lozovik@isan.troitsk.ru

Abstract

We considered the non-dissipative entrainment effect between the Cooper-pair condensate in superconductor and Bose-condensate of microcavity polaritons. We calculated the drag density in realistic conditions with heterostructures of various two-dimensional materials embedded into the microcavity, and show, that the currents, induced by the non-dissipative entrainment effect in realistic systems, can be large enough to become observable in systems with small enough interlayer distance.

Key words: Theoretical physics, mesoscale physics, superconductivity

The non-dissipative entrainment (drag) effect between substances in superconducting or superfluid states manifests itself in the induction of the non-dissipative current in one constituent in response to the condensate motion in the other constituent. The effect was predicted by A. F. Andreev and E. P. Bashkin for mixtures of superfluid ^{3}He and ^{4}He [1], superconductors [2], nucleons in the cores of neutron stars [3], and Bose-condensed ultracold atomic gases [4], however, it lacks convincing experimental evidence yet. According to the theory [1], the superfluid currents in the system, consisting of two interacting superfluid substances, are coupled:

$$\begin{cases} \mathbf{j}_a = n_a^{\mathrm{s}} \mathbf{v}_a + n_a^{\mathrm{dr}} \mathbf{v}_b, \\ \mathbf{j}_b = n_b^{\mathrm{dr}} \mathbf{v}_a + n_b^{\mathrm{s}} \mathbf{v}_b. \end{cases} \tag{1}$$

Here $\mathbf{j}_i$ is the superfluid particle current, $\mathbf{v}_i$ is velocity of the condensate, and n_i^{s} is the superfluid density of the substance i, and the non-diagonal terms n_i^{dr} are called drag densities, they characterize the entrainment effect. To deal with particles having generally non-quadratic dispersions and hence ill-defined effective masses, we consider particle currents $\mathbf{j}_i$ instead of mass ones $\mathbf{g}_i = m_i \mathbf{j}_i$ [1].

In our recent works [5, 6] we considered the superfluid drag effect between the indirect or direct polaritons in Bose-condensed state and superconducting Cooper-pair condensate in various geometries, the system schematics are presented in Fig 1. In our

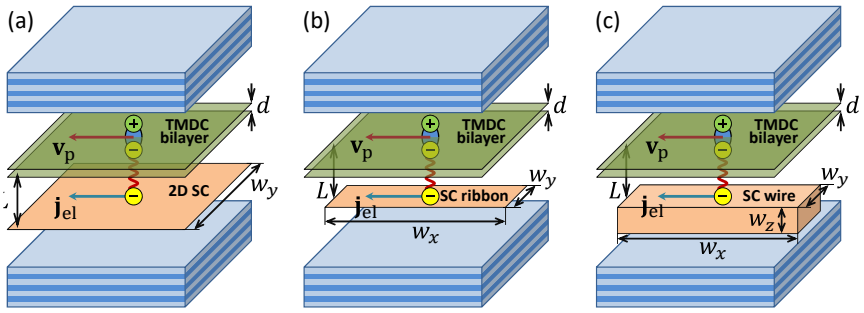

Figure 1: System schematic [6]: excitons in bilayers of semiconducting layers of 2D transition metal dichalcogenides (TMDC) embedded into an optical microcavity interact with (a) 2D atomically thin superconductor (SC), (b) 1D atomically thin superconducting ribbon or (c) 1D wire. Due to electron-exciton interaction, the superfluid drag appears when the motion of exciton-polariton Bose-Einstein condensate (BEC) with the velocity $\mathbf{v}_p$ entrains Cooper pair condensate giving rise to the non-dissipative current of electrons $\mathbf{j}_{el}$.

first work [5] we considered the superconductors with polariton-induced mechanism of superconductivity, when electrons couple via excitation of bogolons in polariton BEC, and investigated the plane-parallel geometry systems (Fig. 1a). The excitons considered were either direct or indirect. In the second work [6] we considered wire-like and ribbon-like (Fig. 1b and 1c) preexisting superconductors ($NbSe_2$, FeSe, YBCO, LSCO, NbN and NbTiN). Another difference between these two works is that in the first we calculated the mass drag density $\rho_{dr} = m^*_{el} n^{dr}_{el}$, which is well-defined whenever electrons have definite effective mass m^*_{el}, while in the second work the drag particle density of electrons $n^{dr}_{el} \equiv n_{dr}$ was our main focus.

The calculations were performed using the Feynman diagrammatic technique in the second order over the polariton-electron interaction, which was screened in the random phase approximation. To describe the polaritonic system, the Bogoliubov theory was used, while the Bardeen–Cooper–Schrieffer theory was applied in regards to the electronic subsystem.

We showed, that the drag density decreases with increasing temperature, linearly vanishes near the critical temperature of the superconductor, and tends to a constant value at much lower temperatures (Fig. 2). The drag density rapidly decreases with the increase of the interlayer distance L: for instance, as $\sim L^{-7}$ for direct and $\sim L^{-1}$ for indirect exciton-polaritons (Fig. 3).

The highest values of drag density is expected for FeSe planar and ribbon-like superconductors, while results for NbN and NbTiN relatively thick superconducting wires are expected to be the lowest. The maximum induced superconducting currents in typical experimental setups are several nA, which are low, but measurable in accurate experiments. Thus the superfluid drag effect can be measured on the electron-polariton

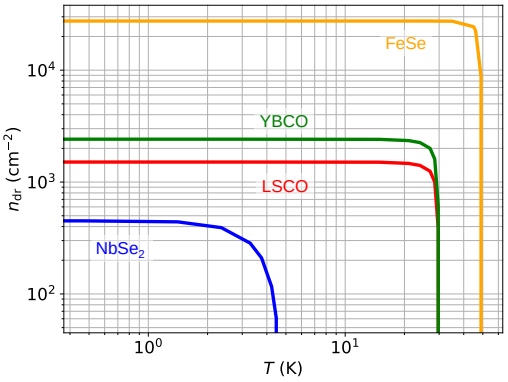

Figure 2: The temperature dependence of the drag density $n_{\rm dr}$ between indirect polaritons and various 2D superconductors.

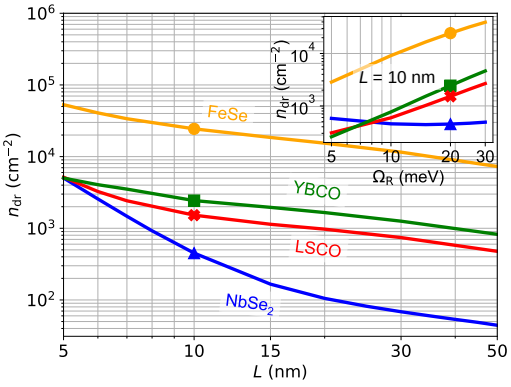

Figure 3: Drag density $n_{\rm dr}$ between indirect polaritons and 2D superconductors as function of interlayer distance L. The inset shows the dependence of the drag density on the Rabi splitting.

platform based on the state-of-the-art two-dimensional materials.

The work was supported by the Russian Foundation for Basic Research (RFBR) within the Project No. 21–52–1203, project FFUU-2021-0003 of the Institute of Spectroscopy of the Russian Academy of Science, and by Program of Basic Research of the Higher School of Economics.

References

1. A. F. Andreev and E. P. Bashkin, Three-velocity hydro-dynamics of superfluid solutions, Sov. Phys. JETP **42**, 164 (1975).

2. J.-M. Duan and S. Yip, Supercurrent drag via the Coulomb interaction, Phys. Rev. Lett. **70**, 3647 (1993).

3. M. A. Alpar, S. A. Langer, and J. A. Sauls, Rapid post-glitch spin-up of the superfluid core in pulsars, Astrophys. J. **282**, 533 (1984).

4. D. V. Fil and S. I. Shevchenko, Non-dissipative drag of superflow in a two-component Bose gas, Phys. Rev. A **72**, 013616 (2005).

5. A. F. Aminov, A. A. Sokolik, and Y. E. Lozovik, Superfluid drag between excitonic polaritons and superconducting electron gas, Quantum **6**, 787 (2022).

6. A. F. Aminov, A. A. Sokolik, and Y. E. Lozovik, Superconductor-polariton non-dissipative drag in optical microcavity, arXiv:2304.10483, to be published.

Optical whispering gallery mode microresonators based on special glasses

E.A. Anashkina[1], A.V. Andrianov[2]

[1,2]Institute of Applied Physics of the Russian Academy of Sciences

[1] elena.anashkina@gmail.com, [2] andrian@ipfran.ru,

Abstract

Optical microresonators with whispering gallery modes play an extremely important role in modern optics and photonics. Microresonators based on dielectric materials provide unique capabilities for controlling fundamental properties of coherent light. They have huge Q-factors and large nonlinearity due to extremely small mode volume, which make it possible to obtain nonlinear effects at very low pump powers. Search for new materials for microresonators is highly interesting, as they may provide wider opportunities for photonic devices as well as new regimes of nonlinear light conversion. From this point of view, highly-nonlinear tellurite and chalcogenide glasses seem to be suitable candidates. In the presentation, we will discuss in detail the features of microresonators made of these special glasses and the special possibilities of light conversion that can be realized in them. A special attention will be paid to nontrivial dynamics of tellurite Raman microlasers with the coexistence of different interacting modes and their controllable switching.

Key words: optical microresonators, whispering gallery modes, tellurite glasses, Raman nonlinearity, microlasers, mode switching.

Introduction

Optical microresonators with whispering gallery modes play an extremely important role in modern optics and photonics. Microresonators based on dielectric materials provide unique capabilities for controlling fundamental properties of coherent light. They have huge Q-factors (10^6-10^{10} and even higher) and large nonlinearity due to extremely small mode volume, which make it possible to obtain nonlinear effects at very low pump powers (of order 0.01-1 mW) [1]. Microresonators are attractive for various applications, including sensing and biosensing, optical filtering and switching, frequency stabilization, and so on. In microresonators, it is possible to generate optical frequency combs (OFCs) which are periodic trains of ultrashort laser pulses with equidistantly spaced spectral lines. Using OFC expands the application range of microresonators in telecommunications, dual-comb spectroscopy, optical atomic clock, ultrafast optical ranging, and in many other areas [1].

Search for new materials for microresonators is highly interesting, as they may provide wider opportunities for photonic devices as well as new regimes of nonlinear light conversion [1]. From this point of view, tellurite (TeO_2-based) and chalcogenide glasses seem to be suitable candidates. They have large nonlinear refractive indices 1-3 orders of magnitude higher compared to silica glass. Tellurite and chalcogenide glasses are characterized by huge Raman gains ($g_R \sim 10^{-11}$ m/W for TeO_2-WO_3 glasses, $g_R = 4.3\times10$ m/W for As_2S_3 glass and $g_R = 5.1\times10^{-11}$ m/W for As_2Se_3 glass) which are two orders of magnitude higher than the maximum Raman gain for silica glasses and many other materials used in microresonator optics [2]. Tellurite and chalcogenide glasses are transparent in the near-IR and mid-IR and demanded for these spectral ranges while silica glasses have very large losses at wavelengths >2.3 μm. In the presentation, we discuss in detail the features of microresonators made of these special glasses and the special possibilities of light conversion that can be realized in them.

Main text

As a good example, we consider controlled Raman generation in tellurite microresonators where theoretical insight is confirmed by experimental study [2]. The research and implementation of Raman microlasers has been attracting increasing attention in recent years. Unlike population inversion lasers, which can generate coherent light in a certain spectral range in the gain band of the active medium, Raman lasers do not have such restrictions on operating wavelengths. The dynamics of intracavity radiation under the action of stimulated Raman scattering can be quite rich and complex and its understanding is very important from the applied and fundamental points of view. Tellurite glasses have a very wide Raman gain band containing, as a rule, two or three pronounced maxima. We studied microresonators based on TeO_2–WO_3–La_2O_3 glass with three maxima (at about 14, 20, and 27 THz; the global one at 20 THz) and found interesting multimode regimes associated with competition of the generated Raman modes (near different maxima of Raman gain spectra) and their cascade interaction [2]. To theoretically describe an unusual behavior of Raman lasing in tellurite microresonators, we developed an analytical model based on nonlinearly-coupled mode theory using the schematic diagram of Raman amplification shown in Figure 1. The obtained analytical solution has confirmed and explained the coexistence of different interacting modes near the Raman gain maxima shifted by ~21 and ~27 THz in the first and second cascades and their switching with a change in pump detuning and pump power (Figure 1). We calculated the diagrams demonstrating different steady-state regimes of Raman generation and their switching with the variation of pump frequency detuning and pump power. We analyzed the behavior of Raman modes in different regimes and obtained a good agreement with the experimental results (Figure 1) [2].

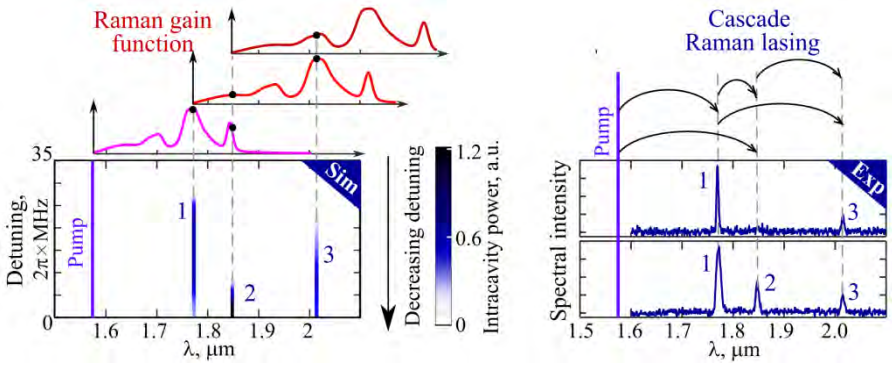

Figure 1: Theoretically simulated (Sim) spectra depending on detuning of pump frequency from the exact resonance that demonstrate controllable switching between steady-state regimes of Raman lasing. The model Raman gain functions and the scheme illustrating the interaction between modes (top). Experimental (Exp) spectra for different values of detuning qualitatively consistent with theoretical results.

References

1. A. Kovach *et al.*, Emerging material systems for integrated optical Kerr frequency combs, Adv. Opt. Photonics **12**, 135 (2020).
2. E.A. Anashkina, A.V. Andrianov, Switchable cascade Raman lasing in a tellurite glass microresonator," ACS Photonics **10**, 1485–1494 (2023).

Coaxial and eccentric states of coupled vortex and skyrmion in superconductor-ferromagnetic heterostructures

S. Apostoloff[1], E. Andriyakhina[2], I. Burmistrov[3]

[1,2,3]L. D. Landau Institute for Theoretical Physics, Chernogolovka, Russia

[2]Moscow Institute for Physics and Technology, Moscow, Russia

[1,3]Laboratory for Condensed Matter Physics, HSE University, Moscow, Russia

[1]ssapostoloff@yandex.com, [3]burmi@itp.ac.ru

Abstract

We study theoretically interaction between a Pearl superconducting vortex and a Néel-type magnetic skyrmion in superconductor-chiral ferromagnetic (SF) heterostructures. Using several complementary approaches, we identify qualitatively different types of the coupled states, coaxial and eccentric. We show that the stray magnetic field of the vortex can significantly change the size and invert chirality of the skyrmion in the coaxial state, and warps the skyrmion in the eccentric state. Moreover, for certain parameters we predict that several different states of coupled vortex and skyrmion can be realized in the same SF heterostructure.

Key words: Superconducting vortex, magnetic skyrmion, chiral ferromagnetic.

Introduction

The interplay of magnetism and superconductivity in heterostructures has attracted attention in recent years. In particular, two topologically nontrivial objects, magnetic skyrmions and superconductor vortices, was realized experimentally in SF bilayers [1]. Skyrmions in SF heterostructures demonstrate interesting physics as they can induce Yu-Shiba-Rusinov-type bound states, modify the Josephson effect, and change the superconducting critical temperature. Skyrmion-vortex pairs can host Majorana modes and serve as a scalable topological quantum computing platform [2].

Superconducting vortices and magnetic skyrmions can couple in SF heterostructures due to proximity effect and via stray fields [3]. Traditionally, analysis of Majorana modes in skyrmion-vortex pairs ignores the effect of stray fields. However, the interaction due to stray fields can result in the repulsion of a Néel–type skyrmion from a Pearl vortex to an eccentric stable state [4].

Model, methods, and results

We consider a heterostructure consisting of two films, superconducting and ferromagnetic, separated by a thin insulating layer that suppresses the proximity effect. The superconducting film contains a Pearl vortex, the ferromagnetic film hosts a Néel–type skyrmion, and the distance a between their centers is assumed to be not equal to zero in the stable state. We use a model with the free energy $\mathcal{F}$ of ferromagnetic film,

$$\mathcal{F}[\vec{m}] = d_F \int d^2\vec{r}\big\{A(\nabla\vec{m})^2 + K(1-m_z^2) + D[m_z\nabla\cdot\vec{m} - (\vec{m}\cdot\nabla)m_z] - M_s\vec{m}\cdot\vec{B}_{\rm V}\big\},$$

accounting for the Dzyaloshinskii–Moriya interaction and the stray field $\vec{B}_{\rm V}$ of the Pearl vortex. We use three complementary approaches: optimizing the free energy with an ansatz for the skyrmion magnetization texture, direct solving of the Euler-Lagrange equation and the micromagnetic simulations.

Comparing the results obtained in the approaches used, we distinguish two types of stable states of coupled vortex and skyrmion, coaxial ($a = 0$) and eccentric ($a \neq 0$). Moreover, we develop a novel ansatz for the skyrmion texture in the presence of the vortex. This ansatz significantly reduces the computational costs and allows to analyze the stable states more precisely than micromagnetic simulations. Basing on it, we study the coaxial state and reveal changing of the size and inversion of the chirality of the skyrmion. For the eccentric state we study the dependence of distance a on the effective vortex strength and determine the conditions, when the skyrmion settles exactly at the top of the vortex. For certain parameters of SF heterostructure we predict that several different states, (i) eccentric, (ii) coaxial with direct chirality, (iii) coaxial with inverted chirality of coupled skyrmion and vortex can be realized.

The work was funded by Russian Science Foundation under Grant No. 21-42-04410.

References

1. A. P. Petrović *et al*, Skyrmion-(Anti)vortex coupling in a chiral magnet-superconductor heterostructure, Phys. Rev. Lett. **126**, 117205 (2021).

2. J. Nothhelfer *et al*, Steering Majorana braiding via skyrmion-vortex pairs: A scalable platform, Phys. Rev. B **105**, 224509 (2022).

3. R. M. Menezes *et al*, Manipulation of magnetic skyrmions by superconducting vortices in ferromagnet-superconductor heterostructures, Phys. Rev. B 100, 014431 (2019).

4. E. S. Andriyakhina and I. S. Burmistrov, Interaction of a Néel-type skyrmion with a superconducting vortex, Phys. Rev. B 103, 174519 (2021).

5. E. S. Andriyakhina, S. Apostoloff, and I. S. Burmistrov, Repulsion of a Néel-type skyrmion from a Pearl vortex in thin ferromagnet–superconductor heterostructures, JETP Letters 116, 825 (2022).

Mean field study of 2D quasiparticle condensate formation in presence of strong decay

N.A. Asriyan[1*], A. A. Elistratov[1], Yu. E. Lozovik[2]

[1]N.L. Dukhov Research Institute of Automatics (VNIIA), Moscow 127030, Russia

[2]Institute for Spectroscopy RAS, Troitsk 108840, Moscow, Russia;

[*]naasriyan@vniia.ru

Abstract

Bose-condensation in a system of 2D quasiparticles is considered in the scope of a microscopic model. Mean-field dynamical equations are derived with the help of the Schwinger-Keldysh formalism and a simple model is proposed which allowes to descibe key features of condensate formation in systems with various quasiparticle decay rates. By analysing stationary solutions of this equation, we obtain the phase diagram of quasiparticle gas, finding a bistability region in the parameter space of the system.

Introduction

Due to finite quasiparticle lifetime in solid state systems (such as quantum well excitons [1, 2], exciton-polaritons [3, 4], magnons [5] and microcavity photons [6]), condensates there are non-equilibrium ones. This complicates the use of standard approaches for describing them (e.g. using the Gross-Pitaevskii equation). In order to overcome this issue numerous techniques were proposed which add pump and decay terms to the evolution equation [7, 8, 9, 10]. However, existing models have several drawbacks when describing significantly non-equilibrium condensates of intensely decaying particles. These are due to the time-local form of the equations and not considering the memory effects.

We develop an approach, based on the Schwinger-Keldysh technique [11], which allows to treat properly memory effects. Deriving an evolution equation we propose several simplifications and express steady-state solutions. Analysing them, we demonstrate that memory effects lead to appearance of an overlap of condensate and normal phases on the phase diagram where the system demonstrates bistable behaviour.

Main results

We deal with a 2D single-level condensate model of finite-lifetime quasiparticles embedded in a long-living particle reservoir, which is assumed to be a quasi-equilibrium

system with well defined effective temperature and chemical potential. The system is treated as a 2D bose gas with contact interparticle interaction and leakage from the condensate. The model Hamiltonian is as follows ($\hat{\psi}_{\boldsymbol{q}}$ is the quasiparticle annihilation operator with wavevector $\boldsymbol{q}$, therefore $\hat{\psi}_0$ corresponds to the condensate mode):

$$\hat{H} = \left(\varepsilon - i\frac{\Gamma}{2}\right)\hat{\psi}_0^\dagger\hat{\psi}_0 + \sum_{\boldsymbol{q}\neq\boldsymbol{0}} \varepsilon_{\boldsymbol{q}}\hat{\psi}_{\boldsymbol{q}}^\dagger\hat{\psi}_{\boldsymbol{q}} + g_0 \sum_{\boldsymbol{q}_1,\boldsymbol{q}_2,\boldsymbol{q}'} \hat{\psi}_{\boldsymbol{q}_1+\boldsymbol{q}'}^\dagger\hat{\psi}_{\boldsymbol{q}_2-\boldsymbol{q}'}^\dagger\hat{\psi}_{\boldsymbol{q}_1}\hat{\psi}_{\boldsymbol{q}_2} \tag{1}$$

Here $g_0 = \frac{V_0}{2L^2}$ stands for contact interparticle interaction with V_0 being the interaction potential and L^2 denoting the quantization area. ε denotes the possible energy detuning of the condensate level with respect to the reservoir dispersion curve $\varepsilon_{\boldsymbol{q}\to 0} = 0$. A decay rate Γ is introduced to describe condensate particle finite lifetime.

Using Schwinger-Keldysh action in path-integral formalism, we integrate out reservoir degrees of freedom to derive an evolution equation for the condensate order parameter in the form:

$$i\dot{\phi}_c = \left[\varepsilon - i\frac{\Gamma}{2} + \Sigma_0^\delta + g_0|\phi_c|^2\right]\phi_c(t) + \int_{t_0}^{t} d\tau \Sigma_0^+(t,\tau)\phi_c(\tau). \tag{2}$$

with the memory kernel being given by the retarded component of the self-energy term given by a diagram depicted on Fig. 1.

$$-\Sigma_{\boldsymbol{q}}^\delta(t,t') = 2$$
$$-\Sigma_{\boldsymbol{q}}(t,t') = 8i$$

Figure 1: Time-local term and the contribution to the self-energy term due to interaction with reservoir. Here the filled vertex corresponds to the factor $(-g_0)$, solid lines are reservoir Green's functions $G_{\boldsymbol{q}}^{\text{res}}$.

We show that the memory kernel may be be expressed in a simplified model form:

$$i\partial_t\phi_c = \left(\tilde{\varepsilon} + g|\phi_c|^2 - i\frac{\Gamma}{2}\right)\phi_c - \Lambda^+\left(1 - i\frac{\mu}{\gamma}\right)\int_0^t e^{-\gamma(t-t')}\phi_c(t')dt' \tag{3}$$

with Λ and γ being density and temperature dependent parameters.

This equation may be solved with the help of Markovian embedding. By doing so we demonstrate that the phase diagram of the system has a bistable region for large decay rates, where both the normal phase ($\phi_c = 0$) and the condensate phase with $\phi \neq 0$ are stable. By applying this technique to the condensate of exciton-polaritons in CdTe microcavities, we conclude that this effect is observable for experimentally relevant polariton densities/temperatures.

References

1. A. A. High, J. R. Leonard, A. T. Hammack, M. M. Fogler, L. V. Butov, A. V. Kavokin, K. L. Campman et A. C. Gossard Nature 483, 584–588 (2012).

2. A. A. High, J. R. Leonard, A. T. Hammack, M. M. Fogler, L. V. Butov, A. V. Kavokin, K. L. Campman et A. C. Gossard Nano Lett., 12, 5 (2012).

3. J.Kasprzak et al., Nature **443**, 409 (2006).

4. R.Balili et al., Science **316**, 1007 (2007).

5. S.O. Demokritov et al., Nature **443**, 430 (2006).

6. J.Klaers, J.Schmitt, F.Verwinger, and M.Weitz, Nature **468**, 545 (2010).

7. M. Wouters and I. Carusotto, Phys. Rev. Lett. **99**, 140402 (2007) PPhys. Rev. Lett. **99**, 140402 (2007).

8. J. Keeling, N. G. Berloff, Phys. Rev. Lett. 100, 250401(2008).

9. H. Haug, T. D. Doan, and D. B. Tran Thoai, Phys. Rev. B **89**, 155302 (2014).

10. A. A. Elistratov and Yu. E. Lozovik, Phys. Rev. B **97**, 014525 (2018).

11. Preprint on ArXiv: 2209.09710, to be published.

Generalized multifractality in the spin quantum Hall symmetry class with interaction

I.S.Burmistrov[1]

[1]L.D. Landau Institute for Theoretical Physics

[1]burmi@itp.ac.ru

Abstract

In this talk I present recent results on generalized multifractality in the spin quantum Hall symmetry class transitions in the presence of interaction.

Key words: Theoretical physics

Introduction

Anderson transition is a fascinating example of a disorder-driven quantum phase transition separating metallic and insulating phases. A nontrivial topology, e.g. as in the integer quantum Hall effect, makes Anderson transition to occur between distinct topological phases. Although more than 60 years past from the seminal paper by Anderson, localization–delocalization transitions in disordered media are still a subject of intense research. A striking feature of Anderson transition is strong mesoscopic fluctuations of electron wave functions or, equivalently, the local density of states. At criticality the disorder averaged moments of the local density of states demonstrate pure power-law scaling with the system size, $\langle \rho^q \rangle \sim L^{-x_{(\mathsf{q})}}$, with the *multifractal* exponents $x_{(\mathsf{q})}$ whose values depend on a symmetry class. In fact, there are much more observables than just the moments of the local density of states that demonstrate pure scaling with L at critically.

Results

In this talk I present the theory of the generalized multifractality for the spin quantum Hall symmetry class in the presence of electron-electron interaction. Within the Finkel'stein nonlinear sigma model I review the results known in the literature for the one-loop renormalization of the spin conductance, dimensionless interaction, the Finkel'stein frequency renormalization parameter, and the averaged density of state.

Next, using Finkel'stein nonlinear sigma model for class C, I argue that the pure scaling derivativeless operators can be constructed by straightforward generalization of the pure scaling operators without derivatives known in the absence of interaction. Within the two-loop approximation we compute how the anomalous dimensions of the pure scaling derivativeless operators are affected by the presence of interaction.

Applying our results to the Anderson-Mott transition in $d = 2 + \epsilon$ dimensions, we illustrate breakdown of the exact symmetry relations between generalized multifractal exponents for class C in the presence of interaction.

The details can be found at Refs. [1, 2]

References

1. S. S. Babkin and I. S. Burmistrov, Generalized multifractality in the spin quantum Hall symmetry class with interaction, Phys. Rev. B **106**, 125424 (2022).

2. S.S. Babkin, J.F. Karcher, I.S. Burmistrov, and A.D. Mirlin, Generalized surface multifractality in 2D disordered systems, arxiv:2306.09455 .

Time-reversal and spatial parity violation in atomic systems

Dmitry V. Chubukov

ITMO University, St. Petersburg, Russia

NRC "Kurchatov Institut" — Petersburg Nuclear Physics Institute, Gatchina, Russia

dmitry.chubukov@metalab.ifmo.ru

Abstract

In this talk, different mechanisms of the $\mathcal{P}$, $\mathcal{T}$-violating electron electric dipole moment and pseudoscalar-scalar electron-nucleus interaction in frames of the Standard Model are considered. Still, there remains a significant gap between the theoretical predictions of the Standard Model and experimental constraints on the $\mathcal{P}$, $\mathcal{T}$-odd interactions in atomic systems. Therefore, in this talk, the experimental prospects of searching for the $\mathcal{P}$, $\mathcal{T}$-odd interactions via the $\mathcal{P}$, $\mathcal{T}$-odd Faraday effect are also discussed.

Key words: $\mathcal{T}$-noninvariance, electron electric dipole moment, Higgs boson, $\mathcal{P}$, $\mathcal{T}$-odd Faraday effect

Introduction

Investigation of spatial parity ($\mathcal{P}$) and time-reversal invariance ($\mathcal{T}$) violation effects at low energies is an effective tool for developing various models of fundamental interactions in physics. Such investigations with atomic and molecular systems appear to be important, inexpensive (reactors and accelerators are not required) and highly precise alternative to high-energy physics experiments to the search for the so-called "new physics" beyond the Standard Model (SM). However, the nature of the $\mathcal{T}$-noninvariant interactions is still unclear.

Theoretical predictions of the Standard Model

The theoretical predictions for the $\mathcal{P}$, $\mathcal{T}$-violating electron electric dipole moment (eEDM) are rather uncertain. The recent estimate at the hadronic level gives the result $\sim 10^{-39}$ $e$cm [1]. In the same paper, estimate at the quark level gives the value for the eEDM $\sim 10^{-50}$ $e$cm. It is known that the $\mathcal{P}$, $\mathcal{T}$-odd electron-nucleus interaction in atomic (molecular) systems can be only of the scalar-pseudoscalar type. It is convenient to express the magnitude of this interaction in terms of the equivalent eEDM, which produces the same Stark shift of atomic energy levels in the same external

electric field. In Ref. [2], this interaction was estimated on the basis of two-photon exchange model with the result of the equivalent eEDM $\sim 10^{-38}$ $e$cm at the hadronic level. In Ref. [3], we proposed to consider the electron-nucleus interaction on the basis of another model (exchange by the Higgs boson) at the quark level. The estimate of the equivalent eEDM for such a mechanism $\sim 10^{-43}$ $e$cm. The largest predicted value for the electron-nucleus interaction has been recently reported on the basis of the exchange by neutral K-meson $\sim 10^{-35}$ $e$cm [4]. There exists a vast literature on the various extensions of the SM which predict larger values for the eEDM (see, for instance, Ref. [5]). None of these predictions have been yet approved, and some of them have already been ruled out by existing experiments.

$\mathcal{P}$, $\mathcal{T}$-odd Faraday effect

The present constraint (up to recent time) on the eEDM is based on the observation of the electron-spin precession in an external electric field using the ThO molecule [6] ($\sim 10^{-29}$ $e$cm). Until recently, a new upper bound for the eEDM (improvement by a factor ~ 2.4) has been established in an experiment with the trapped molecular ions HfF^+ in a rotating electric field [7]. Still, there remains a wide gap between the SM theoretical predictions on the eEDM and the experiment. Therefore, it is highly desirable to develop alternative methods for measuring the eEDM such as that based on the $\mathcal{P}$, $\mathcal{T}$-odd Faraday rotation. The $\mathcal{P}$, $\mathcal{T}$-odd Faraday effect manifests itself as a rotation of the polarization plane of linearly polarized light propagating through a gas medium in an external electric field. Our alternative approach is to observe such an effect using the cavity-enhanced polarimetric scheme in combination with a molecular beam crossing the cavity. A principle scheme of the proposed experimental setup is shown in Fig. 1. Theoretical simulation of the proposed experiment with the PbF and ThO molecular beams indicates that it could potentially improve the current constraint on the eEDM by several orders of magnitude [8].

Acknowledgements

This work was supported by the President of Russian Federation Stipend No. SP1213.2021.2.

References

1. Y. Yamaguchi and N. Yamanaka, Phys.Rev. D **103**, 013001 (2021).

2. M. Pospelov and A. Ritz, Phys.Rev. D **89**, 056006 (2014).

3. D. V. Chubukov and L. N. Labzowsky, Phys.Rev. A **93**, 062503 (2016).

4. Y. Ema, T. Gao, and M. Pospelov, Phys.Rev.Lett. **129**, 231801 (2022).

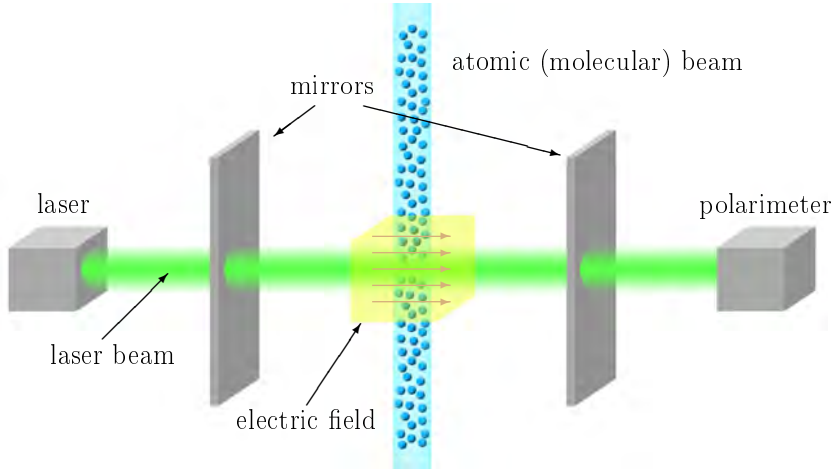

Figure 1: Principle scheme of the experimental setup. An atomic (molecular) beam (blue) traverses a high-finesse optical cavity and interacts with a linearly polarized laser beam (green). The interaction region is located in a background electric field (yellow) directed along the laser beam axis. The laser radiation transmitted through the two mirrors is detected by means of a polarimeter.

5. J. Engel, M. J. Ramsey-Musolf, and U. van Kolck, Prog. Part. Nucl. Phys. **71**, 21 (2013).

6. V. Andreev et al. (ACME collaboration), Nature **562**, 355 (2018).

7. T. S. Roussy et al. (JILA Collaboration), arXiv:2212.11841v3.

8. D. V. Chubukov, L. V. Skripnikov, A. N. Petrov, V. N. Kutuzov, and L. N. Labzowsky, Phys.Rev. A **103**, 042802 (2021).

Radiative properties of nanoscale systems with photobleaching

I. Doronin[1,2,3], A. Zyablovsky[2], E. Andrianov[3]

[1,2,3]Moscow Institute of Physics and Technology, Dolgoprudny, Moscow Oblast

[1,2,3]Federal State Unitary Enterprise Dukhov Automatics Research Institute (VNIIA), Moscow

[1]Institute of Spectroscopy Russian Academy of Sciences, Troitsk, Moscow

[1]ildoron2@gmail.com, [2]zyablovskiy@mail.ru, [3]andrianov.es@mipt.ru

Abstract

We develop a model that describes photobleaching in hybrid nanoparticle in strong coupling regime. We show that there is an optimal concentration of dye molecules in shell of plasmonic nanoparticle at which photobleaching rate is greatly decreased. Theoretical prediction shows reasonable agreement with experimental data. This result paves the way for facilitating dye molecules for many applications, primarily probing and spectroscopy, since it enables a way to combat one of main disadvantages of dye molecules - their short lifetime.

Key words: Plasmonics, photobleaching, strong coupling

Introduction

Dye molecules are popular in many photonic application due to low price and high brightness [1]. However, they have limitations primarily due to high rate of photodegradation [2]. Photodegradation is caused by chemical reaction between dye molecules and oxygen. Such reactions typically occur when dye molecules transition to an excited non-radiating long-living state as a result of interplay between optical pumping and, e.g., vibrational excitations in molecule. There are several approaches to prevent photodegradation, first, reducing oxygen concentration (via coating or other methods), second, decreasing the population of excited states of dye molecule. The latter is the focus of this study. Decreasing of excited states of dye molecules can be achieved by coupling them to plasmonic nanoparticle. This results in higher emission rate and, therefore, lower population inversion and lower chance for a molecule to transition to undesired non-radiative states. This method can be easily combined with reduction of oxygen access via coating plasmonic nanoparticle in non-active polymer, such as polydopamine, and embedding dye molecules in said polymer

In this work we show that concentration of dye molecules in shell plays a large role in resulting energy levels of the system. We develop a model that enables description of photodegradation of dye molecules strongly coupled to a plasmon particle. We show that there is an optimal concentration of dye molecules at which the photobleaching rate is greatly decreased by more than an order of magnitude. We attribute this optimum to interplay between several changes in energy structure of the resulting emitter.

Main text

To describe the hybrid system we employ a well-known approach based on Lindblad equations [3], which are then used to write rate equations on populations of all relevant energy levels of the emitter, namely, unexcited state, lower and upper polaritons (excited states originating from hybridization of plasmonic states and dye radiating states), dark states (non-radiating combination of initially radiating states of dye molecules, note that molecules in this state do not directly interact in oxygen in this state), and, crucially, non-radiating molecule state that interacts with oxygen. To take into account photodegradation we assume that system in this state may either transition to other states (listed above), or irreversibly degrade. The resulting degradation rate is what we aim to describe.

Our model predicts that at low concentration the photodegradation rate decreases with increase of concentration. However, at certain concentration the trend reverses, and further increase of concentration causes increase of photodegradation rate. Results of calculations and comparison to experimental data are shown in Figure 1. As seen from the comparison, the model manages to predict the magnitude of the effect and presence of the optimal concentration. The optimal concentration can explained as the result of competition between two processes. First, high concentration increases the coupling strength between dye molecules and plasmonic particle, which increases particle lifetimes. However, at very high concentration the energy levels of the system shift due to strong concentration quenching which ultimately results in dark states energy dropping below polariton energy. This drop results in population inversion accumulating in dark states, which are unaffected by plasmonic particle and therefore, do not benefit from lifetime increase. At high concentrations the latter effect prevents plasmonic particle from shielding dye molecules from oxidization, and leads to decrease of emitter lifetime.

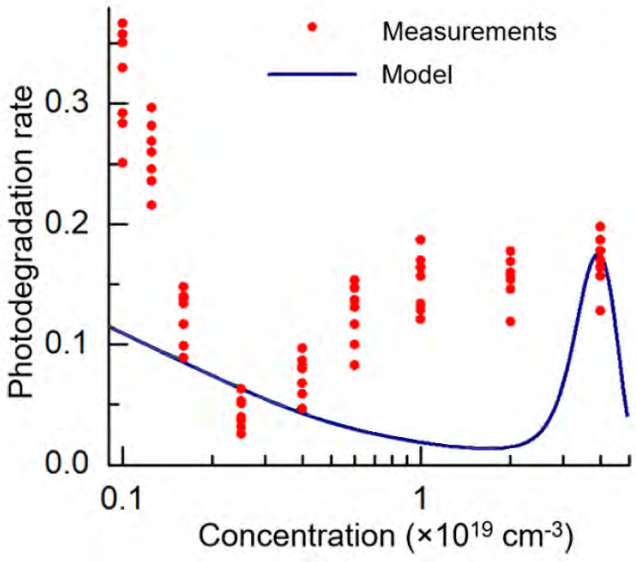

Figure 1: Normalized photodegradation rate of dye molecules within polydopamine shell of plasmonic nanoparticle. Rate of 1 corresponds to about $0.2s^{-1}$. Red dots – experimental data. Blue curve – model. Figure is taken from our work [4].

In conclusion, we demonstrate a model capable of qualitative description of radiative characteristics of nanoscale hybrid system. We predict that there is an optimal concentration that enables highest lifetime and thus greatly increases longevity of dye molecules. Our results show qualitative agreement with experiment. Our result paves the way for facilitating use of dye molecules in probing and imaging techniques.

References

1. M. Mycek, B. Pogue. Handbook of biomedical fluorescence. CRC Press (2003).
2. J. Widengren, J., R. Rigler, R. Mechanisms of photobleaching investigated by fluorescence correlation spectroscopy. Bioimaging, **4**(3), 149, (1996)
3. H. Carmichael. Statistical methods in quantum optics 1: master equations and Fokker-Planck equations (Vol. 1). Springer Science & Business Media (1999).
4. I. Doronin, A. Kalmykov, A. Zyablovsky, et al. Resonant concentration-driven control of dye molecule photodegradation via strong optical coupling to plasmonic nanoparticles. Nano Letters, **22**(1), 105, (2021).

High-quality Resonances in Spherical Nanoparticles with Radial Anisotropy

Amir Eghbali[1*], Andrey A. Vyshnevyy[1]

[1]Center for Photonics and 2D Materials, Moscow Institute of Physics and Technology, 9 Institutsky Lane, Dolgoprudny 141700, Russian Federation

[*] eghbali.amir@phystech.edu,

Abstract

The possibility of obtaining resonances with a high quality factor is one of the topical topics of research in the field of nanophotonics. High-Q resonators are required to achieve a high degree of field amplification/localization and to reduce optical losses, and provide an efficient platform for strong interaction of radiation and matter for applications in nonlinear optics, lasers, and sensors. In this work, we study the effect of radial anisotropy on the optical properties of spherical nanoparticles, including homogeneous spheres and core-shell nanoparticles. Furthermore, we show that over 30-fold increase in Q-factor is possible compared to isotropic nanospheres. Our findings demonstrate that optical anisotropy is a valuable resource for nanophotonics and open new avenues for designing high-performance nanophotonic devices.

Key words: nanophotonics, dielectric resonators, Radial anisotropy,

High-quality resonances

Introduction

Many significant phenomena in nanophotonics are based on the interaction of eigenmodes of nanosized resonators with quantum emitters. Nanolasers and single-photon sources are subject to the influence of the Purcell effect, which consists in changing the rate of spontaneous emission in the resonator. In this case, the higher the quality factor of the resonator mode, the more significant deviations in the rate of spontaneous emission can be achieved. It is generally accepted that nanoparticles, being open resonators, have resonances with a very low quality factor of the order of 5–10, which does not allow them to be used to create nanolasers and other applications that require a high quality factor. To increase the quality factor, it is customary to surround the particles with metal layers that reflect radiation, but this leads to a decrease in the total quantum yield due to absorption losses in the metal, which, in addition, lead to undesirable heating. An alternative approach is to fabricate a non-spherical resonator in which hybridization of different multipole modes can result in a high-Q "supermode" [1], but there is no known way to obtain pure multipole high-Q modes. However, such modes can be obtained using anisotropic optical materials with giant anisotropy which is discussed in the next section.

Main text

For the initial study of the effect of anisotropy on the quality factor of multipole resonances, a uniform radially anisotropic sphere was first investigated. The tangential

component of the refractive index was assumed to be 4, which corresponds to semiconductor dichalcogenides of transition metals in the transparency region, while the radial component was assumed to be variable and varied over a wide range. Due to the spherical symmetry of radially anisotropic spheres, their eigenmodes are eigenfunctions of the total angular momentum operator, i.e., are spherical harmonics. In this case, in magnetic multipole modes, the radial component of the electric field is zero everywhere, due to which they are insensitive to the radial anisotropy of the permittivity. Therefore, only electric multipole modes were analyzed. In particular, a radially anisotropic sphere has an electric dipole quasi-normal mode with a relatively high quality factor, which increases as the radial component of the refractive index of the nanosphere material decreases (Fig. 1a).

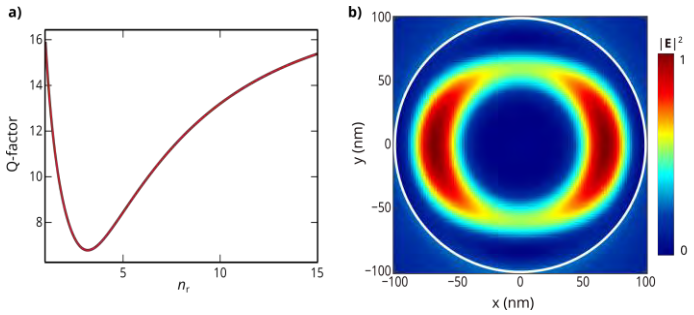

Figure 1: Quality factor of an electric dipole quasi-normal mode in a radially anisotropic nanosphere as a function of the radial component of the refractive index. b) Distribution of the electric field of the mode at n_t=4, n_r=1.

To explain the nature of the increase in the quality factor, the distribution of the electric field of the mode was plotted (Fig. 1b). In contrast to the dipole mode of isotropic spheres, the field at the center of the sphere turns out to be very small. Also, due to the small radial component, the interface between the material of the sphere and the air is less permeable, which leads to more efficient retention of the field energy inside the sphere. However, as the radial component decreases, the Q-factor of the mode increases rather moderately.

Further, the eigenmodes in the core-shell system were studied, in which the core was an isotropic material with a refractive index of 4, and the shell was radially anisotropic with n_t=4, n_r=1. By continuously changing the ratio between the radius of the core and the total radius of the particle, it is possible to achieve a quality factor of the electric dipole resonance in excess of 300 (Fig. 2a). The high-Q mode appears as a narrow peak in the scattering spectrum (Fig. 2b).

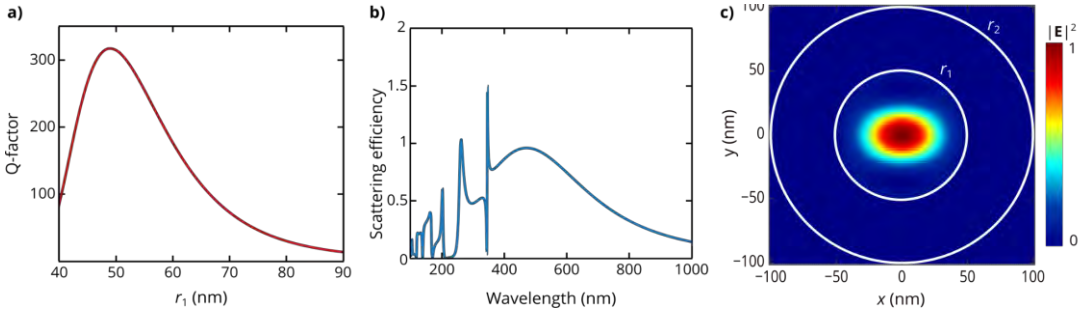

Figure 2: High -Q resonance with the core-shell system. a) the quality factor of the electric dipole mode as a function of the core radius r_1. r_2 = 100 nm. b) Scattering spectrum of a nanoparticle with $r_1=r_2/2$. c) Distribution of the electric field of the electric dipole mode at $r_1=r_2/2$.

References

1. Rybin, M. V., Koshelev, K. L., Sadrieva, Z. F., Samusev, K. B., Bogdanov, A. A., Limonov, M. F., and Kivshar, Y. S., High-Q Supercavity Modes in Subwavelength Dielectric Resonators, Phys. Rev. Lett. 119, 243901 (2017).

Current-induced valley polarization in transition metal dichalcogenide monolayers

Daniil S. Eskoskin[1] and Mikhail M. Glazov[2]

[1] Moscow Institute for Physics and Technology, 141700 Moscow, Russia

[2] Ioffe Institute, 194021 Saint Petersburg, Russian Federation

[1]eskoskin.ds@phystech.edu, [2]glazov@coherent.ioffe.ru

Abstract

Here we study the relation between the electron spin polarization and electric current in monolayers of transition metal dichalcogenides. Such systems are described by the D_{3h} point group, which belongs to the class of noncentrosymmetric and nongyrotopic groups. In such a system, the linear relationship between spin and current is forbidden by symmetry. Phenomenological analysis based on group theory has shown that the spin polarization is proportional to the third power of the current magnitude and the cosine of the triple angle between the current and the crystallographic axis. In the framework of the kinetic equation a microscopic theory of the effect was constructed. The polarization degree has been calculated. A physically grounded estimation of the effect has been made from qualitative considerations.

Key words: spin polarization, transition metal dichalcogenide monolayers, electric current

Peculiarities of the density of states in superconductor/normal-metal junctions

Ya. V. Fominov[1,2] and A. A. Mazanik[3,4]

[1]L. D. Landau Institute for Theoretical Physics RAS, 142432 Chernogolovka, Russia

[2]Laboratory for Condensed Matter Physics, HSE University, 101000 Moscow, Russia

[3]Moscow Institute of Physics and Technology, 141700 Dolgoprudny, Russia

[4]BLTP, Joint Institute for Nuclear Research, 141980 Dubna, Russia

[1]fominov@itp.ac.ru

Abstract

We study the density of states (DoS) $\nu(E)$ in a normal-metallic (N) film contacted by a bulk superconductor (S). We assume that the system is diffusive and the SN interface is transparent. In the limit of thin N layer (compared to the coherence length), we analytically find three different types of the DoS peculiarity at energy equal to the bulk superconducting order parameter Δ_0. (i) In the absence of the inverse proximity effect, the peculiarity has the check-mark form with $\nu(\Delta_0) = 0$ as long as the thickness of the N layer is smaller than a critical value. (ii) When the inverse proximity effect comes into play, the check-mark is immediately elevated so that $\nu(\Delta_0) > 0$. (iii) Upon further increasing of the inverse proximity effect, $\nu(E)$ gradually evolves to the vertical peculiarity (with an infinite-derivative inflection point at $E = \Delta_0$). This crossover is controlled by a materials-matching parameter which depends on the relative degree of disorder in the S and N materials.

Key words: Superconductivity, Proximity effect, SN junction, Density of states

References

1. A. A. Mazanik, Ya. V. Fominov, Peculiarities of the density of states in SN junctions, Annals of Physics **449**, 169199 (2023).

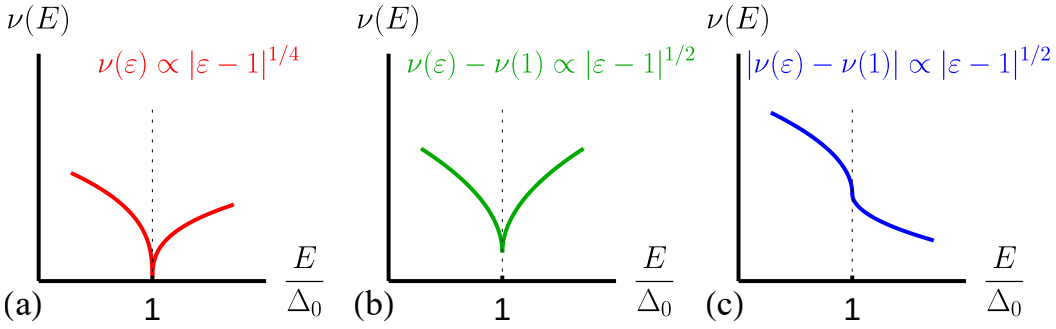

Figure 1: Schematic plot of three different types of the DoS peculiarity at $E = \Delta_0$: (a) full check-mark peculiarity, (b) elevated check-mark peculiarity, (c) vertical peculiarity. The elevated check-mark peculiarity is symmetric, while the full check-mark and the vertical peculiarity are asymmetric.

Nonlinear XUV-optics with IR-dressed atoms: theoretical challenge

M. V. Frolov[1,2]

[1]Voronezh State University, Voronezh 394018, Russia

[2]University of Nizhny Novgorod, Nizhny Novgorod 603950, Russia

frolov@phys.vsu.ru

Abstract

The theoretical description of nonlinear phenomena in atoms jointly interacting with an intense IR and attosecond XUV pulses is discussed. We show that the adiabatic approach together with the perturbation theory may be conveniently utilized for accurate description of nonlinear phenomena caused by the attosecond XUV pulse in IR-dressed atom: strong IR field effects can be treated within the adiabatic approach, while the nonlinear XUV-induced effects can be considered within the perturbation theory. Details of the perturbation theory based on the adiabatic IR-dressed states expansion is discussed. The proposed theory is used for the calculation of the XUV-assisted high harmonic generation, XUV rectification effect, second harmonic generation of the XUV field with further application to the attosecond and IR pulse metrology.

Key words: Intense IR pulse, attosecond XUV pulse, adiabatic theory, perturbation theory, nonlinear XUV-optics phenomena

The quantum mechanical description of fundamental processes in an intense laser field consists in the calculation of corresponding transition matrix elements, which involve the exact wave function of an electron dynamically interacting with an intense laser field. This wave function obeys the time-dependent Schrödinger equation (TDSE), whose solution for a given atomic potential and electron-laser interaction cannot be found in a closed analytic form. This obstacle can be overcome either by getting this wave function numerically from the TDSE or by applying some approximations ensuring different levels of accuracy for the transition matrix element. In this talk we give overview of the adiabatic approach, which is applied for description of the joint interaction of an intense IR and attosecond XUV pulses with unpolarized atom.

It is well known that the interaction of IR and XUV pulses with an atomic system is realized predominantly on the different time scales, which are determined by the carrier frequencies of the corresponding pulses ($\omega_{\rm IR}$ and $\omega_{\rm XUV}$ for IR and XUV pulses, respectively): $\omega_{\rm IR}/I_p \ll 1$ and $\omega_{\rm XUV}/I_p > 1$, where I_p is the ionization potential of an atomic level. If the peak field strengths ($F_{\rm IR}$ and $F_{\rm XUV}$) for both pulses are considered to be lower than the atomic field strength ($F_{\rm at} = \kappa^3$, where $\kappa = \sqrt{2I_p}$), that makes possible to apply the adiabatic approach [1–3] for IR field (describing all nonlinear

IR-induced effects) and the non-stationary perturbation theory for XUV pulse [4]. For synchronized IR and XUV pulses, the adiabatic wave functions in the IR field can be used to develop a formal perturbation theory in the interaction with the XUV field [5].

The theoretical origin of the adiabatic approach lies in the low-frequency approximation, which was proposed in the end of XX century for accurate description of the nonperturbative interaction of an intense low-frequency IR field with an atomic system [1]. The theoretical background of the low-frequency approximation was based on the assumption that the laser field changes much slower than internal dynamics of an atomic system. Within this assumption the shape of the wave function is given by the quasistationary state in the DC field, whose strength is determined by the instant strength of the laser electric field. The further development of the low-frequency approximation was focused mostly in two directions: (i) the decomposition in a series in frequency for the wave function [1] and (ii) the development of an asymptotic solution of TDSE based on the solutions in the DC field [2, 3]. In the latter case, the developed approach was successfully applied for description of plateau effects in spectra of the above-threshold detachment (ATD) and high harmonic generation (HHG).

Recently we have renewed the adiabatic approach to describing the IR-dressed wave function and develop the perturbation theory for IR-dressed atom [5, 6]. Within this approach the wave function is partitioned into "slow" and "fast" parts describing different dynamics of the IR-dressed atom. The slow part is given by the zero order of the low-frequency theory, while the fast (or rescattering) part is presented by a superposition of outgoing-wave scattering states with modified asymptotic momenta in the atomic potential. The slow part presents the IR-dressed wave function, which instantaneously formed by the IR field at the given moment, while the fast part describes the specific IR-induced electron dynamics associated with closed classical trajectories in a laser field. Applying this result to the calculation of strong-field processes amplitudes, we show that amplitudes parametrizations are the result of specific properties of the wave function in an intense laser field. Moreover, we utilize the analytic results for the wave functions in an intense low-frequency laser field to develop the perturbation theory in weak attosecond pulse, whose duration is sufficiently less than IR pulse. The adiabatically-based perturbation theory for XUV field interacting with IR-dressed atom is developed in terms of IR-dressed Green function. This Green function has analytic and non-analytic parts with respect to the IR field strength. We have found that the level of accuracy of the adiabatic approach prescribes to utilize only analytical parts in calculation of a corresponding matrix element of the perturbation theory.

Within the first and second order of the adiabatically-based perturbation theory, we consider the XUV-assisted high-harmonic generation, XUV rectification effect and second harmonic generation of the XUV field by IR-dressed atom. The XUV field is presented by an attosecond pulse, whose unique duration is sufficiently less than the period of IR pulse. The interaction of these two pulses having predominantly different time scales with atoms induces effects, which make a base for an avenue in the developing of new optical methods for tracing the IR-induced electron dynamics and detecting the waveform of IR and XUV pulses. Our analytical analysis and

ab initio numerical simulations demonstrate that the XUV-assisted HHG yield as a function of the time delay between IR and XUV pulses and harmonic energy mimics the short-time Fourier transform of the dipole acceleration induced by the laser field, thereby providing possible *in-situ* experimental access for tracing electron dynamics in strong field phenomena. Moreover, we show analytically that the high-order harmonic generation yield for an intense IR pulse and time-delayed attosecond pulse keeps encoded waveform of the attopulse, which can be decoded by the time delay measurements of the HHG yield, thereby utilizing the XUV-assisted HHG for attosecond pulse metrology. We also show that joint interaction of IR and XUV pulses with unpolarized atom can induce new nonlinear effects: the generation of doubled frequency XUV pulse and the induction of quasistatic dipole moment (QSDM) or the XUV rectification effect. The yield of harmonics in the frequency band of the generated doubled frequency XUV pulse as a function of the time delay between XUV and IR pulses replicates the time dependence of the IR-field intensity, thereby providing an alternative to the streak camera method for retrieving the waveform of an intense IR pulse. Our theoretical analysis also shows that QSDM can be induced on the time scale determining the XUV pulse duration. The direction of QSDM is given by the opposite direction of IR-field strength at the instant corresponding to the time delay between IR and XUV pulses. The short duration of QSDM and it's IR-controllable direction make possible to use the XUV rectification for ultrafast optical gating.

The work is supported by the Russian Science Foundation (Grant No. 22-12-00223).

References

1. M. Pont, R. M. Potvliege, R. Shakeshaft, and Z. Teng, Low-frequency theory of multiphoton ionization. II. general formulation and further results for ionization of H(1s), Phys. Rev. A **4**5, 8235, (1992).

2. O. I. Tolstikhin and T. Morishita, Adiabatic theory of ionization by intense laser pulses: Finite-range potentials, Phys. Rev. A **8**6, 043417, (2012).

3. Y. Okajima, O. I. Tolstikhin, and T. Morishita, Adiabatic theory of high-order harmonic generation: One-dimensional zero-range-potential model, Phys. Rev. A **8**5, 063406, (2012).

4. E. A. Pronin, A. F. Starace, M. V. Frolov, and N. L. Manakov, Perturbation theory analysis of attosecond photoionization, Phys. Rev. A **8**0, 063403, (2009).

5. A. V. Flegel, N. L. Manakov, I. V. Breev, and M. V. Frolov, Adiabatic expressions for the wave function of an electron in a finite-range potential and an intense low-frequency laser pulse, Phys. Rev. A **1**04, 033109, (2021).

6. A. V. Flegel, N. L. Manakov, A. V. Sviridov, M. V. Frolov, L. Geng, and L.-Y. Peng, Analytic description of the above-threshold detachment in the adiabatic limit, Phys. Rev. A **1**02, 063119, (2020).

Diffusion in Bose-Fermi mixtures

M.M. Glazov[1] and Z.A. Iakovlev[1]

[1]Ioffe Institute, 194021, St. Petersburg, Russia

[1]glazov@coherent.ioffe.ru

Abstract

Transport properties of two-dimensional (2D) systems attact significant interest due to evergreen motives of weak and strong localization, electron-electron interaction effects, and non-markovian dynamics. Recent experiments have provided an access to the transport of excitons, neutral quasiparticles formed of a conduction band electron and a valence band hole, in 2D transition metal dichalcogenides [1]. Such systems are known for strong Coulomb correlations and manifest spectacular optical effects [2]. Particularly, in the presence of resident electrons and holes exciton binds with carries forming three-particle complexes, trions. In manybody language, excitons get dressed by the Fermi sea excitations giving rise to the repulsive and attractive Fermi polarons (Suris tetrons) [3].

Here we present the theory of diffusion of excitons immersed in the Fermi sea of free charge carriers. We show that, contrary to naive expectations, the exciton (repulsive polaron) diffusion coefficient strongly decreases with increase in the resident carrier density, while the trion (attractive polaron) diffusion coefficient is only weakly affected by the carriers. We describe experimental data on the exciton transport in 2D WSe_2 and explain non-monotonous dependence of the observed diffusion coefficient, Fig. 1, as function of doping [4].

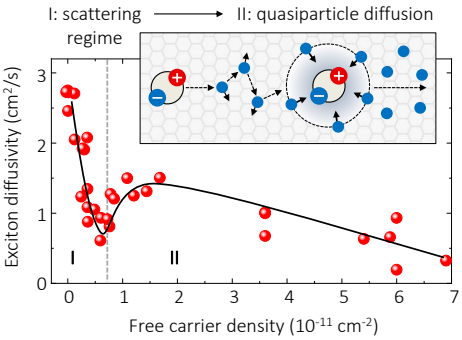

Figure 1: Exciton effective diffusion coefficient measured on WSe_2 monolayer as a function of the free carrier density [4]. Dots show experimental data.

References

1. Marvin Kulig, Jonas Zipfel, Philipp Nagler, Sofia Blanter, Christian Schüller, Tobias Korn, Nicola Paradiso, Mikhail M. Glazov, and Alexey Chernikov, Exciton Diffusion and Halo Effects in Monolayer Semiconductors, Phys. Rev. Lett. **120**, 207401 (2018).

2. Gang Wang, Alexey Chernikov, Mikhail M. Glazov, Tony F. Heinz, Xavier Marie, Thierry Amand, and Bernhard Urbaszek, Colloquium: Excitons in atomically thin transition metal dichalcogenides, Rev. Mod. Phys. **90**, 021001 (2018).

3. R. A. Suris, Correlation between trion and hole in Fermi distribution in process of trion photo-excitation in doped QWs, in *Optical Properties of 2D Systems with Interacting Electrons* ed. by W. Ossau and R. Suris, NATO ASI (2003).

4. Koloman Wagner, Zakhar A. Iakovlev, Jonas D. Ziegler, Marzia Cuccu, Takashi Taniguchi, Kenji Watanabe, Mikhail M. Glazov, and Alexey Chernikov, Diffusion of Excitons in a Two-Dimensional Fermi Sea of Free Charges, Nano Lett. 10.1021/acs.nanolett.2c03796 (2023)

GOODNESS AJAMU

15 Alpiyskiy Street, St. Petersburg, Russia. +79217955136
goodnessajamu6@gmail.com

OBJECTIVE STATEMENT:

Curiosity-driven physicist with research interests spanning areas of quantum mechanics, photonics, and hybrid materials, passionate about developing novel, low-cost, versatile, highly reproducible, and highly integrable materials.

EDUCATION:

ITMO University, St. Petersburg, Russia. August – June 2024.
Master of Science (M.Sc.) Degree in Advanced Quantum and Nanophotonic Systems

- Concentration: Hybrid Materials

University of Ilorin (UIL), Kwara State, Nigeria. (Visit Website) Aug 2021.
Bachelor of Science (B.Sc.) Degree in Physics. (View Certificate)

- CGPA: 4.50/5.00 ~ 90% (First Class Honors)

RESEARCH EXPERIENCE:

University of Ilorin (UIL), Ilorin, Kwara State, Nigeria. Oct 2019 – Aug 2021.
Bachelor's Research Thesis
Thesis: *Solution to Quantum Mechanical problems Employing the Variational Method in the Vicinity of the Kratzer Potential.*

- Investigated and obtained approximate solutions – variational estimates – of heteronuclear and homonuclear diatomic molecules, in the vicinity of the Kratzer potential, within the framework of the variational scheme.
- Compared approximate values obtained within the framework of the variational scheme with those obtained using computational results from Maple software and also illustrative plots from MATLAB, to check for the degree of accuracy of the variational method when the hydrogen-like ansatz is used.

CONFERENCE(S) AND WORKSHOP(S) ATTENDED:

- Second International Perovskite Workshop in Lund: Toward fundamental Understanding of Optoelectronic Properties of Metal Halide Perovskite Semiconductors, organized by the Center for Nanoscience, Lund University. 9th – 11th May 2023.
- 5TH African Light Source E-Conference organized by the African Physical Society. 14th -18th Nov 2022.

TEACHING EXPERIENCE and MENTORSHIP:

University of Ilorin, Kwara State, Nigeria. Aug 2018 – July 2021.
Undergraduate Assistant

- Taught courses such as, Quantum Mechanics, Nuclear and Particle Physics, Electromagnetic Theory, Solid-State Physics, and Computational Physics (MATLAB), to over 50 third year and final year physics undergrads; consequently, over 80% of these students reported an upshift in their academic grades.

Hallmark International School, Niger State, Nigeria.
High School Science Instructor. Aug 2020 – Nov 2020.

- Mentored over 30 High School Seniors of Hallmark International School; consequently, about seven of them obtained over six distinctions in their West African Senior Secondary Certificate Examination (WASSCE).
- Taught the MATLAB software to over 40 high school students. By the end of the term, about 80% of these students became proficient with the use of MATLAB, utilizing the software to solve quadratic and cubic equations; also, to plot illustrative 2-D and 3-D graphs of statistical data.
- Administered quizzes and assessment tests, proctored, and graded these tests to help gauge students' understanding and retention level of course material.
- Facilitated bi-weekly mentorship sessions to help students get acquainted with skills required to communicatetheir thoughts and reports of their findings – be it scientific or in the humanities - clearly.

LEADERSHIP, VOLUNTEER EXPERIENCE, and COMMUNITY DEVELOPMENT:

NYSC Education Community Development Group, Kebbi State, Nigeria. Feb – October 2022.
General Secretary/Acting President

- Spearheaded science inclined sensitization programmes in schools with a combined population of over 500; in addition, talked about the pertinence and role of STEAM courses in nation building and development.

National Youth Service Corps (NYSC), Kebbi State, Nigeria. Nov – Dec 2021.
Platoon Leader

- Successfully led over 140 platoon members to victory in varied platoon competitions; also, gathered over NGN 100,000, in donations, with the help of other executives, to fund various platoon activities.
- Served as a liaison officer between platoon members and the platoon officer, helping to relay camp related issues faced by platoon members: from missing identity cards, theft cases, to misplaced meal tickets.

Planetary Health Alliance (PHA), University of Abuja, Nigeria. July – Aug 2021.
Student Volunteer

- Participated in a 4-week online campaign against open defecation, leveraging social media platforms such as Facebook and WhatsApp, to sensitize over 120 people about the damaging effects of open defecation on communal health.
- Effectively utilized statistical data from various world organizations such as WHO and UNICEF, to back up claims throughout the course of the online campaign; also, gave actionable recommendations, as part of a team, on how best to tackle the menace.

TECHNICAL COMPETENCIES and INTERESTS:

- *Programming Languages and Software Skills*: Comsol Multiphysics, CST Microwave Studio Suite, MATLAB, Python, and CorelDraw.
- *Interests*: Scientific and Creative Writing, Communication, Leadership, Public Speaking, Teaching and Mentoring, Project Management, Traveling and Music.

AWARD(S) and HONOR(S):

- *M.Sc. Scholarship Award (fully funded):* in Advanced Quantum Science and Nanophotonic Systems (Hybrid Materials Track), ITMO University, St. Petersburg, Russia. (Declined). August 2022.
- *E-Passport Funding Award*: Among 60 successful applicants selected from a pool of 1152 applicants, to benefit from the Scholarships Café E-Passport funding initiative, which helped me financially to obtain the Nigerian E- Passport. Jan 2022.
- *Tutor of the Year*: Awarded by the National Association of Physics Students (NAPS), University of Ilorin branch,from a pool of ten physics tutors, for exceptional teaching. Aug 2021.

MOOCs and PROFESSIONAL CERTIFICATIONS:

- Understanding Research Methods (Certified by the University of London) View
- Foundations of Project Management (Certified by Google and MSI) View
- Introduction to Quantum Information (Certified by KAIST) View
- Density Functional Theory (Certified by Ecole Polytechnique) View
- Introduction to Particle Accelerators (NPAP MOOC) (Certified by Lund University) View
- Learning MATLAB (Certified by LinkedIn Learning) View
- Communication and Interpersonal Skills at Work (Certified by the University of Leeds) View
- Improving Communication Skills (Certified by the University of Pennsylvania) View
- Thinking Creatively (Certified by LinkedIn Learning) View
- Lean Six Sigma White Belt (Certified by the Management and Strategy Institute) View
- Digital Literacy Certificate (Certified by Microsoft) View

SCHOLARLY and PROFESSIONAL AFFLIATIONS:

- Member, EducationUSA (EdUSA). 2022 – Present.
- Member, African Physical Society (AfPS). 2021 – Present.

Ginzburg-Landau approximation for the Hubbard model in the external magnetic field

L. B. Dubovskii and S. N. Burmistrov
NRC "Kurchatov Institute", 123182 Moscow, Russia

The Hubbard model is studied in the external magnetic field. The analysis is carried out phenomenologically within the framework of the Ginzburg-Landau theory with the order parameter describing the opposite spin electrons. The study is performed for the nearly half-filled lower Hubbard band in the metallic state. The final equations are the Pauli-like ones for the opposite spins and nonlinear as a result of interaction between electrons with the opposite spins. The equations can analytically be solved for the spatially homogeneous distributions in a number of most interesting cases. In particular, the problem on the metal-insulator transition is analyzed for the nearly half-filled Hubbard sub-bands. The critical magnetic field at which the transition from the metallic state to the insulator one takes place is found under the paramagnetic spin effect.

I. INTRODUCTION

The traditional electronic theory of metals starts from the weakly interacting electrons moving in the periodic crystal field and is described by the standard band theory [1]. According to the band theory of metals, various transition metal oxides should be conductors since they have an odd number of electrons per unit cell. The typical system of this kind is nickel oxide NiO. However, it is found that such compounds behave like insulators in reality. Nevill Mott [2] predicted that the anomaly could be explained by involving the Coulomb interaction between electrons and proposed the model for NiO as an example of an insulator for transition metal oxides. Such anomalous state is called the Mott insulator. The Mott insulator state appears provided that the repulsive Coulomb potential is sufficiently large in order to produce the gap in the electron energy spectrum.

The simplest approach to this problem is to apply the Hubbard model [3]. Describing the metal system, J. Hubbard starts from the usual electron-ion Hamiltonian for a hypothetical partly-filled narrow s-band containing n electrons per atom. In the case of narrow energy bands J. Hubbard has emphasized that one can take into account the atomicity of the electron distribution and employ a very simple approximate representation of the electron-electron interactions. In fact, this approximation is mathematically much simpler to handle than the Coulomb interaction in itself.

On the whole, the analysis leads to the simplified Hamiltonian as

$$\hat{H} = \sum_{i,j,\sigma} T_{ij} c^{+}_{i\sigma} c_{j\sigma} + \frac{1}{2} I \sum_{i,\sigma} n_{i,\sigma} n_{i,-\sigma} - I \sum_{i,\sigma} \nu_{ii} n_{i,\sigma} \tag{1}$$

where $n_{i,\sigma} = c^{+}_{i\sigma} c_{i\sigma}$. Here $c_{\boldsymbol{k}\sigma}$ and $c^{+}_{\boldsymbol{k}\sigma}$ are the annihilation and creation operators of electrons with spin σ in the Bloch state and the transition amplitude reads

$$T_{ij} = N^{-1} \sum_{\boldsymbol{k}} \epsilon_{\boldsymbol{k}} \exp i\boldsymbol{k}(\boldsymbol{R}_i - \boldsymbol{R}_j), \quad \nu_{ii} = N^{-1} \sum_{\boldsymbol{k}} \nu_{\boldsymbol{k}} \,,$$

N being the number of atoms. The sum in (1) runs over all the atomic sites $\boldsymbol{R}_i$. The magnitude I is the Coulomb repulsion of the electrons at the same transition oxide atom. The quantity $\epsilon_{\boldsymbol{k}}$ is the electron band spectrum and magnitude $\nu_{\boldsymbol{k}}$ is the occupation number of the electron states in the band.

It should be emphasized that the interactions in the Hamiltonian $\hat{H}$ are between the opposite-spin electrons alone and these interactions are completely local. The physical reason for the completely on-site interactions in $\hat{H}$ (1) is determined by the fact that the electron interaction is only significant for the electrons belonging to the same transition atom. The electron interaction from various transition atoms is negligible. So, despite the band motion of d-electrons, the electrons at the same atom are strongly correlated with each other and correlated weakly with the electrons from other atoms. Such intra-atomic correlations are responsible for the physical properties as compared with the system of isolated atoms.

The most significant result from this Hamiltonian [3] is that the electron conduction bands, arising in the conventional electron theory of metals at half-filling, prove to be split into two bands. The lower subband is completely

filled with the conduction electrons. The upper subband proves to be completely empty. In the Hubbard electron conduction band there are electrons of the spin-up and spin-down directions with the purely local interaction.

The purpose of our paper is a construction of phenomenological approach for the Hubbard model in the Ginzburg-Landau approximation and application it for most significant problems [4]. The behavior in the magnetic field is significant for the metal-insulator transitions in the first turn. This is interesting both for the paramagnetic case and for the case of the orbital electron motion. The static spin structures and spin wave problems can be analyzed within the framework of this approach as well.

II. HUBBARD MODEL IN THE GINZBURG-LANDAU APPROACH

The description of Hubbard model in the Ginzburg-Landau approximation can be done by introducing of the order parameter with two components $u_{\uparrow}(\vec{r})$ and $u_{\downarrow}(\vec{r})$. This order parameter can be represented by the column $\hat{\Upsilon}(\vec{r})$ with two components (cf. [6]):

$$\hat{\Upsilon}(\vec{r},t) = \begin{pmatrix} u_{\uparrow}(\vec{r},t) \\ u_{\downarrow}(\vec{r},t) \end{pmatrix}.$$

The component $u_{\uparrow}(\boldsymbol{r})$ describes a spin-up electron and component $u_{\downarrow}(\boldsymbol{r})$ does a spin-down one. The Hermitian-conjugated operator represents the row:

$$\hat{\Upsilon}^{+}(\vec{r},t) = \left(u^{*}_{\uparrow}(\vec{r},t) \;\; u^{*}_{\downarrow}(\vec{r},t)\right).$$

$$\hat{(\Upsilon^{+}\hat{\Upsilon})} = u^{*}_{\uparrow}u_{\uparrow} + u^{*}_{\downarrow}u_{\downarrow}\,.$$

$$\hat{\beta} = \begin{pmatrix} 0 & \beta\exp(i\varphi) \\ \beta\exp(-i\varphi) & 0 \end{pmatrix}.$$

$$\hat{(\beta\ \Upsilon)} = \begin{pmatrix} \beta\exp(i\varphi)\,u_{\downarrow} & 0 \\ \beta\exp(-i\varphi)\,u_{\uparrow} & 0 \end{pmatrix}.$$

$$\hat{(\Upsilon^{+}\beta\ \Upsilon)} = \beta\exp(-i\varphi)u^{*}_{\downarrow}u_{\uparrow} + \beta\exp(i\varphi)u^{*}_{\uparrow}u_{\downarrow}$$

$\varphi = 0$

$$\hat{(\Upsilon^{+}\beta\ \Upsilon)} = \beta(u^{*}_{\downarrow}u_{\uparrow} + u^{*}_{\uparrow}u_{\downarrow})$$

The interactions in the Hamiltonian $\hat{H}$ (1) are between the opposite-spin electrons alone. We introduce the same in the Ginzburg-Landau approximation.

In zero magnetic field the components $u_{\uparrow}(\boldsymbol{r})$ and $u_{\downarrow}(\boldsymbol{r})$ are real quantities. However, the components become the complex quantities in the finite magnetic field. The construction of the Ginzburg-Landau functional Φ can be performed as usual (cf. [4–6])

$$\Phi = \Phi[\hat{\Upsilon}(\vec{r}),\hat{\Upsilon}^{+}(\vec{r})] = \int d\vec{r}F(\hat{\Upsilon}(\vec{r}),\hat{\Upsilon}^{+}(\vec{r}))\,,$$
$$F(\hat{\Upsilon}(\vec{r}),\hat{\Upsilon}^{+}(\vec{r})) = \alpha\left(\hat{\Upsilon^{+}\Upsilon}\right)$$
$$-\frac{1}{2}\left(\hat{\Upsilon}^{+}\hat{\beta}\hat{\Upsilon}\right)^{2} + \frac{\hbar^{2}}{2m}\left(\nabla\hat{\Upsilon}^{+}(\vec{r})\nabla\hat{\Upsilon}\right). \qquad (2)$$

The coefficient minus in the second term of the right-hand part of the last equation is connected with repulsion between the electrons on the same atom of the transition metal.

(3) can be represented in components as follows:

$$F(u^*_\uparrow(\boldsymbol{r},t),u^*_\downarrow(\boldsymbol{r},t),u_\uparrow(\boldsymbol{r},t),u_\downarrow(\boldsymbol{r},t)) = \alpha\sum_\sigma\left(u^*_\sigma(\boldsymbol{r},t)u_\sigma(\boldsymbol{r},t)\right)$$
$$-\frac{1}{2}\beta^2\sum_{\sigma,\sigma_1}\left(u^*_\sigma(\boldsymbol{r},t)u_{-\sigma}(\boldsymbol{r},t)\right)\left(u^*_{-\sigma_1}(\boldsymbol{r},t)u_{\sigma_1}(\boldsymbol{r},t)\right)$$
$$+\frac{\hbar^2}{2m}\sum_\sigma\left(\nabla u^*_\sigma(\boldsymbol{r},t)\nabla u_\sigma(\boldsymbol{r},t)\right). \tag{3}$$

The variable α characterizes the electron spectrum with the both spins $\sigma =\uparrow,\downarrow$. The magnitude β^2 determines the Coulomb interaction between electrons with opposite spins $\sigma =\uparrow,\downarrow$.

Varying the functional (3) leads to the following equation:

$$-\imath\hbar\frac{\partial}{\partial t}u_\sigma(\vec{r},t) = -\frac{\hbar^2}{2m}\nabla^2u_\sigma(\vec{r},t)+\alpha u_\sigma(\vec{r},t)$$

$$-\beta^2\left(u^*_{-\sigma}(\vec{r},t)u_\sigma(\vec{r},t)+u^*_\sigma(\vec{r},t)u_{-\sigma}(\vec{r},t)\right)u_{-\sigma}(\vec{r},t),\quad \sigma =\uparrow,\downarrow. \tag{4}$$

Varying the functional (3) leads to the following equation:

$$-i\hbar\frac{\partial}{\partial t}u_\sigma(\boldsymbol{r},t) = -\frac{\hbar^2}{2m}\nabla^2u_\sigma(\boldsymbol{r},t)+\alpha u_\sigma(\boldsymbol{r},t)$$
$$+\beta\left(u^*_{-\sigma}(\boldsymbol{r},t)u_{-\sigma}(\boldsymbol{r},t)\right)u_\sigma(\boldsymbol{r},t),\quad \sigma =\uparrow,\downarrow. \tag{5}$$

Equation (5) allows us to determine the excitation spectrum in the electronic system. As a first step, we consider only the static and homogeneous coordinate-independent electron density ρ_σ in the metal for a fixed spin. In this case the magnitude $\rho_\sigma(\boldsymbol{r},t) = (u^*_\sigma(\boldsymbol{r},t)u_\sigma(\boldsymbol{r},t)) \equiv n_\sigma(0)$ is independent of coordinate $\boldsymbol{r}$ and t. The two equations for different spins (5) represent the linear system for $u_\sigma(\boldsymbol{r},t)$ with $\sigma =\uparrow,\downarrow$

$$-i\hbar\frac{\partial}{\partial t}u_\sigma(\boldsymbol{r},t) = -\frac{\hbar^2}{2m}\nabla^2u_\sigma(\boldsymbol{r},t)+\alpha u_\sigma(\boldsymbol{r},t)$$
$$+\beta\left(u^*_{-\sigma}(\boldsymbol{r},t)u_{-\sigma}(\boldsymbol{r},t)\right)u_\sigma(\boldsymbol{r},t),\quad \sigma =\uparrow,\downarrow. \tag{6}$$

The order parameter $u_\sigma(\boldsymbol{r})$ corresponds fully to the description of the Hubbard model (1) with the interactions between the opposite-spin electrons. In addition, the electron interactions are completely local as in the Hubbard model.

For the case of homogeneous coordinate-independent density of electrons, the system in Eq. (5) reduces to

$$\alpha u_\sigma+\beta n_{-\sigma}(0)u_\sigma = 0,\quad \sigma =\uparrow,\downarrow,$$
$$n_\uparrow(0) = n_\downarrow(0) = -\alpha/\beta. \tag{7}$$

The value $\beta<0$ refers to the Coulomb repulsion. If $\alpha \gg \mid\beta\mid$, the magnitude $n_\sigma(0)$ can arbitrarily be large and is limited by the electron Fermi statistics alone. Correspondingly, no more than two electrons with the opposite spins can be in the conduction band:

$$n_\sigma(0)+n_{-\sigma}(0)\leqslant 2,\quad \sigma =\uparrow,\downarrow.$$

For $\mid\beta\mid\gg\alpha$, we have $n_\sigma(0)\ll 1$. The system (6) can exactly be solved using the Fourier transformation. We can seek for the solution as

$$u_\sigma(\boldsymbol{r},t) = u_{\sigma\varepsilon}(\boldsymbol{k})\exp\left[\frac{i}{\hbar}(\boldsymbol{kr}+\varepsilon t)\right].$$

As a result, we arrive at two connected linear equations with $\sigma =\uparrow,\downarrow$

$$\varepsilon u_{\sigma\varepsilon}(\boldsymbol{k}) = \frac{k^2}{2m}u_{\sigma\varepsilon}(\boldsymbol{k})+\alpha u_{\sigma\varepsilon}(\boldsymbol{k})+\beta n_{-\sigma}(0)u_{\sigma\varepsilon}(\boldsymbol{k}).$$

So, we obtain two different electronic energy branches for various spins. At the same time these energy branches are connected with each other via electron densities

$$\varepsilon_\sigma = \frac{k^2}{2m} + \alpha_\sigma + \beta n_{-\sigma}(0), \quad \sigma = \uparrow, \downarrow .$$

Introducing the magnetic field $\boldsymbol{h}(\boldsymbol{r})$ and vector potential $\boldsymbol{A}(\boldsymbol{r})$ into the system is performed by the conventional way [5, 6] similar to that in superconductor. So, we write the magnetic field-dependent part of the total functional as

$$F_h = \frac{\boldsymbol{h}^2}{8\pi} + \frac{\hbar^2}{2m}\sum_\sigma \left| \left(\nabla - \frac{ie}{\hbar c}\boldsymbol{A} \right) u_\sigma(\boldsymbol{r}) \right|^2 , \tag{8}$$

$$\boldsymbol{h} = \operatorname{curl} \boldsymbol{A}, \quad \operatorname{div} \boldsymbol{h} = 0, \quad \operatorname{curl} \boldsymbol{h} = \frac{4\pi}{c}\boldsymbol{j}(\boldsymbol{r}),$$

$$\boldsymbol{j}(\boldsymbol{r}) = \sum_\sigma \left(\frac{ie\hbar}{2m}\left[\big(\nabla u_\sigma^*(\boldsymbol{r})\big) u_\sigma(\boldsymbol{r}) - u_\sigma^*(\boldsymbol{r}) \nabla u_\sigma(\boldsymbol{r}) \right] \right.$$

$$\left. - \frac{e^2}{mc}\boldsymbol{A} u_\sigma^*(\boldsymbol{r}) u_\sigma(\boldsymbol{r}) + \mu \operatorname{curl}\left[u_\sigma^*(\boldsymbol{r}) \boldsymbol{\sigma} u_\sigma(\boldsymbol{r}) \right] \right),$$

μ being the effective Bohr magneton. In the magnetic field the order parameter $u_\sigma(\boldsymbol{r})$ satisfies the following equation:

$$-\frac{\hbar^2}{2m}\left(\nabla - \frac{ie}{\hbar c}\boldsymbol{A}(\boldsymbol{r}) \right)^2 u_\sigma(\boldsymbol{r}) + \alpha u_\sigma(\boldsymbol{r})$$

$$+ \beta |u_{-\sigma}(\boldsymbol{r}, t)|^2 u_\sigma(\boldsymbol{r}) + \mu\big(\boldsymbol{\sigma}\boldsymbol{h}(\boldsymbol{r})\big) u_\sigma(\boldsymbol{r}) = 0 \tag{9}$$

where $\sigma = \uparrow, \downarrow$. This system of equations (9) is nonlinear. Provided that the quantity $|u_{-\sigma}(\boldsymbol{r}, t)|^2 \equiv$ const and is spatially homogeneous, nonlinear Eq. (9) becomes linear and can exactly be solved. In this case the quantity $|u_{-\sigma}(\boldsymbol{r}, t)|^2 \equiv n_{-\sigma}(0)$ represents the number of electrons in the cell with $\sigma = \downarrow, \uparrow$ and does not depend on the coordinate $\boldsymbol{r}$.

The term with vector potential $\boldsymbol{A}(\boldsymbol{r})$ in Eq. (9) describes the orbital motion of electrons in the metal and the term $\mu\boldsymbol{h}(\boldsymbol{r})$ represents the Pauli paramagnetism.

III. METAL-INSULATOR TRANSITION

One of most significant results of analyzing Hamiltonian $\hat{H}$ (1) is that the conduction bands, arising in the traditional electronic theory of metals at half-filling, turn out to be split into two subbands (Hubbard subbands, see [3, 7–18]). In this case the lower subband proves to be completely filled with the conduction electrons and the upper one proves to be completely empty. The energy gap appears between these two subbands. It is necessary to emphasize that the Coulomb interaction should be sufficiently strong in this scenario. The system becomes an insulator. This is the physical reason for the Mott insulator. The transition metal oxides are the brilliant examples of Mott insulator.

If $\alpha = \mid \beta \mid$, we have according to (7)

$$n_\uparrow(0) = n_\downarrow(0) = -\alpha/\beta = 1. \tag{10}$$

So, the lower Hubbard subband will completely be filled. For the almost filled Hubbard band, this means that the phenomenological constants in the Ginzburg-Landau equations are connected by the following relation:

$$|\beta| = \frac{\alpha}{1-\delta}. \tag{11}$$

The small constant δ shows how much the filling in the lower Hubbard band differs from the full filling. The complete filling corresponds to an insulator. At $\delta = 0$, the metal goes over to the insulator state.

We will consider simplest problem when the Pauli paramagnetism near the half-filling of the electron band transfers the metal state to the insulator one under influence of external magnetic field. The case of small $\delta \ll 1$ will be considered in the following magnetic field:

$$\boldsymbol{h} = \boldsymbol{i}h_x + \boldsymbol{k}h_z(x),$$

$\boldsymbol{i}$ and $\boldsymbol{k}$ being unit vectors in the coordinate directions. Let magnetic field vary in the metal in the x direction. The axis z is normal to the the metal surface. The axis x is parallel to the metal surface. The appropriate magnitude of the vector potential, directed along the y axis, reads

$$\boldsymbol{A} = \boldsymbol{j}\left(\int_{-\infty}^{x} h_z(x')dx' - zh_x\right).$$

Here component h_z is a function of x and the component h_x is independent of x since the Maxwell equation $\mathrm{div}\,\boldsymbol{h} = 0$ should be satisfied.

For simplicity, we assume that, due to scattering in the system, the orbital motion of electrons is suppressed in the metal and we neglect the vector potential $\boldsymbol{A}$. The equations (9) take the form

$$-\frac{\hbar^2}{2m}\nabla^2 u_\sigma(\boldsymbol{r}) + \alpha u_\sigma(\boldsymbol{r}) + \beta n_{-\sigma}(0)u_\sigma(\boldsymbol{r}) + \mu(\boldsymbol{h}(\boldsymbol{r})\boldsymbol{\sigma})u_\sigma(\boldsymbol{r}) = 0, \quad \sigma = \uparrow, \downarrow. \tag{12}$$

Here we have replaced the magnitude $|u_{-\sigma}|^2$ with $n_{-\sigma}(0)$ as we consider the static and homogeneous coordinate-independent density of electrons in the metal.

We use the following notation:

$$(\boldsymbol{\sigma h}) = \begin{pmatrix} h_z & h_x \\ h_x & -h_z \end{pmatrix}.$$

The homogeneous and coordinate-independent solution for $u_\sigma(\boldsymbol{r})$ $(\sigma = \uparrow, \downarrow)$ can be written as the following system of equations:

$$\begin{aligned} &\alpha u_\uparrow + \beta n_\downarrow(0)u_\uparrow + \mu(h_z u_\uparrow + h_x u_\downarrow) = 0, \\ &\alpha u_\downarrow + \beta n_\uparrow(0)u_\downarrow + \mu(h_x u_\uparrow - h_z u_\downarrow) = 0. \end{aligned} \tag{13}$$

Let us put $u_\uparrow \neq 0$ and $u_\downarrow \neq 0$. Then from this equation we arrive at the following one:

$$\alpha + \beta n_\downarrow(0) + \mu h_z + \frac{(\mu h_x)^2}{\alpha + \beta n_\uparrow(0) - \mu h_z} = 0. \tag{14}$$

If the number of electrons with the both spin directions equals each other, i.e. $n_\downarrow(0) = n_\uparrow(0) = n$, we have

$$n = \frac{\alpha}{|\,\beta\,|} \pm \frac{\mu}{|\,\beta\,|}\sqrt{(h_z^2 - h_x^2)}. \tag{15}$$

Here we use that β is negative $(\beta < 0)$ for the Coulomb interaction between two electrons. Then we can write Eq. (15) for $h_x = 0$ in the simplified form

$$n = \frac{\alpha}{|\,\beta\,|} + \frac{\mu}{|\,\beta\,|}h_z. \tag{16}$$

If we put the magnetic field as

$$h_z = \alpha\frac{\delta}{\mu},$$

the magnitude n becomes unity. Then the system goes over from the metallic state to insulator one. The critical magnetic field reads

$$h_{cr} = \frac{\alpha\delta}{|\mu|} \tag{17}$$

and means that the lower Hubbard band becomes completely filled. The same situation realizes as well when certain number of electrons is in the upper Hubbard subband. We can transfer the system to the insulator state by appropriate selection of the direction and magnitude of the magnetic field in (17).

In the case when the electron densities with the different spin projections are not equal to each other, such system becomes ferromagnetic according to [3]. By governing the magnetic field according to Eq. (14), it is possible to control the states of the ferromagnetic system.

IV. CONCLUSION

To conclude, we have considered the Hubbard model [3] in the external magnetic field within the Ginzburg-Landau approximation. The starting point is the introduction of two-component order parameter with components $u_{\uparrow}(\boldsymbol{r})$ and $u_{\downarrow}(\boldsymbol{r})$. The component $u_{\uparrow}(\boldsymbol{r})$ describes an electron with spin-up and the component $u_{\downarrow}(\boldsymbol{r})$ describes an electron with spin-down. The electron interactions are significant only for the electrons at the same transition atom. The electron interactions at various transition atoms are neglected. This implies that the electron interactions are fully local and effective only between electrons with the opposite spins. The external magnetic field mediates an additional interaction between electrons of different spin directions even for the homogeneous system, see (12) and (14). The strong Coulomb repulsion results in the low density of electrons in the conduction band.

The resulting equations (9), which are the Pauli-like ones for the opposite spins and nonlinear due to interaction of electrons with different spins, can analytically be solved in a number of important cases. For example, the problem of metal-insulator transition in the external magnetic field is exactly solved for the case of the nearly half-filled lower Hubbard sub-band. The critical magnetic field $h_{cr} \sim \alpha\delta/|\mu|$ (17) is governed by the parameters of electron spectrum and Coulomb repulsion. Provided that the electron densities with various spin projections are different, the system becomes ferromagnetic. Varying the magnetic field makes it possible to control the ferromagnetic behavior in the system.

[1] A. A. Abrikosov, *Fundamentals of the Theory of Metals* (Groningen, Elsevier, North-Holland, 1980).
[2] N. F. Mott, Proc. Phys. Soc. A **62**, 416 (1949).
[3] J. Hubbard, Proc. Roy. Soc. A **276**, 238 (1963).
[4] L. B. Dubovskii, Physica B **536**, 469 (2018).
[5] E. M. Lifshitz and L. P. Pitaevskii, *Statistical Physics, Part II* (Pergamon Press, Oxford, 1980).
[6] L. B. Dubovskii, JETP Lett. **99**, 22 (2014); J. Low. Temp. Phys. **182**, 192 (2016); J. Phys.: Conf. Ser. **2164**, 021071 (2022).
[7] J. Hubbard, Proc. Roy. Soc. A **277**, 237 (1964).
[8] J. Hubbard, Proc. Roy. Soc. A **281**, 41 (1963).
[9] J. Hubbard, Proc. Roy. Soc. A **285**, 542 (1965).
[10] J. Hubbard, Proc. Roy. Soc. A **296**, 82 (1966).
[11] J. Hubbard, Proc. Roy. Soc. A **296**, 100 (1966).
[12] J. Hubbard, Proc. Roy. Soc. A **296**, 82 (1967).
[13] R. O. Zaitsev, Sov. Phys. JETP **43**, 574 (1976).
[14] M. I. Vladimir and V. A. Moskalenko, Theor. Math. Phys. 82, 301 (1990).
[15] D. P. Arovas, E. Berg, S. A. Kivelson, and S. Raghu, Annu. Rev. Condens. Matter Phys. **13**, 239 (2022).
[16] A. Sherman, J. Low Temp. Phys. **209**, 96 (2022).
[17] Y. Niu, J. Sun, Y. Ni, J. Liu, Y. Song, and S. Feng, Phys. Rev. B **100**, 075158 (2019).
[18] Y. Niu, Y. Ni, J. Wang, L. Chen, Y. Xing, Y. Song, and S. Feng, arXiv: 2112.0466 (2021).

Hubbard model in an external magnetic field in the Ginzburg-Landau approximation.

Dubovskii L.B., Burmistrov S.N.
NRC "Kurchatov Institute 123182 Moscow, Russia (E-mail: ldubovskii@mail.ru)

1. INTRODUCTION

The traditional electronic theory of metals starts from the weakly interacting electrons moving in the periodic crystal field and is described by the standard band theory [1]. According to the band theory of metals, various transition metal oxides should be conductors since they have an odd number of electrons per unit cell. The typical system of this kind is nickel oxide NiO. However, it is found that such compounds behave like insulators in reality. Nevill Mott [2] predicted that the anomaly could be explained by involving the Coulomb interaction between electrons and proposed the model for NiO as an example of an insulator for transition metal oxides. Such anomalous state is called the Mott insulator.

2. HUBBARD MODEL

The simplest approach to this problem is the Hubbard model of 1963 [3]. An essential result of the Hubbard model is that the conduction bands arising in the standard electronic theory of metals, when half-filled, are split into two subzones (Hubbard zones). In this case, the lower subzone turns out to be completely filled with conduction electrons, and the upper one turns out to be completely empty. An energy gap appears between these two subzones.

3. METAL-INSULATOR TRANSITION

We consider a construction of phenomenological approach for the Hubbard model in the Ginzburg-Landau approximation and application it for the most significant problems [4].

The behavior in the magnetic field is significant for the metal-insulator transitions in the first turn. This is interesting both for the paramagnetic case and for the case of the orbital electron motion.

---

[1] A.A. Abrikosov. Fundamentals of the theory of metals, NY Butterworth-Heinemann, 1988.
[2] *N.F. Mott. Proc. Phys. Soc. A 62*, 416-22, 1949.
[3] *J. Hubbard, Proc. Roy. Soc. A 276*, 238, 1963.
[4] *L.B. Dubovskii,JETP Letters* **99**, *No.1*, 22-26, 2014; *J. Low. Temp. Phys. 182*, 192-205, 2016; *Physica B* **536**, 469, 2018; *J. Phys. : Conf. Ser. 2164*, 021071, 2022 - IOPscience.

PARTIAL-SECULAR APPROXIMATION FOR THE DESCRIPTION OF THE DISSIPATION IN STRONGLY COUPLED SYSTEMS

I. V. Vovcenko[1], T. T. Sergeev[2], V. Y. Shishkov[3], A. A. Zyablovskiy[4],

E. S. Andrianov[5]

[1,2,3,4,5] Moscow Institute of Physics and Technology

[2,3,4,5] Institute of Theoretical and Applied Electrodynamics

[1,4] Kotelnikov Institute of Radioengineering and Electronics

[2,3,4,5] Dukhov Automatics Research Institute

[1]vovchenko@phystech.edu

Abstract

The reliability of the description of the dissipation in quantum systems is important in many applications. We studied the effects induced by the usage of the partial-secular approximation, which has no restrictions on the ratio of coupling constants and dissipation rates, such as the manifestation of the exceptional point, suppression of the energy flows by high dissipation rates, environment-assisted strong coupling regime. The existence of a long-living entangled state in the system of two strongly coupled qubits with different dephasing reservoirs is shown.

Key words: Master equation, photonics, strong coupling, partial-secular approximation, exceptional point, entanglement, energy flows

Introduction

A precise description of the dissipation in quantum systems is important in many applications such as quantum computing, photonics, phononics, sensors, etc. Markovian approaches to the description of dissipation are very popular among researchers. The final master equation for the density matrix in Markovian approaches has the form of a differential equation. However, many Markovian approaches have a limited range of applicability, depending on the system parameters.

We studied the partial-secular approximation as one of the most promising approaches having no restrictions on the ratio of coupling constants and dissipation rates. The manifestation of the exceptional point in this approach is shown. The dependences of the energy flow on coupling constant between subsystems and on dissipation rates were studied. It is shown that large derivatives of the state density in a reservoir can cause a transition to the so-called environment-assisted strong coupling regime. The existence of a long-living entangled state in the system of two strongly coupled qubits with separate dephasing reservoirs is shown.

Main text

There are three main Markovian approaches to the description of the dissipation in quantum systems: local, global, and partially-secular. In the local approach, the dissipation of coupled subsystems into different reservoirs is described under the

assumption that the interaction between subsystems does not affect the type of relaxation operators of the subsystems. In the global approach, the system is treated as a single, and the type of relaxation operators significantly depends on the eigenstates of the whole subsystem. The local approach is reliable if the energy dissipation rates are much higher than the coupling between the subsystems. The global approach is reliable if the coupling between subsystems is much greater than the rates of energy dissipation. Another approach has recently been proposed – a partial-secular one. It has no restrictions on the ratio of coupling and dissipation rates.

Non-Hermitian systems with dissipation, in which there is a so-called exceptional point: a point in the parameter space of the system where both the eigenvalues and the eigenvectors of the system coincide, are of interest. It can be shown that a phase transition occurs near an exceptional point of the system [1]. Root-like splitting of the eigenvalues is observed in the vicinity of the exceptional point, which finds application in sensors, photonics, and laser technology due to frequency selective amplification or absorption [2]. From a theoretical point of view, the description of such systems is of great interest, since in the local approach the exceptional point is clearly expressed, and in the global approach the exceptional point is completely absent. At the same time, near the exceptional point, the coupling constants between subsystems and the dissipation rates are comparable, thus both approaches are not applicable. The partial-secular approach is the main candidate for the description of systems with an exceptional point since it is applicable for any ratios of coupling constants and dissipation rates [3, 4].

Transition through the exceptional point is associated with the transition to the strong coupling regime. However, there are several cases in which this definition loses its physical meaning. In this cases the transition to the strong coupling regime can be determined by the maximization of the stationary energy flow through the system [5].

In the example of a system of two coupled oscillators, it will be shown that at small coupling constants, the partially secular approach asymptotically turns into a local approach, and at large coupling constants into a global approach [3]. It will be shown that in the partial secular approximation, the system eigenvalues are split all the time, but there is a manifestation of the exceptional point and there is a critical coupling constant, such that if the coupling constant is larger the system is in the so-called environment-assisted strong coupling regime [6]. An alternative way to determine the transition to the strong coupling regime is proposed in terms of stationary energy flows. The suppression of energy flows at high dissipation rates is shown [5]. The existence of a long-living entangled state in the system of two strongly coupled qubits with separate dephasing reservoirs is shown [7].

References

1. T.T. Sergeev, A.A. Zyablovsky, E.S. Andrianov, A.A. Pukhov, Y.E. Lozovik, A.P. Vinogradov, A new type of non-Hermitian phase transition in open systems far from thermal equilibrium. Scientific reports, **11**(1), 1, (2021).
2. M.-A. Miri, A. Alu, Exceptional points in optics and photonics. Science, **363**, 6422, (2019).
3. I. V. Vovchenko, V. Y. Shishkov, A. A. Zyablovsky, E.S. Andrianov, Model for the description of the relaxation of quantum-mechanical systems with closely spaced energy levels. JETP Letters, **114**, 51, (2021).
4. M. Cattaneo, G.L. Giorgi, S. Maniscalco, R. Zambrini, Local versus global master equation with common and separate baths: superiority of the global approach in partial secular approximation. New Journal of Physics, **21**(11), 113045, (2019).

5. I.V. Vovcenko, A.A. Zyablovsky, A.A. Pukhov, E.S. Andrianov, Energy Transport Induced by Transition from Weak to Strong Coupling Regime Between Non-Hermitian systems. arXiv preprint arXiv:2211.08484, (2022).
6. T.T. Sergeev, I.V. Vovcenko, A.A. Zyablovsky, and E.S. Andrianov, Environment-assisted strong coupling regime, Quantum, **6**, 684, (2022).
7. I.V. Vovcenko, V.Y. Shishkov, E.S. Andrianov, Dephasing-assisted entanglement in a system of strongly coupled qubits. Optics Express, **29**(6), 9685, (2021).

Non-Hermitian phase transitions in open systems

T. T. Sergeev[1], I. V. Doronin[2], E. S. Andrianov[3], A. A. Zyablovsky[4]

[1,2,3,4]Moscow Institute of Physics and Technology

[1,2,3,4]Dukhov Research Institute of Automatics

[4]ziablovskii.aa@mipt.ru, [4]zyablovskiy@mail.ru

Abstract

Open systems demonstrate a non-Hermitian phase transition, when, as the parameters change, they pass through an exceptional point. Near the transition point, the open systems have unique properties that are used to create new types of devices. In this report, we discuss various implementations of the systems with the exceptional points. The non-Hermitian phase transitions in the open systems interacting with reservoirs of finite size are considered. A concept of a laser without inversion based on the system with an exceptional point is proposed.

Keywords: exceptional point, non-Hermitian phase transition, open system, laser without inversion

Introduction

Currently, non-Hermitian systems with exceptional points are of great interest [1, 2]. An exceptional point is a singularity in a space of the system eigenstates [1, 2]. At the exceptional point, two or more eigenstates become linearly dependent and its eigenvalues coincide with each other [1, 2]. The passing through the exceptional point occurring when the system parameters change is often accompanied by the spontaneous symmetry breaking in the eigenstates [2]. This serves as a source of the non-Hermitian phase transition, which manifests in the system spectrum. Near the transition point, non-Hermitian systems demonstrate unique behavior, which is used to create new types of devices such as sensors [3], lasers without inversion [4-6], etc. In recent years, it has been demonstrated that exceptional points (EPs) can take place in the quantum-mechanical [7] and optical systems [1, 2], etc.

In this report, we discuss the various realizations of the systems with the exceptional points [4-6, 8-10] including experimental implementation of a magnonic waveguide structure [11]. We study the interaction of open systems with the reservoirs of various types [12, 13]. In particular, we consider the open system interacting with the reservoirs of finite size [13]. It is shown that the dynamics of this system demonstrates a transition, which takes place at the coupling strength corresponding to the parameters of the exceptional point in the system with infinite reservoirs. We show that such a transition manifests itself in the system dynamics even when the observation time is much greater than the return time and the non-Markovian effects play an important role. An order parameter was found that describes the transition in the systems with both finite and infinite reservoirs [13].

We propose a concept of laser without inversion based on the system with the exceptional point [4-6]. The spectral and coherent properties of a radiation from this laser are calculated. We demonstrate that the laser radiation can become coherent even without population inversion in the active medium [4, 5]. We show that the operation near the exceptional point promotes a decrease in the line width of laser radiation [5].

Main text

We consider the various realizations of the systems with the exceptional points. The coupled waveguides with loss and gain are a widespread type of such systems. Usually, the optical waveguides possessing PT-symmetry [8] are used to create the systems with the exceptional points. The PT-symmetry breaking taking place in these systems is often associated with a non-Hermitian phase transition. We study the same transition in a system of two coupled magnonic waveguides [11], in which an external optical wave is used to control losses. In addition, the influence of the periodic modulation of the waveguides parameters on the wave propagation is studied. We demonstrate that near the exceptional point, the system is instable to periodic modulation of the parameters. We show that such instability also takes place in other systems with exceptional points. In what follows, we use this effect to achieve lasing without inversion [4-6].

We study the system of two coupled cavities interacting with their own reservoirs having different temperatures. We find the coupling strength, for which the spectrum of the energy flow through system splits. We demonstrate that this splitting relates with a new type of non-Hermitian phase transition [12]. In addition, we predict an existence of a non-Hermitian phase transition in the cavity-free laser [10]. We take into account the infinite number of free-space modes interacting with the active atoms. We demonstrate that an increase in the pump rate of the active atoms leads to form a lasing mode, which is a linear combination of free-space modes [10]. Formation of the lasing mode is a necessary condition of the lasing. For this reason, we call the predicted non-Hermitian phase transition a lasing pre-threshold [10].

We consider the open system interacting with the reservoirs of finite size [13]. Due to finite size of the reservoirs, the dynamics of this system demonstrate the collapses and revivals [13]. When the observation time is less than the return time, the system dynamics are similar to the one in the non-Hermitian system. When the observation time is greater than the return time, the presence of the collapses and revivals breaks this similarity. Despite this fact, such a system exhibits a signature of the non-Hermitian phase transition even when the observation time is much greater than the return time. We find an order parameter that describes the non-Hermitian phase transition in the systems with both finite and infinite reservoirs [13].

We propose a concept of laser without inversion based on a system with an exceptional point [4-6]. We consider an optical mode strongly coupled to active atoms. We demonstrate that there is a pump rate of the active atoms, for which the exceptional point takes place in the system. Near the exceptional point, the periodic modulation of the pump rate results in the parametric instability in the system. This instability leads to the light generation even without population inversion in the active atoms. We calculate the spectral and coherent properties of a radiation from the considered system. We show that the radiation can become coherent even without population inversion in the active medium [4, 5]. That is, the system can operate like a laser without inversion. We demonstrate that the operation near the exceptional point promotes a decrease in the line width of laser radiation [5].

References

1. M. A. Miri, A. Alu, Exceptional points in optics and photonics, Science. **363**, 6422, (2019).

2. S. K. Ozdemir, S. Rotter, F. Nori, L. Yang, Parity–time symmetry and exceptional points in photonics, Nature Mater. **18**, 783, (2019).

3. J. Wiersig, Review of exceptional point-based sensors, Photonics Res. **8**, 1457, (2020).

4. I. V. Doronin, A. A. Zyablovsky, E. S. Andrianov, A. A. Pukhov, A. P. Vinogradov, Lasing without inversion due to parametric instability of the laser near the exceptional point, Phys. Rev. A. 100, 021801(R), (2019).

5. I. V. Doronin, A. A. Zyablovsky, E. S. Andrianov, Strong-coupling-assisted formation of coherent radiation below the lasing threshold, Opt. Express. **29**, 5624, (2021).

6. A. Mukhamedyanov, A. A. Zyablovsky, E. S. Andrianov, Subthreshold phonon generation in an optomechanical system with an exceptional point, Opt. Letters. **48**, 1822, (2023).

7. N. Moiseyev. Non-Hermitian quantum mechanics, Cambridge University Press (2011).

8. A. A. Zyablovsky, A. P. Vinogradov, A. A. Pukhov, A. V. Dorofeenko, A. A. Lisyansky, PT-symmetry in optics, Phys. Usp. **57**, 1063, (2014).

9. A. A. Zyablovsky, E. S. Andrianov, A. A. Pukhov, Parametric instability of optical non-Hermitian systems near the exceptional point, Sci. Rep. **6**, 29709, (2016).

10. A. A. Zyablovsky, I. V. Doronin, E. S. Andrianov, A. A. Pukhov, Yu. E. Lozovik, A. P. Vinogradov, A.A. Lisyansky. Exceptional points as lasing prethresholds, Laser Photonics Rev. **15**, 2000450, (2021).

11. A. V. Sadovnikov, A. A. Zyablovsky, A. V. Dorofeenko, S. A. Nikitov, Exceptional-point phase transition in coupled magnonic waveguides, Phys. Rev. Appl. **18**, 024073, (2022).

12. T. T. Sergeev, A. A. Zyablovsky, E. S. Andrianov, A. A. Pukhov, Yu. E. Lozovik, A new type of non-Hermitian phase transition in open systems far from thermal equilibrium, Sci. Rep. **11**, 24054, (2021).

13. T. T. Sergeev, A. A. Zyablovsky, E. S. Andrianov, Yu. E. Lozovik, Signature of exceptional point phase transition in Hermitian systems, Quantum. **7**, 982, (2023).

Coexistence of superconductivity and magnetism at the nanoscale

Alexander Buzdin

University of Bordeaux, LOMA, 33405, Bordeaux, France

alexandre.bouzdine@u-bordeaux.fr

Abstract

The main mechanisms of the interplay between magnetism and superconductivity and the coexistence between these two different long ranged orders in the bulk magnetic superconductors will be reviewed. The antagonism of ferromagnetism with a singlet superconductivity leads to spectacular effects such as a re-entrant superconductivity and the nanoscopic domain magnetic structure formation. In the case of the weak exchange interaction (or triplet superconductivity), the competition between a self-induced vortex phase and a short-period domain structure may occur.

The very special character of the proximity effect in superconductor-ferromagnet heterostructures is revealed in the damped oscillatory behaviour of the Cooper pair wave function and the formation of the special π-Josephson junctions is possible. Such "π - junction" incorporated in a superconducting circuit may generate a spontaneous current. The quantum oscillations and the "π"-states should also be present in multiply connected ferromagnet–superconductor hybrids, for example in a thin-walled superconducting shell surrounding a ferromagnetic cylinder.

The proximity effect in S/F structures is usually short-ranged though it can become long ranged when the magnetic structure is non-collinear. It has been demonstrated that the Josephson junctions with a composite ferromagnetic interlayer indeed reveal the triplet long-ranged superconducting current. The triplet superconducting correlations provide the possibility to generate the magnetization in the Josephson junction. Such induced magnetization occurs at a relatively large distance, and is sensitive to the superconducting phase difference. By tuning the Josephson current, one may manipulate the long-range induced magnetic moment. This magnetic moment controlled by the Josephson current may therefore be used in spintronics devices instead of the spin-torque effect.

Coupling between the superconducting current and magnetization opens the very interesting perspectives for emerging superconducting spintronics.

New effects in open quantum optical systems with strong coupling

T.T. Sergeev[1,2,3], I.V. Vovcenko[1,2,4], I.V. Doronin[1,2,5], V. Yu. Shishkov[1,2,3],
A.A. Zyablovsky[1,2,3,4], E.S. Andrianov[1,2,3,6,*]

[1]Dukhov Research Institute of Automatics (VNIIA), Moscow, Russia

[2]Moscow Institute of Physics and Technology, Moscow, Russia

[3]Institute for Theoretical and Applied Electromagnetics, Moscow, Russia

[4]Kotelnikov Institute of Radioengineering and Electronics RAS, Moscow, Russia

[5]Institute of Spectroscopy Russian Academy of Sciences, Moscow, Russia

[6]Laboratories for Hybrid Photonics, Skolkovo Institute of Science and Technology, Moscow, Russia

[*]andrianov.es@mipt.ru

Abstract

In this talk, it will be given the review of physical properties and new effects in open quantum optical systems with strong coupling between subsystems.

Key words: Open quantum systems, strong coupling,

Introduction

Recently, open quantum-optical systems, consisting of coupled subsystems and interacting with external reservoirs, have attracted considerable interest [1]. An increase in the coupling constant between subsystems results in a transition from the weak coupling regime to the strong coupling regime through an exceptional point [2]. In the strong-coupling regime, there is the formation of hybrid eigenstates of interacting subsystems and a change in the physical properties of such systems that are promising for various applications [2]. In this talk, it will be given the review of physical properties and new effects in open quantum optical systems with strong coupling between subsystems.

Main text

In the framework of the Born-Markov approximation, there are two main approaches to describe the relaxation processes in open quantum systems. The first one is the local approach in which the relaxations processes are supposed to be as for noninteracting subsystems. Though such approach is widely used, it may lead to violation of second order of thermodynamics. The second approach is the global approach for which it is necessary to find eigenstates of interacting subsystems. This approach is derived from Bloch-Redfield master equation for the system density matrix using full-secular approximation. This approximation is to average the terms in the Bloch-Redfield equation that oscillate at any non-zero frequencies. For the system near an exceptional point, we develop the partial-secular approximation for the Bloch-Redfield equation. This approximation is to average only the terms that oscillate at fast optical frequencies and to conserve time-dependent terms that oscillate at the Rabi frequency. We show that the

master equation obtained with the aid of partial-secular approximation asymptotically tends to the master equation in local approach at small Rabi interaction frequency and tends to the master equation in global approach at large Rabi interaction frequency [3].

Usually, it is assumed that increasing of interaction between system and reservoirs increases dissipations rates and, thus, weakens the effective coupling between subsystems and results in transition from strong to weak coupling regime. We show that the increase in interaction with reservoirs results not only to increasing of dissipation rates but also in non-Hermitian coupling between subsystems which is proportional to the Hermitian coupling constant between subsystems and frequency dispersion of the reservoir density of states. When subsystems interact with the reservoir with sharp frequency dispersion, there is a critical value of Hermitian coupling constant between subsystems above which the system stays in the strong coupling regime at any relaxation rates. We call this regime as environment-assisted strong coupling regime [4].

We show that in the system of strongly coupled qubits dephasing can results in formation of long-lived mixed entangled state. This state is close to subradiant state known from Dicke model. We demonstrate that the time of existence of entanglement is much larger than the time of dephasing and dissipation. We show that long-lived entanglement is robust to detuning between eigenfrequencies of the qubits [5].

It is known that strong coupling between plasmonic nanoparticle and j-aggregated molecules, the rate of photooxidation of j-aggregates can be suppressed by order of magnitude [6]. We show, both theoretically and experimentally, that when molecules of Cy7.5 are strongly coupled with plasmonic gold nanorod, there is optimal concentration of Cy 7.5 molecules, at which the rate of photooxidation is minimal. We demonstrate that the existence of optimal concentration is the results of competition of two effects: increasing of effective Rabi constant of interaction and concentration quenching [7].

The strong coupling between electromagnetic field of resonator and polarization of organic molecules results in formation of polaritons. Recently, vibron-mediated Bose-Einstein condensation of polaritons has been demonstrated. We show, both theoretically and experimentally, that formation of Bose-Einstein condensation results in nonlinearity at the single-photon level [8]. We develop full quantum mechanical theory that explains this phenomenon and describse coherent properties of polariton Bose-Einstein condensate [9].

The study was financially supported by a grant from Russian Science Foundation (project № 20-72-10057).

References

1. R. Chikkarady, et al., Single-molecule strong coupling at room temperature in plasmonic nanocavities, Nature. **535**, 127, (2016).

2. M. A. Miri, A. Alu, Exceptional points in optics and photonics, Science. **363**, eaar7709, (2019).

3. I. V. Vovcenko, V. Yu. Shishkov, A. A Zyablovsky, E. S. Andrianov, Model for the Description of the Relaxation of Quantum-Mechanical Systems with Closely Spaced Energy Levels, JETP Letters. **114**, 51, (2021).

4. T. T. Sergeev, I. V. Vovcenko, A. A. Zyablovsky, E. S. Andrianov, Environment-assisted strong coupling regime, Quantum. **6**, 684, (2022).

5. I. V. Vovcenko, V. Yu. Shishkov, E. S. Andrianov, Dephasing-assisted entanglement in a system of strongly coupled qubits, Opt. Exp. **29**, 9658, (2021).

6. B. Munkhbat, et. al., Suppression of photo-oxidation of organic chromophores by strong

coupling to plasmonic nanoantennas, Sci. Adv. **4**, eaas9552, (2018)

7. I. V. Doronin, et. al., Resonant Concentration-Driven Control of Dye Molecule Photodegradation via Strong Optical Coupling to Plasmonic Nanoparticles, Nano Lett. **22**, 105, (2022).

8. A. V. Zasedatelev, et al., Single-photon nonlinearity at room temperature, Nature. **597**, 493, (2021).

9. V. Yu. Shishkov, et al., Exact Analytical Solution for the Density Matrix of a Nonequilibrium Polariton Bose-Einstein Condensate, Phys. Rev Lett. **128**, 065301, (2022).

Coexistence of superconductivity and magnetism at the nanoscale

Alexander Buzdin

University of Bordeaux, LOMA, 33405, Bordeaux, France

alexandre.bouzdine@u-bordeaux.fr

Abstract

The main mechanisms of the interplay between magnetism and superconductivity and the coexistence between these two different long ranged orders in the bulk magnetic superconductors will be reviewed. The antagonism of ferromagnetism with a singlet superconductivity leads to spectacular effects such as a re-entrant superconductivity and the nanoscopic domain magnetic structure formation. In the case of the weak exchange interaction (or triplet superconductivity), the competition between a self-induced vortex phase and a short-period domain structure may occur.

The very special character of the proximity effect in superconductor-ferromagnet heterostructures is revealed in the damped oscillatory behaviour of the Cooper pair wave function and the formation of the special π-Josephson junctions is possible. Such "π - junction" incorporated in a superconducting circuit may generate a spontaneous current. The quantum oscillations and the "π"-states should also be present in multiply connected ferromagnet–superconductor hybrids, for example in a thin-walled superconducting shell surrounding a ferromagnetic cylinder.

The proximity effect in S/F structures is usually short-ranged though it can become long ranged when the magnetic structure is non-collinear. It has been demonstrated that the Josephson junctions with a composite ferromagnetic interlayer indeed reveal the triplet long-ranged superconducting current. The triplet superconducting correlations provide the possibility to generate the magnetization in the Josephson junction. Such induced magnetization occurs at a relatively large distance, and is sensitive to the superconducting phase difference. By tuning the Josephson current, one may manipulate the long-range induced magnetic moment. This magnetic moment controlled by the Josephson current may therefore be used in spintronics devices instead of the spin-torque effect.

Coupling between the superconducting current and magnetization opens the very interesting perspectives for emerging superconducting spintronics.

Exceptional point phase transition in Hermitian systems

T. T. Sergeev[1,2,3,5], A. A. Zyablovsky[1,2,3,4], E. S. Andrianov[1,2,3], Yu. E. Lozovik[2,5,6]

[1]Moscow Institute of Physics and Technology, 141700, 9 Institutskiy pereulok, Moscow, Russia
[2]Dukhov Research Institute of Automatics (VNIIA), 127055, 22 Sushchevskaya, Moscow, Russia
[3]Institute for Theoretical and Applied Electromagnetics, 125412, 13 Izhorskaya, Moscow, Russia
[4]Kotelnikov Institute of Radioengineering and Electronics RAS, 125009, 11-7 Mokhovaya, Moscow, Russia
[5]Institute of Spectroscopy Russian Academy of Sciences, 108840, 5 Fizicheskaya, Troitsk, Moscow, Russia
[6]MIEM at National Research University Higher School of Economics, 123458, 34 Tallinskay, Moscow, Russia

Abstract

Non-Hermitian systems are actively studied recently [1]. These systems are characterized by the presence of an exceptional point (EP) in them. At the EP, the degeneracy of the eigensubspaces occurs, that is, the eigenvalues coincide, and the eigenvectors are collinear [1]. The transition through the EP is associated with a phase transition, which is also called the non-Hermitian phase transition or exceptional point phase transition [1]. The EP phase transition can be observed in many physical systems: atom-cavity systems [1, 2], optomechanical systems [3], etc. The main problem with the use of exceptional points is the presence of dissipation or amplification in the system.

In this paper, we show that the signature of exceptional point phase transition [4] exists in Hermitian systems, in which there is no dissipation or amplification. The paper considers a Hermitian system, which is presented in the form of two harmonic oscillators, each of which interacts with its own finite reservoir. Reservoirs, in turn, are also represented as a set of a finite number of harmonic oscillators. The Hamiltonian of considered system has the following form:

$$\begin{aligned}\hat{H} &= \omega_0 \hat{a}_1^\dagger \hat{a}_1 + \omega_0 \hat{a}_2^\dagger \hat{a}_2 + \Omega(\hat{a}_1^\dagger \hat{a}_2 + \hat{a}_2^\dagger \hat{a}_1) + \sum_{k=1}^{N_1} \omega_k^{(1)} \hat{b}_k^\dagger \hat{b}_k \\ &+ \sum_{k=1}^{N_2} \omega_k^{(2)} \hat{c}_k^\dagger \hat{c}_k + \sum_{k=1}^{N_1} g_1(\hat{b}_k^\dagger \hat{a}_1 + \hat{a}_1^\dagger \hat{b}_k) + \sum_{k=1}^{N_2} g_2(\hat{c}_k^\dagger \hat{a}_2 + \hat{a}_2^\dagger \hat{c}_k)\end{aligned} \quad (1)$$

In the present work [4] we show the qualitative change in the dynamics of the system occurring at the coupling strength between oscillators corresponding to the EP in the non-Hermitian system. Moreover, we also demonstrate that phase transition manifests itself even in the non-Markovian regime of dynamics, where collapses and revivals take place. Additionally, we introduce an order parameter that describes the exceptional point phase transition in a non-Hermitian system, and also show that this order parameter describes the signature of exceptional point phase transition in Hermitian system (see Figure 1).

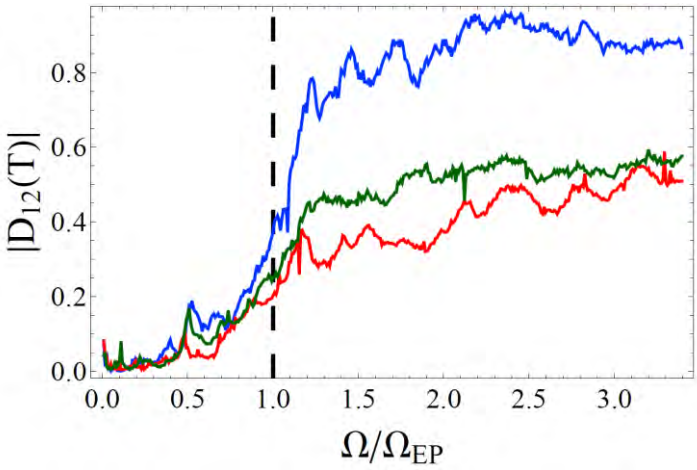

Figure 1. Dependence of the order parameter $D_{12}(T)$ on coupling strength in the Hermitian system. The numbers of the modes in the reservoirs are $N_1 = N_2 = 40$ (the blue line); $N_1 = N_2 = 30$ (the green line); $N_1 = N_2 = 20$ (the red line). The vertical dashed line corresponds to the exceptional point. Figure reprinted from [4]: *Quantum* **7**, 982 (2023).

We believe that presented results can help to overcome the limitations from dissipation or amplification in the system. The results open the way for constructing new devices for laser and sensoric applications.

References

[1] Miri, M. A., and Alu, A. (2019). Exceptional points in optics and photonics. *Science*, **363**(6422), eaar7709.

[2] Khurgin, J. B. (2020). Exceptional points in polaritonic cavities and subthreshold Fabry-Perot lasers. *Optica*, **7**(8), 1015-1023.

[3] Xu, H., Mason, D., Jiang, L., and Harris, J. G. E. (2016). Topological energy transfer in an optomechanical system with exceptional points. *Nature*, **537**(7618), 80-83.

[4] Sergeev, T. T., Zyablovsky, A. A., Andrianov, E. S., and Lozovik, Y. E. (2023). Signature of exceptional point phase transition in Hermitian systems. *Quantum*, **7**, 982.

Generalizations of adiabatic theorems for the harmonic oscillator and a charged particle in a magnetic field

Viktor V. Dodonov and Alexandre V. Dodonov

Institute of Physics,, University of Brasilia, 70910-900 Brasilia, Federal District, Brazil
International Center for Physics, University of Brasilia, Brasilia, DF, Brazil

Correspondence: vicdod@gmail.com

Abstract

We study the evolution of energy, magnetization and initial Fock states of the harmonic oscillator and a charge in a homogeneous time-dependent magnetic field, when the frequencies slowly vary with time and pass through zero value. In this case, the original Born-Fock adiabatic theorem is obviously broken. However, its generalization is found: the initial Fock state becomes a wide superposition of many Fock states, whose weights do not depend on time in the new adiabatic regime. We show that after a single frequency passage through zero value, the famous adiabatic invariant ratio of energy to frequency (which does not hold for zero frequency) is reestablished again, but with the new proportionality coefficient, which is bigger than unity. The concrete value of the mean proportionality coefficient depends on the power index of the frequency dependence on time near zero point. In particular, the mean energy triplicates if the frequency tends to zero linearly. If the frequency attains zero more than once, the adiabatic proportionality coefficient strongly depends on the lengths of the time intervals between zero points, so that the mean energy behavior turns out quasi-stochastic after many frequency passages through zero value. Generalizations to the case of non-Hermitian PT-symmetric Hamiltonians with real energy spectra are considered. The role of the statistical correlations between the coordinate and momentum is emphasized.

References

[1] Viktor V. Dodonov and Alexandre V. Dodonov, Adiabatic amplification of the harmonic oscillator energy when the frequency passes through zero, Entropy 25, 2 (2023) https://doi.org/10.3390/e25010002

[2] Viktor V. Dodonov and Alexandre V. Dodonov, Adiabatic amplification of energy and magnetic moment of a charged particle after the magnetic field inversion, Entropy 25 (4), art. 596 (2023) https://doi.org/10.3390/e25040596

Oblique solitons in Bose-Einstein condensates

A. M. Kamchatnov

Institute of Spectroscopy, Russian Academy of Sciences

kamch@isan.troitsk.ru

Abstract

We shall consider the story of prediction and observation of oblique solitons in Bose-Einstein condensates. The notion of oblique solitons appeared in the context of study of superfluidity of quantum gases. Stability of oblique solitons observed in numerical experiments apparently contradicted to the 'common wisdom' which was then generally accepted that such solitons must be unstable with respect to bending or 'snake' perturbations. We will explain the solution of this conundrum and discuss experimental observations of oblique solitons in polariton condensates.

Key words: Bose-Einstein condensate, nonlinear dynamics

As is well known, if a gas of Bose atoms is cooled down very low temperature, it experiences the phase transition to the Bose-Einstein condensate state. In such a state, slow enough flow of the gas past an obstacle is superfluid what means that no any excitations are excited by the flow. However, if the flow velocity u exceeds the velocity c_s of long sound waves which can propagate through the condensate, then this flow past an obstacle is accompanied by the Cherenkov-like radiation of sound waves. This means loss of superfluidity according to the Landau criterium. In fact, the superfluidity is lost even at smaller velocity because of generation of vortex pairs in vicinity of the obstacle's boundary.

Quite unexpectedly, it was found [1] that this simple physical picture changes at high enough supersonic velocities: dark solitons were observed in numerical experiments instead of 'streets' of vortices if

$$u > 1.46c_s.$$

These oblique solitons have a form of dips in the condensate's density distributions and slopes of such dips with respect to the flow direction depend on their depth; see Fig. 1. Formal solutions of the two-dimensional Gross-Pitaevskii equation which describes the condensate's dynamics can be easily obtained in the form of oblique solitons, however it is well known that such solitons correspond to unstable excitations decaying to vortex pairs because of bending or 'snake' instability.

The way out of this dilemma was found in Refs. [2, 3] and the solution is the following. If there is a flow of condensate along an oblique soliton, then this flow convects the unstable growing modes so that they can be 'washed' away when the flow velocity is large enough. As a result, the length of an oblique soliton increases with time after switching on the flow past an obstacle, as is shown in Fig. 1. It means that

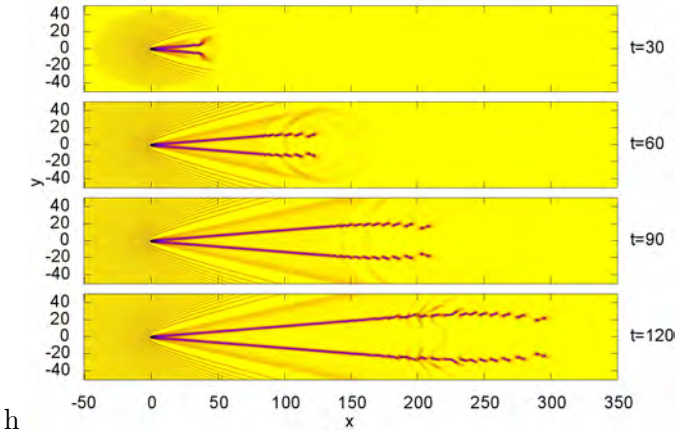

h

Figure 1: Growth of oblique solitons with time after switching on the flow of condensate past an obstacle.

the bending instability is convective, that is it can be removed by the flow, and an oblique soliton becomes stable in the reference frame attached to the obstacle.

After this theoretical prediction oblique solitons were observed in experiments with polariton condensates [4, 5] in qualitative agreement with theoretical predictions. These theoretical and experimental results provide a simple example of the modern 'fluid of light' dynamics.

References

1. G. A. El, A. Gammal, A. M. Kamchatnov, Oblique dark solitons in supersonic flow of a Bose-Einstein condensate, Phys. Rev. Lett., **97,** 180405 (2006).

2. A. M. Kamchatnov, L. P. Pitaevskii, Stabilization of solitons generated by a supersonic flow of Bose-Einstein condensate past an obstacle, Phys. Rev. Lett., **100,** 160402 (2008).

3. A. M. Kamchatnov, S. V. Korneev, Dynamics of ring dark solitons in Bose-Einstein condensates and nonlinear optics, Phys. Lett. A, **374,** 4625-4628-2580 (2010).

4. A. Amo, S. Pigeon, D. Sunvitto, V. G. Sala, R. Hivet, I. Carusotto, F. Pisanello, G. Leménager, R. Houdré, E. Giacobino, C. Ciuti, and A. Bramati, Polariton superfluids reveal quantum hydrodynamic solitons, Science, **332,** 1167 (2011).

5. G. Grosso, G. Nardin, F. Morier-Genoud, Y. Léger, and B. Deveaud-Plédran, Soliton Instabilities and Vortex Street Formation in a Polariton Quantum Fluid, Phys. Rev. Lett. **107,** 245301 (2011).

High-order harmonic generation by H_2^+ molecular ion in time-delayed bichromatic few-cycle counter-rotating laser fields

N. V. Knyazev[1] and D. A. Telnov[2]

[1]NRC "Kurchatov Institute", Petersburg Nuclear Physics Institute, Gatchina 188300, Russia

[2]Department of Physics, St. Petersburg State University, St. Petersburg 199034, Russia

[1]knyazev_nv@pnpi.nrcki.ru, [2]d.telnov@spbu.ru

Abstract

In this work, we investigate high-order harmonic generation by bichromatic $(\omega_0, 2\omega_0)$ few-cycle counter-rotating circularly polarized laser pulses with wavelengths 800 nm and 400 nm and intensities 1×10^{14} W/cm^2 and 2×10^{14} W/cm^2 for the laser pulse component with frequency ω_0 and intensities 5×10^{13} W/cm^2 and 1×10^{14} W/cm^2 for the component with frequency $2\omega_0$.

Key words: Theoretical physics, nonlinear optics, harmonic generation, circular polarization

Introduction

High-order harmonic generation (HHG) is an attractive table-top source of coherent, bright, and tunable extreme ultraviolet (XUV) and soft X-ray radiation with applications in coherent diffractive imaging, ultrafast holography, and time-resolved measurements [1]. Moreover, circularly polarized HHG may find additional applications in nanolithography, ultrafast spin dynamics, and magnetic circular dichroism [1, 2].

Main text

In this work, we study HHG by the H_2^+ molecule in the $1\sigma_g$ ground electronic state in bichromatic counter-rotating circularly polarized sine-squared pulses with the carrier wavelengths 800 nm and 400 nm. Both components are circularly polarized in $x - y$ plane and have the same duration (10 optical cycles of wavelength 400 nm). The molecular axis is oriented along the z axis, which is perpendicular to the polarization plane of the laser field.

To solve the time-dependent Schrödinger equation, we use the generalized pseudospectral method in prolate spheroidal coordinates [3]. We also employ the split-opeartor method in energy representation [4] for propagation of the electron wave function in time.

The spectral density of the radiated energy $S(\omega)$ can be obtained by the Fourier transformation of the time-dependent dipole acceleration, which is calculated by employing the semiclassical approach, where the basis expressions come from classical electr
quant

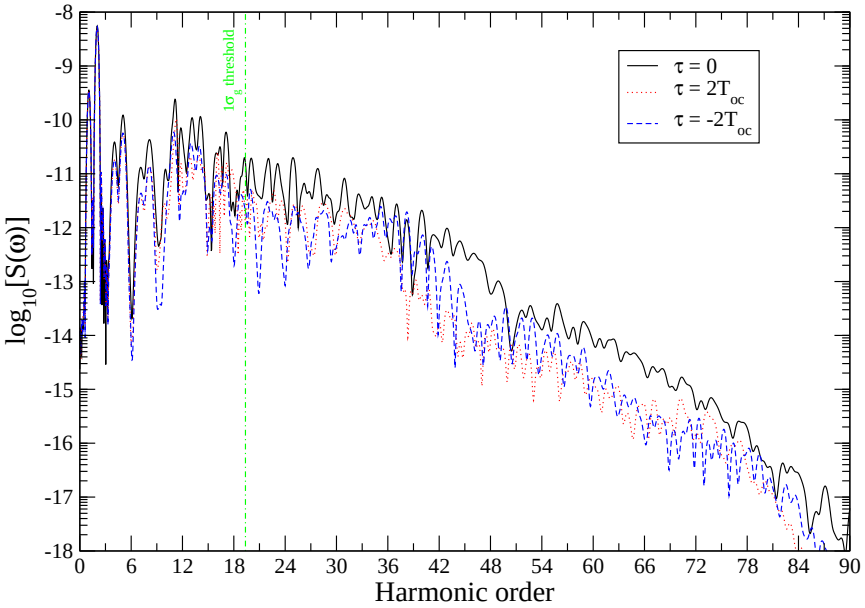

Figure 1: HHG spectrum $S(\omega)$ of the H_2^+ molecule subject to the counter-rotating few-cycle circularly polarized sine-squared laser pulses. The pulse duration is 10 optical cycles of frequency $2\omega_0$ and peak intensities are 1×10^{14} W/cm^2 for the ω_0 component and 1×10^{14} W/cm^2 for the $2\omega_0$ component. Solid (black) line: $\tau = 0$ (zero time delay), dotted (red) line: $\tau = 2T_{oc}$ (positive time delay corresponds to the ω_0 field arriving first), dashed (blue) line: $\tau = -2T_{oc}$ (negative time delay corresponds to the $2\omega_0$ field arriving first), where $T_{oc} = \pi/\omega_0$. The green vertical dashed line indicates the corresponding ionization threshold (I_p) marked by the $1\sigma_g$ threshold.

We calculate the HHG spectra depending on the intensity ratio of the components and the time delay between them. As a result, a distinct doublet structure of peaks with opposite circular polarization for low-order harmonics was revealed, explained by selection rules. It was found that the strongest signal in all parts of the spectrum is observed when the components completely overlap when there is no time delay between

them. The values of the total radiated energy in the below-threshold, plateau, and cutoff regions were also obtained. With a negative delay (the 400 nm component starts earlier than the 800 nm component), the signal level is lower than with a positive delay, with the same absolute value both in the low-frequency part of the spectrum and in the plateau region. The opposite picture is observed in the cutoff region, where the signal level with a negative delay is higher than with a positive delay with the same absolute value.

Table 1: Radiated energy of harmonics in different frequency intervals for pulses with duration 10 optical cycles of wavelength 400 nm and intensities 1×10^{14} W/cm^2 for ω_0 and 1×10^{14} W/cm^2 for $2\omega_0$

Time delay between pulses in π/ω_0 units	Energy of the below-threshold region (3H–20H) (a.u.)	Energy of the plateau region (21H–55H) (a.u.)	Energy of the cutoff region (56H–90H) (a.u.)
0	4.71×10^{-10}	8.87×10^{-11}	1.82×10^{-13}
1	3.44×10^{-10}	6.87×10^{-11}	0.51×10^{-13}
-1	3.66×10^{-10}	6.73×10^{-11}	1.24×10^{-13}
2	1.72×10^{-10}	2.38×10^{-11}	2.46×10^{-14}
-2	1.56×10^{-10}	2.17×10^{-11}	3.02×10^{-14}
3	4.44×10^{-11}	4.21×10^{-12}	5.93×10^{-15}
-3	4.11×10^{-11}	3.25×10^{-12}	1.14×10^{-14}

References

1. C. Hernández-García, C. G. Durfee, D. D. Hickstein,T. Popmintchev, A. Meier, M. M. Murnane, H. C. Kapteyn, I. Sola, A. Jaron-Becker, and A. Becker,, Physycal Review A **93**, 043855, (2016).

2. A. Fleischer, O. Kfir, T. Diskin, P. Sidorenko, and O. Cohen, Nat. photonics **8**, 543, (2014).

3. D. A. Telnov, S. I. Chu, Physical Review A **80**, 043412, (2009).

4. X. M. Tong, S. I. Chu, Chem. Phys. **217**, 119, (1997).

Two-photon $2s \to 1s$ decay in one-electron and one-muon ions

V. A. Knyazeva[1,2], K. N. Lyashchenko[3,1], O. Yu. Andreev[1,3]

[1]Department of Physics, St. Petersburg State University, St. Petersburg 199034, Russia

[2]D. I. Mendeleev Institute for Metrology, St.Petersburg 190005, Russia

[3]Petersburg Nuclear Physics Institute named by B.P. Konstantinov of National Research Centre Kurchatov Institute, Gatchina, Leningrad District 188300, Russia

[1]viknyazeva16@gmail.com

Abstract

The radiative decay of the $2s$ state of one-electron and one-muon ions is investigated. Based on the accurate relativistic calculation, we introduce a two-parameter approximation, which makes it possible to describe the two-photon angular-differential transition probability for the polarized emitted photons with high accuracy. The emission of photons with linear and circular polarizations is studied separately. We also investigate the transition probabilities for the polarized initial and final states. The investigation is performed for ions with atomic numbers $1 \leq Z \leq 120$.

Key words: Theoretical physics

Introduction

Two-photon transitions represent a fundamental process in atomic physics. Two-photon decay is best studied for one- electron ions, which is the dominant decay channel of the 2s-electron state for low- and medium-Z H-like ions, where Z is the atomic number. The probabilities of one- and two- photon transitions become comparable for $Z \approx 40$. Unlike one-photon decay, the emission spectrum of two- photon decay has a continuous distribution determined by the energy conservation law. The study of differential transition probabilities is of particular interest.

The record accuracy of measurement of the transition frequency in hydrogen was obtained in the reverse process, two-photon excitation $1s \to 2s$ [1]. For one-muon ions, two-photon decay is the main radiative channel for all ions. An experimental investigation of the 2s $\to$ 1s transition in muon ions was performed in [2, 3]. Since significant progress was recently made in the quality of muon beams [4], the study of muon ions has become relevant.

Main text

For both electron and muon ions the most long-lived state of the L shell is the $2s$ state. We investigated the radiative decay of the $2s$ state of one-electron and one-muon ions with respect to the polarization of the emitted photons. The investigation was performed for the ions with nuclear charge numbers $1 \leq Z \leq 120$. Particular attention was paid to the role of the two-photon decay channel.

The radiative decay of the 2s state in the electron and muon ions is qualitatively different. In particular, in contrast to electron ions, in the case of muon ions the cascade ($2s \to 2p_{3/2} \to 1s$ and $2s \to 2p_{1/2} \to 1s$) channels are of great importance. For the muon ions, taking into account the nuclear size corrections may change the transition probability by several orders of magnitude.

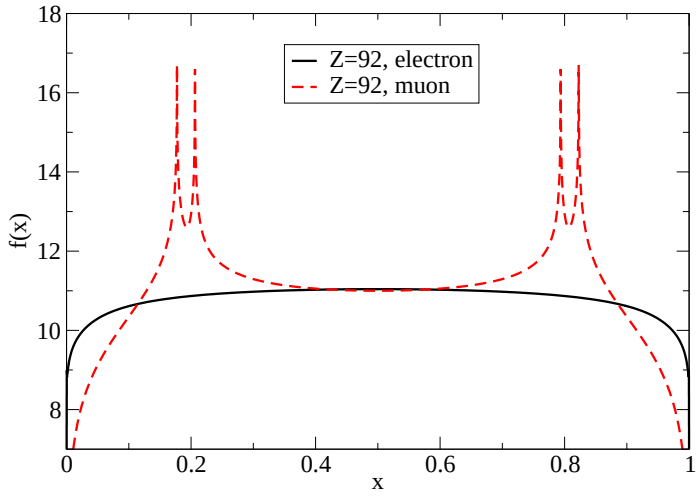

Figure 1: Differential transition probabilities $f(x) = \frac{dW^{(e,\mu)}}{d\omega_1}$ (in $\mathrm{s}^{-1}\mathrm{keV}^{-1}$) for electron and muon ions for $Z = 92$ as a function of the energy sharing fraction x ($x = \frac{\omega_1}{\varepsilon_i - \varepsilon_f}$). The differential transition probabilities are given on a logarithmic scale as $\log_{10} f(x)$.

The two-parameter approximation was introduced, which made it possible to describe with high accuracy the two-photon angular-differential transition probability for the polarized emitted photons. The accuracy of this approximation was $10^{-3}\%$ for light ions, remaining within 1% even for the superheavy ions (for the photons with equal energies). Within the two-parameter approximation, the asymmetry factor completely determines the asymmetry of the differential transition probability. For the one-muon

ions the asymmetry is very small. For the one- electron ions the main contribution to the asymmetry factor is made by the negative continuum of the Dirac spectrum. A nonzero asymmetry factor even for light ions can be a source of nonresonant corrections, which can be important for precision experiments.

We study the differential transition probabilities for the emission of a photon with certain linear and circular polarizations, as well as the transition probabilities for polarized initial and final states. Recently, it was reported that the detector technology for the measurement of linear photon polarization (appearing in K-shell radiative electron capture by heavy ions) was significantly improved [5]. We used the two-parameter approximation for the differential transition probabilities to analyze different polarizations of photons even in the relativistic domain. The angular dependence of the differential transition probabilities for the emission of circularly polarized photons is clearly related to the transition probabilities for linearly polarized photons.

The work was supported by the Russian Science Foundation under Grant No. 22-12-00043.

References

1. A. Matveev, C. G. Parthey, K. Predehl, J. Alnis, A. Beyer, R. Holzwarth, T. Udem, T. Wilken, N. Kolachevsky, M. Abgrall, D. Rovera, C. Salomon, P. Laurent, G. Grosche, O. Terra, T. Legero, H. Schnatz, S. Weyers, B. Altschul, and T. W. Hänsch, Phys. Rev. Lett. **110**, 230801 (2013).

2. J. Missimer and L. M. Simons, Phys. Rep. **118**, 179 (1985).

3. R. Pohl, A. Antognini, F. Nez et al., Nature (London) **466**, 213 (2010).

4. M. Bogomilov, R. Tsenov, G. Vankova-Kirilova, Y. P. Song et al., Nature (London) **578**, 53 (2020).

5. M. Vockert, G. Weber, H. Bräuning, A. Surzhykov, C. Brandau, S. Fritzsche, S. Geyer, S. Hagmann, S. Hess, C. Kozhuharov, R. Märtin, N. Petridis, R. Hess, S. Trotsenko, Y. A. Litvinov, J. Glorius, A. Gumberidze, M. Steck, S. Litvinov, T. Gaßner et al., Phys. Rev. A **99**, 052702 (2019).

Decay of Flexural Phonons in 2D Membrane

A.D. Kokovin[1,3] and I.S. Burmistrov[1,2]

[1]L. D. Landau Institute for Theoretical Physics, Semenova 1-a, 142432, Chernogolovka, Russia

[2]Laboratory for Condensed Matter Physics, HSE University, 101000 Moscow, Russia

[3]Moscow Institute for Physics and Technology, 141700 Moscow, Russia

kokovin.ad@phystech.edu

This work explores the dynamic behavior of flexural phonons in two-dimensional crystalline membranes at the room temperature. We studied the decay of flexural phonons due to interaction with in-plane phonons with the help of the Matsubara diagram technique.

At first we found that the decay rate of flexible phonons is independent of temperature, unlike the standard lifetime in three-dimensional crystals due to three-phonon processes. Our analysis show that this unexpected result is because of the strong screening of the interaction at small momenta $q < q_*$ where $q_* \sim \sqrt{YT}/\varkappa$. Here Y and $\varkappa$ denote the Young's modulus and the bending rigidity, respectively. For static out-of-plane deformations the strong screening of the interaction results, as well-known, in power-law dependence of the Young's modulus and the bending rigidity on momentum, $Y \sim q^{2-2\eta}$ and $\varkappa \sim q^{-\eta}$ [1]. These power-law scaling of elastic moduli persits in the dynamic.

We studied the behavior of the imaginary part of the self-energy for flexural phonons as a function of frequency. We found the power-law behaviour of imaginary part of the self-energy $\mathrm{Im}\Sigma(q,\omega) \sim \rho\omega\omega_q F(\omega/\omega_q)$, where $\omega_q = (\varkappa q^{4-\eta} q_*^{\eta}/\rho)^{1/2}$ with ρ being the mass density of the membrane. The obtained result suggests the exact relation for the dynamical exponent: $z = 2 - \eta/2$. We find that the function $F(z)$ has the following asymptotic behavior at $x \gg 1$, $F(x) \sim x^{-3\eta/(4-\eta)}$.

Finally, behaviour of mean squared displacement, $\langle (h(t) - h(0))^2 \rangle$, was analysed as a function of time. At long times, $t \gg \sqrt{\rho/(\varkappa q_*^4)}$, we obtain $\langle (h(t) - h(0))^2 \rangle \propto t^{1-\beta}$, where $\beta = \frac{\eta}{4-\eta} > 0$. The latter implies that fluctuations behave subdiffusively in quantitative agreement with the experiment.

References

1. Pierre Le Doussal, Leo Radzihovsky «Anomalous elasticity, fluctuations and disorder in elastic membranes», Annals of Physics 392 (2018) 340-410

Superferromagnetic sensors

V.N. Kondratyev, V.A. Osipov

Bogolubov Laboratory of Theoretical Physics, JINR, 141980, Dubna, Russia

Abstract

Properties of ferromagnetic nanoparticles are considered using the band structure based shell model. As is demonstrated such an approach allows to describe the observed superparamagnetic features of such nanocrystals. Arrays of these superparamagnets embedded in nonmagnetic insulator, semiconductor or metallic substrates are shown to display ferromagnetic coupling leading to a superferromagnetic structure properties. Such structures are studied accounting for quantum fluctuations due to the discrete electronic levels and disorder within the randomly jumping interacting moments model. The occurrence of self-organized criticality is found to indicate an existence of spinodal regions and critical points in magnetic state equation and phase diagram. The magnetodynamics represent jerky behaviour displayed as erratic stochastic discontinuities for magnetic induction. Considerations of magnetic noise correlations are proposed as model-independent analytical tools employed in order to specify, quantify and analyse magnetic structure and origin of superferromagnetism. We discuss some results for a sensor mode of superferromagnetic reactivity associated with spatially local external fields, e.g., a detection of magnetic particles. Transport of electric charge carriers between superparamagnetic particles is considered as the Landau level state dynamics. Arising giant magnetoresistance is determined by ratio of respective time of flight and relaxation and can be significant at room temperatures. Favorable designs of superferromagnetic systems for sensor implications are revealed.

Key words: suprparamagnetism; superferromagnetism; giant magnetoresistance, sensor

Precision Physics and the Nonrelativistic QED

Vladimir I. Korobov
Bogoliubov Laboratory of Theoretical Physics
Joint Institute for Nuclear Research
Dubna 141980, Russia
korobov@theor.jinr.ru

Abstract

A review of modern precision physics of atomic scale will be given. We discuss determination of the fundamental physical constants [1] such as the fine structure and Rydberg constant, masses of electron and light nuclei from precision experiments. Along with the Rydberg constant, the problem of the proton charge radius is debated. Spectroscopy of exotic atoms, tests of the CPT invariance, constrains on the hadronic fifth force is considered.

In the second part of the talk the Nonrelativistic quantum electrodinamics (NRQED) [2] as a tool for precision theoretical studies will be outlined. We start from the NRQED Lagrangian and derive the basic corrections to the bound systems such as the leading order relativistic Breit-Pauli Hamiltonian, leading order radiative corrections. Then we discuss how complex particles (hadrons) may be incorporated into the low-energy QED theory. Finally, we show how corrections of order $m\alpha^7$ inclusive may be derived and calculated from the NRQED formalism.

Keywords: Spectroscopy of light atoms and molecules, exotic atoms, bound states, effective field theories, radiative and relativistic corrections.

References

[1] E. Tiesinga, P.J. Mohr, D.B. Newell, and B.N. Taylor, CODATA recommended values of the fundamental physical constants: 2018, Rev. Mod. Phys. **93**, 025010 (2021).

[2] W.E. Caswell and G.P. Lepage, Effective Lagrangians for bound state problems in QED, QCD, and other field theories. Phys. Lett. B **167**, 437 (1986).

Electron-loop corrections of order $\alpha^5 m_\mu$ to the Lamb shift in light muonic atoms

E. Korzinin

D.I.Mendeleyev Institute for Metrology (VNIIM)

korzinin@vniim.ru

Abstract

We consider two kinds of contributions to the Lamb shift in light muonic hydrogenlike atoms: one-loop light-by-light-scattering contributions and three-loop vacuum polarization corrections. The contributions are of the order $\alpha^5 m_\mu$ (with diverse dependence on the nuclear charge Z). Those include the contributions of the so-called Wichmann-Kroll potential $[\alpha(Z\alpha)^4 m_\mu]$, the virtual Delbrück scattering $[\alpha^2(Z\alpha)^3 m_\mu]$, etc.

Key words: muonic hydrogen, QED

Muonic atoms give an opportunity to develop and test a bound-state QED theory and probe a nuclear structure with a specific range of parameters not available with ordinary [electronic] atoms. Recently the accuracy of the measurement of the 2s–2p Lamb shift in some light hydrogenlike muonic atoms has been dramatically improved [1, 2]. The QED theory of the energy levels in muonic atoms is somewhat different from that in ordinary atoms. The Bohr radius in muonic atoms is comparable with the Compton wavelength of an electron. Because of that, an important role is played by the diagrams with the closed electron loops. Those contributions are specific for muonic atoms. The most important are those due to vacuum polarization. Their contribution to the energy is of the order $\alpha(Z\alpha)^2 m_\mu$.

Effects of the virtual light-by-light scattering contribute to higher orders. There are three types of such contributions, characteristic diagrams which are presented in Fig.1. They are all of the order $\alpha^5 m_\mu$, but their dependence on the value of the nuclear Z charge is different. It was proven in [3, 4] that an approximation of a static muon, where its nonrelativistic propagator is presented with a δ function over the energy (see Fig.2), is a valid one. For the calculation of the virtual-Delbrück-scattering contribution (diagrams 2:2 in Fig.2), one can use an effective potential in the coordinate space which was constructed in [5].

The other kind of the contribution under consideration is irreducible VP3 diagrams Fig.3. The only available result for the contribution is on μH [6]. In other papers only bold estimations have been made. We recalculate it using new available asymptotics of vacuum polarization operator [7].

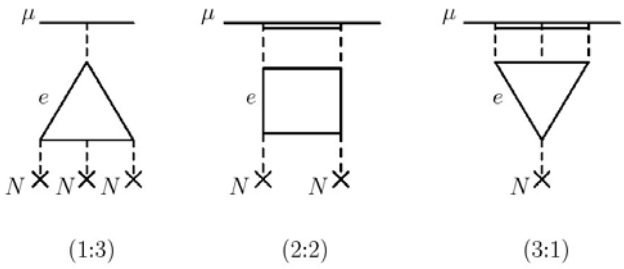

Figure 1: Characteristic diagrams induced by the light-by-light scattering. The double horizontal line is for the nonrelativistic Coulomb Green's function of a muon.

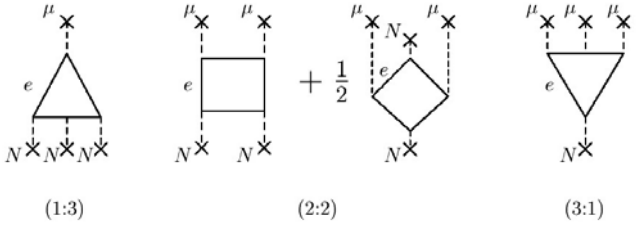

Figure 2: "Double-external-field" approximation with a static nucleus and a static muon.

Figure 3: Characteristic irreducible VP3 diagrams: VP with VP inside and VP with 2γ inside. For VPinVP the masses of the particle in the loop are the same.

References

1. A. Antognini, F. Nez, K. Schuhmann, F. D. Amaro, F. Biraben, J. M. R. Cardoso, D. S. Covita, A. Dax, S. Dhawan, M. Diepold, L. M. P. Fernandes, A. Giesen, A. L. Gouvea, T. Graf, T. W. Hänsch, P. Indelicato, L. Julien, C.-Y. Kao, P. Knowles, F. Kottmann et al., Science 339, 417 (2013).

2. R. Pohl, F. Nez, L. M. P. Fernandes, F. D. Amaro, F. Biraben, J. M. R. Cardoso, D. S. Covita, A. Dax, S. Dhawan, M. Diepold, A. Giesen, A. L. Gouvea, T. Graf, T. W. H?nsch, P. Indelicato, L. Julien, P. Knowles, F. Kottmann, E.-O. Le Bigot, Y.-W. Liu et al., Science 353, 669 (2016).

3. S. G. Karshenboim, E. Yu. Korzinin, V. G. Ivanov, and V. A. Shelyuto, PisЎma v ZhETF 92, 9 (2010) [JETP Lett. 92, 8 (2010)].

4. S. G. Karshenboim, V. G. Ivanov, E. Yu. Korzinin, and V. A. Shelyuto, Phys. Rev. A 81, 060501 (2010).

5. E. Yu. Korzinin, V. A. Shelyuto, V. G. Ivanov, R. Szafron, S. G. Karshenboim, Phys. Rev. A 98, 062519 (2018)

6. T. Kinoshita and M. Nio, Phys. Rev. Lett. 82, 3240 (1999); Erratum, Phys. Rev. Lett. 103, 079901 (2009)

7. A.I. Onishchenko, arXiv:2212.03502 [hep-ph] (2022)

Time-depending screening effects in relativistic evaluations of electronic quantum dynamics in ion-atom collisions

Y. S. Kozhedub[1] and V. M. Shabaev[1,2]

[1]Department of Physics, St. Petersburg State University, 7/9 Universitetskaya nab., 199034 St. Petersburg, Russia

[2]B. P. Konstantinov Petersburg Nuclear Physics Institute of National Research Centre "Kurchatov Institute", Gatchina, 188300 Leningrad District, Russia

[1]ykozhedub@spbu.ru

Abstract

We present the results of non-perturbative relativistic calculations of electronic quantum dynamics in low-energy ion-atom collisions taking into account time-depending screening effects. Method of calculations employs an independent particle model with effective single-electron Dirac-Kohn-Sham operator. For the inclusion of the time-depending screening effect we use a simple model. Calculations are performed for Ne-$F^{8+}(1s)$ collision at the projectile energy 130 keV/u.

Introduction

Low-energy heavy-ion collisions play a very important role in studying relativistic quantum dynamics of electrons in the presence of strong electromagnetic fields [1]. What is more, if the total charge of the colliding nuclei is larger than the critical one spontaneous electron-positron pair production becomes possible, observation of the effect can shed light on quantum electrodynamics at supercritical fields [2, 1]. Experimental investigations aimed at comprehensive study of various processes in low-energy heavy ion-atom collisions are planned in the nearest future. The corresponding theoretical calculations are urgently required. The present work is devoted to development of effective methods for evaluation quantum dynamic of electrons in ion-atom collisions including time-dependent screening effect.

Theory

Here we briefly present the formalism used, for a complete description see Refs. [3]. Using the semiclassical approximation, where the atomic nuclei move along the classical trajectories and are considered as sources of a time-dependent external potential, we

have to solve the time-dependent many-particle Dirac equation for the electrons involved in the process. We employ a method based on an independent-particle model, where the many-electron Hamiltonian $\hat{H}$ is approximated by a sum of effective single-electron Hamiltonians, $\hat{H}^{\rm eff} = \sum \hat{h}^{\rm eff}$, reducing the electronic many-particle problem to a set of single-particle Dirac equations for all (N) electrons of the colliding system with the initial conditions:

$$i\frac{\partial\psi_k(\vec{r},t)}{\partial t} = \hat{h}^{\rm eff}\,\psi_k(\vec{r},t), \quad \lim_{t\to-\infty}(\psi_k(\vec{r},t) - \psi_k^0(\vec{r},t)) = 0, \quad k = 1,\ldots,N, \qquad (1)$$

The many-electron wave function is given by a Slater determinant made-up from the single-particle wave functions. As the effective single-electron Hamiltonian $\hat{h}^{\rm eff}$ we use the two-center Dirac-Kohn-Sham Hamiltonian:

$$\hat{h}^{\rm eff} = c(\vec{\alpha}\cdot\vec{p}) + \beta\,c^2 + V^A_{\rm nucl}(\vec{r}_A) + V^B_{\rm nucl}(\vec{r}_B) + V^A_{\rm scr}(\vec{r}_A,t) + V^B_{\rm scr}(\vec{r}_B,t)\,, \qquad (2)$$

where c is the speed of light and $\vec{\alpha}$, β are the Dirac matrices. Index $\mu = A, B$ indicates the centers, $\vec{r}_\mu = \vec{r} - \vec{R}_\mu$, $\vec{r}$ is the electron radius-vector, $\vec{R}_\mu$ is the radius-vector of the centers (nucleus), $V^\mu_{\rm nucl}(\vec{r}_\mu)$ and $V^\mu_{\rm scr}(\vec{r}_\mu,t)$ are the electron-nucleus and the electron-electron interaction potentials, respectively,

Relatively simple model, which does not increase the computational cost significantly compared to a calculation with a frozen target and projectile potentials was suggested in work [4]:

$$V^\mu_{\rm scr}(\vec{r},t) = \frac{Q^\mu_{\rm eff}(t)}{N^\mu} V^{\mu,0}_{\rm scr}(r), \qquad (3)$$

where N^μ is the initial number of the target or projectile electrons. In other words the time-dependent screening potential is presented as the frozen one multiplied by a coefficient. There are different ways to defined the coefficient $Q^\mu_{\rm eff}(t)$, here we consider the following:

1. $Q^\mu_{\rm eff}(t) = \int_{V_\mu}\rho(\vec{r})/|e|d^3r$, V_μ is the target (projectile) space volume
2. $Q^\mu_{\rm eff}(t) = Q^\mu(t) \equiv \sum_{i=1}^{N^\mu}\sum_{v=1}^{M}|\langle\varphi^\mu_v|\psi_i(t)\rangle|^2$;
   the set $\{|\varphi^\mu_v\rangle, \quad v = 1,...,V\}$ contains all bound states of the target (projectile)
3. $Q^\mu_{\rm eff}(t) = (Q^\mu(t) - P^{\rm loss}_0)\frac{N^\mu}{N^\mu-1}$
   $P^{\rm loss}_q$ are the probabilities to lose charge q from the target (projectile)

Solving the effective single-particle Eq. (1) is based on the coupled-channel approach with atomic-like Dirac-Fock-Sturm orbitals, localized at the ions (atoms) [5]. The many-particle probabilities are calculated in terms of the single-particle amplitudes employing the formalism of inclusive probabilities [6], which allows one to describe the many-electron collision dynamics.

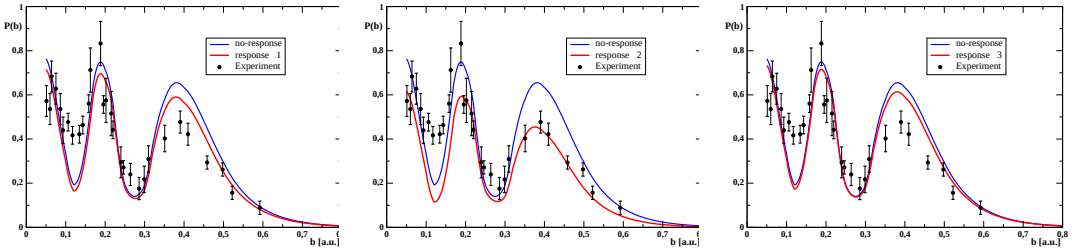

(a) response type (1) (b) response type (3) (c) response type (3)

Figure 1: The average number $P(b)$ of the Ne K-shell-vacancy production as function of the impact parameter b for the Ne-$F^{8+}(1s)$ collisions at the projectile energy of 130 keV/u. Comparison of the no-response calculation with the response type (1) (fig. a), (2) (fig. b), (3) (fig. c) results and experimental data by Hagmann *et al.* [7].

Results of calculations

In the present work the average number of the Ne K-shell-vacancy production as function of the impact parameter b for the Ne-$F^{8+}(1s)$ collisions at the projectile energy of 130 keV/u has been calculated. The calculations were performed for the no-response screening potential as well as for time-dependent (response) case. Three types of inclusion of the time-dependent screening effect were considered. The results are presented in Fig. 1. One can see considerable influence of the effect.

Acknowledgments

This work was supported by the Russian Science Foundation (Grant No. 22-62-00004).

References

1. W. Greiner and B. Müller and J. Rafelski, Quantum Electrodynamics of Strong Fields, Springer-Verlag, Berlin, Heidelberg (1985).
2. S.S. Gershtein and Y.B. Zeldovich, Zh. Eksp. Teor. Fiz. 57, 654 (1969).
3. Y. S. Kozhedub *et al.*, Phys. Rev. A 90, 042709 (2014).
4. T. Kirchner *et al.*, Phys. Rev. A 62 042704 (2000).
5. I. I. Tupitsyn *et al.*, Phys. Rev. A 82, 042701 (2010).
6. H. J. Lüdde and R. M. Dreizler, J. Phys. B 18, 107 (1985).
7. S. Hagmann *et al.*, Phys. Rev. A 36, 2603 (1987).

Using atoms and molecules to search for New Physics

M. G. Kozlov[1,2]

[1]Petersburg Nuclear Physics Institute of NRC "Kurchatov Institute", Gatchina, 188300, Russia

[2]St. Petersburg Electrotechnical University "LETI", Prof. Popov Str. 5, St. Petersburg 197376, Russia

[1]kozlov_mg@pnpi.nrcki.ru

Abstract

Spectroscopic experiments with atoms and molecules have unique accuracy. In the optical domain the part per billion precision in frequency measurements is routinely achieved, while the atomic optical clocks at present have relative accuracy on the level of 10^{-17} – 10^{-18}. This opens a variety of possibilities to test New Physics beyond the Standard Model by studying minute effects in atoms and molecules. Atomic experiments include tests of the violation of the fundamental symmetries, such as spacial parity non-conservation, or time-reversal invariance and local Lorenz invariance violation. Another direction is the search for the possible variation of the effective fundamental constants, including the fine structure constant α and the electron to proton mass ratio μ. Atomic physics places very strong constrains on the exotic long-range interactions. Such interactions are predicted in a large number of theoretical models, where the cosmological Dark Matter supposed to be formed by the light bosonic field(s). Atomic table-top experiments are complementary to the extremely expensive high-energy experiments with particle accelerators. In this talk I will stop on some of the recent advances in this field and will discuss several proposals of the new experiments.

Key words: atomic physics, optical clocks, fundamental constants, exotic bosons

Electromagnetic-field-phase effect on charge transfer and ionization in laser-assisted collisions of protons with hydrogen atoms

D. A. Krapivin[1] and D. A. Telnov[2]

[1,2]St. Petersburg State University, St. Petersburg, Russia
[1]st033103@student.spbu.ru, [2]d.telnov@spbu.ru

Abstract

We perform a theoretical and computational study of laser-assisted collisions of protons with hydrogen atoms. The incident proton energy is equal to 0.25 keV, and the laser field is linearly polarized in the collision plane. For the infrared laser field (frequency $\omega_0 = 0.01$ a.u.) and small impact parameters ($0.125 - 1.5$ a.u), our results demonstrate a strong dependence of the charge transfer and ionization probabilities on the phase of the field at the moment when the proton approaches the hydrogen atom most closely. On the contrary, for the field in the extreme ultraviolet region (frequency $\omega_0 = 2$ a.u.), the charge transfer and ionization probabilities do not depend on the phase of the field irrespective of the impact parameter value.

Key words: Charge transfer, Ionization probability, Capture cross section

Introduction

Revolutionary changes in the experimental technique made it possible to observe and measure various processes with diatomic molecules and quasimolecules in laser fields. An external electromagnetic field makes it possible to control the process of electron capture during collisions. In particular, it was demonstrated [1, 2] that the phase of the electromagnetic field has a significant influence on the probability of the charge transfer in collisions of various ions with a hydrogen atom.

Here we present a theoretical and numerical study of the effect of the phase and intensity of the laser field on the charge transfer and ionization processes in a homonuclear $H–H^+$ quasimolecular system [3]. The field is linearly polarized in the collision plane along the initial direction of the inrenuclear axis. The collision dynamics is studied solving the time-dependent Schrödinger equation in the center-of-mass coordinate system. Then a transition to a non-inertial reference frame rotating with the internuclear axis is made, which leads to appearance of an additional term in the Hamiltonian that takes the rotational coupling into account. The velocity of the incident proton is chosen to be rather low ($v_0 = 0.1$ a.u., which corresponds to an energy of 0.25 keV). The main goal was to obtain the dependence of the charge transfer probability and cross section, as well as the ionization probability on the field

parameters, such as intensity, frequency and phase at the ahortest distance between the nuclei. The calculations were carried out at the peak intensities 1×10^{12} W/cm^2 and 1×10^{13} W/cm^2 for the frequency 0.01. a.u. and 5×10^{14} W/cm^2 for frequency 2 a.u.; the phase values were 0°, 90°, 180°, and 270°.

Main text

Assuming that collision of a proton with a hydrogen atom occurs in the $x - z$ plane, the Schrödinger equation in the rotating frame of reference can be written in the following form:

$$i\frac{\partial}{\partial t}\Psi(\mathbf{r},t) = [-\frac{1}{2}\nabla^2 + U(\mathbf{r}) + V(\mathbf{r},t) - \omega(t)L_y]\Psi(\mathbf{r},t), \tag{1}$$

where $U(\mathbf{r})$ is the interaction of the electron with the nuclei; $V(\mathbf{r},t)$ is the interaction of the electron with the laser field; $\omega(t)$ is the angular velocity; L_y is the operator of the angular momentum projection on the y axis. Using the velocity gauge in the dipole approximation, the operator $V(\mathbf{r},t)$ is written as:

$$V(\mathbf{r},t) = -i(\mathbf{A}\cdot\nabla) + \frac{1}{2}A^2, \quad \mathbf{A}(t) = -\frac{F_0}{\omega_0}\cos(\omega_0 t + \phi)\mathbf{e}_z, \tag{2}$$

where F_0 is the peak field strength, ω_0 is the carrier frequency of the electromagnetic wave, and ϕ is the field phase at $t = 0$. The time-dependent Schrödinger equation is solved on a symmetrical time interval, where the moment $t = 0$ corresponds to the shortest distance between the nuclei. The equation (1) is solved using generalized pseudospectral discretization in prolate spheroidal coordinates and Crank-Nicolson algorithm for time propagation.

The dynamics of the charge transfer and ionization is determined by the superposition of the Coulomb forces from the nuclei and the force from the electromagnetic field in the region where the projectile is close to the target. The force from the electromagnetic field in this region is in turn determined by the phase of the field at the moment of the shortest distance between the projectile and the target. Our results for the frequency $\omega_0 = 0.01$ a.u. demonstrate a significant influence on the charge transfer and ionization from the phase of the electromagnetic field.

If the impact parameter is sufficiently small ($b < 2$ a.u.), the excited electronic states of the quasimolecule H_2^+ get substantial population while the projectile is in close proximity to the target. In this case, the portions of the nuclear motion when the projectile approaches the target and when it flies away differ significantly in their role in the charge transfer and ionization processes. When the projectile still approaches the target, the electron dynamics is mainly to interference of initially populated $1\sigma_g$ and $1\sigma_u$ molecular orbitals. However, when the projectile flies away, higher-lying electronic states are already populated thus affecting the dynamics of the charge transfer and ionization in the external field. The charge transfer and ionization probabilities are different for different phases of the field at the same intensity.

At large impact parameters ($b > 2$ a.u.), the probability of excitation of the quasimolecule to higher-lying electronic states is small, and the charge transfer dynamics is mainly determined by the interference of the initially occupied $1\sigma_g$ and $1\sigma_u$ molecular orbitals. In this case, the portions of the nuclear motion before and after the point of the shortest distance between the projectile and the target are equivalent with respect to the charge transfer. In the vicinity of this point, the molecular axis is almost perpendicular to the direction of the force from the external field. In this geometry, dependence on the sign of the field disappears. Then the charge transfer probability is the same for both field phases within the pairs 0°, 180° and 90°, 270° but differs from the probability for the other pair. The effect of the field phase on the charge transfer is also well pronounced in the cross section upon integration of the probability with respect to the impact parameter, as one can see in Table 1.

Table 1: Phase-dependent charge transfer cross sections (10^{-16} cm^2) for the laser field frequency $\omega = 0.01$ a.u.

Phase	Intensity	
	1×10^{12} W/cm^2	1×10^{13} W/cm^2
0°	20.62	22.94
90°	23.37	24.48
180°	20.91	23.24
270°	23.69	24.83

For the frequency of the electromagnetic field $\omega = 2$ a.u. and intensity $I_0 = 5 \times 10^{14}$ W/cm^2, we do not observe the effect of the phase of the electromagnetic field on the charge transfer and ionization probabilities. This is well explained by much more rapid oscillations of the electromagnetic field compared to oscillations of the electron density between the target and the projectile.

References

1. F. J. Domínguez-Gutiérrez and R. Cabrera-Trujillo, Eur. Phys. J. D **68**, 226 (2014).

2. T. Kirchner, Phys. Rev. Lett. **89**, 093203 (2002).

3. D. A. Krapivin and D. A. Telnov, Eur. Phys. J. D (accepted for publication).

Geometric phase for nonlinear oscillators from perturbative renormalization group

D. A. Khromov[1], M. S. Kryvoruchko[2], D. A. Pesin[3]

[1,2]Moscow Institute of Physics and Technology, Russia

[3]University of Virginia, USA

[1]krivoruchko.ms@phystech.edu, [2]khromov.da@phystech.edu, [3]dp7bx@virginia.edu

Abstract

We formulate a renormalization group approach to a general nonlinear oscillator problem. The approach is based on the exact group law obeyed by solutions of the corresponding ordinary differential equation. We consider both the autonomous models with time-independent parameters, as well as nonautonomous models with slowly varying parameters. We show that the renormalization group equations for the nonautonomous case can be used to determine the geometric phase acquired by the oscillator during the change of its parameters. We illustrate the obtained results by applying them to the Van der Pol, and Van der Pol-Duffing models.

Key words: Renormalization group

Introduction

It was shown in Refs. [1-3] that classical dissipative systems with a limit cycle admit the notion of a geometric phase accumulated when the system's parameters undergo a slow change. This geometric phase is analogous to the Hannay angle [4] in classsical Hamiltonian systems with adiabatic invariants, and to the Berry phase [5] in quantum mechanics. In this work, we show how to calculate this phase for models describable with nonlinear oscillators based on the renormalization group (RG) approach.

The renormalization group method turned out to be a powerful way to regularize secular terms in the perturbation theory for dynamical systems, and study their asymptotic behavior, see Refs. [8-9]. As demonstrated in Ref. [10], the method is extremely versatile, and can in principle replace most known methods of asymptotic analysis, such as multiplescale analysis, time-averaging techniques, and so on.

Main text

In this work, we present a formulation of the renormalization group procedure for nonlinear oscillators based on the exact group law obeyed by the solutions of the

corresponding differential equations, similar to the approach of Ref. [7, 11]. As a result, we are able to show that the nonlinear oscillator models are perturbatively renormalizable to any order. The renormalization group equations are obtained directly from the linear in time secular terms at the prime frequency of the unperturbed oscillator in a completely mechanistic way. We then use these equations to calculate the geometric phase shifts for nonlinear oscillators.

We will consider a situation in which the small parameters in a nonlinear oscillator problem are time-dependent, but this time dependence is slow. Having in mind applications for calculation of geometric phases for oscillators, we will assume that these small parameters are taken through a cycle in the parameters space, and the duration of the cycle. In calculating these corrections, we restrict ourselves to the linear order in nonadiabaticity, since only such terms lead to the appearance of geometric phases.

We show how to use formalism to describe the geometric phase for a nonlinear oscillator with a limit cycle, especially to Van der Pol-type oscillators (Eq. 1).

$$\ddot{y} + \omega^2 y = \mu(1 - y^2)\dot{y} - \beta y^3. \tag{1}$$

In general geometric phase can be represented as in Eq. 2 with the corresponding curvature (Eq. 3).

$$\theta_{\text{geom}} = \int (a_\mu d\mu + a_\beta d\beta) \tag{2}$$

$$\chi = \partial_\mu a_\omega - \partial_\omega a_\mu \tag{3}$$

Recently, a way to study the geometric phases in dissipative systems was proposed by their “Hamiltonization" in Ref.[6]. In this work, we adopt the perturbative renormalization group to study changes in the limit cycle of the VdPD oscillator under slow time evolution of its parameters, and to determine the associated geometric phase. We will start with the VdP model to reproduce some known results using the RG. Later we will turn to the VdPD model, and show that in that case, the curvature in the parameter space is singular and scales as $1/\mu^2$. For the curvature we obtain

$$\chi_{\text{vdpd}} = \partial_\mu a_\beta - \partial_\beta a_\mu = \frac{3}{2}\frac{\beta}{\mu^2\omega^3}. \tag{4}$$

To give quality observation, we used Wolfram Mathematica for getting results with different parameters (Fig. 1).

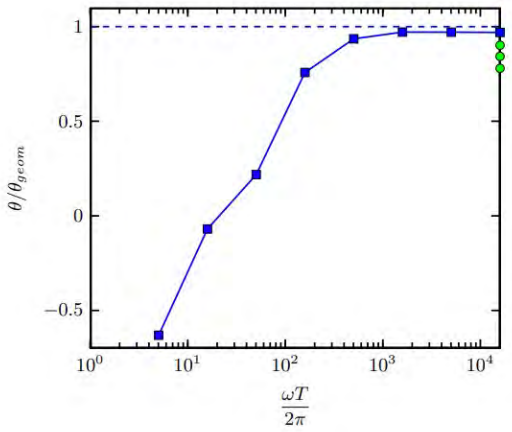

Figure 1: Geometric phase accumulated during a cycle in the (μ, β) space as a function of the time to complete the cycle, T (blue squares). The parameters used for the simulation, in appropriate units, are $\beta = 0.005$, $\delta\beta = 0.001$, $\mu = 0.01$, $\delta\mu = 0.0005$, $\omega = 1$. Geometric phase calculated using Eq. 4: $\theta_{geom} = 1.31 \cdot 10^{-4}$. Green circles: the geometric phase obtained for the longest cycle, $\omega T = 10^5$, and different values of $(\mu, \beta) = (0.015, 0.01125), (0.02, 0.02), (0.025, 0.03125)$, for which $\beta/\mu^2 = 50$.

References

1. T. B. Kepler and M. L. Kagan, Phys. Rev. Lett. **66**, 847 (1991).

2. M. L. Kagan, T. B. Kepler, and I. R. Epstein, Nature **349**, 506 (1991).

3. C. Z. Ning and H. Haken, Phys. Rev. Lett. **68**, 2109 (1992).

4. J. H. Hannay, J. Phys. A **18**, 221 (1985).

5. M. V. Berry, Proc. R. Soc. London Ser: A **392**, 45 (1984).

6. R. Chattopadhyay, T. Shah, and S. Chakraborty, Phys. Rev. E **97**, 062209 (2018).

7. M. A. Mnatsakanyan, Sov. Phys. Dokl. **262**, 856 (1982)

8. D. Shirkov, Int. J. Mod. Phys. A **3**, 1321 (1988).

9. N. Goldenfeld, *Lectures on phase transitions and the renormalization group* (CRC Press, 2018).

10. L.-Y. Chen, N. Goldenfeld, and Y. Oono, Phys. Rev. E **54**, 376 (1996).

11. S.-I. Ei, K. Fujii, and T. Kunihiro, Ann. Phys. **280**, 236 (2000).

Metamaterials: Conceptual highlights and recent trends

M. Lapine[1,2]

[1]ITMO University, Saint Petersburg, Russia

[2]University of Technology Sydney, Australia

[1,2]mikhail.lapine@gmail.com

Abstract

In this talk, I provide an overview of the theoretical development of selected topics in metamaterials research over the past decades. The main emphasis is on the effective medium theory for metamaterials, specifically for artificial magnetics; peculiarities owing to discrete structure of metamaterials and finite size of practical samples; methods to provide nonlinearity and tunability to metamaterials; and I will point out the arising open questions along all the topics.

Key words: Metamaterials

Introduction

The research area of metamaterials — as long as we adhere to the explicit use of terminology, as indeed some of the relevant ideas are more than a century old — is currently at a mature age of 23 years, and a wide range of specific research directions has emerged in this context, even if we only look at the first decade only, and a limited selection of topics, as shown in Table 1.

It is certainly impossible to address all the relevant aspects within a single review talk, however quite a few textbooks and a number of review articles are published to date, covering various specific topics.

Table 1: Brief timeline of metamaterial research (first decade)

Research direction	Year	Research direction	Year
Negative refraction	1945	Magnetoinductive waves	2002
Negative ε and μ	1959	Nonlinear metamaterials	2003
Metamaterials	**2000**	Acoustic metamaterials	2004
Superresolution	2001	"Cloaking"	2006
Artificial magnetism	2002	Hyperbolic dispersion	2008
Wire media	2002	"Metasurfaces"	2009

Main text

As I have worked in the area of metamaterials from its very beginning, it might be even of interest to trace, retrospectively, the evolution of perception of the progress of the relevant research as reflected in review papers written in earlier years, addressing the general conceptual and strategic aspects [1, 2], artificial magnetics [3], wire media [4], nonlinearity [5], metasurfaces [6] and new degrees of freedom [7]; therein, some thousand of relevant references are found.

For this report however, I will only focus on a few specific topics as outlined in the main section. In general, I will primarily address peculiarities of artificial magnetic response achieved with metamaterials, and highlight various phenomena which can be observed in such metamaterials.

As the primary point, the fundamental question to address is the effective medium theory for magnetic metamaterials, whereby strong mutual interaction between individual elements is quite essential [8] and leads to a number of curious effects. In particular, I will point out an exceptionally strong effect of metamaterial boundaries and shape of metamaterial samples on their observable properties [10]. The effect owes to extraordinarily strong mutual interaction between closely positioned elements, which enhances the boundary role and results in remarkable deviations between the effective medium predictions and realistic properties if finite samples. The eventual convergence towards a homogenisable response is quite slow [11], which poses direct implications for any conceivable practical designs.

Strong mutual interaction also paves a route towards implementation of nonlinear response and tunable properties in metamaterials [5]. In particular, I will discuss various links between mechanical and magnetic response, emerging in the so-called magnetoelastic metamaterials [9] and similar structures.

A somewhat related direction points to opto-acoustic metamaterial designs, which offer artificial electrostriction and enhanced stimulated Brillouin scattering (SBS) [12]. On this track, a simple and non-resonant composite medium, such as an array of spheres embedded in a matrix of a different material, attains an artificial term in the electrostriction coefficient so the resulting photoelasticity can exceed that of the individual components.

Another example of non-resonant metamaterials is a simple but efficient design of artificial diamagnetics [13]. Diamagnetic metamaterials are scalable to work in a huge range of frequencies, and provide exceptionally strong diamagnetism compared to conventional materials . The strong role of mutual interaction in a very dense uniaxial lattice of meta-atoms, is once again a key feature here, leading to a magnitude of effective permeabilities below 0.1, further armed with efficient reconfigurability, and playing a step on the way to light-weight magnetic levitation.

Finally, a remark should be made on the extreme importance of spatial dispersion in metamaterials, naturally arising from their typical design [4, 14, 15].

Research on the discrete metamaterials of finite size was supported by the Russian Science Foundation (grant no. 22-11-00153).

References

1. M. Gorkunov, M. Lapine and S. A. Tretyakov, Methods of crystal optics for studying electromagnetic phenomena in metamaterials: Review, *Crystallography Reports*, **51** (6), 1048–1062 (2006).

2. M. Lapine and S. A. Tretyakov, Contemporary notes on metamaterials, *IET Proc. Microwaves, Antennas & Propagation*, **1** (1), 3–11 (2007).

3. R. Marqués, L. Jelinek, M. J. Freire, J. D. Baena and M. Lapine, Bulk metamaterials made of resonant rings, *Proc. IEEE*, **99**, 1660–1668 (2011).

4. C. R. Simovski, P. Belov, A. Atrashchenko, Y. Kivshar, Wire metamaterials: Physics and applications, Advanced Materials **24** (31), 4229–4248 (2012).

5. M. Lapine, I. V. Shadrivov and Yu. S. Kivshar, Nonlinear metamaterials, *Rev. Mod. Phys.*, **86** (3), 1093–1123 (2014).

6. S. B. Glybovski, S. A. Tretyakov, P. A. Belov, Yu. S. Kivshar, C. R. Simovski, Metasurfaces: From microwaves to visible, *Physics Reports*, **634**, 1–72 (2016).

7. M. Lapine, New degrees of freedom in nonlinear metamaterials *Phys. Status Solidi B* **254** (4), 1600462 (2017).

8. M. Gorkunov, M. Lapine, E. Shamonina, and K. H. Ringhofer, Effective magnetic properties of a composite material with circular conductive elements, *Eur. Phys. J. B*, **28**, pp. 263–269 (2002).

9. M. Lapine, I. V. Shadrivov, D. A. Powell and Yu. S. Kivshar, Magnetoelastic metamaterials, *Nature Materials*, **11**, pp. 30–33 (2012).

10. M. Lapine, L. Jelinek and R. Marqués, Surface mesoscopic effects in finite metamaterials, *Opt. Express*, **20** (16), pp. 18297–18302 (2012).

11. M. Lapine, R. C. McPhedran, and C. G. Poulton, Slow convergence to effective medium in finite discrete metamaterials, *Phys. Rev. B*, **93**, 235156 (2016).

12. M. J. A. Smith, C. M. de Sterke, C. Wolff, M. Lapine, and C. G. Poulton, Enhanced acousto-optic properties in layered media *Phys. Rev. B* **96**, 064114 (2017).

13. M. Lapine, A. K. Krylova, P. A. Belov, C. G. Poulton, R. C. McPhedran and Yu. S. Kivshar, Broadband diamagnetism in anisotropic metamaterials, *Phys. Rev. B*, **87**, 024408 (2013).

14. M. A. Gorlach, M. Lapine, Boundary conditions for the effective-medium description of subwavelength multilayered structures, *Phys. Rev. B* **101**, 075127 (2020).

15. M. Lapine, M. A. Gorlach, Current trends and nonlinear effects in multilayered metamaterials, *Ceramics International* **49**, 24422–24427 (2023).

Fractal geometry methods by improving image quality in atomic force microscopy

A. Lelekova [1], V. Samyshkin[1], S. Kavokina[1,2]

[1]Vladimir state university

[2] Abrikosov Center for Theoretical Physics, Moscow Institute for Physics and Technology
[1]lelekova@vlsu.ru, [1]samyshkin@vlsu.ru, [1,2]11stella@mail.ru

Abstract

The methods of atomic force microscopy (AFM) are increasingly being used to study nanoscale objects and structures. The approaches used make it possible to obtain a high-resolution map of surface properties. This paper proposes a method for programmatic improvement of the quality of measurements in terms of increasing their information content.

Key words: atomic force microscopy, fractal dimension, Hurst exponent

It is shown that the determination of the fractal properties of the structure makes it possible to control the quality of the obtained images by getting rid of redundant measurements and by improving the detail of the height map of the analyzed relief. Improving the quality of the image occurs according to the Foss random addition algorithm by determining the initial variance and the Hurst exponent. Due to the calculation of the Hurst exponent, it is possible to speak about the presence of a trend in the distribution of heights of the measured relief. The more the value of the indicator deviates from ½, the more predictable the distribution of heights in the study area becomes. This fact opens up the possibility of using the Hurst exponent to improve the quality of the resulting images. The essence of the method lies in the fact that, having some arbitrary dependence, it is possible to build a random relief using the following recursive algorithm. Between the starting points of the sequence, new points of the sequence are added in randomly addition; the initial point value corresponds to the arithmetic mean of two adjacent measurements.

This study was funded by the Russian Science Foundation (project no. 23-29-10016, https://rscf.ru/en/project/23-29-10016/)

Title

V.G. Lukyanchuk[1], N.D. Kondratyuk[2], I.M. Saitov[3]

[1,2,3]Moscow Institute of Physics and Technology

[1,2,3]Joint Institute for High Temperatures RAS

[2,3]National Research University Higher School of Economics

[1]lukianchuk.vg@phystech.edu, [2]kondratyuk.nd@mipt.ru, [3]saitovilnur@gmail.com

Abstract

This research pioneers the study of nuclear quantum effects on metastable states of high-pressure liquid hydrogen using advanced computational methods, revealing a first-order phase transition. A new method for modeling these states across isotherms was successfully developed and applied, leading to valuable thermodynamic insights.

Key words: Equations of state, Phase transitions, Critical phenomena

Introduction

Currently, there is a sufficiently large number of works in which the influence of accounting for quantum effects of nuclei on the thermodynamic properties of systems containing hydrogen at high pressures is investigated [1, 2]. The method of integrals on trajectories together with the density functional theory allows us to effectively calculate these corrections [3].

Main text

In this work we propose to study the influence of this effect on the region of existence of metastable states (atomic and molecular) of liquid hydrogen at high pressures (100-200 GPa) for the first time. The technique of calculations within the method of molecular dynamics on integrals on trajectories with the use of software packages VASP and PIMD is mastered. Metastable states in the hydrogen fluid, the existence of which is an unambiguous indication that the observed transition is, indeed, a phase transition of the first kind, were discovered. This fact is especially important for phase transitions with small density jumps.

Isotherms for the temperature range 700-1500 K were calculated. A method for modeling metastable states for all isotherms under study has been developed and successfully applied. The phase curve and evaluation on the metastable regions were obtained. The preservation of the molecular phase along the metastable branches is evidenced by the high values of the heights of the first peaks of the paired correlation function. An estimate of the heat of the phase transition through the jump of the pair entropy is obtained. This work was carried out within the framework of the Priority 2030 Strategic Academic Leadership Program (agreement 075-02-2021-1316 dated September 30, 2021).

References

1. Deemyad S, Silvera IF. Melting Line of Hydrogen at High Pressures. Phys. Rev. Lett. 2008;100(15).
2. Celliers PM, Millot M, Brygoo S, et al. Insulator-metal transition in dense fluid deuterium. Science. 2018;361(6403):677–682.
3. Morales MA, McMahon JM, Pierleoni C, et al. Nuclear Quantum Effects and Nonlocal Exchange-Correlation Functionals Applied to Liquid Hydrogen at High Pressure. Phys. Rev. Lett. 2013;110(6).

Diffusive modes in a two-dimensional fermionic gas with number conserving dissipative dynamics

A.A. Lyublinskaya[1] and I.S. Burmistrov[2]

[1]Moscow Institute of Physics and Technology

[1,2]L.D. Landau Institute for Theoretical Physics (RAS)

[1]lyublinskaya.aa@phystech.edu, [2]burmi@itp.ac.ru

Abstract

We consider a two-band 2D fermionic system subject to dissipation, described in terms of the Gorini-Kosakovski-Sudarshan-Lindblad equation. Using the Keldysh functional integral approach, the presence of an interval of length- and time-scales with diffusion motion of quasiparticles is shown by calculating the ladder series. The first orders of the diffuson's self-energy are taken into account, which lead to a change in the diffusion coefficient and determine whether the trivial stationary state is stable.

Key words: non-equilibrium field theory, Keldysh functional integrals, driven open quantum systems

Introduction

Recently, active research has been carried out on open quantum many-body systems with dissipative dynamics [1], [2], [3], [4]. Having non-thermal stationary states with non-equilibrium transient dynamics, such systems show interesting and unexpected physical results.

The main technical tool for constructing a theory in the field of quantum systems with dissipative dynamics is the Gorini-Kossakovski-Sudarshan-Lindblad (GKSL) equation [5], which describes both the Hamiltonian and nonunitary evolution of the density matrix, determined by the jump operators. The Keldysh formalism [6] is often used to construct diagramatics. In the presence of diffusion modes, it also opens the way to the construction of the Keldysh sigma-model [7], [8], [9].

Main text

Within the framework of this scientific activity, in a recent paper [2] a paradigmatic two-band model was presented. It is determined by the quadratic Hamiltonian and particle number conserving jump operators that empty the upper band of the spectrum and fill the lower one. Analysis using the mean field method shows that, as a result

of dissipation, the system tends to occupy the ground state of the Hamiltonian, the so-called dark state, at a rate that does not depend on the system size.

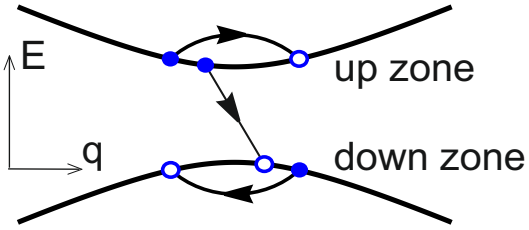

Figure 1: Action of jump operators: redistribution of particles within one zone, or moving them from top to bottom.

In the paper [3] that followed, the question of what happens beyond the mean field approximation was investigated. In this work, an analysis of vertex corrections in the diagramatics of the Keldysh formalism was carried out and the presence of a diffusion regime in the dynamics of particle and hole density modes was shown. Also, recombination of particles from the upper zone with holes in the lower one was described in the second order in particle density deviation from the dark state filling, and pumping from bottom to top was detected in the second order in the dissipation constant. These two effects of interband transitions, combined with diffusion, lead to a description of the particle density in terms of the Fisher-Kolmogorov-Petrovsky-Piskunov (FCP) equation, and also indicate the instability of the dark state.

Our work is devoted to a more rigorous description of the diffusion regime in the presented fermionic system. Using the Keldysh formalism, the ladder diagram for the diffuson is calculated and the diffusion coefficient obtained in [3] is reproduced. Further, self-energy insertions are added to this series, which in the leading order in the dissipation coefficient give a correction to the diffusion coefficient, and in the next order introduce the final mass for diffusons. This mass either confirms the [3] authors' prediction about the existence of pumping and dark state instability, being formally negative, or refutes it otherwise.

In addition to studying diffusion, we asked ourselves about possible physical implementations of the model under consideration and tried to derive a description of a bosonic system suitable for the role of a bath for creating the corresponding jump operators. This system must have noise with nonequilibrium correlators of a specific form and formally corresponds to the infinite temperature of the bath particles.

The work is supported by the RSF project 22-22-00641.

References

1. Victor V. Albert, Barry Bradlyn, Martin Fraas, Liang Jiang, Geometry and Response of Lindbladians, Phys. Rev. X **6**, 041031 (2016).

2. F. Tonielli, J. C. Budich, A. Altland, and S. Diehl, Topological Field Theory Far from Equilibrium, Phys. Rev. Letters **124**, 240404 (2020).

3. P. A. Nosov, D. S. Shapiro, M. Goldstein, and I. S. Burmistrov, Reaction-diffusive dynamics of number-conserving dissipative quantum state preparation, Phys. Rev. B **107**, 174312 (2023).

4. Gabriele Perfetto, Federico Carollo, Juan P. Garrahan, Igor Lesanovsky, Reaction-Limited Quantum Reaction-Diffusion Dynamics, Phys. Rev. Lett. **130**, 210402 (2023).

5. L. M. Sieberer, M. Buchhold, and S. Diehl, Keldysh field theory for driven open quantum systems, Rep. Prog. Phys. **79**, 096001 (2016).

6. Alex Kamenev, Alex Levchenko, Keldysh technique and non-linear sigma-model: basic principles and applications, Advances in Physics **58**, 197 (2009).

7. Qinghong Yang, Yi Zuo, Dong E. Liu, Keldysh Nonlinear Sigma Model for a Free-Fermion Gas under Continuous Measurements, arXiv:2207.03376 (2023).

8. Michele Fava, Lorenzo Piroli, Tobias Swann, Denis Bernard, Adam Nahum, Non-linear sigma models for monitored dynamics of free fermions, arXiv:2302.12820 (2023).

9. Igor Poboiko, Paul Pöpperl, Igor V. Gornyi, Alexander D. Mirlin, Theory of free fermions under random projective measurements, arXiv:2304.03138 (2023).

Nonlinear thermo-optical effects in a system of coupled optical microresonators

M.P. Marisova[1], A.V. Andrianov[2], E.A. Anashkina[3]

[1,2,3]A.V. Gaponov-Grekhov Institute of Applied Physics of the Russian Academy of Sciences

[1]marisova.mariya@rambler.ru, [2]andrian@ipfran.ru, [3]elena.anashkina@ipfran.ru

Abstract

We theoretically studied nonlinear thermo-optic effects in a system of two coupled silica glass microresonators with whispering gallery modes (WGMs). The steady-state stability map and the intracavity powers were obtained as a function of the system parameters. It was found that, contrary to the case of a single nonlinear resonator, up to 9 steady-state solutions are possible for a given parameter set, and that not more than 4 of them are stable. For sufficient pump powers, one of the symmetric solutions becomes unstable and the system is expected to switch to a stable asymmetric solution.

Key words: whispering-gallery mode, coupled microresonators, thermo-optic nonlinearity

Introduction

Optical microresonators with whispering-gallery modes (WGMs) have been extensively studied in the recent years. Their unique features, namely, ultra-high quality factors and field localization, make them a convenient platform for the study of various photonic phenomena. Although the majority of the research is related to studies of a single microresonator, several unique effects have been observed in systems of coupled microresonators, for example, PT-symmetry breaking and coupled-resonator-induced transparency. The use of coupled optical microcavities with WGMs was proposed for synchronized generation of optical frequency combs, measurements with enhanced precision, construction of optical delay lines, as well as for various laser applications [1].

Thermal effects usually play significant role in the performance of WGM-based devices, as the value of thermally-induced resonance frequency shift may be several magnitudes larger than the resonance linewidth. This work is dedicated to the study of nonlinear thermo-optical effects in a system of two coupled silica glass WGM microresonators.

Main text

The considered system of microresonators is shown schematically in Fig. 1a; for simplicity, we assume that the interacting fundamental WGMs have the same structure. As the circulating optical power in each of the microresonators $P_{1,2}$ is partially absorbed, resonator temperatures $T_{1,2}$ rise. This shifts partial WGM frequencies $\omega_{1,2}$ due to the effect of thermal expansion and the thermo-optic effect (dn/dT), which causes changes in the refractive index n. The variations in partial WGM frequencies lead to redistribution of optical power across the modes, thus creating the thermo-optical nonlinearity in the system. It is important to note that for a stable-state problem this nonlinearity is analogous to Kerr nonlinearity.

To study the nonlinear thermo-optical effects in the considered system we used coupled-mode theory (CMT) equations combined with heat equations for $\Delta T_{1,2}$ [2]. The thermo-optical characteristics of the microresonators ($d\omega_{1,2}/dT_{1,2}$, temperature relaxation time) were calculated according to the previously developed and experimentally verified numerical and analytical models [3]. The linear characteristics of the coupled modes (WGM frequencies, WGM coupling

coefficient κ and taper coupling characteristics) were obtained numerically using a specially developed finite-element model. Only stable-state solutions were considered.

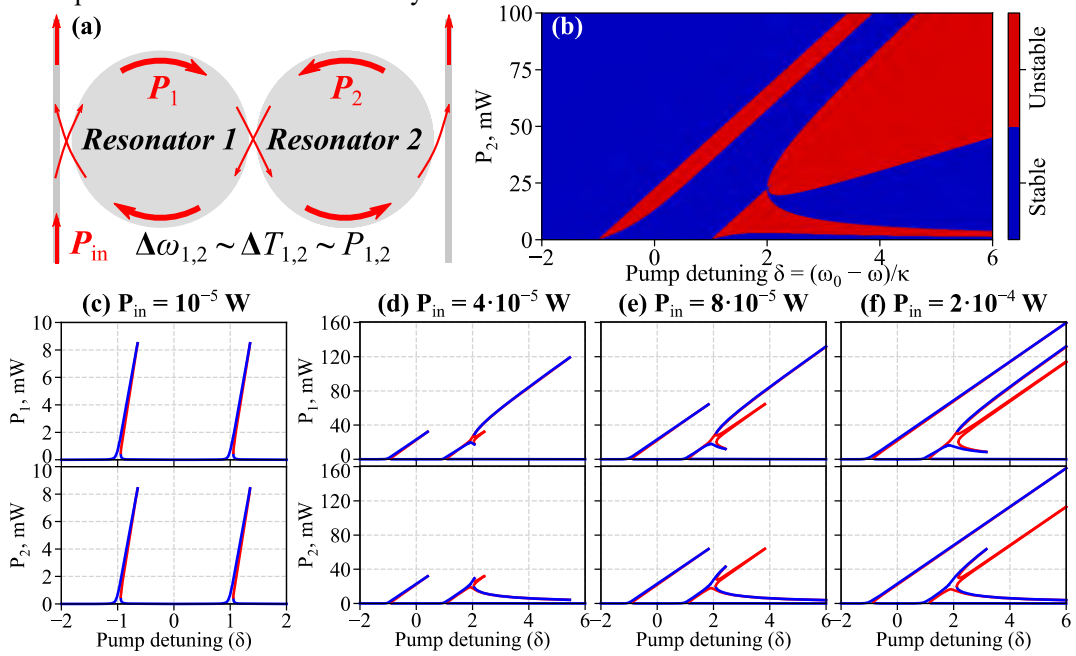

Figure 1: (a) Schematic of the considered system of coupled microresonators. Resonator diameters are ~50 μm. Red arrows show light propagation direction. (b) Stability map of the system of coupled microresonators with thermo-optical nonlinearity. (c–f) Calculated stable-state intracavity powers as a function of pump detuning for different input powers. Color legend is the same for (b–f).

The calculation results are shown in Figs. 1b–f. It was found that up to 9 stationary states are possible, and that the number of stable states cannot exceed 4. This behavior differs drastically from the case of a single nonlinear resonator, where up to 3 stationary states are possible, with 1 or 2 of them being stable. Fig. 1b shows the calculated stability map of the system. Figs. 1c–f illustrate the intracavity powers for various pump power P_{in}. For small P_{in} (Fig. 1c), the dependencies are similar to the case of a single nonlinear resonator, and the power distribution across the WGMs is symmetric. With the increase in P_{in} (Fig. 1d–f), one of the symmetric solutions becomes completely unstable, and the system is forced to switch to one of the two new asymmetric stable solutions. We also investigated the role of a small frequency detuning between the WGMs, which can be controlled externally, for example, via the thermo-optic effect.

References

1. Y. Li et al., Whispering gallery mode hybridization in photonic molecules, Laser Photonics Rev. **11**, 1600278, (2017).
2. C. Huang et al., Dynamic nonlinear thermal optical effects in coupled ring resonators, AIP Adv. **2**, 032131, (2012).
3. A.V. Andrianov et al., Thermo-Optical Sensitivity of Whispering Gallery Modes in As2S3 Chalcogenide Glass Microresonators, Sensors. **22**, 4636, (2022).

Ultracold rotating molecules inside the Rydberg atom

G. Adamyan[1], A. Volosnev[2], M. Lemeshko[2]

[1] Moscow Institute of Physics and Technology, Russia

[3] Institute of Science and Technology Austria, Klosterneuburg, Austria

[1] adamian.gg@phystech.edu

Abstract

In the process of studying the behavior of ultracold molecules inside the Rydberg atom (RA), a phenomenon similar to the Rydberg blockade was discovered. So called, Rydberg-molecular blockade consists in the fact that when molecules are found inside an atom, the energy levels of the Rydberg states are shifted and thereby removed from resonance. In such a system were investigated the different regimes of interaction with light.

Key words: Rydberg atoms, Rydberg blocckade, ultracold molecules

Introduction

Due to molecule inside the RA, the its spectrum slightly changed. This means that the energy required to excite the eigenstates is tuned out.

This effects depends on molecule's coordinates. Qualitatively speaking, the stronger the interaction between RA and molecule, the stronger the expansion of energy levels. On the Fig. 1 there are shifting of energy for 98D and 99P Rydberg's and P and D molecule's resonant states.

Thus, we could excite with specific frequency of light systems with a certain position of the molecule. It is something like Rydberg blockade when we block the excitement with non-resonant molecular position.

Main text

Our Hamiltonian with interaction with light after rotating-wave approximation is writes as

$$\hat{\mathcal{H}} = \hat{V}_{\text{opt}} + \hat{\mathcal{H}}_0 = \Delta \hat{a}_g^\dagger \hat{a}_g + \Omega_R \hat{a}_g \hat{a}_R^\dagger + \Omega_R^* \hat{a}_g^\dagger \hat{a}_R + \sum_{i=1}^{N} (J_i \hat{a}_R \hat{a}_i^\dagger + J_i^* \hat{a}_R^\dagger \hat{a}_i) \qquad (1)$$

and in matrix form

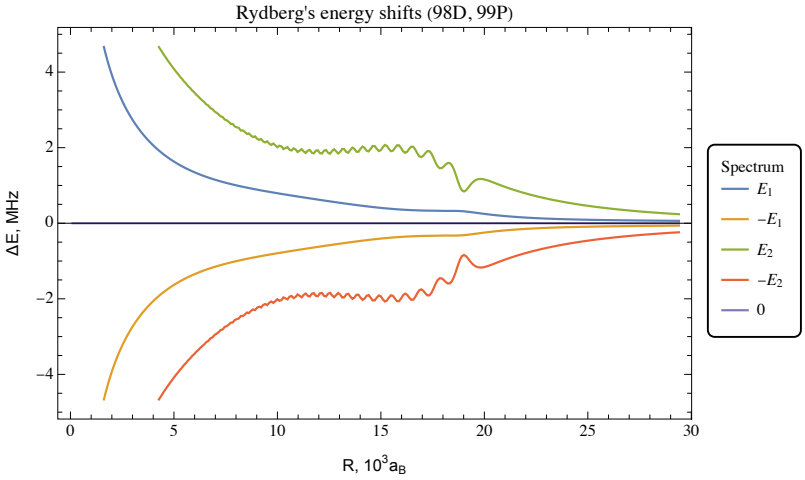

Figure 1: Energy spectrum for the Rydberg atom with a single molecule located at the position R.

$$\hat{\mathcal{H}} = \begin{pmatrix} \Delta & \Omega_R^* & & 0 & ... & 0 \\ \Omega_R & 0 & J_1^* & J_2^* & ... & J_N^* \\ 0 & J_1 & 0 & 0 & ... & 0 \\ 0 & J_2 & 0 & 0 & ... & 0 \\ ... & ... & ... & ... & ... & ... \\ 0 & J_N & 0 & 0 & ... & 0 \end{pmatrix} \tag{2}$$

where $\Delta = \hbar\omega - E_{Rg}$ is detuning the frequency of the electric field relative to the gap between excited $|R\rangle$ and ground $|g\rangle$ Rydberg's states.

Then analyze the case $\Omega_R \ll J_i$ when optical interaction is just perturbation. After diagonalization of the system "Rydberg+molecules" we have states

$$\begin{cases} |\psi_\pm\rangle = \frac{1}{\sqrt{2}} \left(\pm |R\rangle |0\rangle + \sum\limits_{m=1}^{N} j_m |r\rangle |m\rangle \right), & E_\pm = \pm J_0 \\ |\psi_m\rangle = \frac{1}{\sqrt{|j_1|^2 + |j_m|^2}} \left(j_1 |r\rangle |m\rangle - j_m |r\rangle |1\rangle \right), & E_m = 0 \end{cases} \tag{3}$$

.

If we want to excite states $|\psi_\pm\rangle$, we have to fulfill resonance condition $E_{Rg} \pm J_0 = \hbar\omega$ ($\Delta = \pm J_0$). Then the wave function will be depends from time as

$$|\psi_\pm(t)\rangle = \cos\left(\frac{|\Omega_R|}{\sqrt{2}} t\right) |g\rangle - i \sin\left(\frac{|\Omega_R|}{\sqrt{2}} t\right) |\psi_\pm\rangle \tag{4}$$

But what about $|\psi_m\rangle$ states? Because of matrix element $\langle\psi_m| V_{opt} |g\rangle = 0$ (since $\langle\psi_m|$ does not contain a component of non-excited molecules), then there are no

transitions in this states in first order of perturbation theory. This is actually the Rydberg-molecular blockade. The molecules push Rydberg's energy levels apart and allow states to be excited when the light frequency is tuned to $\Delta = \pm J_0$. Thus, if light's frequency is $\hbar\omega = E_{Rg}$ and there are molecules inside the RA, then there will be no significant excitations and dynamics.

References

[1] González-Férez, R., Sadeghpour, H. and Schmelcher, P., 2015. Rotational hybridization, and control of alignment and orientation in triatomic ultralong-range Rydberg molecules. New Journal of Physics, 17(1), p.013021.

Self-organization of charged particles in lateral potentials with a high symmetry

R. Nazmitdinov

Joint Institute for Nuclear Research, Dubna, Russia

rashid@theor.jinr.ru,

The problem of the optimal configuration of a finite number of particles in a plane has been a difficult problem of both physics and mathematics for many centuries. Back in 1611, Kepler posed the question of why a snowflake has perfect hexagonal symmetry [1]. At present, increased interest in the problem of the optimal configuration is also due to the development of nanotechnologies which make it possible to form systems of similarly charged particles confined by external potentials with a high symmetry. For example, this problem arises when analyzing the behavior of quantum vortices in a Bose condensate [2]; electrons in quantum dots [3]; and the self-organization of colloidal particles at the interface between two different liquids [4, 5].

In this communication we discuss the basic principles of self-organization of one-component charged particles, confined in disk and circular parabolic potentials. A system of equations is derived, that allows to determine equilibrium configurations for arbitrary, but finite, number of charged particles that are distributed over several rings [6,7]. The main idea is based on the cyclic symmetry and periodicity of the Coulomb interaction between particles located on several rings. Our approach reduces significantly the computational effort in minimizing the energy of equilibrium configurations and demonstrates a remarkable agreement with the values provided by molecular dynamics calculations [8]. With the increase of particle number $n \geq 180$ we find a steady formation of a centered hexagonal lattice. At the same time, the energetic preferences for nonuniform local density then favor ground states where this locally hexagonal structure is isotropic dilated and contracted throughout the structure. In fact, the equilibrium configuration is determined by the need to achieve equilibrium through the formation of a hexagonal lattice on one side and a ring-like structure on the other. This competition leads to the formation of internal defects in such systems, in contrast to the case of unlimited regions, where the ground state of the system has no defects. Finally, this structure smoothly transforms to valence circular rings in the ground state configurations for both potentials. We briefly discuss the precursors of the phase transition of the type "hexagonal lattice - hexatic phase" with the increase of a particle number in the system at zero temperature.

References

1. J. Kepler, *The Six-Cornered Snowflake* (Clarendon, Oxford, 1966).

2. H. Saarikoski, S. M. Reimann, A. Harju, and M. Manninen, Rev. Mod. Phys. **82**, 2785 (2010).

3. J. L. Birman, R. G. Nazmitdinov, and V. I. Yukalov, Phys. Rep. **526**, 1 (2013).

4. B. P. Binks and T. S. Horozov, *Colloidal Particles at Liquid Interfaces* (Cambridge Univ. Press, Cambridge, 2006).

5. M. E. Leunissen, A. van Blaaderen, A. D. Hollingsworth, M. T. Sullivan, and P. M. Chaikin, Proc. Natl. Acad. Sci. U. S. A. **104**, 2585 (2007).

6. M. Cerkaski, R. G. Nazmitdinov, and A. Puente, Phys. Rev. E **91**, 032312 (2015).

7. R. G. Nazmitdinov, A. Puente, M. Cerkaski, and M. Pons, Phys. Rev. E **95**, 042603 (2017).

8. E. G. Nikonov, R. G. Nazmitdinov, and P. I. Glukhovtsev, Journal of Surface Investigation: X-ray, Synchrotron and Neutron Techniques **17**, 235 (2023).

Double layer in asymmetric ionic liquids: molecular scale roughness effect

I. Nesterova[1,*], A. Khlyupin[1], K. Gerke[2]

[1]Moscow Institute of Physics and Technology

[2]Schmidt Institute of Physics of the Earth of Russian Academy of Sciences

[*]irina.nesterova@phystech.edu

Abstract

In this work we propose a new analytical form of the nonlinear Poisson-Fermi equation that includes additional term, describing the perturbation driven by molecular scale roughness of electrode surface. Soft repulsion induced by molecular rough surface enhances ion separation and allows to store higher values of electric charge. The presented result is beneficial for optimal design of electric double layer capacitors required for effective energy storage.

Key words: Electric Double Layer, Surface Roughness, Asymmetric Ionic Liquids.

Introduction

The formation of electric double layer (EDL) is the phenomenon underlying the work of electric double layer capacitors (EDLC), which are promising tools for energy storage. As EDL occurs near the electrode surface, the morphological characteristics of the surface impact EDL capacitance properties and its structure. While, little attention was paid to this aspect before.

We provide a new analytical solution for electrostatic characteristics of EDL to account for ion size asymmetry and roughness of electrode surface. We use results of the work by Kornyshev [1] as a reference solution without perturbation and the expression for ion distribution function from Aslyamov et al [2], which includes permitted area due to surface roughness. Then, we solve the nonlinear Poisson-Fermi equation for electrostatic potential and after can obtain expressions for: (i) cumulative charge of EDL, (ii) the potential of zero charge (PZC) and (iii) differential capacitance.

Main text

Let us consider electrode rough surface that is described by Gaussian random field $Z(x, y, z)$. Molecular interactions between solid particles of electrode and ions define

the area that is available for ions to localize. To determine this, we introduce the characteristic function $S(z) = A_{open}(z)/(A_{open}(z) + A_{solid}(z))$, which has the form of the Gauss cumulative function, that brings the character of the effective solid potential $U_{eff}(z) = -(1/\beta)\log S(z)$. In the model, we replace the exact solid potential by effective one that reflects the properties of random one and modify the free energy of ions averaged by $Z(x, y, z)$ in the same way with accuracy of $O(\beta)$ [3].

The characteristic function $S(z)$ define permitted area for a non-size particles on each level z. But for particles with size this available area become smaller depending on its size $S(z - \xi(d))$. It is included into ion charge distribution function as a factor (see Eq.(6) from [2]). To obtain the total ion charge distribution, we use $S_2(z) = S_1(z) - \Phi(z)$, then ion charge distribution has the form:

$$\rho(z) = -2ec_0 S_1(z)\frac{\sinh(\beta e\phi)}{1 + \sum_i \gamma_i \left[e^{-Z_i\beta e\phi} - 1\right]} + ec_0\Phi(z)\frac{e^{\beta e\phi}}{1 + \sum_i \gamma_i \left[e^{-Z_i\beta e\phi} - 1\right]} \quad (1)$$

with two terms in r.h.s.: the main term and the perturbation term.

Substituting Eq.1 into Poisson equation, turning to dimensionless variables ($u = \beta e\phi, x = z/L_D$), and considering the solution in the form: $u = u_0 + \mu u_1$, where $\mu = \Delta/\sigma \ll 1$, we obtain the following system for perturbation:

$$\begin{cases} \Delta u_1 = \left.\frac{\partial f}{\partial u}\right|_{u_0} u_1 & -\frac{1}{2}\tilde{g}(x)e^{u_0} \\ u_1|_{x=0} = 0, & u_1|_{x\to\infty} = 0 \end{cases} \quad (2)$$

here, f is the r.h.s in the equation in the system for u_0, u_0 is taken from Eq.16 in the work [1], and $\Phi(x) = \mu g(x)$.

The system for perturbation includes screened Poisson equation that can be solved using the Green function. But here, due to boundary conditions, we use the "method of images" to find the Green function. Then, the solution for electrostatic potential perturbation u_1 expresses as:

$$u_1(x) = \frac{1}{4\lambda}\int_0^\infty \tilde{g}(x_0)e^{u_0(x_0)}\left[e^{-\lambda|x-x_0|} - e^{-\lambda|x+x_0|}\right]dx_0 \quad (3)$$

References

1. Kornyshev A. A. Double-layer in ionic liquids: paradigm change? //The Journal of Physical Chemistry B. – 2007. – Т. 111. – №. 20. – С. 5545-5557.

2. Aslyamov T., Sinkov K., Akhatov I. Electrolyte structure near electrodes with molecular-size roughness //Physical Review E. – 2021. – Т. 103. – №. 6. – С. L060102.

3. Khlyupin A., Aslyamov T. Random process theory approach to geometric heterogeneous surfaces: Effective fluid–solid interaction //Journal of Statistical Physics. – 2017. – Т. 167. – №. 6. – С. 1519-1545.

Helical Aharonov-Bohm Interferometers: Shot Noise and Conductance

R. Niyazov[1], D. Aristov[2], V. Kachorovskii[3]

[1,2]NRC "Kurchatov Institute", Petersburg Nuclear Physics Institute

[2,3]Ioffe Institute

[1]niyazov_ra@pnpi.nrcki.ru

Abstract

We study Aharonov-Bohm interferometers based on helical edge state. The conductance and the shot noise were calculated. We demonstrate that interference effects survive in a relatively high-temperature regime. There are periodic antiresonances in the observable quantities as a function of magnetic flux. Their magnitude is greater for the shot noise than for the conductance. Remarkably, the interference in shot noise remains even in the absence of a magnetic impurity, which is not the case for conductance.

Key words: helical edge states, Aharonov-Bohm interferometers, shot noise

Introduction

Great attention is paid to the study of two-dimensional topological insulators (2D TIs) [1]. They are insulators in the bulk, but conducting helical electronic states may exist at the edge. Due to this, 2D TIs are naturally quantum electronic interferometers if metal electrodes are attached to them (see Fig. 1 (a)). In this case, there is no scattering of electrons at the points of their contact, and backscattering occurs only in the presence of a magnetic defect at the edge. Observables in such systems can be controlled due to Aharonov-Bohm (AB) effect: they periodically depend on the magnetic flux piercing the area encompassed by the electronic states.

Early, the conductance of helical AB interferometer was studied [2]. At the same time, there is another observable quantity – shot noise. Shot noise is a consequence of the discreteness of the charge carrier and is expressed in terms of the standard deviation of the current. Its measurement can be used to obtain information not available from conductance measurements: to determine the charge and statistics of current carriers and the internal energy scales of the system [3]. One can explore the Fano factor, F, which is the ratio of the shot noise and the Schottky noise value. For example, the value $F = 1/3$ is universal for a diffusion conductor. It does not depend on the conductor's shape, length, and conductance.

Experimental measurement of the Fano factor for the edge states of 2D TI gives the value F=0.29, which still does not have a good enough explanation [4]. As far as

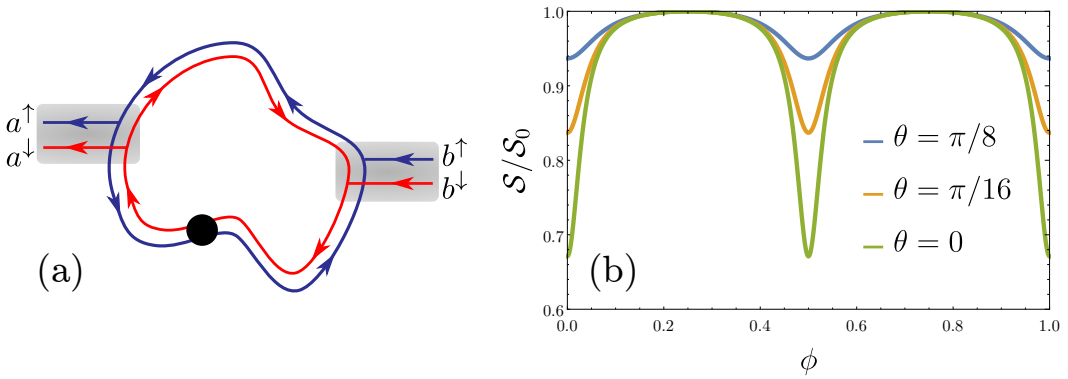

Figure 1: (a) Helical Aharonov-Bohm interferometer. The black dot denotes the magnetic impurity. The gray area represents the electrodes. (b) Dependence of shot noise on magnetic flux at different strengths of scattering by a magnetic impurity.

we know, measurements of the dependence of the shot noise on the magnetic field in such systems and their theoretical estimates have not been carried out. In the next section, we will calculate the shot noise.

Shot noise and conductance

Shot noise is associated with fluctuations in the electric current relative to its average value $\delta\hat{I}(t) = \hat{I}(t) - \langle\hat{I}\rangle$. The noise-related current correlation function is defined as follows $S(t-t') = \frac{1}{2}\langle\delta\hat{I}(t)\,\delta\hat{I}(t') + \delta\hat{I}(t')\,\delta\hat{I}(t)\rangle$. Its Fourier transform yields an expression for the noise power. Of all the contributions to noise, we are interested in the contribution associated with the discreteness of charge carriers – the shot noise. To extract it, we need to consider the case of zero frequency at a temperature much less applied voltage. Then only the shot noise remains in the expression for the noise power. For two-terminal devices, it can be expressed as [3]

$$\mathcal{S} = \frac{2e^2}{h}\int_{E_F}^{E_F+eV} d\varepsilon\, T(\varepsilon)\,(1 - T(\varepsilon))\ , \tag{1}$$

here $T(\varepsilon) = \frac{1}{2}Tr\left[\hat{t}\hat{t}^{\dagger}\right]$ is the energy-dependent transmission coefficient which is related to the transfer matrix, $\hat{t}$. The conductance can be calculated as $G = \frac{2e^2}{h}\int d\varepsilon\, T(\varepsilon)$.

The transfer matrix of the helical AB interferometer, $\hat{a} = \hat{t}\hat{b}$ (see Fig. 1 (a)), has a rather complicated expression [5] and is proportional to

$$\hat{t}(k,\phi) \propto \begin{pmatrix} 0 & 0 \\ 0 & \cos\theta \end{pmatrix} + \sum_{\alpha=\pm}\frac{1 + \alpha\hat{H}(k,\phi)}{1 - t^2 e^{i(kL+\alpha 2\pi\phi_0)}}\ .$$

Here, $\cos(2\pi\phi_0) = \cos\theta\cos(2\pi\phi)$, θ is the scattering strength of electrons on the magnetic impurity ($\theta = 0$: no scattering, $\theta = \pi/2$: a case of a strong magnetic impurity, all electrons are backscattered on it), ϕ is the magnetic flux penetrating the system in units of a magnetic flux quantum, t is the transmission amplitude of contact inside the ring, k is the wave vector of the electron and L is the length of the "ring".

An exact expression for shot noise (1) can be obtained in the limit of a sufficiently large temperature when many levels are involved in the transport: $eV \gg T \gg \Delta$, Δ is the energy spacing in the "ring". However, it is rather cumbersome. The dependence of the obtained expression on the magnetic flux is shown in Fig. 1 (b). It is normalized to $\mathcal{S}_0 = \mathcal{S}(\phi = 1/4)$. There are antiresonances For integer and half-integer values ϕ. Their depth increases with a decrease of θ and can reach several tens of percent of the $\mathcal{S}$ value far from half-integer values. This differs significantly from the conductance behavior in such systems. There are no interference effects in the conductance without a magnetic impurity, and the depth of antiresonances reaches no more than a few percent [2].

This can be seen for the expressions for the shot noise and the conductance near antiresonances ($\delta\phi = \frac{n}{2} + \delta\phi \ll 1$) for small values of scattering by the magnetic impurity ($\theta \ll 1$) and low transparency contacts ($t = e^{-\lambda},\ \lambda \ll 1$):

$$\mathcal{S}/\mathcal{S}_0 \ = 1 - \frac{\frac{4}{3}\lambda^2}{4\left(\pi^2\delta\phi^2 + \lambda^2\right) + \theta^2}\,, \quad G/G_0 = 1 - \frac{\theta^2\lambda^2}{4\left(\pi^2\delta\phi^2 + \lambda^2\right) + \theta^2}\,.$$

As the scattering force on the magnetic impurity increases, the interference effects decrease, and for $\theta = \pi/2$, the normalized shot noise and conductance are equal to 1.

Acknowledgment

The study was partly funded by the Russian Federation President Grant No. MK-2918.2022.1.2 (R.N.). The Russian Science Foundation funded the work of D.A. and V.K., Grant No. 20-12-00147-П.

References

1. B. Bernevig and T. Hughes, *Topological Insulators and Topological Superconductors* (Princeton University Press, 2013).

2. R. Niyazov, D. Aristov and V. Kachorovskii, Phys. Rev. B **98**, 045418 (2018).

3. Ya. M. Blanter and M. Büttiker, Phys. Rep. **336**, 1 (2000).

4. S. U. Piatrusha, L. V. Ginzburg, E. S. Tikhonov, et.al. JETP Lett. **108**, 71, (2018).

5. R. Niyazov, D. Aristov and V. Kachorovskii, npj Comp. Mat. **6**, (2020).

Mathematical models for predicting volt-ampere characteristics and heat release in high-temperature superconductors at alternating currents

K. Osipov[1]

[1]Central Institute of Aviation Motors named after P.I. Baranov

[1]kaosipov@ciam.ru

Abstract

Transient processes in superconductors that occur when a key switch is closed in an electric circuit at direct current, as well as processes with a harmonic change in the electromotive force of a current supply, are considered. To describe transient processes, the paper presents an equivalent electrical circuit of superconductors in accordance with a two-fluid model. Inertial inductances for superconducting and normal electrons L_s and L_n characterizing the dynamics of acceleration of various types of electrons due to the excitation of an electric field, as well as effective resistance R_n for describing energy dissipation during the excitation of normal electrons, were introduced. An equivalent electrical circuit of a high-temperature superconducting tape of the company SuperOx is developed taking into account the layering of the structure with alternating electromotive force of the current source. The vortex mass is obtained, which is determined exclusively through fundamental constants. The resulting mass of the isolated vortex far exceeds all previously known contributions to the mass by several orders of magnitude. The dependence of the vortex mass in the vortex lattice on the magnitude of the magnetic field relative to the second critical magnetic field in the superconductor is also obtained.

Key words: Superconductivity, high-temperature superconductivity, two-fluid model, normal electrons, superconducting electrons, inertial inductances for superconducting and normal electrons, Abrikosov vortex mass, Ginzburg-Landau equations, penetration depth of the magnetic field, equivalent electrical scheme of high-temperature superconducting tapes.

Introduction

Globally, the task is set in such a way that theoretically, from the first physical principles, to predict the volt-ampere characteristics and heat generation in high-temperature superconducting (HTS) tapes under variable conditions (currents and external fields). The potential solution to this problem has not only fundamental, but also practical use, since it will theoretically predict the characteristics of electric motors and electric generators using HTS-technologies (efficiency, electromagnetic torque and power) at various temperatures (for example, liquid nitrogen – 77 [K] or liquid hydrogen 20 [K]), magnetic fields and frequencies. Based on this, it will be possible to assess the feasibility of using HTS tapes in electric machines in comparison with cryoconductors. The corresponding refinement of mathematical models for predicting volt-ampere charachteristics and heat generation, taking into account various effects occurring in the HTS, will allow us to follow the path of computer-aided design of materials (HTS tapes).

Mathematical models for predicting volt-ampere characteristics and heat release in HTS at alternating currents

The paper presents an equivalent electrical scheme of superconductors in accordance with a two-fluid model for both alternating and direct currents, taking into account the transient process (oscillatory and aperiodic) when the key switch is closed (or opened) in an electrical circuit. To describe transient effects in superconductors, some macroscopic parameters were introduced for the first time in the branches for normal and superconducting currents – inertial inductances L_n and L_s for normal and superconducting electrons, respectively, as well as effective resistance R_n to describe energy dissipation during excitation of normal electrons. The main physical meaning of the introduced inertial inductances L_n and L_s is that they reflect the dynamics of acceleration of two types of electrons under the action of alternating electric fields in a superconductor.

The parameters L_n and L_s were determined by comparing the macroscopic equations for the entire electrical circuit with the microscopic equations of motion of normal and superconducting electrons. It is found that the inertial inductances are determined by the fractions of the concentrations of normal α_n and superconducting electrons α_s, as well as by the square of the penetration depth of the magnetic field into the superconductor λ_L^2.

This approach makes it possible to determine the dependences of superconducting and normal currents, as well as electric fields on time, frequency, temperature and other parameters of the electrical circuit under consideration. Knowing the currents and electric fields, it is possible to estimate the heat release in the volume of a superconductor when normal electrons are excited at alternating current. It is also possible to evaluate the influence of temperature and frequency of alternating current on heat generation.

In this paper, an equivalent electrical circuit of a high-temperature superconducting tape of the company SuperOx is developed taking into account the layering of the structure with alternating electromotive force of the current source. When currents are excited in different layers, energy dissipation occurs, therefore the thermal conductivity equations for each individual layer were solved simultaneously with the addition of source terms.

An integro-differential equation is derived for the penetration of a magnetic field into a superconductor with an arbitrary change in the external magnetic field, taking into account the excitation of normal electrons under the action of an induced vortex electrical field. With a sinusoidal change of the magnetic field or transport current a modified London equation for the magnetic field in a superconductor is obtained. The dependence of the penetration depth of the magnetic field into the superconductor λ_ω^2 on the external frequency and concentration of normal electrons is also obtained.

To consider non-stationary processes in a vortex state, it is necessary to solve the non-stationary equation for the motion of the Abrikosov vortex. It is necessary to determine the mass of the vortex per unit length. The problem of determining the mass of a vortex has a long history, starting with the theoretical work of 1965. The most optimistic calculations for estimating the magnitude of the vortex mass do not exceed 10^{-20} g/cm. It is possible to outline the main contributions to the vortex mass proposed theoretically in earlier works: mass of the core $\mu_{\text{core}} = \frac{3}{8\pi}\frac{\Phi_0}{\upsilon_F^2}\frac{H_{c1}}{\ln\kappa} \approx 3\times10^{-22}$ g/cm; electromagnetic mass $\mu_{\text{em}} = \frac{\Phi_0}{16\pi c^2}H_{c2} \approx 10^{-26}$ g/cm; mass due to deformation of the vortex core zone $\mu_{\text{defl}} \approx \pi\rho\xi^2\gamma^2 \approx 10^{-24}$ g/cm; dynamic mass $\mu_{\text{dyn}} \approx 10^{-21}$ g/cm; mass associated with a backflow having a hydrodynamic nature. It can be seen that these contributions to the vortex mass do not exceed the value of 10^{-21} g/cm.

In this paper, the mass of the Abrikosov vortex (both as a single vortex and as part of a

vortex lattice) is obtained, which is determined exclusively through fundamental constants. The resulting mass of the isolated vortex far exceeds all previously mentioned contributions to the mass by several orders of magnitude. The obtained estimates of the vortex masses are in accordance with the experimental results. The dependence of the vortex mass in the vortex lattice on the magnitude of the magnetic field relative to the second critical magnetic field in the superconductor is also obtained. The introduced mass of the vortex makes it possible to solve a full non-stationary equation of its motion, which makes it possible to obtain non-stationary characteristics under variable conditions.

The paper considers the resistive regime in type II superconductors at alternating currents. Nonstationary volt-ampere characteristics are obtained, which corresponds to the nonstationary flow regime in superconductors. To construct an equivalent electrical circuit of a type II superconductor in a vortex state (in the presence of an external magnetic field), an effective resistance R_v is introduced at alternating currents to describe energy dissipation due to the viscous motion of the vortex lattice. Vortex inductance L_v is also introduced due to the fact that the vortex lattice has its inertial characteristics under the influence of the alternating Lorentz force.

In the case when the Lorentz force acting on the Abrikosov vortices from the transport current is variable (due to the alternating electromotive force of the current source), the resistive response acquires an imaginary component due to the introduction of the vortex mass to the motion equations and the presence of pinning forces. For this reason, the study of the dependence of the complex resistive response (impedance $Z(\omega)$) will allow us to extract significant information about the pinning forces.

In this work a complex resistance $Z(\omega)$ is obtained for viscous motion of vortices that make small oscillations and are in the pinning potential. The depinning frequency at which the complex impedance becomes active is obtained. The study of harmonic oscillations of pinned vortices makes it possible to extract information about the pinning potential without overheating of superconducting materials at direct current. The results on the frequency of depinning, previously obtained by other researchers, are incorrect due to the fact that the vortex mass was not introduced into the equations of motion of vortices.

Since the oscillations of the transport current and, accordingly, vortices are in the radio frequency and microwave ranges, it is necessary to take into account radiation friction due to energy radiation in the equations of vortex motion. Taking into account the term describing radiation dissipation, corrections are made to the decay coefficients 2γ and viscosity of vortices η depending on the external frequency.

The processes of vortex motion on a constant subcritical transport current with a small amplitude of the variable component of the current are also considered. Oscillations under the action of a small variable external Lorentz force in the vicinity of a shifted equilibrium point in the pinning potential (due to the action of a constant component of the Lorentz force) are considered, the depinning frequency is obtained. The obtained equations allow us to determine the pinning potential depending on the coordinate according to a certain algorithm.

The classical Maxwell equations are generalized taking into account the anisotropic properties of superconductors in the Meissner state through the Levi-Civita pseudotensor. The agreement of the derived equations with the phenomenological Ginzburg-Landau equations for the anisotropic case during the transition to the "classics" is obtained. A second-rank tensor is introduced for the square of the penetration depth of the magnetic field.

Instanton effects in spin quantum Hall effect

M. V. Parfenov[1,*], **I. S. Burmistrov**[1]
[1] *L. D. Landau Institute for Theoretical Physics, Semenova 1-a, 142432, Chernogolovka, Russia*
*email: *maksimqwery@gmail.com*

Recently, studing of criticality in quantum systems has attracted a great interest. There are some theoretical evidences of SQHE in two dimensional superconducting system with $d_{x^2-y^2} + id_{xy}$ pairing [1]. In this study we develop the theory of the spin quantum Hall transition, using the generalization of Pruisken replica NLσM with θ-term [2] on superconducting class C [3,4]. Using NLσM action, we show presence of the non-trivial topological configurations of Q-matrix field, called instantons. To find the analytical form of such configurations with topological charge equals to one, we construct solutions of self-duality (anti-self-duality) equations, using the symmetries of target coset space $G/K = \mathrm{Sp}(2N)/\mathrm{U}(N)$. In Gaussian approximation we find action for small fluctuactions around the instanton. We find whole instanton manifold and identify eight instanton eigenparameters as zero modes of kinetic operators for fluctuations. Our aim is to compute instanton contribution to the partition function, density of states, longitudinal and transverse spin conductivities. This work was supported by the Russian Science Foundation (Grant No. 22-42-04416)

Bibliography

[1] Senthil, T., and M. P. A. Fisher, Phys. Rev. B 60 (1999)

[2] A. M. M. Pruisken, Nucl. Phys. B 285, 719 (1987).

[3] Ferdinand Evers and Alexander D. Mirlin "Anderson transitions". Rev. Mod. Phys. 80 (2008)

[4] Babkin, S. S., and I. S. Burmistrov, Physical Review B 106.12 (2022).

HfF^+ spin-rotational Hamiltonian for eEDM search

Alexander N. Petrov [1,2], Leonid V. Skripnikov [1,2], Anatoly V. Titov [1,2]

[1]NRC "Kurchatov Institute" - PNPI, RUSSIA

[2]Saint Petersburg State University, RUSSIA

petrov_an@pnpi.nrcki.ru

Abstract

The current limit on the electron electric dipole moment (eEDM), $|d_{\rm e}| < 4.1 \times 10^{-30}$ e·cm was recently established using the trapped $^{180}Hf^{19}F^+$ molecular ions [T. S. Roussy, L. Caldwell, T. Wright, et al., arxiv:2212.11841]. We developed theoretical approaches which can fully reproduce the latest experimental data. The excellent agreement between theory and experiment is very important for the examination of modern molecular theory as well as experimental data and understanding of possible systematic uncertainties in the experiment.

Key words: New physics, electron electric dipole moment

Introduction

The non-zero electron electric dipole moment (eEDM, $d_{\rm e}$) value measured at the level of the current experimental sensitivity would be a clear signature of the physics beyond the Standard model (SM) [1]. Recently the JILA group has obtained a new constraint on the electron electric dipole moment (eEDM), $|d_{\rm e}| < 4.1 \times 10^{-30}$ e·cm (90% confidence) [2], using the $^{180}Hf^{19}F^+$ ions trapped by the rotating electric field. It further improves the latest ACME collaboration result obtained in 2018, $|d_e| \lesssim 1.1 \cdot 10^{-29}$ $e \cdot$ cm [3], by a factor of 2.4 and the first result $|d_{\rm e}| \lesssim 1.3 \times 10^{-28}$ on the $^{180}Hf^{19}F^+$ ions [4] by a factor of about 32.

1. Level scheme of $^{180}Hf^{19}F^+$ for the electron EDM search

The energy splitting, f, between the sublevels $m_F = \pm 3/2$ (projection of the total momentum) is measured in the experiments. The measurement of f is repeated under different conditions which can be characterized by binary switch parameters such as $\tilde{\mathcal{B}}$, $\tilde{\mathcal{D}}$, $\tilde{\mathcal{R}}$ being switched from $+1$ to -1. $\tilde{\mathcal{B}} = +1(-1)$ means that the rotating magnetic field, $\mathbf{B}_{\rm rot}$, is parallel (antiparallel) to the rotating electric field $\mathbf{E}_{\rm rot}$; $\tilde{\mathcal{D}} = +1(-1)$ means that the measurement was performed for lower (upper) Stark level; and $\tilde{\mathcal{R}}$ defines direction for the rotation of the fields. Let $f^{S_1,S_2\cdots}$ be a component of f which is odd under the switches $S_1, S_2, ...$ Then the eEDM signal manifests as the main

contribution to $f^{\mathcal{BD}}$ channel. Beyond the $f^{\mathcal{BD}}$ other components f^0 (even under all switches), $f^{\mathcal{D}}$, $f^{\mathcal{B}}$ are measured with high accuracy [2, 5], which, in particular, is required to control a number of systematic effects. As a matter of fact, all the components are measured with the same scheme but with different treatment of the raw experimental data. In turn in Refs. [6, 7] the precise scheme for theoretical calculation of Stark and Zeeman effects in rotating fields was developed.

The main goal of our work [8] is to calculate parameters $f^{\mathcal{BD}}$, f^0, $f^{\mathcal{D}}$ and $f^{\mathcal{B}}$ from the *first principles* and to compare them with the experimental data.

2. Results

In Fig. 1 the calculated values of $f^{\mathcal{D}}$ as function of f^0 and in Fig. 2 $f^{\mathcal{BD}}$ as function of f^B [8] in comparision with experimental values [5] are given.

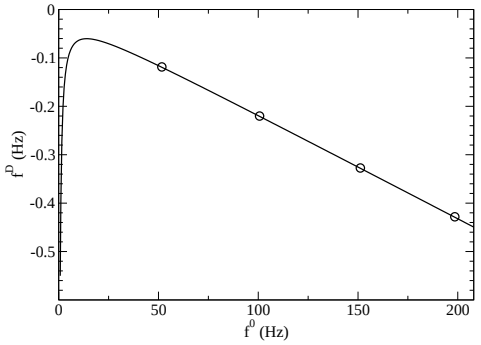

Figure 1: $f^{\mathcal{D}}$ as a function of f^0. Circles – the experimental values [5]. Solid curve - calculation [8].

The agreement between the measured and calculated values of $f^{S_1,S_2\cdots}$ is a good test for examination of possible systematic uncertainties. For example, at the first stage of the ^{180}Hf^{19}F$^+$ experiment the disagreement between calculated and measured $f^{\mathcal{D}}$ values as a function of f^0 led to a conclusion about the existence of a large (the largest, see Table II in Ref. [4]) "doublet population background" systematic error. Then it was shown in Refs. [6, 7] that the disagreement between calculation and experiment in Ref. [4] is on the level of interactions with $^3\Pi_{0^\pm}$ and $^3\Delta_2$ states which were not taken into account and new advanced scheme which included all the perturbations important for the eEDM spectroscopy was proposed. However, the previous experimental data were not accurate enough (there was only one experimental point with an error bar just on the level of the influence of the interaction with $^3\Pi_{0^\pm}$ and $^3\Delta_2$ states, see Fig. 4 in Ref. [7]) to check our method. Excellent agreement of our new calculations [8] with new highly accurate experimental data (four points) on Fig. 1 resolves the problem, declare

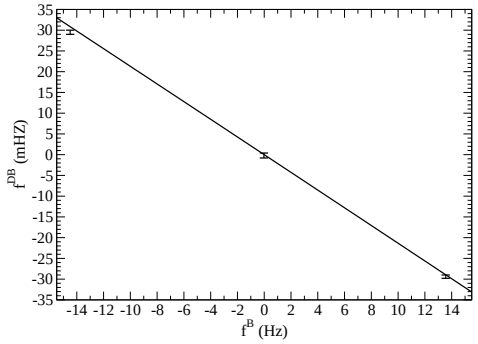

Figure 2: $f^{\mathcal{DB}}$ as a function of $f^{\mathcal{B}}$. Horizontal bands – the experimental values, bandwidths is the experimental uncertainty [5]. Solid curve - calculation [8].

the accurate theoretical tool and give prospect to control the systematics on the level of 10^{-31} e·cm and lower for the HfF^+ (and similar systems like ThF^+) experiment. Good agreement of the theory and experiment on Fig. 2 points on a reliable control of systematics related with stray magnetic field.

References

1. R. Alarcon, J. Alexander, V. Anastassopoulos, T. Aoki, R. Baartman, S. Baeßler, L. Bartoszek, D. H. Beck, F. Bedeschi, et al., arXiv:2203.08103 [hep-ph](2022).

2. T. S. Roussy, L. Caldwell, T. Wright, W. B. Cairncross, Y. Shagam, K. B. Ng, N. Schlossberger, S. Y. Park, A. Wang, J. Ye, et al., (2022), `arXiv:2212.11841`.

3. V. Andreev, D. Ang, D. DeMille, J. Doyle, G. Gabrielse, J. Haefner, N. Hutzler, Z. Lasner, C. Meisenhelder, B. O'Leary, et al., Nature **562**, 355 (2018).

4. W. B. Cairncross, D. N. Gresh, M. Grau, K. C. Cossel, T. S. Roussy, Y. Ni, Y. Zhou, J. Ye, and E. A. Cornell, Phys. Rev. Lett. **119**, 153001 (2017).

5. L. Caldwell, T. S. Roussy, T. Wright, W. B. Cairncross, Y. Shagam, K. B. Ng, N. Schlossberger, et al. (2022), URL `https://arxiv.org/abs/2212.11837`.

6. A. N. Petrov, L. V. Skripnikov, and A. V. Titov, Phys. Rev. A **96**, 022508 (2017).

7. A. N. Petrov, Phys. Rev. A **97**, 052504 (2018).

8. A. N. Petrov, L. V. Skripnikov, and A. V. Titov (2023), Phys. Rev. A, accepted, URL `https://arxiv.org/abs/2302.02856`.

Nonlinear dissipative exciton-polariton condensate dynamics

M. A. Posazhenkov[1] and N. S. Voronova[2]

[1,2]Russian Quantum Center, Skolkovo IC, 121205 Moscow, Russia

[1,2]National Research Nuclear University (Moscow Engineering Physics Institute), Moscow, 115409 Russia

[2]nsvoronova@mephi.ru

Abstract

Spatiotemporal dynamics of coherently excited exciton-polariton Bose condensate and its distortions due to nonlinearities of various nature is considered. The two-component Gross-Pitaevskii based approach allows to track both the photon-exciton Rabi oscillations and the difference between the decoherence rates of the upper and lower polaritons.

Key words: Exciton-polaritons, Rabi oscillations, differential decay.

Introduction

Exciton-polaritons are new normal modes arising in the system of excitons and photons in an optical microcavity in the strong-coupling regime, hybrid quasi-particles having the properties of light and matter. Their tendency to macroscopically occupy one quantum state makes them attractive for fundamental and applied research.

The most common way to describe this system is based on the Gross-Pitaevskii equation (GPE) for the condensate wave function of lower polaritons. Alternatively, a set of coupled GPEs for the photon and exciton condensate wave functions can be considered. Despite the success of such models in describing experimental observations, plenty of existing effects are difficult to account for. Some of these effects are added with the help of phenomenological modifications of the GPEs, but most of them bring significant nonlinearities, making the equations challenging for numerical simulation [1].

A posteriori, the upper polariton (UP) mode has the decay rate order(s) of magnitude larger than that of the lower mode (LP), which allows to describe the system with one equation for lower polaritons. This approach, however, does not track the inherent two-component nature of the polariton system and its key feature: the Rabi oscillations. At the same time, the two-component coupled GPEs for exciton and photon subsystems that combine the oscillatory dynamics with nonlinearities in space and time present a more difficult numerical task, in which the higher decay rate of upper polariton is usually ignored. In this case, however, adding the polariton decay as a simple photon leakage brings erroneous dynamics into simulations [1, 2].

Nonlinear Rabi oscillations with differential decay

In this work, we consider the spatiotemporal dynamics of the exciton-polariton Bose condensate using a modified set of two Gross-Pitaevskii-like equations:

$$i\hbar\partial_t\psi_{ph} = \left(\frac{\Delta}{2} - \frac{\hbar^2\vec{\nabla}^2}{2m_{ph}}\right)\psi_{ph} + \frac{\Omega\hbar}{2}\left(1 - \frac{|\psi_{ex}|^2}{n_{sat}}\right)\psi_{ex} - i\hat{\Gamma}_{ph}[\psi_{ph}, \psi_{ex}] + iS_{ph},$$
$$i\hbar\partial_t\psi_{ex} = \left(-\frac{\Delta}{2} - \frac{\hbar^2\vec{\nabla}^2}{2m_{ph}} + g|\psi_{ex}|^2\psi_{ex}\right)\psi_{ex} + \frac{\Omega\hbar}{2}\left(1 - \frac{|\psi_{ex}|^2}{n_{sat}}\right)\psi_{ph} - i\hat{\Gamma}_{ex}[\psi_{ph}, \psi_{ex}], \quad (1)$$

where $\psi_{ph}(\vec{r}, t)$, $\psi_{ex}(\vec{r}, t)$ are the two-dimensional condensate wave functions of photons and excitons, respectively, Δ is the energy detuning between the photon and exciton energy dispersions, $\Omega\hbar$ is the Rabi-splitting energy, g is the exciton-exciton interaction constant, n_{sat} is the density of exciton saturation, $S_{ph}(\vec{r}, t)$ represents the resonant pump which is here assumed radially symmetric and pulsed, $\hat{\Gamma}_{ph}$ and $\hat{\Gamma}_{ex}$ are the integral operators describing the polariton decay. Energy reference is taken at $(E_{ph} - E_{ex})/2$, where E_{ph} and E_{ex} are the photon and exciton energies at $k = 0$.

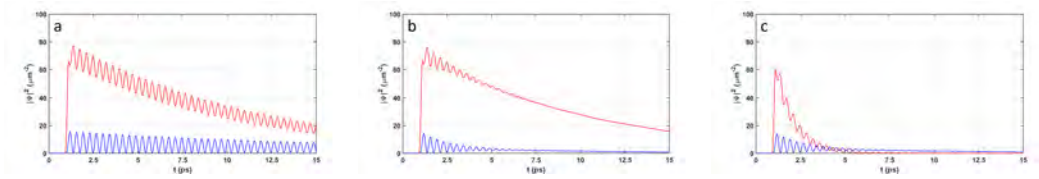

Figure 1: Numerical modeling of the exciton-polariton Rabi oscillations in the center of the spot ($r = 0$) after the excitation with a short (150 ps) resonant pulse. The red lines describe the photon density, the blue lines correspond to the exciton density. $\Omega\hbar = 5.0$ meV, $g = 1.5$ μeV μm^2. (a) $|\Delta| = 10$ meV, with the photon decay only. (b,c) $\Delta = -10$ meV and $+10$ meV, respectively, with the differential UP-LP polariton decay added to the equations.

Fig. 1 (a) shows an example of modeling such system with a constant photon decay, as it is usually done for simplicity. Eqs. (1), instead, contain the polariton decay described by integral operators that are obtained by transforming the photon and exciton wave functions into the UP-LP basis and back, in order to account for the faster decoherence of the upper mode. The examplary results of such simulations are shown in Fig. 1 (b) and (c): the decay of oscillations amplitude and the dependence of upper polariton lifetime on the detuning is clearly seen. One notes the striking difference of both the positive and the negative detuning cases with the simulations made with the photon decay only (Fig. 1 (a)).

Fig. 2 shows the Rabi oscillations in the linear regime (a,b) and with the two added nonlinearities: the exciton interaction term and the exciton saturation (c, d). As one can see, the nonlinearities make the Rabi oscillation frequency dependent on

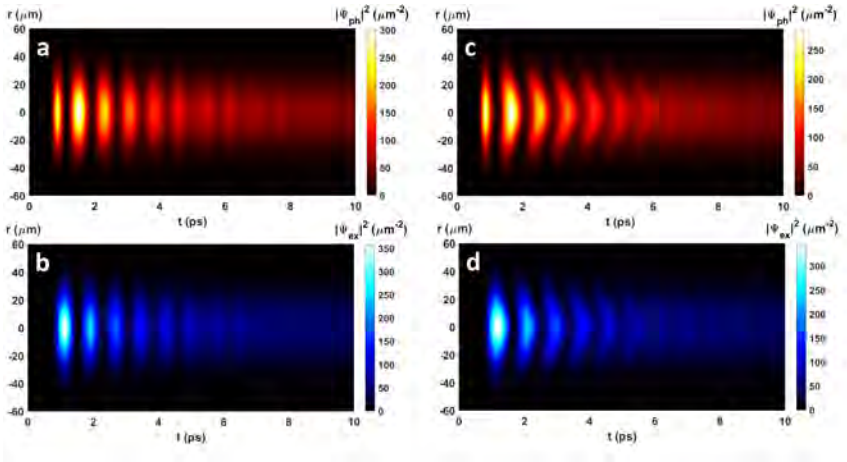

Figure 2: Numerical modeling of the exciton-polariton Rabi oscillations in space and time after the excitation by a short (150 ps) resonant Gaussian pulse. (a,b) for the linear case ($g = 0$, $n_{sat} = \infty$). (c,d) for the nonlinear case ($g = 1.5$ μeV μm^2, $n_{sat} = 1000$ μm^{-2}). $\Delta = 0$, $\Omega\hbar = 5.4$ meV.

the density, thus the oscillations in the center of the pump spot (where the densities are higher) can be retarded or accelerated, depending on the detuning.

This work is financially supported by the Russian Foundation for Basic Research within the Project No. 20–52–7816 (joint with CNR).

References

1. M. Kira, S.W. Koch, Progress in Quantum Electronics, 30, 5 (2006)

2. L. Dominici, D. Colas, S. Donati, et al., Phys. Rev. Lett. 113, 226401 (2014)

The magnetic exchange coupling to the skyrmion crystal on the electronic states of topological insulator

G. Rakhmanova[1], P. Shaban[2], I. Iorsh[3]

[1,2,3]Department of Physics, ITMO University, St. Petersburg, 197101, Russia

[3]Abrikosov Center for Theoretical Physics, MIPT, Dolgoprudnyi, Moscow Region 141701, Russia

[1]gulnaz.rahmanova@metalab.ifmo.ru,
[2]polina.shaban@metalab.ifmo.ru,[3]i.iorsh@metalab.ifmo.ru

Abstract

The effect of magnetic exchange coupling to the spatially inhomogeneous fields of a skyrmion crystal on the electronic spectrum of the surface electronic states of topological insulator was discovered. It was shown that periodic magnetic and pseudomagnetic fields leads to a nontrivial topology of the electronic bands, namely the localized topologically protected edge states appears in the band gap of energy spectrum. It was analytically demonstrated that the magnetic field created by a skyrmion crystal can be represented as an effective vector potential, which is proportional to the topological charge.

Key words: Van der Waals materials, skyrmionic crystal, spin-orbit coupling

Introduction

In recent years, the progress in nanofabrication techniques allowed to routinely stack monolayers to Van der Waals (vdW) heterostructures, combining different properties, which opened new avenues for perspective applications [1]. But for a long time no atomically thin intrinsic magnets have been realized in experiments. The first experimental realization of two-dimensional (2D) vdW magnets was reported in 2017 [2]. In addition, many 2D magnets have been reported to host non-collinear magnetic phases such as helices and skyrmions [3]. At the same time, as has been already demonstrated, interfacing vdW magnets with non-magnetic monolayers leads to the emergence of strong magnetic proximity effects in the non-magnetic material, namely the periodic magnetic and pseudo magnetic fields may lead to the non-trivial topology of the electronic band structures [4]. The magnetization of the magnetic layer acts as an effective Zeeman field for the electrons in the non-magnetic one. Here we consider the effect of magnetic exchange coupling to the spatially inhomogeneous fields of a skyrmion crystal on the electronic spectrum of the surface electronic states of

topological insulator. In the paper [5] a quantized topological Hall effect in a magnetic skyrmion crystal was discovered. Also, it has been shown that the skyrmion-induced superconductivity can exhibit nontrivial topological properties, such as Majorana fermions at the interface between the magnetic and superconducting regions [6].

Results and discussions

The system is described by the Hamiltonian:

$$\hat{H} = v[\hat{\boldsymbol{\sigma}} \times \hat{\boldsymbol{p}}]_z + \hat{\boldsymbol{\sigma}} \cdot \boldsymbol{B}(\boldsymbol{r}), \tag{1}$$

where the first term corresponds to Rashba spin-orbit coupling and the last term describes the strength of exchange coupling to the non-collinear magnetization of the skyrmionic crystal, where $\boldsymbol{B}(\boldsymbol{r})$ is periodic, space dependent magnetization of skyrmion crystal (For details see [7]).

The eigenenergy spectrum is shown in Fig. 1. The skyrmion crystal magnetization plays a role of an external potential for the conduction electrons. It is seen that at the boundaries where magnetic field of skyrmion crystal changes sign (for 2D the boundaries close into a ring) localized topologically protected edge states appear in the band gap. Our investigation focuses on a specific scenario of a skyrmion crystal, where the spacing between the skyrmions is sufficiently large, allowing magnetic field's sign changing. Specifically, we observe that over a large period, a discrete spectrum of states appears, while for shorter periods, the edge states combine into a single zone within the energy gap. This phenomenon arises due to the ability of the edge states to tunnel. Furthermore, we find that the thickness of the domain wall of the skyrmion also plays a role in the localization of the edge states. The degree of smoothness exhibited by the skyrmion directly impacts the effectiveness of localization. In other words, a smoother skyrmion results in poorer localization of the edge states. As the thickness of the domain wall increases to a significant extent, the edge state ultimately disappears.

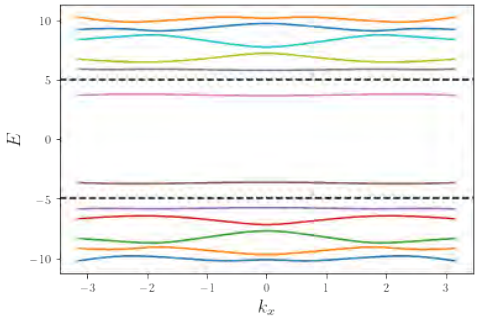

Figure 1: The dispersion of the structure. Dashed line corresponds to magnetic field amplitude, domain wall width is 0.01

We explore how the real space topological invariant of the skyrmion crystals maps to the reciprocal space topological invariants (Chern numbers) of the electronic bands. It is analytically shown that the magnetic field created by a skyrmion crystal can be represented as an effective magnetic field, which is proportional to the topological charge. We try to find such field $\boldsymbol{F}$, that

$$div\boldsymbol{F} = Q, \tag{2}$$

where Q is the topological charge density. Further, a unitary coordinate-dependent transformation was found, which makes it possible to transfer the dependence on the coordinate from the magnetic field to the vector potential in the spin-orbit part. Such a unitary transformation makes it possible to obtain constructions in the vector potential that are proportional to the topological charge. In this way, we got our introduced field $\boldsymbol{F}$ which is actually some effective field, generated by the topological charge. Thus, it was shown that periodic magnetic and pseudomagnetic fields can lead to a nontrivial topology of the electron bands.

References

1. K. Novoselov, A. Mishchenko, et. al, 2D materials and van der Waals heterostructures, Science. **353**, aac9439, (2016).

2. C. Gong, L. Li, et.al, Discovery of intrinsic ferromagnetism in two-dimensional van der Waals crystals, Nature. **546**, 265, (2017).

3. Wu Y, et al, Néel-type skyrmion in WTe2/Fe3GeTe2 van der Waals heterostructure, Nat. Commun. **11**, 3860, (2020)

4. Phong, Võ Tien and Mele, E. J., Boundary Modes from Periodic Magnetic and Pseudomagnetic Fields in Graphene, Phys. Rev. Lett. **128**, 176406 (2022)

5. Keita Hamamoto, Motohiko Ezawa, and Naoto Nagaosa, Quantized topological Hall effect in skyrmion crystal, Phys. Rev. B. **92**, 115417, (2015)

6. Kristian Mæland and Asle Sudbø, Topological Superconductivity Mediated by Skyrmionic Magnons, Phys. Rev. Lett. **130**, 156002, (2023)

7. Daniel Hill, Valeriy Slastikov, Oleg Tchernyshyov, Chiral magnetism: a geometric perspective, SciPost Phys. **10**, 078 (2021)

Renormalization group analysis of the Kardar-Parisi-Zhang model in turbulent environment

M. Reiter[1]

[1] Department of Physics, Saint Petersburg State University,
Universitetskaya nab. 7/9, St. Petersburg, 199034, Russia

[1]mikh.reiter@gmail.com

Abstract

Kinetic roughening of a randomly growing surface can be modelled by the Kardar-Parisi-Zhang equation with a time-independent ("spatially quenched" or "columnar") random noise. Field-theoretic renormalization group approach is used to investigate how randomly moving medium affects the kinetic roughening. The medium is described by the stochastic differential Navier-Stokes equation for incompressible viscous fluid with an external stirring force, which allows to consider both turbulence and a fluid in thermal equilibrium. Action functional for the full stochastic problem should be extended to be renormalizable: a new nonlinearity must be added. Moreover, in order to correctly couple the scalar and velocity fields, a new dimensionless parameter must be introduced as a factor in the covariant derivative of the scalar field. Critical indices, responsible for long - time large - scale asymptotic behavior of the correlation functions, are found in the leading order of perturbation theory (one-loop approximation).

Key words: Theoretical physics, kinetic roughening, turbulence, renormalization group

Introduction

The phenomenon of "kinetic roughening" describes the process of growth of random surfaces, in which they become increasingly "rough" with time. Flame fronts, surfaces of tumours or bacterial colonies, and landscape profiles are most notable examples of such surfaces [1]. It is important to study various growth processes and the models proposed to describe them. One such model is the Kardar-Parisi-Zang (KPZ) model, originally proposed to explain the universal scaling behavior in various physical systems [2]. The KPZ model is described by a nonlinear differential equation on the field h:

$$\partial_t h = \varkappa_0 \partial^2 h + \frac{\lambda_0}{2}(\partial h)^2 + f, \tag{1}$$

where $\partial_t = \frac{\partial}{\partial t}$, $\partial_i = \frac{\partial}{\partial x_i}$, $(\mathbf{x}, t)$ are the space-time coordinates, $i = 1, .., d$, d is the dimension of space, $\partial^2 = \partial_i \partial_i$, $(\partial h)^2 = (\partial_i h)(\partial_i h)$, $\varkappa_0 > 0$ is the coefficient of surface

tension, f is a random noise, usually assumed to be Gaussian and delta correlated in time and space.

The study of the KPZ model by field-theoretic renormalization group (RG) methods shows that there are no infrared (IR–) attractive fixed points of the RG equations, at least within the perturbation theory. For this reason, interest arises in studying various modifications of the KPZ. "Frozen" (time-independent) random noise, proposed in [3] for modeling the process of landscape erosion with correlation function of the form:

$$\langle f(x)f(x')\rangle = D_0\delta^{(d)}(x-x'), \tag{2}$$

with positive amplitude factor D_0, is considered.

Movement of the environment is also taken into account. It is important to study turbulent motion because turbulence itself is an important stochastic process. The external velocity field is described by the stochastic Navier–Stokes (NS) equation for an incompressible viscous fluid:

$$\nabla_t v_i = \nu_0\partial^2 v_i - \partial_i P + F_i. \tag{3}$$

Here P is pressure, ν_0 is kinematic viscosity coefficient, F is a random force with zero mean and pair correlator of the form

$$\langle F_i(t,\mathbf{x})F_j(t',\mathbf{x}')\rangle = \delta(t-t')\int \frac{d\mathbf{k}}{(2\pi)^d}P_{ij}(\mathbf{k})d_f(k)e^{i\mathbf{k}\cdot(\mathbf{x}-\mathbf{x}')}, \tag{4}$$

$P_{ij}(k) = \delta_{ij} - k_ik_j/k^2$ is orthogonal projector, $k = |\mathbf{k}|$ is wave number, and the function $d_f(k)$ consists of two terms (D_0, $D_0' \geq 0$) [4]:

$$d_f(k) = D_0k^{4-d-y} + D_0', \tag{5}$$

corresponding to both turbulent fluid and fluid in a thermal equilibrium. The advection by the velocity field is provided by a "minimal" replacement in the eq. (1):

$$\partial_t h \to \nabla_t h \;=\; \partial_t h \;+\; (v_i\partial_i)h. \tag{6}$$

RG analysis of the problem, results

Stochastic problem under consideration is equivalent [5] to the field theoretic model with an increased number of fields and action of the form:

$$\begin{aligned} S_h(\Phi) = \frac{1}{2}h'h' + h'\{-\partial_t h - v_i\partial_i h + \varkappa_0\partial^2 h + \frac{1}{2}\lambda_0(\partial_i h\partial_i h)\}+ \\ +v_i'\{-\partial_t v_i - v_j\partial_j v_i + \nu_0\partial^2 v_i\} + \frac{1}{2}v_i'D_F v_i'. \end{aligned} \tag{7}$$

Here, integrations over $\mathbf{x}$ and t are implied. Dimensional analysis shows that in order to ensure the renormalizability of the theory, it is necessary to add a nonlinearity

proportional to the square of the velocity field ($h'vv$) and introduce an additional parameter in the covariant derivative for the scalar field. The logarithmic dimension of the resulting theory is $d = 4$. Dimensional regularization ($\varepsilon = 4 - d$) is used. An analysis of the RG equations reveals the presence of three stability regions for three fixed points:

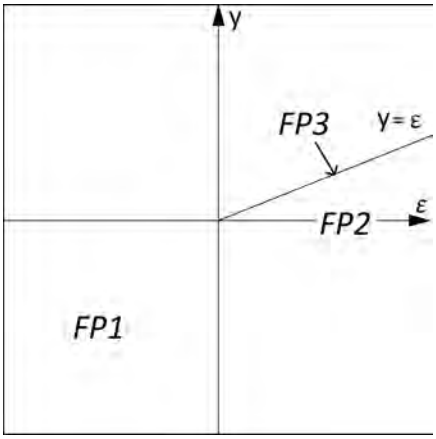

Figure 1: Stability regions on the plane (ε, y).

The critical dimensions responsible for the asymptotic behavior of the correlation functions of the original problem are found in all the regions.

References

1. Halpin-Healy, T.; Zhang, Y.-C. Kinetic roughening phenomena, stochastic growth, directed polymers and all that. Aspects of multidisciplinary statistical mechanics. *Phys. Rep.* **1995** *254*, 215.

2. Kardar, M.; Parisi, G.; Zhang, Y.-C. Dynamic Scaling of Growing Interfaces. *Phys. Rev. Lett.* **1986**, *56*, 889.

3. Caldarelli, G.; Giacometti, A.; Maritan, A.; Rodriguez-Iturbe, I.; Rinaldo, A. Randomly pinned landscape evolution. *Phys. Rev. E* **1997**, *55*, R4865(R).

4. Forster, D.; Nelson, D.R.; Stephen, M.J. Long-Time Tails and the Large-Eddy Behavior of a Randomly Stirred Fluid. *Phys. Rev. Lett.* **1976**, *36*, 867.

5. Vasiliev A.N. *The Field Theoretic Renormalization Group in Critical Behaviour Theory and Stochastic Dynamics*; Chapman & Hall/CRC: Boca Raton, FL, USA, 1998.

Plasmons in stripe with anisotropic two-dimensional electron gas fully screened by metal gate

D.A. Rodionov[1] and I.V. Zagorodnev[2]

[1] Moscow Institute of Physics and Technology

[1,2]Kotelnikov Institute of Radioengineering and Electronics of Russian Academy of Sciences

[1]rodionov.da@phystech.edu

Abstract

Magnetoplasma oscillations in a stripe with an anisotropic two-dimensional electron gas near a metal gate are theoretically investigated. We considered two-dimensional electron systems the Fermi surface of which is an ellipse and used an anisotropic Drude like conductivity. We obtained analytical expressions for the frequency and damping of the oscillations taking into account the effects of electromagnetic retardation and arbitrary orientation of the main axes of the effective electron mass tensor.

Key words: Two-dimensional plasmons, laterally confined electron systems, anisotropic conductivity

Introduction

The excitation of collective oscillations of electrons, called plasmons, in two-dimensional electron systems is of particular interest for applications in the field of generation and detection of radiation, in particular, in the terahertz range. The main characteristics of these oscillations are their frequency and damping which depend on the conductivity and geometry of the considered system. Recently, there has been an interest in plasmons in various anisotropic systems, since the presence of anisotropy provides an additional opportunity to control their propagation direction. Among such system, quantum wells based on stressed AlAs stand out, since, on the one hand, they have high mobility at low ("helium") temperature, and, on the other hand, the anisotropy in them is very sensitive to the deformation of the quantum well [1]. At certain thicknesses, growth directions of quantum wells and deformation stress the Fermi surface is an ellipse. Below we assume this situation.

Main text

Consider an infinite stripe of width W with a two-dimensional electron gas. Let's direct the x, y axes across and along the stripe, respectively. There is an infinite ideally

conductive metal gate under the stripe in the $z = -d$ plane. The two-dimensional electron system is placed in a constant homogeneous magnetic field B, the lines of which are perpendicular to the stripe. We work in the CGS system of units.

To obtain the magnetodispersion, we derive an equation for the current density of the plasma eigenmodes in the two-dimensional electron system under consideration. We look for plasma excitation whose electromagnetic fields, as well as their current density and charge density perturbation, are proportional to $e^{iq_y - i\omega t}$, where q_y is the real wave vector along the stripe and ω is the complex frequency the imaginary part of which defines damping in the system. We consider the dynamic anisotropic Drude like conductivity of a two-dimensional electron gas and assume that the relaxation time of electrons is independent of their momentum direction and energy [2]. Using Maxwell's equations, the Ohm's law and requiring that the tangential component of the electric field is equal to zero on the gate, we obtain an integro-differential equation for the current density.

To simplify the analysis, we consider the case of a fully screened stripe in which the current equation becomes differential. In this case, the relation between the induced electric field and the current becomes localized. It means that electrons within the stripe interact with their images in the metal rather than with each other. Notice, due to such proximity plasma oscillations, including modes whose dispersion is greater than the light dispersion, do not radiate electromagnetic waves. This is explained by that the interference of the electromagnetic fields originated from the stripe and the nearby metal suppresses the total radiation. For the local interaction limit to be applicable, the distance between the electron gas and the gate d must be much smaller than any characteristic length in the system.

In the infinite stripe we describe various plasma modes by a non-negative integer number n. The frequency and damping of plasma modes can be written as

$$(\operatorname{Re}\omega_n(q_y))^2 = q_y^2 v(\theta)^2 + \left(\frac{n\pi}{W}\right)^2 \frac{v_1^2 v_2^2}{v(\theta)^2} + \omega_c^2 \left(1 - \frac{v_1^2}{c^2}\right)\left(1 - \frac{v_2^2}{c^2}\right)(1 - \delta_{n,0}), \quad (1)$$

$$\operatorname{Im}\omega_n(q_y) = \\ = -\frac{\gamma}{2}\left[2 - \frac{v_1^2 + v_2^2}{c^2} - \frac{q_y^2 v(\theta)^2 \left(1 + \frac{v(\theta)^2 - v_1^2 - v_2^2}{c^2}\right)}{\left(\operatorname{Re}\omega_n(q_y,\theta)\right)^2} - \frac{\left(\frac{n\pi}{W}\right)^2 \frac{v_1^2 v_2^2}{v(\theta)^2}\left(1 - \frac{v(\theta)^2}{c^2}\right)}{\left(\operatorname{Re}\omega_n(q_y,\theta)\right)^2}\right], \quad (2)$$

where $\delta_{n,n'}$ – the Kronecker delta. Here we introduce velocities

$$v_i^2 = c^2\left(\frac{m_i c^2}{4\pi n_s e^2 d} + 1\right)^{-1}, \quad i = 1, 2, \quad v(\theta)^2 = \frac{v_1^2 v_2^2}{v_1^2 \cos^2\theta + v_2^2 \sin^2\theta}, \quad (3)$$

where n_s, $m_{1,2}$, γ and e are the two—dimensional concentration, the effective mass along the main axes, the inverse relaxation time and the electron charge, respectively,

$\omega_c = eB/c\sqrt{m_1 m_2}$ is the cyclotron frequency, c is the speed of light in vacuum, θ is the angle between the axis corresponding to the mass m_1 and the positive direction of the x axis. It turned out that the fundamental mode $n = 0$ corresponds to the edge magnetoplasmon. Its frequency, velocity and damping do not depend on the magnetic field, while its localization length near the edge which is given by the following expression

$$l = \frac{v_1 v_2}{\sqrt{1 - \frac{v_1^2}{c^2}}\sqrt{1 - \frac{v_2^2}{c^2}} v(\theta)\omega_c} \tag{4}$$

is inversely proportional to the magnetic field. The frequency of the other modes with number $n = 1, 2, ...$, unlike the isotropic case [3], is not able to be obtained from the plasma dispersion in the infinite electron system by quantization of the transverse component of the wave vector. As in the isotropic case, the square of the frequency of a magnetoplasmon is the sum of the square of the frequency of a plasmon without a magnetic field and a term proportional to the square of the cyclotron frequency. The last term does not depend on the orientation of the conduction tensor and is always less than the square of the cyclotron frequency. The damping of the magnetoplasmon in strong magnetic fields also does not depend on the orientation of the effective mass tensor.

The work was supported by the Foundation for the Advancement of Theoretical Physics and Mathematics “BASIS”.

References

1. M. Shayegan, E.P. De Poortere, O. Gunawan, Y.P. Shkolnikov, E. Tutuc, K. Vakili, Two-dimensional electrons occupying multiple valleys in AlAs, phys. stat. sol. (b) **243**, 3629, (2006).

2. B. Lax, H.J. Zeiger, and R.N. Dexter, Anisotropy of cyclotron resonance in germanium, Physica **20**, 818, (1954).

3. I.V. Zagorodnev, A.A. Zabolotnykh, D.A. Rodionov, V.A. Volkov, Two-Dimensional Plasmons in Laterally Confined 2D Electron Systems, Nanomaterials **13**, 975, (2023).

Few- and half-cycle electromagnetic pulses

N.N. Rosanov[1]

[1]Ioffe Institute

[1]nnrosanov@mail.ru

Abstract

Extremely short electromagnetic pulses, including laser pulses, are necessary for metrology and control of ultrafast processes. I consider the question of the limit of shortening of such pulses. In addition, extremely short pulses should not be weak. Then the question of the criterion for the effectiveness of the impact of extremely short pulses on microobjects is further considered.

Key words: Few-cycle electromagnetic pulses, unipolar pulses

Introduction

Ever shorter electromagnetic pulses are needed for observation of the dynamics and control ever faster processes. As the duration of the pulses decreases, the oscillations of atoms in molecules (scale 10^{-14} s), the movement of electrons in atoms (10^{-16} s), intranuclear processes (10^{-22} s), etc., become available for observation. At present, the main method of shortening electromagnetic pulses is the summation of the higher harmonics of radiation, while pulse durations of 43 as (1 as = 10^{-18} s) have been achieved [1]. Such pulses are multi-cycle and bipolar, with a change in the direction of the electric field strength to the opposite after half the period of field oscillations. Another approach, when fixing the maximum available radiation frequency, is to reduce the number of half-periods of field oscillations. The limit is the pulse in the form of a half wave, which is therefore unipolar. At the same time, the possibility of the existence and formation of unipolar electromagnetic pulses still causes discussion in the literature. Therefore, one of the main tasks of this report is to derive a criterion for the formation of these pulses. More precisely, it is required to obtain a criterion for the formation of pulses with a nonzero electric area $\mathbf{S}_E(\mathbf{r}) = \int_{-\infty}^{+\infty} \mathbf{E}(\mathbf{r}, t)dt$, defined as the time integral of the electric field strength $\mathbf{E}$ ($\mathbf{r}$ – radius-vector). This problem is solved for the electrodynamics of charges in vacuum. Some simple examples of unipolar pulses in the presence of continuous media are also given. Next, I analyze the effectiveness of the interaction of extremely short pulses with micro-objects. In all these cases, it turns out that, under the condition of a sufficiently short pulse duration, the interaction efficiency is determined not by the maximum intensity or energy of this pulse, but by its electric area $\mathbf{S}_E$.

Charges in a vacuum

In a vacuum without charges, the possibility of propagating unipolar (with non-zero electric area) pulses in 1D-geometry follows from d'Alembert's solution of the wave equation. Unipolar pulses in 2D-dimensional geometry are also possible. However, in 3D-space their energy is infinitely large. The report shows that effectively finite-energy unipolar pulses can propagate in a hollow coaxial waveguide. In an unbounded vacuum without charges, such pulses cannot propagate. In the presence of moving electric charges with a charge density $\rho(\mathbf{r}, t)$, in an unbounded vacuum, the nature of the spatial distribution of the electric area is determined by the distribution of the integral charge density $Q(\mathbf{r}) = \int_{-\infty}^{+\infty} \rho(\mathbf{r}, t)dt$. The electric area is identically zero if and only if in the entire space $Q(\mathbf{r}) \equiv 0$. Examples of the formation of electromagnetic pulses with a nonzero electric area when this condition is violated are presented. The asymptotic behavior of the area distribution $\mathbf{S}_E(\mathbf{r})$ far from the bounded system of charges is also given.

Charges in dielectrics

A single uniformly moving in vacuum charge creates unipolar pulse with electric area inversely proportional to the distance from the charge trajectory and charge velocity. In dielectrics, the area is inversely proportional to the dielectric index and therefore increases significantly for epsilon-near-zero materials. During transition radiation, when the charge crosses the interface between two dielectrics, in addition to the transverse radial component, there also arises a longitudinal component of the electric area localized near the interface.

Interaction with micro-objects

For a single electron, both classical and quantum (with spin), interacting with a plane-wave short electromagnetic pulse, just the pulse electric area determines the efficiency of the interaction. For quantum objects, such as molecules, atoms, and quantum dots, appropriate is the Migdal sudden perturbation approximation. In this case, the efficiency of objects excitation or ionization is also determined by the area $\mathbf{S}_E(\mathbf{r})$, and the efficiency is inversely proportional to the object size.

Acknowledgments

I am grateful to my colleagues M.V. Arkhipov, R.M. Arkhipov, I.A. Alexandrov, S.V. Fedorov, A.V. Pakhomov, D.A. Tumakov, N.A. Veretenov, and others for joint research in the topics. The current research has been supported by the Russian Scientific Foundation, grant 23-12-00012.

Deep strong light-matter coupling with artificial metallic nanostructures

Evgeny Ryabkov[1,*], Ivan Kharichkin[1], Benjamin Rousseaux[2], and Denis G. Baranov[1]

[1]Center for Photonics and 2D Materials, Moscow Institute of Physics and Technology, Dolgoprudny 141700, Russia

[2]Laboratoire Interdisciplinaire Carnot de Bourgogne, CNRS UMR 6303, Universite de Bourgogne, BP 47870, 21078 Dijon, France

[*]ryabkov.e@phystech.edu

Abstract

Various coupling regimes are normally characterized with coupling strength and describe how fast resonant optical modes exchange energy with material excitations in comparison to losing it to the environment. Reaching high coupling efficiency traditionally implies the use of some sorts of quantum emitters and special conditions, including high vacuum, strong magnetic fields, and extremely low temperatures. However, in this work, we show that deep strong coupling is reachable at ambient conditions with metallic nanoresonators [1,2]. Using a Hamiltonian approach we theoretically analyze the formation of polaritonic states in a number of such dense assemblies. We obtain results that let analyze various geometries and determine their universal normalized collective constants of coupling with free-space photons. The results could be valuable for the field of polaritonic studies [3-5], quantum technologies, modifying material properties [6] and controlling chemical reactions [7-11].

Introduction

Stationary eigenstates of a coupled system, also known as polaritons, are of the photonic and the matter nature simultaneously. This calls for numerous useful applications. One of the core characteristics in the polariton studies is the interaction strength between the two components of the coupled system. As might be expected, the question of improving the coupling strength in polaritonic systems (with the lowest cost, preferably) is the main to focus on.

We study periodic plasmonic nanostructures consisting of closely packed metallic nanoparticles, whose hybrid polaritonic states have harmonic energy ladder, which lets these nanoparticles play the role of quantum emitters interacting with free-space photons. This approach has enabled the exotic regimes of ultra-strong (USC) and even deep strong coupling (DSC) at ambient conditions, which was previously unavailable with more traditional quantum emitter platforms.

Formulating a proper Hamiltonian model, we theoretically analyze the formation of

polaritonic states including their dependance on primitive microscopic geometry and dielectric characteristics of the artificial nanostructures. Our results suggest that deep strong coupling is reachable at ambient conditions with such systems.

Main text

Considering an ensemble of nanoparticles, each of volume V_j and single resonance frequency ω_j, Fig. 1, we show that the Hamiltonian:

$$H = \underbrace{\sum_j \int_{V_j} \mathrm{d}^3 r \left(\frac{\mathbf{\Pi}_j^2}{2\rho} + \frac{1}{2}\rho\omega_j^2 \mathbf{X}_j^2 \right)}_{\text{nanoparticles}} + \underbrace{\int_{\mathbb{R}^3} \mathrm{d}^3 r \left(\frac{\mathbf{\Pi}_A^2}{2\epsilon_0} + \frac{(\nabla \times \mathbf{A})^2}{2\mu_0} \right)}_{\text{radiation}} + \underbrace{\sum_j \int_{V_j} \mathrm{d}^3 r \frac{\mathbf{P}_j^2}{2\epsilon_0}}_{\mathbf{P}^2\text{-term}} + \underbrace{\sum_j \int_{V_j} \mathrm{d}^3 r \frac{\mathbf{P}_j \cdot \mathbf{\Pi}_A}{\epsilon_0}}_{\text{interaction}} \quad (1)$$

generates the source-free Maxwell's equations $\nabla \cdot \mathbf{D} = 0, \nabla \cdot \mathbf{B} = 0, \nabla \times \mathbf{E} = -\frac{\partial}{\partial t}\mathbf{B}, \nabla \times \mathbf{H} = \frac{\partial}{\partial t}\mathbf{D}$, as well as the equation of motion of the macroscopic polarization $\mathbf{P} = \sum_j \mathbf{P}_j$:

$$\left(\frac{\partial^2}{\partial t^2} + \omega_j^2 \right) \mathbf{P}_j(\mathbf{r}, t) = \beta_j(\mathbf{r}) \mathbf{E}(\mathbf{r}, t), \quad (2)$$

where $\beta_j(\mathbf{r}) = \alpha_j(\mathbf{r})/\rho$, ρ being the carrier volumic mass in the medium of the resonators, and $\alpha_j(\mathbf{r})$ being the displaced carrier density in resonator j. The displacement of the carriers is contained in the vector field $\mathbf{X}_j(\mathbf{r}, t)$, whose canonical momentum is $\mathbf{\Pi}_j = \rho \frac{\partial}{\partial t} \mathbf{X}_j$. The radiation field with vector potential $\mathbf{A}$ and canonical momentum $\mathbf{\Pi}_A = -\mathbf{D}$ is purely transverse in the Coulomb gauge. We emphasize that, in the picture given by Hamiltonian (1), Ohmic dissipation is disregarded.

We next focus on the light-matter interaction term, assuming the array is homogeneous in the dipole orientation, along the z-axis. In the original basis, involving the operators $b_{\mathbf{Q}}, b_{\mathbf{Q}}^\dagger$, the light-matter interaction term corresponding to the last term of Eq. (1) takes the form:

$$H_{\text{light-mat}} = -i\hbar g_{\mathbf{k}} (a_{\mathbf{k}} - a_{-\mathbf{k}}^\dagger)(b_{-\mathbf{k}} + b_{\mathbf{k}}^\dagger), \quad (3)$$

where $a_{\mathbf{k}}$ is the annihilation operator for a transverse magnetic photon with wave vector $\mathbf{k}$ and frequency $\omega_k = c|\mathbf{k}|$, and the array excitation wavevector $\mathbf{Q}$ must now match the photon wave vector $\mathbf{k}$. The *collective* coupling constant is given by

$$\hbar g_{\mathbf{k}} = \mathcal{E}_{\text{vac}}(\mathbf{k}) \boldsymbol{\mu}_N \cdot \boldsymbol{\epsilon}_{\mathbf{k}} \quad (4)$$

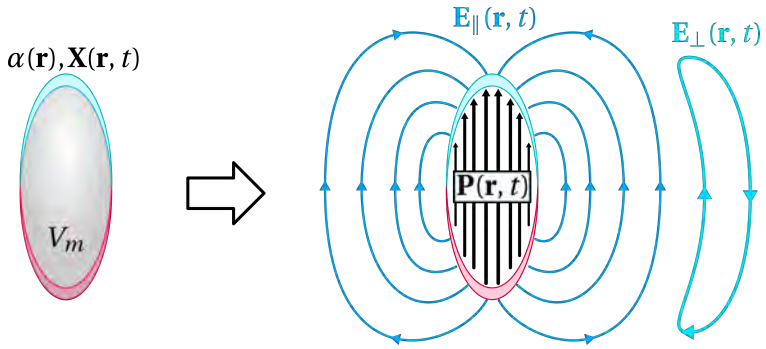

Figure 1: Description of a single nanoparticle of volume V_m. The charge density $\alpha(\mathbf{r})$ is displaced with a vector field $\mathbf{X}(\mathbf{r},t)$, and the associated polarization density is $\mathbf{P}(\mathbf{r},t) = \alpha(\mathbf{r})\mathbf{X}(\mathbf{r},t)$. This system couples to the electric field $\mathbf{E} = \mathbf{E}_\parallel + \mathbf{E}_\perp$, where $\mathbf{E}_\parallel = -\nabla\Phi$ is the longitudinal field created by the charge density and $\mathbf{E}_\perp$ is a divergence-less field from either the radiation of the nanoparticle or external waves.

where

$$\mathcal{E}_{\text{vac}}(\mathbf{k}) = \sqrt{\hbar\omega_{\mathbf{k}}/(2\varepsilon_0 V_{\text{cell}})} \tag{5}$$

is the vacuum electric field of the photonic mode confined to the quantization box of volume V_{cell} and $\boldsymbol{\epsilon}_{\mathbf{k}}$ is the unit transverse magnetic polarization vector. Plugging the vacuum field into Eq. (4) allows us to express the collective coupling constant via the photon frequency, transition dipole moment, and the nanoparticles' spatial density:

$$g_{\mathbf{k}} = \sqrt{\frac{f}{V_0}\frac{\omega_{\mathbf{k}}}{2\hbar\varepsilon_0}}\boldsymbol{\mu}_{01}\cdot\boldsymbol{\epsilon}_{\mathbf{k}} \tag{6}$$

where V_0 is the physical volume of a single nanoresonator and f is the filling factor of a unit cell.

In the new basis involving the diagonalized matter part, the Hamiltonian is, for a given wavevector $\mathbf{k}$:

$$H = \hbar\omega_k a^\dagger_{\mathbf{k}} a_{\mathbf{k}} + \hbar\Omega_{pl} B^\dagger_{\mathbf{k}} B_{\mathbf{k}} - i\hbar\widetilde{g}_{\mathbf{k}}\left(a_{\mathbf{k}} - a^\dagger_{-\mathbf{k}}\right)\left(B_{-\mathbf{k}} + B^\dagger_{\mathbf{k}}\right), \tag{7}$$

where $\widetilde{g}_{\mathbf{k}} = g_{\mathbf{k}}\sqrt{\omega_{pl}/\Omega_{pl}}$ is the rescaled coupling strength. The resonant *transition* frequencies of the polaritonic system given by the eigenvalues of the Hopfield matrix associated to the Hamiltonian (7) can be denoted as:

$$\Omega_\pm = \frac{\sqrt{\omega^2_{\mathbf{k}} + \Omega^2_{pl} \pm \sqrt{\left(\omega^2_{\mathbf{k}} - \Omega^2_{pl}\right)^2 + 16\widetilde{g}^2_{\mathbf{k}}\omega_k\Omega_{pl}}}}{\sqrt{2}} \tag{8}$$

References

1. R. Ameling and H. Giessen, "Cavity Plasmonics: Large Normal Mode Splitting of Electric and Magnetic Particle Plasmons Induced by a Photonic Microcavity", Nano letters 10, 4394 (2010).
2. A. Bisht, J. Cuadra, M. Wersall, A. Canales, T. J. Antosiewicz, and T. Shegai, "Collective strong light-matter coupling in hierarchical microcavity-plasmon-exciton systems",Nano letters 19, 189 (2018).
3. G. Khitrova, H. Gibbs, M. Kira, S. W. Koch, and A. Scherer, "Vacuum rabi splitting in semiconductors", Nature Physics 2, 81 (2006).
4. P. T orm a and W. L. Barnes, "Strong coupling between surface plasmon polaritons and emitters: a review", Reports on Progress in Physics 78, 013901 (2014).
5. D.G. Baranov, M. Wers all, J. Cuadra, T. J. Antosiewicz, and T. Shegai, "Novel nanostructures and materials forstrong light–matter interactions", ACS Photonics 5, 24 (2018).
6. T.W. Ebbesen, "Hybrid light–matter states in a molecular and material science perspective", Accounts of Chemical Research 49, 2403 (2016).
7. A. Thomas, J. George, A. Shalabney, M. Dryzhakov, S. J. Varma, J. Moran, T. Chervy, X. Zhong, E. Devaux, C. Genet, et al., "Ground-state chemical reactivity under vibrational coupling to the vacuum electromagnetic field", Angewandte Chemie International Edition 55, 11462 (2016).
8. B. Munkhbat, M. Wers all, D. G. Baranov, T. J. Antosiewicz, and T. Shegai, "Suppression of photo-oxidation of organic chromophores by strong coupling to plasmonic nanoantennas", Science Advances 4, eaas9552 (2018).
9. A. Thomas, L. Lethuillier-Karl, K. Nagarajan, R. M. Vergauwe, J. George, T. Chervy, A. Sha-labney, E. Devaux, C. Genet, J. Moran, and T. W. Ebbesen, "Tilting a ground-state reactivity landscape by vibrational strong coupling", Science 363, 615 (2019).
10. V. N. Peters, M. O. Faruk, J. Asane, R. Alexander, A. P. D'angelo, S. Prayakarao, S. Rout, and M. Noginov, "Effect of strong coupling on photodegradation of the semiconducting polymer p3ht", Optica 6, 318 (2019).
11. K. Stranius, M. Hertzog, and K. B orjesson, "Selective ma-nipulation of electronically excited states through strong light–matter interactions", Nature Communications 9, 1 (2018).

Creation of a photocell based on titanium dioxide scrolls

V. Samyshkin[1], S. Kutrovskaya[1,2], A. Kucherik[1]

[1]Vladimir State University

[2] The Moscow Institute of Physics and Technology

samyshkin@vlsu.ru

Abstract

An experimental method for the fabrication of nanocomposite metamaterial based on self-assembled titanium dioxide microtubes with gold nanoparticles is proposed. The obtained titanium dioxide scrolls have a high optical absorption coefficient, which can be enhanced by increasing the concentration of linear carbon chains with gold nanoparticles. The possibility of using arrays of oriented microtubes as absorbing n-doped layers for solar cells was investigated.

Key words: titanium dioxide microtubes, laser ablation, metasurfaces

Introduction

The development and creation of spatially ordered metamaterials is one of the main tasks of modern nanotechnology. One of the promising directions of creating such metasurfaces is self- assembly. This method demonstrates a high potential for fabrication of nanostructures [1]. One of the most significant areas where this method can be applied is photonics. Due to the special geometry of the metasurfaces, the optical response has tunable properties that can be controlled. Nanophotonics is aimed in particular at the development of ideal absorbers that would absorb 100% of the incident light in a selected narrow spectral range. The proposed method of obtaining metasurfaces, can also be used in the creation of broadband absorbers in the form of photocells[2].

Materials and Methods

We used a laser ablation method to synthesize metastable forms of TiO_2. Thin films of titanium dioxide were deposited on a solid transparent substrate due to the rapid cooling of the molten phase created by laser ablation of a titanium target in air. To scan the surface of the bulk titanium target, a laser beam with a focal spot diameter of 30 μm was used by moving around circles with a diameter of 3 mm (see Fig. 1a). Assembly of the obtained material on the substrate surface is achieved by direct vapor deposition in the presence of a spatially homogeneous magnetic field generated by two rectangular NdFeB magnets. The effect of the magnetic field during tube formation exhibits threshold behavior. A field of 500 mTl effectively disrupts the film, and rolls are formed as shown in Fig. 1d.

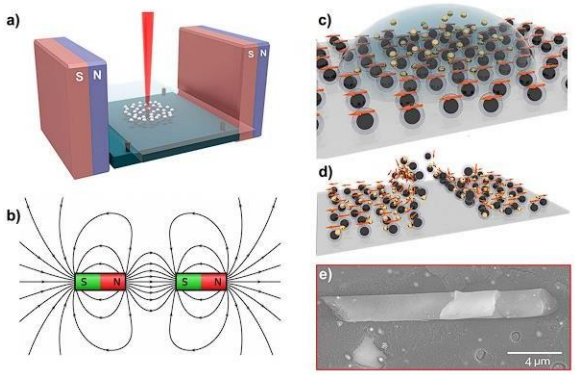

Figure 1: The experimental setup for the deposition of thin flms of titanium oxide: (a,b) the schematic distribution of the magnetic field lines; (c,d) is the schematic presentation of the procedure of introduction of gold NPs and the self-induced formation of microtubes by rolling thin flms of titanium dioxide. The formation of microtubes is controlled by the spatially homogeneous magnetic field. (c) The schematic orientation of the magnetic momenta of TiO_2 NPs on the surface of the substrate in the presence of the external magnetic field with (d) showing the subsequent disorientation of magnetic momenta due to the effect of the gradient of the magnetic field on the magnetically oriented NPs. (e) shows the SEM image of the microtube.

Based on the results obtained, the concept of creating a photocell based on titanium dioxide scrolls was proposed (see Fig. 2): 1, 2 - top and bottom contacts, 3 - top transparent electrode, 4 - silicon layer (p-type), 5 is titanium oxide microtubes doped gold NPs (n-type). The orientation and size of the titer can be estimated from the SEM image of the structure shown in the inset.

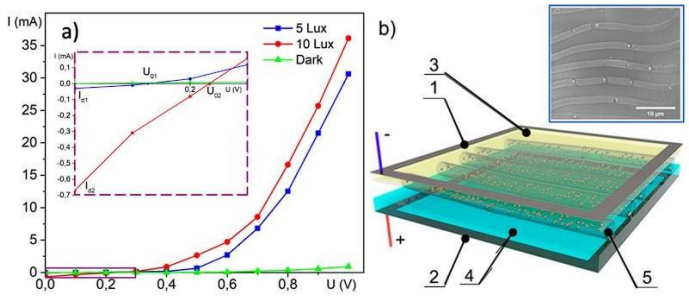

Figure 2: Schematic representation of a photocell based on titanium dioxide scrolls.

Conclusions

As one can conclude from Fig. 2, the tested structure is characterised by the intrinsic photo-electromotive force and a short-circuit current. This explains the existence of zero-voltage current and zero current at U=0.16V and the light power of 5 Lux (also at U=0.23V and the light power of 10 Lux). Under the effect of the irradiation, the diffusion carrier current (Id) is induced due to the generation of additional carriers in the p-n junction region. The current is caused by holes, mostly. The variation of the light intensity leads to the variation of the photocurrent. The current-voltage curves taken at different light intensities demonstrate a similar non-linear behaviour. We anticipate that higher values of the photocurrent are achievable if using a semiconductor with a lattice constant closely matching one of the bottom element of the cell. Overall, these measurements show the high potentiality of TiO_2 microtubes for photovoltaic applications[3].

Acknowlegment

This study was funded by the Russian Science Foundation (project no. 23-29-10016, https://rscf.ru/en/project/23-29-10016/).

References

1. H. B. Bohidar & K. Rawat, Design of nanostructures: self-assembly of nanomaterials. Weinheim, Wiley press (2017).
2. N.I. Landy, S. Sajuyigbe, J.J.Mock, D.R. Smith & W.J. Padilla, Perfect metamaterial absorber. Phys. Rev. Lett. 100, 207402 (2008).
3. S. Kutrovskaya, A. Kucherik, A. Osipov, V. Samyshkin, A. Istratov & A Kavokin, Nanocomposite Metamaterials Based on Self-assembled Titanium Dioxide Rolls with Embedded Gold Nanoparticles. Scientific Reports, 9(1), 7023, (2019).

Excitons and trions with negative effective masses in 2D semiconductors

M.A. Semina[1], J.V. Mamedov[2], M.M. Glazov[3]

[1,3]Ioffe Institute, St. Petersburg, Russia

[2]National Research University Higher School of Economics, St. Petersburg, Russia

[1]semina@mail.ioffe.ru, [2]javi-m@mail.ru, [3]glazov@coherent.ioffe.ru

Abstract

We develop a theory describing fundamental Coulomb-correlated complexes: neutral and charged excitons, also known as trions, in transition metal dichalogenides monolayers in unusual situation where one of the electrons occupies excited, high-lying, conduction band characterized by a negative effective mass. We present simple, accurate and physically justified trial wavefunctions for calculating the binding energies of excitons and trions and compare the results of variational calculations with those of a fully numerical approach. We demonstrate the importance of taking into account the nonparabolicity of high-lying conduction band dispersion.

Introduction

Due to very small thickness and characteristics of dielectric environment, Coulomb correlations are especially pronounced in two-dimensional semiconductors based on transition metal dichalcogenides, for example, in MoS2 or WSe2, where the binding energies of excitons – electron-hole pairs – are hundreds of meV, and trions or charged excitons – three-particle complexes of an electron and two holes or two electrons and a hole - tens of meV [1, 2]. In recent experimental works [3, 4], the observation of "high-lying" excitons and trions in such atomically thin semiconductors, where one of the electrons is located in the remote (excited) conduction band, was reported. The peculiarity of the band structure of these materials is such that this band is characterized by a negative effective mass [3, 4]. It gives rise to the question on how the Coulomb-correlated states can be formed in such a case. Here we present the results of a theoretical study of the states of excitons and trions in atomically thin semiconductors, where one of the charge carriers is in the remote band and has a negative effective mass.

Binding energies of excitons and trions

In the framework of the model with parabolic dispersion, we obtained a criterion for the ratio between the effective masses of charge carriers, under which Coulomb

complexes, excitons and trions, can be bound. The region of existence of stable trions turns out to be narrow, and it does not correspond to the known values of effective masses in the remote bands [3, 4]. This fact distinguishes the complexes under study from conventional trions with two identical charge carriers. The complexes can be stabilized by taking into account the contributions of the fourth power in the wave vector to the electron dispersion in the remote band. The binding energies of excitons and trions have been calculated both within the framework of the variational method and by numerical diagonalization of the Hamiltonian on the Gaussian basis [5]. Based on analytical calculations with a short-range potential, variational functions with a small number of adjustable parameters are proposed, which are applicable for any type of interparticle interaction and arbitrary signs of the effective masses. For our calculations we used Coulomb and Rytove-Keldysh potentials to describe interparticle interaction. The dependences of the exciton and trion binding energies on both the reduced mass of the high-lying exciton (both positive and negative) and on the parameter describing the nonparabolicity of the dispersion of the excited conduction band are analyzed. It was shown, that accounting nonparabolicity of high-lying conduction band dispersion stabilizes exciton with negative reduced mass and significantly widen the region of stability of negative trion. The criterion of stability of the positive trion is stability of high lying exciton.

The asymptotics of the exciton and trion binding energies are obtained within the limits of strong nonparabolicity or a small absolute value and negative effective electron mass. The deviations of the exciton series from the hydrogen-like series are analyzed. The results of recent experiments [4] on the observation and study of positively and negatively charged trions with a negative effective electron mass are described.

This work has been supported by the Russian Science Foundation project 23-12-00142

References

1. G. Wang, A. Chernikov, M. M. Glazov, et al., Rev. Mod. Phys. **90**, 021001 (2018)

2. M. A. Semina, R. A. Suris, Physics-Uspekhi **65**, 111 (2022).

3. K.-Q. Lin, et al., Nature Comm. **12**, 5500 (2021).

4. K.-Q. Lin, M.A. Semina et al., Nature Comm. **13**, 6980 (2022).

5. M.A. Semina, J.V. Mamedov, M.M. Glazov, Oxford Open Materials Science, itad004, doi:10.1093/oxfmat/itad004 (2023).

Quantum electrodynamics at strong and supercritical Coulomb fields

Vladimir Shabaev
St.Petersburg State University, St.Petersburg, 199034, Russia
B. P. Konstantinov Petersburg Nuclear Physics Institute of National Research Centre “Kurchatov Institute”, Gatchina, 188300 Leningrad District, Russia
v.shabaev@spbu.ru

The current status of tests of quantum electrodynamics (QED) at strong and supercritical Coulomb fields with heavy ions is briefly reviewed. Special attention is focused on tests of QED in supercritical regime. It is known that in slow collisions of two bare nuclei with the total charge number larger than the critical value, $Z_1+Z_2 > Z_c =173$, the initially neutral vacuum can spontaneously decay into the charged vacuum and two positrons. Detection of the spontaneous emission of positrons would be the direct evidence of this fundamental phenomenon. However, the spontaneous positron emission is generally masked by the dynamical positron emission, which is induced by a rapidly changing electric field created by the colliding nuclei. For many years it was believed that the vacuum decay can be observed only in collisions with nuclear sticking, when the nuclei are bound for some period of time due to nuclear forces. But to date there is no evidence for the nuclear sticking in such heavy-ion collisions. In our recent papers [I.A. Maltsev et al., PRL, 2019; R.V. Popov et al., PRD, 2020; R.V. Popov et al., PRD, in press], it was shown that the vacuum decay can be observed without any sticking of the nuclei. This can be done via measurements of the pair-production probabilities or the positron spectra for a given set of nuclear trajectories. The results of this study will be presented in the talk.

Dynamics of skyrmions in moiré magnetic materials

P. Shaban[1], I. Lobanov[1], V. Uzdin[1], I. Iorsh[1,2]

[1]Department of Physics, ITMO University, St. Petersburg, 197101, Russia

[2]Abrikosov Center for Theoretical Physics, MIPT, Dolgoprudnyi, Moscow Region 141701, Russia

[1]polina.shaban@metalab.ifmo.ru

Abstract

In this study, we investigate twisted magnetic bilayers under a perpendicular electric field. The interplay of induced Dzyaloshinskii-Moriya interaction and moiré exchange potential leads to complex non-collinear magnetic phases. Our simulations show coexisting intralayer skyrmions and interlayer skyrmion pairs with distinct dynamics under an in-plane electric field. Notably, skyrmions exhibit intriguing movement along domain walls, promising applications in van der Waals magnet-based spintronics.

Key words: Moiré potential, van der Waals magnets, twisted magnets, non-collinear phases, skyrmions

Introduction

Van der Waals materials are layered structures with strong intralayer interactions and weak interlayer interactions. They can be easily exfoliated into monolayers, offering unique electronic and optical properties. By constructing heterostructures from different Van der Waals materials, their properties can be modified.

A new class of Van der Waals materials, known as Van der Waals magnets, exhibits fascinating magnetic properties in two-dimensional structures. These materials are highly sensitive to external perturbations like electric fields, twist angles, or mechanical strain. The Dzyaloshinskii-Moriya interaction, induced by broken inversion symmetry, stabilizes non-collinear structures such as skyrmions.

In twisted magnetic bilayers, an additional interaction called the moiré potential arises due to site-dependent interlayer exchange. The moiré potential's spatial scale is determined by the twist angle θ and is proportional to a/θ, where a is the lattice period.

This work investigates a specific structure composed of a twisted bilayer of ferromagnetic Van der Waals material (Fig. 1).

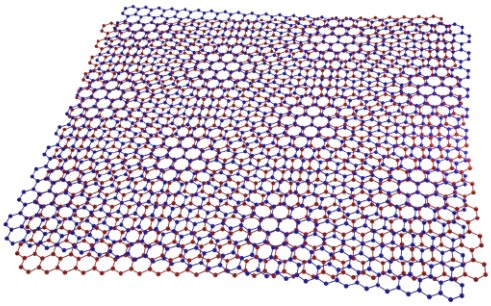

Figure 1: Twisted ferromagnetic biayer.

Results

We consider a continuous generalized Heisenberg-type model with the energy

$$E = \int d^2\mathbf{r} \left[\sum_{i=1,2} \left(\mathcal{A}(\nabla \mathbf{n}_i(\mathbf{r}))^2 - \mathcal{K} n_{zi}^2(\mathbf{r}) + \mathcal{D}\mathbf{n}_i(\mathbf{r}) \cdot (\hat{\mathbf{z}} \times \nabla) \times \mathbf{n}_i(\mathbf{r}) \right) - J_{1,2}\Phi(\mathbf{r})\mathbf{n}_1(\mathbf{r}) \cdot \mathbf{n}_2(\mathbf{r}) \right] \tag{1}$$

Here $\mathbf{n}_1$ and $\mathbf{n}_2$ are the unit vectors along the magnetization in layers 1 and 2, respectively, $\mathcal{A}$ is the exchange stiffness constant, $\mathcal{D}$ is DMI, interlayer exchange equals $J_{1,2}\Phi(\mathbf{r})$. Anisotropy $\mathcal{K} > 0$ corresponds to the easy axis anisotropy.

The moiré potential $\Phi(\mathbf{r})$ (Fig. 2a) is directly related to the lattice period and twist angle. The study employs numerical simulations to explore the magnetic phases in this system, considering the interplay between the intralayer Dzyaloshinskii-Moriya interaction and the spatially dependent interlayer exchange coupling.

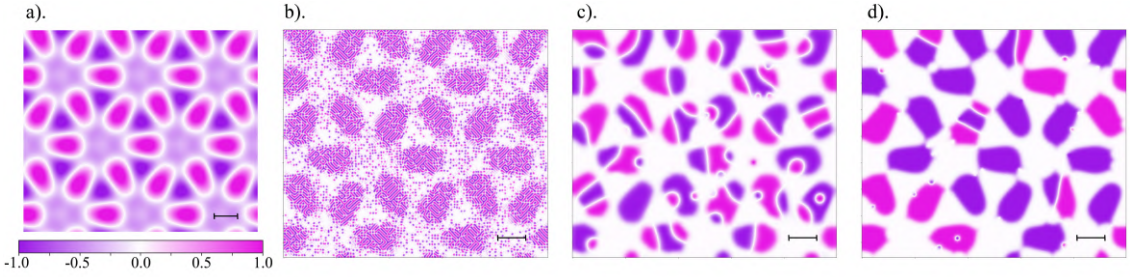

Figure 2: Spatial dependence of interlayer interaction $\Phi(\mathbf{r})$ (a) and z-projection of total bilayer magnetic moments in moiré magnets for $D = 0.9$ (b), $D = 0.11$(c) and $D = 0.07$ (d). Scale bar: 100 lattice constants.

Intriguingly, the system exhibits a variety of intralayer skyrmions and bound interlayer skyrmion pairs (Fig. 3).

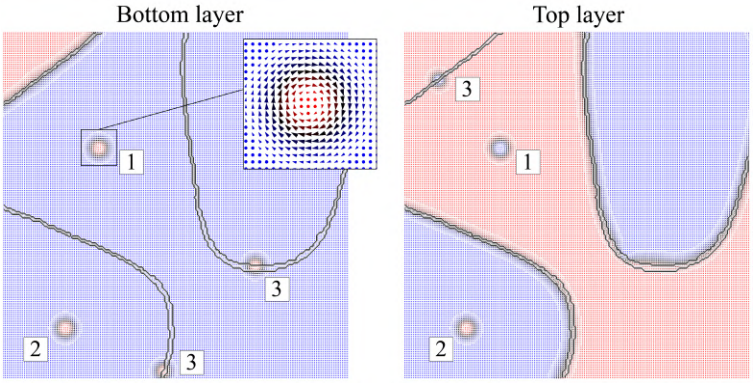

Figure 3: Various types of skyrmions in a twisted bilayer. Pair of AF skyrmions located in the AF IEC grain (1), in the FM IEC grain (2) and a single skyrmion (3) fixed at the border of zero moiré potential.

The Landau-Lifschitz-Gilbert equation and Thiele equation are used to study the dynamics of skyrmions under the influence of external electric current. The calculations predict that single skyrmions exhibit railing behavior along the grain boundary when subjected to an applied current. Using the Thiele equation, we provide an analytical description of this effect. This behavior is not limited to a specific structure but is expected to be observed in various van der Waals moiré magnetic bilayers.

To conclude, the interplay between the moiré potential and DMI in van der Waals magnets results in a diverse range of non-collinear magnetic structures. Three types of skyrmions were identified with distinct topological properties and kinetics under applied in-plane current. The railing of skyrmions in van der Waals magnets paves the way for innovative applications of these heterostructures in spintronics.

References

1. K. S. Novoselov, O. A. Mishchenko, et al., 2d materials and van der Waals heterostructures, Science **353**, aac9439, (2016).

2. Kenneth S Burch, David Mandrus, and Je-Geun Park, Magnetism in two-dimensional van der Waals materials, Nature **563**, 47–52, (2018).

3. Bevin Huang, Genevieve Clark, et al., "Layer-dependent ferromagnetism in a van der Waals crystal down to the monolayer limit," Nature **546**, 270–273, (2017).

4. Cheng Gong, Lin Li, et al., Discovery of intrinsic ferromagnetism in two-dimensional van der waals crystals, Nature **546**, 265–269, (2017).

Simulation of Two-Phase Flow in Porous Media using a Two-Dimensional Network Model

K. Shabbir[1], O. Izvekov[2], A. Konyukhov[3]

[1,2,3]Moscow Institue of Physics and Technology

[1]kafiulshabbir@phystech.edu, [2]izvekov_o@inbox.ru, [3]konyukhov_av@mail.ru

Abstract

Various algorithms and methods used to simulate two-phase flow in porous media has many practical applications in oil recovery, hydrology, electricity production where pressurized water is passed through heated pipes and is transformed into steam, etc. The algorithm presented here is used to find the saturation of a phase with respect to time and model imbibition.

Key words: Two-phase flow, porous body, imhibition

Introduction

Figure 1a is an example of two-phase flow in porous body. The wetting fluid, in this case - water displaces the non wetting fluid - air. The aim is to plot concentration of one of the phases with respect to time for a given region of the porous body, similar to [1].

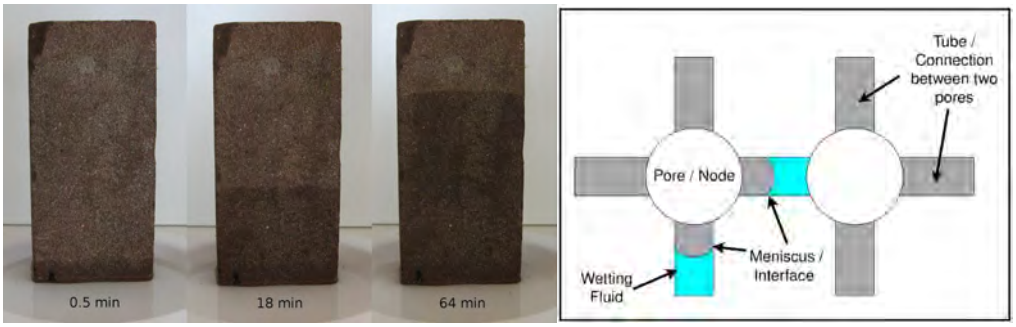

(a) Porous body (b) Model

Figure 1: Example of two-phase flow in porous body and a simplified manner of modeling the process

Model

The flow rate when a tube contain meniscus after necessary derivation is given by a modified Poiseuille's equation:

$$Q_{ij} = \frac{\pi R_{ij}^4}{8 M_{ij} l} \left(\Delta P_{ij} + \frac{2 s_{ij} \sigma}{R_{ij}} \right) \tag{1}$$

Here M_{ij} is:

$$M_{ij} = \sum_k \mu_{ijk} \frac{l_{ijk}}{l} \tag{2}$$

And $s_{ij} = \{-1, 0, +1\}$ depending on the orientation and number of meniscus.
For every node due to conservation of volume:

$$\sum_j Q_{ij} = 0 \tag{3}$$

This produces n linear equations for a model with n nodes. The pressures at each node are the variables. Gaussian-elimination is used to solve the linear equations. This is the most computationally expensive task and defines for how many nodes, the simulation can be performed in a given time. Various methods of optimizations have been presented in [2].

The calculated pressures at each node is used to determine the flow rates according to equation 1. Then the time step is decided and each meniscus in the tubes is displaced according to $d_{ij} = v_{ij} \Delta t_{ij}$. The novelty of our algorithm is the distribution of the phases when more than one phase enters a node. The wetting fluid is distributed first in ascending order of the radius of the tubes. After this if there are more than two meniscus in a tube, the phases are combined such that the center of mass of the phases remain the same. This algorithm can be extended to the case of a 3-D model, such as in [3].

Results

For modeling only the saturation of a phase in a given region [4] when there is an external pressure difference, does not produce oscillations unlike modeling imhibition where the boundaries are closed and the volume of each phase in the system remains the same. Here the fluid does not reach an equilibrium position in a finite amount of time. However the small oscillations dampens over time, as in figure 3. Another significant advantage of this method is that the shape of the tubes are considered to be cylindrical unlike hour glass shape in [5] and and flow is determined by solving a set of linear equations. Computation requires a few hours for 30x30 matrix of tubes on a personal computer.

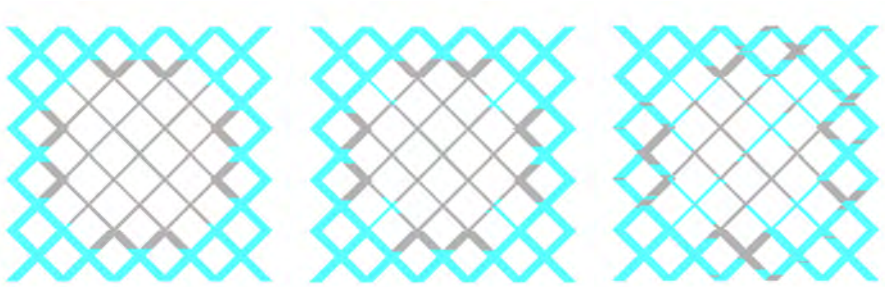

(a) Initial (b) Invasion (c) Final

Figure 2: Showing how a wetting fluid enters the region with thinner radius

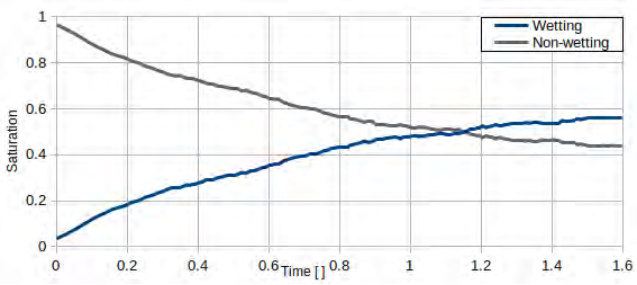

Figure 3: Volumetric saturation of the two-phases in the region of thinner radius with respect to dimensionless time

References

1. Fatt I. The network model of porous media 3, dynamic properties of networks with tube radius distribution Petroleum Trans. AIME 1956. V. 207. P. 164

2. Raoof A., Hassanizadeh S. A new method for generating pore-network models of porous media // Transp. Porous Med. 2010. V. 81. P. 391

3. S. Sinha et al. Effective rheology of two-phase flow in three-dimensional porous media: experiment and simulation // Transp. Porous Med. 2017. V. 119. P. 77

4. K. Shabbir, Sim of Two-Phase flow network model, 65 All Russia Scientific Conference MIPT, Aerospace Section, P. 196, https://mipt.ru/upload/medialibrary/002/aerokosmicheskie-tekhnologii.pdf

5. Aker E., Måløy K et al. A two-dimensional network simulator for two-phase flow in porous media // Transp. Porous Med. 1998 V. 32 P. 163

Optical spin Hall effect in a rigidly rotating system of exciton-polaritons

F. A. Shabunin[1] and N. S. Voronova[1,2]

[1]National Research Nuclear University MEPhI, Moscow, Russia

[2]Russian Quantum Center, Skolkovo Innovation Center, Moscow, Russia

[1]nsvoronova@mephi.ru

Abstract

We derive the change in the effective magnetic field created by the polariton longitudinal-transverse splitting when rotation of the system is considered. Momentum-space and real-space dynamics of the degree of circular polarization of the light emitted from the system is studied and rotational oscillations of the polarization pattern are predicted.

Key words: exciton-polaritons, pseudospin, rotation

Introduction

In this work, we consider a semiconductor microcavity in the strong-coupling regime between the optical mode and excitons in a quantum well. In this regime, the new eigenmodes, called exciton polaritons, appear. Being half light and half matter, they possess a low effective mass and a pseudospin corresponding to the polarization of the emitted light [1]. The longitudinal-transverse (LT) splitting of the polariton dispersion Δ_{LT} creates an effective magnetic field oriented in the microcavity plane. As a result, polaritons with non-zero momentum demonstrate the so-called optical spin Hall effect (OSHE): when excited with the linear polarization, due to the precession of their pseudospin around the effective magnetic field, the domains of predominantly right circular (σ^+) and left circular (σ^-) polarization appear in different regions of momentum space [2], and in real space the degree of circular polarization additionally exhibits beats in the radial direction [3].

Rotational OSHE

In this work, we study a system of exciton-polaritons rigidly rotating around the z-axis (the sample growth direction) with the angular velocity $\vec{\omega}$. In this case, the correspondence of polar angles $\varphi \leftrightarrow \theta$ in real and momentum spaces gives way to $\varphi \leftrightarrow \theta + \pi/2$ (see the sketch in Fig. 1, left). Applying the rotation transformation to the system Hamiltonian describing the LT-splitting, we derive new expressions for the

components of the effective magnetic field. Namely, decomposing the 2×2 polariton Hamiltonian with added rotation in the basis of the identity matrix and the Pauli matrices, we obtain: $\Omega_x^{rot} = \Omega \cos 2(\theta + \omega t)$, $\Omega_y^{rot} = \Omega \sin 2(\theta + \omega t)$, where $\Omega = \Delta_{\mathrm{LT}}/\hbar$. Thus, in the rotating frame, the effective field rotates around the elastic cirle with twice the angular velocity of the system rotation [Fig. 1, right].

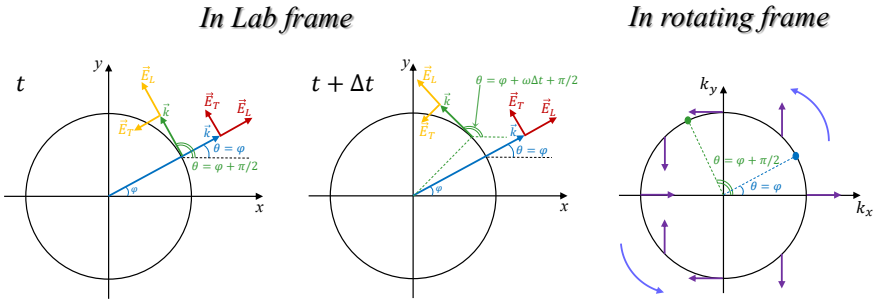

Figure 1: Left: Orientation of the wavevector $\vec{k}$ in the case of radial motion (blue) and rotation (green) in real space and the corresponding directions of the longitudinal and transverse components of the electric field, for the two consequent moments of time. Right: the corresponding distribution of the effective magnetic field in momentum space, in rotating frame, that rotates around the elastic circle in time.

Using the pseudospin evolution equation, we calculate the dynamics of the distribution of the degree of circular polarization (DCP) of light emitted by the rotating system of exciton polaritons, in momentum and real spaces. As follows from the intuitive sketch presented in Fig. 1, the DCP distribution contains not only the term $\propto \sin 2\theta$, but also an additional term $\propto \cos 2\theta$ which vanishes when $\omega = 0$. Analyzing the behavior of the amplitudes of the terms in time, we predict a new observable effect: in the presence of rotation, for small frequencies of rotation ($\omega \lesssim 0.1\Omega$), the typical OSHE polarization pattern experiences rotational oscillations: the angular directions in space corresponding to linear polarization and to the maximum of DCP begin to rotate, then move in the opposite direction, then change direction again to the initial one, etc. The equilibrium position of such oscillations slowly shift against the direction of rotation over time.

References

1. A. V. Kavokin, J. J. Baumberg, G. Malpuech, and F. P. Laussy, Microcavities // Oxford: Oxford University Press / (2nd edition) — 2017.

2. A. V. Kavokin, G. Malpuech and M. M. Glazov, Optical spin Hall effect // Phys. Rev. Lett. — 2005. — Vol. 95. — P. 136601.

3. W. Langbein et al., Polarization beats in ballistic propagation of exciton-polaritons in microcavities // Phys. Rev. B — 2007. — Vol. 75. — P. 075323.

Anomalous Hall effect for intervalley excitons

A. Shubnic[1], V. Shahnazaryan[1,2*], H. Rostami[3], I. Shelykh[1,2,4]

[1]Department of Physics, ITMO University, Saint Petersburg, Russia

[2]Abrikosov Center for Theoretical Physics, MIPT, Dolgoprudnyi, Russia

[3]Department of Physics, University of Bath, Bath, United Kingdom

[4]Science Institute, University of Iceland, Reykjavik, Iceland

vanikshahnazaryan@gmail.com

Abstract

The ability of controllable manipulation of valley degree of freedom in transition metal dichalcogenide monolayers will allow for creation of valleytronic devices. Here we theoretically address an exciton anomalous Hall effect of excitons. We demonstrate that the combined impact of strain-induced gradient of exciton resonance energy and emergent pseudo-magnetic field result in anomalous Hall transport of intervalley excitons. The proposed effect manifests itself in spatially inhomogeneous circular polarization of exciton luminescence.

Tailoring effective axion response via time-modulated metamaterials

L. Shaposhnikov[1] and M.A. Gorlach[2]

[1,2]School of Physics and Engineering, ITMO University, Saint Petersburg, Russia

[1] leon.shaposhnikov@metalab.ifmo.ru

Abstract

We have shown that time-modulated nonreciprocal media exhibit effective axion response. By introducing periodic modulations in the magnetization of a gyrotropic material, we have derived an effective axion response that can be preciesly controlled. This provides a new way to tailor the properties of metamaterials and opens up new possibilities for manipulating electromagnetic fields. In particular, we have shown that it is possible to create arbitrary smooth time modulations that can model cosmic axion fields, which in turn has the potential application for axion detection experiments.

Key words: time-modulated metamaterials, axion electrodynamics, nonreciprocal photonics, magneto-optical materials

Introduction

Axions are hypothetical particles that simultaneously solve multiple problems in modern physics. In field theory, they solve the problem of CP invariance [1, 2]. At the same time, in cosmology they are a promising candidate for the role of dark-matter particles [3]. Axions have not been detected so far, but there are real solid-state structures where light propagation is described by equations of axion electrodynamics. Such media are known as Tellegen media in the simplest case of a constant axion field, and these materials are part of the magnetoelectrics material family [4]. Structures with a strong axion response provide a convenient platform to study the effects of axion electrodynamics.

However, the use of natural materials alone severely limits the research capabilities. The use of artificially structured media allows flexible control of the effective axion response. The possibility of achieving an effective axion response via spatial [7] and space-time [8] metamaterials was recently demonstrated. However, an approach based purely on temporal modulation has not yet been demonstrated to achieve an effective axion response.

Main text

Here, we design a time-modulated metamaterial with an effective axion response. The metamaterial is a continuous gyrotropic medium, in which the magnetization rapidly and periodically changes in time so that the average magnetization of the entire structure equals zero. Hence, its microscopic description is based on the permeability tensor:

$$\hat{\mu} = \begin{pmatrix} \mu & i\,g(t) & 0 \\ -i\,g(t) & \mu & 0 \\ 0 & 0 & \mu \end{pmatrix}, \quad g(t) = \sum_{m\neq 0} g_m\, e^{im\Omega t}, \quad \Omega \gg \omega : \tag{1}$$

The structure of this metamaterial makes it possible create temporal modulations of the effective axion response, as well as to fine-tune its values.

Approach for theorethical analysis of time-modulated structures was developed recently [5, 6]. Based on this approach we obtain the effective axion response:

$$\chi = \frac{q}{2\pi\mu^2} \int_0^{2\pi/\Omega} g(t')(\Omega t' - \pi) dt' \tag{2}$$

We examine dependence of the effective axion response on the the magnetization distribution in time. The magnetization distribution that maximizes the effective axion response is found.

We verify the correctness of the obtained results, by numerical simulations of the reflection of a plane electromagnetic wave from a metamaterial and an isotropic medium with an axion response. The results confirm the emergence of an effective axion response of the structure.

Thus, an original time-modulated photonic structure with a tunable axion response is developed. This structure also provides temporal modulation of the effective axion response. A theoretical analysis of the structure is performed.

In the future, the experimental realization of this structure is planned as well as the study of the possibility to create not only temporal modulation, but also spatial gradients. In this case, it will be possible to create an arbitrary distribution of the effective axion field in the proposed structure. This work was supported by the Priority 2030 Federal Academic Leadership Program and in part by the Foundation for the Development of Theoretical Physics and Mathematics "BASIS".

References

1. Weinberg S. A new light boson? //Physical Review Letters. – 1978. – T. 40. – №. 4. – C. 223.
2. Wilczek F. Problem of Strong P and T Invariance in the Presence of Instantons //Physical Review Letters. – 1978. – T. 40. – №. 5. – C. 279.
3. Bertone G., Hooper D. History of dark matter //Reviews of Modern Physics. – 2018. – T. 90. – №. 4. – C. 045002.

4. Pyatakov A. P., Zvezdin A. K. Magnetoelectric and multiferroic media //Physics-Uspekhi. – 2012. – Т. 55. – №. 6. – С. 557.
5. Pacheco-Peña, V., Engheta, N. (2020). Effective medium concept in temporal metamaterials. Nanophotonics, 9(2), 379-391.
6. Rizza, C., Castaldi, G., Galdi, V. (2022). Nonlocal effects in temporal metamaterials. Nanophotonics, 11(7), 1285-1295.
7. Shaposhnikov L. et al. Emergent axion response in multilayered metamaterials //arXiv preprint arXiv:2302.05111. – 2023.
8. Prudêncio, Filipa R., and Mário G. Silveirinha. "Synthetic axion response with space-time crystals." Physical Review Applied 19.2 (2023): 024031.

Propagation of wave packets along large-scale background waves [1]

D.V. Shaykin[1,2], A.M. Kamchatnov[2,2]

[1]Institute of Spectroscopy, Russian Academy of Sciences, Troitsk, Moscow, 108840, Russia

[2]Moscow Institute of Physics and Technology, Institutsky lane 9, Dolgoprudny, Moscow region, 141700, Russia

[1]shaykin.dv@phystech.edu, [2]kamch@isan.troitsk.ru,

Abstract

We study propagation of high-frequency linear wave packets along large-scale background waves obeying two hydrodynamic equations for fluid density and flow velocity. The influence of the wave packet dynamics on the evolution of the background is disregarded. The geometric optics approximation is used for the investigation of the evolutions of these objects: the dispersionless approximation governs the background dynamics, and the Hamilton equations are used for the dynamics of the wave packet. To study the wave packet propagation we assume the presence of the dependency of the carrier wave number of the packets on the background variables. The obtained theory is applied to the systems reducing to the shallow water equations. The analytical predictions agree well with exact numerical calculations.

Key words: Theoretical physics, linear wave packets, geometric optics approximation

Introduction

The linear wave packet is a long-standing object of physics study. Its characteristic features can be distinguished in many complex wave structures, which makes it possible to consider it as a model object similar to a material point in mechanics. In this regard, the study of its dynamics is an important task that has not yet been solved for non-stationary and inhomogeneous hydrodynamics, where the basic approaches for the simplest cases are usually simply described [2]. Difficulties in such a study arise due to the presence of nonlinear terms inherent in hydrodynamics.

To study the motion of a wave packet along a large-scale background wave, we will use the approximation of geometric optics, relying on the scale separation inherent such a problem: a characteristic packet size $d \ll$ characteristic size of the background l, and we will assume that the packet itself carries a large number of oscillations ($\lambda \ll d$) with a slightly varying wavelength ($\Delta\lambda \ll \lambda$). Thus, following the optical-mechanical analogy, Hamilton's equations can be written for the dynamics of the packet

$$\frac{dx}{dt} = \frac{\partial\omega}{\partial k} = V, \quad \frac{dk}{dt} = -\frac{\partial\omega}{\partial x}, \tag{1}$$

where x can be considered as the “center of mass” of the packet and k being the carrier wave number.

Main text

As a physical system, we will choose a fluid obeying gNLS:

$$i\psi_t + \frac{1}{2}\psi_{xx} - f(|\psi|)\psi = U\psi, \tag{2}$$

which can be easily rewritten in hydrodynamic form by substitution $\psi = \sqrt{\rho(x,t)} * exp\{i\int^x u\,(y,t)dy\}$:

$$\begin{gathered}\rho_t + (\rho u)_x = 0 \\ u_t + uu_x + \frac{c^2}{\rho}\rho_x + \left(\frac{\rho_x^2}{8\rho^2} - \frac{\rho_{xx}}{4\rho}\right)_x = -U_x\end{gathered} \tag{3}$$

where $c^2 = \rho f'(\rho)$. The dispersion law takes the form

$$\omega = k\left(u \pm \frac{1}{2}\sqrt{k^2 + 4c^2}\right). \tag{4}$$

To describe the evolution of a large-scale background wave, we will use the equations (3) in the dispersionless approximation, which instantly leads us to

$$\begin{gathered}\rho_t + (\rho u)_x = 0 \\ u_t + uu_x + \frac{c^2}{\rho}\rho_x = -U_x\end{gathered} \tag{5}$$

The first important case that we will analyze will be the stationary flow due to the potential. In the stationary situation, it is possible to integrate equations (5) and obtain the dependency $u(x), \rho(x)$ according to a given potential $U(x)$. So, to describe the motion of the packet, we need to get the first Hamilton equation (1) in the convenient form, that is not possible while we don't know dependency k from x. In the simple case of stationary flow, we can use the well known energy conservation law: $\omega = const$. It allows us to obtain k from Eq. (4) as a function of x. Thus, we get the ordinary differential equation

$$\frac{dx}{dt} = \frac{\partial}{\partial k}\omega\big(k(x), u(x), \rho(x)\big). \tag{6}$$

The similar approach we use in the case of non-stationary hydrodynamics without a potential. In this sense, the system (3) without a right part has the general solution in terms of Riemann invariants [3], although there is not always a mutual unambiguity between physical variables and Riemann invariants. So, assuming the solution $\rho(x,t), u(x,t)$ is known, we again have only one undetermined parameter $k(x,t)$ on the right side of the first Hamilton equation. Now we will consider k as a function of the background parameters $\rho(x,t), u(x,t)$ and to determine this dependency we will use the second Hamilton equation.

On this way, substituting the system (5) without potential in the second Hamilton equation, one can obtain expression

$$\frac{\partial k}{\partial \rho}[(V-u)\rho_x - \rho u_x] + \frac{\partial k}{\partial u}\left[(V-u)u_x - \frac{c^2}{\rho}\rho_x\right] = -\frac{\partial \omega}{\partial \rho}\rho_x - \frac{\partial \omega}{\partial u}u_x. \tag{7}$$

Assuming that $\rho(x,t), u(x,t)$ are independent from each other, one should collect summands with ρ_x and u_x, therefore we obtain the system

$$\frac{\partial k}{\partial \rho} = \frac{(V-u)\frac{\partial \omega}{\partial \rho} + \frac{c^2}{\rho}\frac{\partial \omega}{\partial u}}{c^2 - (V-u)^2}, \qquad \frac{\partial k}{\partial u} = \frac{(V-u)\frac{\partial \omega}{\partial u} + \rho\frac{\partial \omega}{\partial \rho}}{c^2 - (V-u)^2}. \tag{8}$$

For existence of such a function $k = k(\rho, u)$ these derivatives must commute. For ease of further analysis, we can consider the power-law function $c^2 = \rho^p$. It turns out that case $p = 1$ satisfies this condition, but other cases don't, so for $p = 1$ we obtain the exact conservation law

$$k^2 = (q - u)^2 - 4\rho, \tag{9}$$

where q is constant along the packet motion. Although an exact conservation law cannot be obtained for arbitrary p, in the approximation $k \gg c$, these derivatives again commute and approximate conservation law takes the form

$$k^2 = (q - u)^2 - \frac{2(p+1)}{p}\rho^p. \tag{10}$$

We apply our analytical theory to the initial background flow in the parabolic form

$$\rho(x, 0) = a^2\left[1 - \left({}^{x}/_{l}\right)^2\right], \qquad u(x, 0) = 0. \tag{11}$$

A comparison with the exact numerical solution is reflected on Fig. (1).

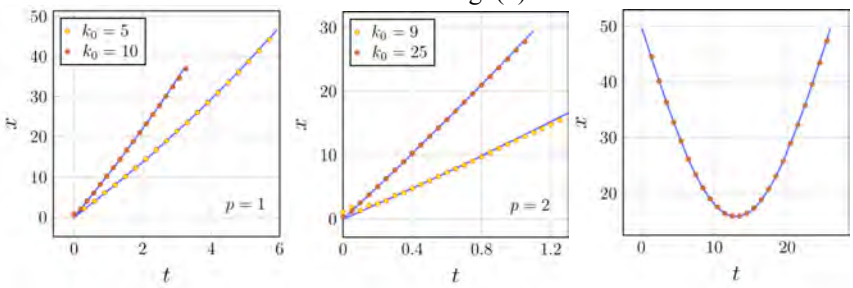

Fig.1 The comparison of developed analytical theory with the exact numerical solutions of gNLS. The circles denote the numerical result and the solid lines denote the analytical predictions. The first two pictures is obtained for the initial parabolic distribution (11) with $a = 5, l = 35$. The last picture is got from the analysis of stationary flow with $U = \frac{15}{\mathrm{ch}(x/15)}$ and $k_0 = 12$.

References

1. D.V. Shaykin and A.M. Kamchatnov, *Propagation of wave packets along large-scale background waves,* Physics of Fluids 35, 062108 (2023).

2. L. Synge, *Geometrical Optics. An Introduction into Hamil- ton's method*, (Cambridge University Press, 1937).

3. L. D. Landau and E. M. Lifshitz, *Course of Theoretical Physics, Vol. 6: Fluid Mechanics*, (Pergamon, New York, 1987).

Universal relations for Bose gases with power-law interaction at $T = 0$

E. Skirdova[1] and N. Voronova[1,2]

[1]National Research Nuclear University MEPhI (Moscow Engineering Physics Institute), Moscow, Russia

[2]Russian Quantum Center, Skolkovo Innovation Center, Moscow, Russia

[2]nsvoronova@mephi.ru

Abstract

Current study is devoted to derivation of universal relations for Bose gases with power-law interactions using the Tan's contact. At short distances, the two-body scattering problem for slow particles is solved to define the wavefunction and the second-order correlation function corresponding to the rarified limit. Universal relation for the potential energy density via the Tan's contact is obtained. At long distances, the pair correlation function is calculated in the Bogoliubov approximation at $T = 0$. The stitching of $g_2(r)$ in the overlap of the two regions allows to find the Tan's contact and a universal relation between the potential energy density and the chemical potential of the system.

Key words: Bose gases, Tan's contact, universal relations

Introduction

The Tan's contact is a universal constant that allows one to describe a large number of properties of low-temperature gases with short-range interactions (when interaction can be described using the s-wave scattering length), such as the interaction energy, the pair correlation function, the dependence of free energy on interactions, and also relation between the pressure and energy density. Initially, this constant was introduced for fermions [1, 2], after which the idea of universal relations was extended to systems of one-dimensional [3] and 2D bosons with dipole interactions [4]. The work is devoted to the derivation of universal relations for Bose gases with an arbitrary (integrable at infinity) power-law interaction potential, by means of calculating the Tan's contact for 2D and 3D systems at $T = 0$.

Universal relations for bosons with power-law interactions

We consider 2D (and 3D) Bose gases with power-law interparticle interaction potential $U(r) = Q/r^\alpha$, where Q is a constant factor and $\alpha > 2$ ($\alpha > 3$ for the 3D case) to assure integrability at all distances. The problem is solved on large and small

scales, after which the independently obtained solutions are stitched in the overlap region, which allows to derive a set of universal relations for such systems.

On small scales ($r \ll n^{1/2}$ in two dimensions or $r \ll n^{1/3}$ in three dimensions, where n is the density of particles) the two-body scattering problem for slow particles of the mass m is considered. The obtained wavefunction allows to define the second-order correlation function of the gas corresponding to the rarified limit (when the influence of all the other particles can be neglected). In this limit, we obtain the relation between the potential energy density and the Tan's contact, which is true at any temperature:

$$u = \frac{U}{S} = \frac{\hbar^2 C}{4(\alpha-2)\pi m}, \quad \text{for the 2D case,} \tag{1}$$

$$u = \frac{U}{V} = \frac{CQ(\alpha-2)^{\frac{2}{\alpha-2}}}{8\sin(\frac{\pi}{\alpha-2})\Gamma^2\Big(\frac{1}{\alpha-2}\Big)}\Big(\frac{mQ}{\hbar^2}\Big)^{\frac{3-\alpha}{\alpha-2}}, \quad \text{for the 3D case.} \tag{2}$$

The above results stand for any interaction exponent α.

On large scales (in the long-wavelength limit $r \gg a$, where a is the s-wave scattering length), the collective behavior of the Bose gas of N particles is considered in the Bogoliubov approximation, and the second-order correlation function $g_2(r)$ is derived for $r \ll \xi$, where ξ is the healing length. Stitching the two solutions at intermediate distances $a \ll r \ll \xi$ allows to determine the Tan's contact C through the particle density and the ratio of the considered scales. In particular, for 2D,

$$C = \frac{4\pi^2 n^2}{\ln^2 \frac{\xi\kappa}{a}} + \mathcal{O}\Big(\frac{1}{\ln^4 \frac{\xi^2\kappa^2}{a^2}}\Big), \tag{3}$$

where $\kappa = \frac{2\sqrt{2}}{e^{\gamma_E+1/2}} \approx 0.96319$. Combining Eq. (3) with (1) and the equation of state, we obtain the universal relation between the chemical potential of the system μ and the potential energy density:

$$u = \frac{m\mu^2}{4\pi\hbar^2(\alpha-2)} + \mathcal{O}\Big(\frac{1}{\ln^4 \frac{\kappa^2\xi^2}{a^2}}\Big). \tag{4}$$

References

1. S. Tan, Energetics of a strongly correlated Fermi gas, Ann. Phys. **323**, 2952 (2008).

2. S. Tan, Generalized virial theorem and pressure relation for a strongly correlated Fermi gas, Ann. Phys. **323**, 2987 (2008).

3. H. Yao, D. Clement, A. Minguzzi, P. Vignolo, and L. Sanchez-Palencia, Tan's Contact for Trapped Lieb-Liniger Bosons at Finite Temperature, Phys. Rev. Lett. **121**, 220402 (2018).

4. J. Hofmann and W. Zwerger, Universal relations for dipolar quantum gases, Phys. Rev. Res. **3**, 013088 (2021).

Use of molecules to measure the parity violating nuclear anapole moment

L.V. Skripnikov[1,2]

[1]Petersburg Nuclear Physics Institute named by B.P. Konstantinov of National Research Center "Kurchatov Institute" (NRC "Kurchatov Institute" – PNPI), 1 Orlova roscha, Gatchina, 188300 Leningrad region, Russia

[2]Saint Petersburg State University, 7/9 Universitetskaya nab., St. Petersburg, 199034, Russia

[1]skripnikov_lv@pnpi.nrcki.ru

Abstract

A novel approach to measure the anapole moment of the nucleus, which arises due to the violation of spatial parity P in intranuclear interactions is proposed [1]. The nuclear anapole moment phenomenon has only been observed once, approximately 25 years ago, for the Cs nucleus. The proposed method involves measuring the P-odd contribution to the spin-spin interaction between the two nuclei of the diatomic molecule TlF. We outline a possible experimental setup and provide an estimate of the signal based on precise calculations using state-of-the-art relativistic coupled cluster theory of the molecular constant that characterizes the coupling of the Tl nuclear anapole moment with the F nuclear magnetic moment via electronic shells. To validate the approach, we also calculate the P-conserving NMR parameters of the molecule and find an excellent agreement with the available experimental data.

Key words: Theoretical physics, anapole moment, symmetry violation, P-odd effects

Introduction

Weak interactions violate the spatial parity (P) symmetry, and several atomic experiments have been conducted to investigate this phenomenon [2]. The P-odd effect that is independent of nuclear spin and mainly arises due to the exchange of Z^0-bosons between electrons and the nucleus is well-established [2]. However, the P-odd effects that are dependent on the nuclear spin and are much smaller in magnitude, primarily caused by the interaction of electrons with the nuclear anapole moment, have only been observed once in atoms with considerable uncertainty [3].

Results

The parity non-conserving (PNC) contribution to the coupling of nuclear spins I and S in a diatomic molecule can be expressed as:

$$H_{\rm PNC} = 2\pi J^{(1),\rm PNC} \boldsymbol{\lambda} \cdot (\mathbf{I} \times \mathbf{S}), \tag{1}$$

where $\boldsymbol{\lambda}$ is the unit vector directed along the internuclear axis, and $J^{(1),\rm PNC}$ is the constant that characterizes the PNC interaction. $J^{(1),\rm PNC}$ is proportional to the dimensionless constant $g_{\rm Tl}$, which characterizes the nuclear anapole moment. Similar to Ref. [4], we have extended the coupled cluster approach to calculate the proportionality coefficient within the Dirac-Coulomb-Gaunt Hamiltonian. The result is

$$J^{(1),\rm PNC} = -3.03 \times 10^{-3} g_{\rm Tl} \text{ Hz}. \tag{2}$$

Our findings indicate that the primary contribution to this molecular electronic structure parameter is due to the negative energy states in the Dirac picture. We demonstrate that the use of the Sternheim's-like approximation, which is often employed for related nuclear magnetic resonance problems, overestimates the effect by a factor of 3.

If $J^{(1),\rm PNC}$ is measured, it would be possible to extract the value of $g_{\rm Tl}$ using the above result (2). To measure $J^{(1),\rm PNC}$, we propose [1] considering an effective two-level system of hyperfine sublevels of a rotational state J of the ^{205}Tl^{19}F molecule ($J = 0$ or $J = 1$). One can consider a molecular beam initially prepared in one of these hyperfine sublevels. The beam enters an interaction region with parallel oscillating magnetic and electric fields and in the presence of an additional static electric field. Both fields can induce transitions between two levels. By measuring the population of one of the hyperfine states, it is possible to extract the interference term (signal), which is proportional to $J^{(1),\rm PNC}$. By considering the actual experimental parameters, we estimated [1] that one can achieve a signal-to-noise ratio of 100 (i.e., measure $g_{\rm Tl}$) in just 3.5 hours.

An important feature of the proposal is that the experiment can be performed by a slight modification in the existing CENTREX facility [5] to measure T,P-violating effects. This work was supported by the RSF grant 19-72-10019-P.

References

1. J.W. Blanchard, D. Budker, D. DeMille, M.G. Kozlov, L.V. Skripnikov "Using parity-nonconserving spin-spin coupling to measure the Tl nuclear anapole moment in a TlF molecular beam", Phys. Rev. Research **5**, 013191 (2023).

2. M. S. Safronova, D. Budker, D. DeMille, D. F. J. Kimball, A. Derevianko, and C. W. Clark, "Search for new physics with atoms and molecules", Rev. Mod. Phys. **90**, 025008 (2018).

3. C. Wood, S. Bennett, D. Cho, B. Masterson, J. Roberts, C. Tanner, and C. E. Wieman, "Measurement of parity nonconservation and an anapole moment in cesium," Science **275**, 1759 (1997).

4. L. V. Skripnikov, S. Schmidt, J. Ullmann, C. Geppert, F. Kraus, B. Kresse, W. Nörtershäuser, A. F. Privalov, B. Scheibe, V. M. Shabaev et al., "New Nuclear Magnetic Moment of ^{209}Bi: Resolving the Bismuth Hyperfine Puzzle", Phys. Rev. Lett. **120**, 093001 (2018).

5. O. Grasdijk, O. Timgren, J. Kastelic, T. Wright, S. Lamoreaux, D. DeMille, et al, "CeNTREX: A new search for time-reversal symmetry violation in the ^{205}Tl nucleus", Quantum Sci. Technol. **6**, 044007 (2021).

Radiative corrections to the bound electron g-factor and level width in the presence of a magnetic field combined with blackbody radiation

D. Solovyev[1], T. Zalialiutdinov[2], D. Glazov[3], Yu. Kozhedub[4]

[1,2,4]Department of Physics, St. Petersburg State University, Petrodvorets, Oulianovskaya 1, 198504, St. Petersburg, Russia

[1,2]Petersburg Nuclear Physics Institute named by B.P. Konstantinov of National Research Centre "Kurchatov Institut", St. Petersburg, Gatchina 188300, Russia

[3]School of Physics and Engineering, ITMO University, Kronverkskiy pr. 49, 197101 St. Petersburg, Russia

[1]d.solovyev@spbu.ru, [2]t.zalialiutdinov@spbu.ru, [3]glazov.d.a@gmail.com, [4]y.kozhedub@gmail.com

Abstract

The discussion is devoted to the evaluation of the radiative one-loop correction with a vertex, where the vertex represents the interaction with an external magnetic field, and the loop refers to a "ordinary" or thermal photon. Within the framework of the rigorous QED theory, corrections to the g-factor of the bound electron and the level width are derived as real and imaginary parts, respectively. The effects are considered for hydrogen and light hydrogen-like ions and are discussed in regard to modern experiments in this field. Temperatures and magnetic field strengths corresponding to various laboratory and astrophysical conditions are taken into account. The discussion is based on our most recent results obtained within the QED approach at the finite temperature being developed by our group.

Key words: Theoretical physics

Introduction

The formation and development of quantum theory for bound states is closely connected with precision spectroscopic experiments performed on the hydrogen atom and a number of hydrogen-like ions. Having their own methodological features, such systems are most accurately theoretically described within the framework of quantum electrodynamics (QED). In the last decades, experimental measurements and theoretical calculations of the hyperfine structure (HFS) and g-factors in simple atomic systems have attracted particular interest. Significant progress in evaluation of QED radiative and nuclear-structure corrections, as well as the improvement of experimental

techniques, make it possible to identify the fundamental parameters of the theory (the electron to proton mass ratio, the Rydberg constant, nuclear parameters, etc.) and to look for manifestations of new physics.

To date, the transition frequencies in various atomic systems are measured with extremely high accuracy and also serve as a tool for building atomic clocks, metrological frequency standards, tests of perturbative quantum electrodynamics and others. In particular, the relative error in measuring the transition frequencies in hydrogen is about $10^{-15} \div 10^{-13}$ [1], the hyperfine interval is determined with an accuracy about 10^{-13} [2], and the g-factor is as accurate as 10^{-12} [3]. Such extraordinary precision stimulates theoretical studies of more subtle effects that are at the level of modern experimental error and less. Along these lines, the influence of the blackbody radiation field (BBR) on these quantities is of particular interest. It is well known that the BBR field leads to a quadratic ac-Stark shift of energy levels and reduces the lifetimes by inducing electron transitions between atomic states. The effects are extremely important in the spectroscopy of Rydberg atoms, the construction of atomic clocks, and the determination of frequency standards. The study of the effect of equilibrium radiation on the characteristics of atomic systems is usually limited to the quantum mechanical approach, in which the root-mean-squared field induced by BBR is considered as a perturbation. In our recent works, bound-state quantum electrodynamics theory at finite temperature (BS-TQED) has been developed to calculate thermal effects in atomic systems.

One-loop with vertex radiative corrections

Within the framework of the present study we discuss radiative corrections that take into account the finite temperature environment affecting the measurement of the g-factor, the HFS, and the determination of the level widths in simple atomic systems [4, 5, 6, 7]. The lower-order radiative corrections relevant to this study can be depicted using Feynman graphs in Fig. 1. Considering various combinations of the vertex part (attributed to interactions with an external magnetic field or hyperfine interaction) and the loop part (attributed to a "ordinary" or thermal photon), corrections can be evaluated to the g-factor, the HFS as the real part and to the level width as the imaginary part of the corresponding contributions.

In particular, the lowest order corrections to the g-factor at different temperatures for the hydrogen and light hydrogen-like ions were described in [4], and within the model potential approach for Rb and Cs atoms in [5]. Thermal radiative corrections to hyperfine structure of light hydrogen-like systems were evaluated in [6]. It is shown that the corrections are at or close to the accuracy level of modern experiments. Further, the discussion of the imaginary part of the contributions corresponding to the graphs in Fig. 1 is considered in detail. The theoretical analysis is devoted to the magnetic interaction given by the vertex part of the diagrams and to two cases: when the loop is attributed to the emission of a photon and its magnitude stimulated by the blackbody radiation. The entire analysis is devoted to the low-lying states of hydrogen and

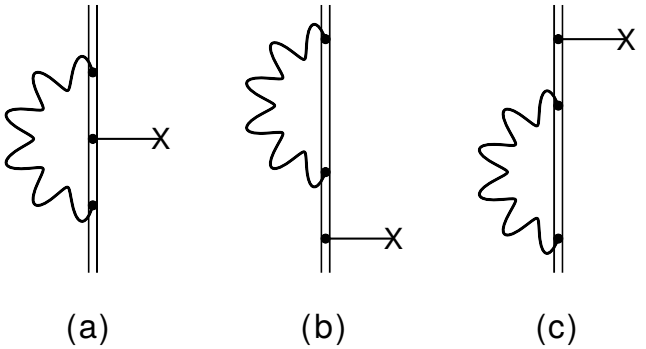

Figure 1: Feynman diagrams describing the TQED contributions to the bound-electron g-factor, HFS and level widths. The tiny line with the cross indicates interaction with an external magnetic field or hyperfine interaction. The double solid line denotes the bound electron in the Furry picture. The bold wavy line represents the "ordinary" or thermal photon propagators.

hydrogen-like ions [7].

Acknowledgments. The work was supported by the Russian Science Foundation under grant No. 22-12-00043.

References

1. P.J. Mohr, D.B. Newell, B.N. Taylor, CODATA recommended values of the fundamental physical constants: 2014, J. Phys. Chem. Ref. Data **45**, 043102 (2016).

2. H. Hellwig et.al., Measurement of the Unperturbed Hydrogen Hyperfine Transition Frequency, IEEE Trans. Instr. Meas., **19**, 200-209 (1970).

3. G. Werth et.al., Zeeman Spectroscopy in Penning Traps, Adv. At. Mol. Opt. Phys, **67**, 257 (2018).

4. T. Zalialiutdinov, D. Glazov, D. Solovyev, Thermal corrections to the bound-electron g-factor, Phys. Rev. A **105**, 012804 (2022).

5. T. Zalialiutdinov, Y. Kozhedub, D. Solovyev, arXiv:2212.12399 [physics.atom-ph] 23 Dec 2022 (accepted for publication in Can. J. Phys).

6. T. Zalialiutdinov, D. Glazov, D. Solovyev, Thermal radiative corrections to hyperfine structure of light hydrogenlike systems, Phys. Rev. A **106**, 062808 (2022).

7. D. Solovyev, T. Zalialiutdinov, Radiative corrections to the level width in the presence of magnetic field, arXiv:2209.01049 [physics.atom-ph] 3 Sep 2022 (under revision in Phys. Scr.).

Theoretical prerequisites for the upcoming generation of precision spectroscopic experiments

D. Solovyev[1], T. Zalialiutdinov[2], A. Anikin[3], L. Labzowsky[4]

[1,2,3,4]Department of Physics, St. Petersburg State University, Petrodvorets, Oulianovskaya 1, 198504, St. Petersburg, Russia

[1,2,4]Petersburg Nuclear Physics Institute named by B.P. Konstantinov of National Research Centre "Kurchatov Institut", St. Petersburg, Gatchina 188300, Russia

[3]D.I. Mendeleev Institute for Metrology, St. Petersburg, 190005, Russia

[1]d.solovyev@spbu.ru, [2]t.zalialiutdinov@spbu.ru, [3]alexey.anikin.spbu@gmail.com, [4]l.labzovskii@spbu.ru

Abstract

The discussion is devoted to a long-standing issue of determining the transition frequency in precision spectroscopic experiments with simple atoms. The problem was first formulated theoretically using the resonance approximation and going beyond it. Recently, the crucial role of effects arising beyond the resonance approximation for determining the transition frequency has been demonstrated in spectroscopic experiments with the hydrogen atom. In particular, we discuss the paradigm for determining the transition frequency through the line profile. Despite the existing ambiguity of the concepts, the adjustment of various possible definitions of the frequency standard is shown using the example of the hydrogen atom.

Key words: Theoretical physics, spectral line profile, transition frequency, resonance approximation

Introduction

The theory of natural line profile in atomic physics was developed since the earlier works [1, 2]. An extended quantum electrodynamics (QED) theory of the line profile for many-electron atoms and highly charged ions (HCI) can be found in [3] (see also references therein), resulting in formulation of the Line Profile Approach to QED calculations in atoms.

The development of the line profile theory is closely related to experimental advances in measuring the transition frequency in the hydrogen atom [4, 5], where the $1s - 2s$ two-photon transition was measured with an accuracy of about 10^{-15} relative magnitude. Such experiments have stimulated interest in theoretical studies of effects beyond the resonance approximation, see, for example, [6, 7]. Relying on theoretical

results, the most important consequences of the line profile theory were found in the form of corrections to the transition frequency arising due to nonresonant terms in the photon scattering cross section [6, 7, 3, 8]. These corrections (called nonresonant) expressly demonstrate the breach of the resonance approximation.

The largest contribution originates from the states most close by energy to the resonant one and corresponds to the differential cross section for the photon scattering process [7] consituting the Quantum Interference Effects (QIE). The interference effect occuring for the pathways between neighboring resonance states described in [7] served as a starting point for further theoretical studies in various atomic systems. The most specific for nonresonant frequency corrections is that they depend on the process used in the experiment and, therefore, are an inherent part for the distinctive experimental conditions. Varying over a wide range of values, nonresonant corrections and, in particular, QIE, as their most significant part, play a decisive role in modern precision spectroscopic experiments [9].

Transistion frequency determination

The experiment [9] can be referred to the first, where nonresonant effects were directly observed in the form of a distorted spectral line profile. As stated in [6, 7], nonresonant effects do not allow the transition frequency to be determined unambiguously because of the asymmetry of the line shape. The result of going beyond the resonance approximation (evaluating the nonresonant contributions in the scattering cross section) leads to an arbitrary determination of the transition frequency within the range of the line profile asymmetry. However, with an appropriate choice of the asymmetry parameter, the observed line profile was symmetrized, thus making the "line center" an evident candidate for the transition frequency [9].

The [9] experiment, at the same time, corresponds rather to a special case in which the excited state decays into any of the allowed lower states. The absence of at least one of the decay channels would violate the definition of the frequency invariant in this manner [10]. In particular, the line profile can be measured when decay goes to a fixed final state. The above case can be implemented by a "matching experiment", where the frequency of emitted photons is detected only for a particular decay (with a certain energy). According to the results of [10], the observed asymmetry should be different from that in [9]. Thus, a similar symmetrization procedure should be applied with a different asymmetry parameter. Without guaranteeing an exact match of the results, the frequencies determined for the partial transitions and the scheme used in the experiment [9] may differ within a few kilohertz. In turn, this discrepancy can be crucial in determining the physical constants.

The present study involves a discussion of the concepts of determining the transition frequency and, as a consequence, the possibility of finding a frequency "invariant" beyond the resonance approximation. The theoretical analysis devoted to the detailed study of the spectral line profile relies primarily on measurements of the transition frequency $2s - 4p$, although it is obviously generalized to arbitrary spectroscopic

experiments, where the photon scattering process is used to determine the transition frequency. It is shown that a thorough evaluation of the process utilized to determine the transition frequency should be carried out theoretically, setting the prerequisites for a forthcoming generation of precision spectroscopic experiments.

References

1. V. Weisskopf and E. Wigner, Berechnung der natürlichen Linienbreite auf Grund der Diracschen Lichttheorie, Zeitschrift für Physik **45**, 043102 (2016).

2. F. Low, Natural Line Shape, Phys. Rev. textbf63, 54-73 (1930).

3. O.Yu. Andreev, L.N. Labzowsky, G. Plunien and D.A. Solovyev, QED theory of the spectral line profile and its applications to atoms and ions, Phys. Rep. **455**, 135-246 (2008).

4. M. Niering et.al., Measurement of the Hydrogen $1S$- $2S$ Transition Frequency by Phase Coherent Comparison with a Microwave Cesium Fountain Clock, Phys. Rev. Lett. **84**, 5496 (2000).

5. A. Matveev et.al., Precision Measurement of the Hydrogen $1S-2S$ Frequency via a 920-km Fiber Link, Phys. Rev. Lett. **110**, 230801 (2013).

6. L.N. Labzowsky, D.A. Solovyev, G. Plunien and G. Soff, Asymmetry of the Natural Line Profile for the Hydrogen Atom, Phys. Rev. Lett. **87**, 143003 (2001).

7. U.D. Jentschura and P.J. Mohr, Nonresonant effects in one- and two-photon transitions, Can. J. Phys. **80**, 633 (2002).

8. T.A. Zalialiutdinov, D.A. Solovyev, L.N. Labzowsky and G. Plunien, QED theory of multiphoton transitions in atoms and ions, Phys. Rep. **737**, 1-84 (2018).

9. A. Beyer et.al., The Rydberg constant and proton size from atomic hydrogen, Science **358**, 79-85 (2017).

10. D. Solovyev, A. Anikin, T. Zalialiutdinov and L. Labzowsky, Importance of nonresonant corrections for the description of atomic spectra, J. Phys. B: At. Mol. Opt. Phys. **53**, 125002 (2020).

On out-of-equilibrium phenomena in pseudogap phase of complex SYK+U model

Artem Alexandrov, Moscow Institute of Physics and Technology

Abstract

We consider the out-of-equilibrium phenomena in the complex Sachdev-Ye-Kitaev (SYK) model supplemented with the attractive Hubbard interaction (SYK+U). This model provides the clear-cut transition from non-Fermi liquid phase in pure SYK to the superconducting phase through the pseudogap phase with non-synchronized Cooper pairs. We investigate the quench of the phase soft mode in this model and the relaxation to the equilibrium state. Using the relation with Hamiltonian mean field (HMF) model we show that the SYK+U model enjoys the several interesting phenomena, like violent relaxation, quasi-stationary long living states, out-of-equilibrium finite time phase transitions, non-extensivity and tower of condensates. We comment on the holographic dual gravity counterparts of these phenomena.

Based on: https://arxiv.org/abs/2305.09767 with A. Gorsky

We start from the complex SYK model. The model involves the complex fermions with four-fermion interaction and random coupling J_{ijkl},

$$H_{\text{SYK}} = \ = \frac{1}{2}\sum_{ijkl,\sigma,\sigma'} J_{ijkl}\left[c^\dagger_{i\sigma}c^\dagger_{j\sigma'}c_{k\sigma'}c_{l\sigma} + c^\dagger_{l\sigma}c^\dagger_{k\sigma'}c_{j\sigma'}c_{i\sigma}\right] \tag{1}$$

It is supplemented with the attractive Hubbard interaction

$$H_{\text{Hub}} = -U\sum_i^N c^\dagger_{i\uparrow}c^\dagger_{i\downarrow}c_{i\downarrow}c_{i\uparrow} - \mu\sum_{i,\sigma}^N c^\dagger_{i\sigma}c_{i\sigma} = \ = -U\sum_i^N b^\dagger_i b_i - \mu\sum_{i,\sigma}^N c^\dagger_{i\sigma}c_{i\sigma}, \quad b^\dagger_i = c^\dagger_{i\uparrow}c^\dagger_{i\downarrow} \tag{2}$$

Hamiltonians above conserve particle number and are symmetric under the time-reversal transformations. States of these models are governed by temperature T, fermion occupation number N_f, along with the dimensionless parameter, U/J, characterizing the attraction strength.

We show that in SYK+U model in the limit of small Hubbard interaction, $U \ll J$ (here U is the Hubbard interaction constant and J is the SYK model interaction constant) the pseudogap phase appears. This phase corresponds to a non-trivial saddle-point in mean-field treatment, where the phases of gaps $\Delta_i = |\Delta|e^{i\theta_i}$ are not fixed by saddle point equation. These phases are soft degrees of freedom and their fluctuations can destroy off-diagonal long-range order (ODLRO) even in $N \to \infty$ limit. The pseudogap phase corresponds to the non-synchronized Cooper pairs. We investigate out-of-equilibrium phenomena in this phase and connect them to the well-known Hamiltonian mean field (HMF) model.

Space-group approach to the Ginzburg-Landau phase in topological superconductors and 4 quantum numbers of a Cooper pair

E. A. Teplyakov[1] and V. G. Yarzhemsky[2]

Landau department of theoretical physics. Moscow Institute of Physics and Technology, Dolgoprudny, 9 Institutskiy lane, 141701, Moscow Region, Russia

[1]egery23@gmail.com, [2]vgyarzh@gmail.com

Abstract

The Ginzburg-Landau phase is considered accounting crystal symmetry and time reversal symmetry in topological superconductors in the space-group approach. The results of this approach are compared with existing experimental data for topological superconductors UTe_2, Sr_2RuO_4.

Key words: Ginzburg-Landau phase, quantum numbers, topological superconductors, space groups

Introduction

The concept of a topological order parameter is established as a key characteristic of condensed matter systems such as topological metals and unconventional superconductors. According to Anderson [1], the wavefunction of a Cooper pair is constructed taking into account the Pauli exclusion principle. Volovik and Gorkov in their work [2] generalized Ginzburg-Landau approach and suggested using spherical functions to describe the superconducting order parameter. In the space-group approach of Yarzhemsky-Murav'ev [3], the wave function of the Cooper pair depends on the irreducible representation of space and point groups. In this work, we consider the Ginzburg-Landau phase $e^{im\phi}$, which follows from the gauge invariance of the superconducting order parameter (SOP), from the point of view of the space-group approach based on the Mackey-Bradley theorem accounting the Shubnikov and the Fedorov symmetry. The phase change is determined by the diagonal element of the matrix of the irreducible representation written as $e^{i\breve{m}\phi}$ for finite rotations. It is obtained that the structure of a Cooper pair depens on the spin multiplicity and the labels of irreducible representations of space group, point group, intermediate group and time reversal symmetry

Main text

In the majority of theoretical works pair momentum and point group symmetry are expressed by the model functions. In our approach these two fundamental properties are not the same but they are related. It is necessary to equate the topological angular momentum m (Ginzburg-Landau phase) in the basis domain of a Brillouin zone and the group-theoretical quasi-momentum $\overline{m}$ for establishing connection between these two concepts. For describing different order parameters belonging to the same representation, additional quantum numbers and time reversal symmetry are introduced [4], [5]. Also, these additional quantum numbers determine the topological structure and angular momentum of Cooper pairs. Theoretical results are compared with experimental data for UTe_2 and Sr_2RuO_4 superconductors. In UTe_2, the spin triplet state with a total phase winding of 2π corresponds to ICR(irreducible corepresentation) B_u^+. If the same spin state is coupled with a spatial chiral part, the angular momentum projection m is equal to 2. Such a state corresponds to ICR A_u^+ and experimental structure. In addition, A_u^+ is nodal but B_u^+ is nodeless in the basal plane which is seen from Figure 1.

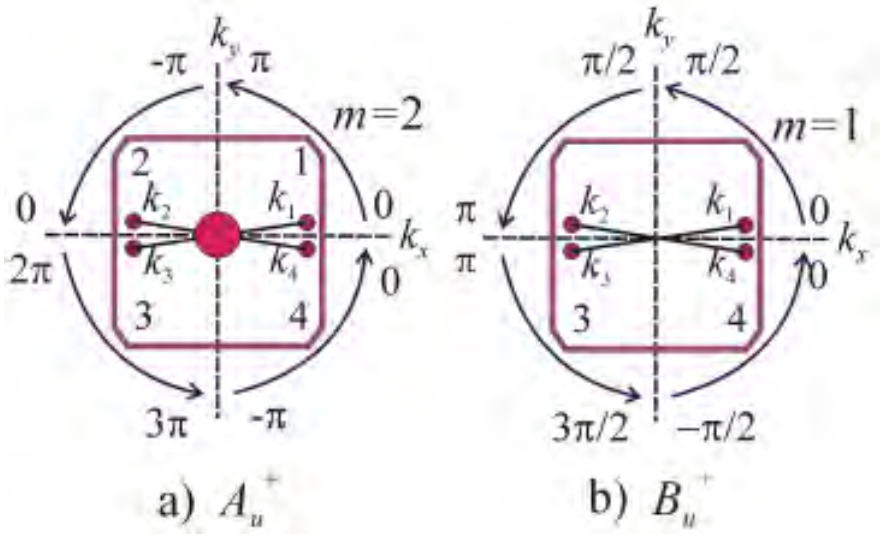

Figure 1: Nodal structure and phase winding of SOP in $m'm'm$ symmetry for odd ICRs (a) A_u^+ (b) B_u^+. Red circle denotes nodal basal plane

In D_{4h} symmetry, the possible vertical nodal planes of E_u and E_g are similar, but these IRs differ by nodes in the basal plane (Figure 2); namely, E_u is nodeless but E_g is nodal. This nodal structure has been confirmed experimentally for Sr_2RuO_4.

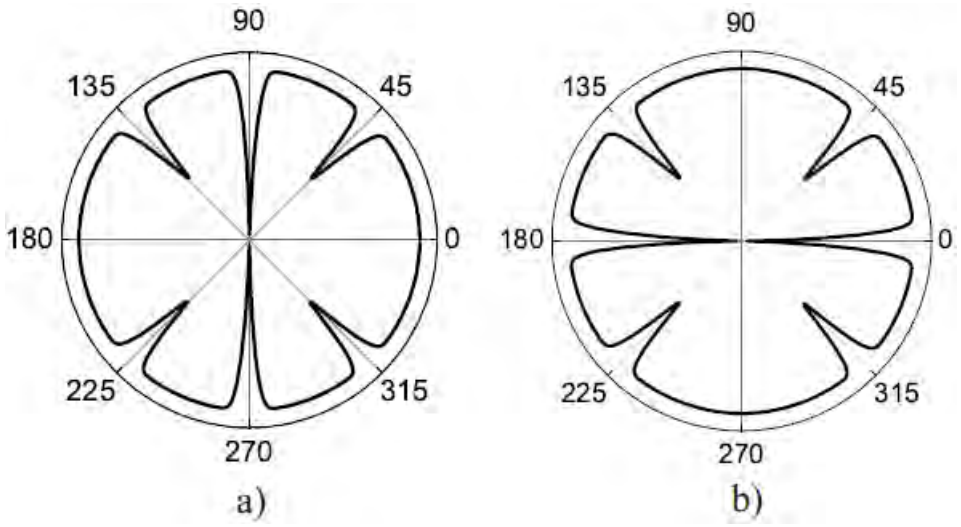

Figure 2: Nodal structures of complex SOPs for Sr_2RuO_4 (a) $E_{g(u)}$ and (b) $E_{g(u)} \times A_{2g}$ in D_{4h} symmetry. In both cases, E_g is nodal and E_u in nodeless in the basal plane.

References

1. P. W. Anderson, Structure of "triplet" superconducting energy gap, Phys. Rev. B **30**, 4000, (1984).

2. G. E. Volovik, L. P. Gor'kov, Superconducting classes in heavy-fermion systems, Sov. Phys. JETP. **61**, 843, (1985).

3. V. G. Yarzhemsky, E. N. Murav'ev, Space group approach to the wavefunction of a Cooper pair, Journal of Physics: Condensed Matter. **4**, 13, 3525, (1992).

4. V. G. Yarzhemsky , E. A. Teplyakov, Additional quantum numbers for two-electron states in solids. Application to topological superconductor UPt_3, J. Phys. Math. Theor. **54**, 455304, (2021).

5. V. G. Yarzhemsky, E. A. Teplyakov, Topological Structure of the Order Parameter of Unconventional Superconductors Based on d- and f - Elements, Symmetry. **15**, 376, (2023).

Influence of active medium vibronic degrees of freedom on operating lasers regimes

E.A. Tereshchenkov[1], E. S. Andrianov[1], A. A. Zyablovsky[1]

[1,2,3]Moscow Institute of Physics and Technology, Moscow

[1,2,3]Dukhov Research Institute of Automatics (VNIIA), Moscow

[1,2,3]Institute for Theoretical and Applied Electromagnetics, Moscow

[1]tereschenkov.ea@phystech.edu

Abstract

It was found that the presence of a large interaction constant between phonons and electrons entails the appearance of new output regimes of laser operation. One of these new regimes characterizes by excitation of coherent joint self-oscillations as an optical field in the resonator and optical phonons in the active medium. We also found that for a quantum dot with a low exciton dephasing regime with coherent phonons can transform into a chaotic regime similar to a strange attractor with a spectrum containing an infinite number of frequencies that are incommensurable with the frequencies of the opticalic phonons. Finally, we show that, in contrast to conventional lasers, there is a range of values of the interaction constant of optical phonons with an electronic subsystem and the pumping magnitude in which one two different regimes are simultaneously stable. These regimes can be any pair of the following: trivum regime, regular laser regime, coherent phonon generation regime, and chaotic regime. Which regime is implemented in practice is determined by the initial conditions.

Key words: Theoretical physics, quantum mechanics, nonlinear optics, nonlinear phenomena, lasers, quantum dots, strong coupling, phonons

Introduction

We considered an ordinary single-mode laser consisting of the resonator and the active medium. Previous laser systems research neglected the high cross section of the combination seeding of active molecules caused by strong coupling between excitons and optical phonons. In this work, to the best of our knowledge, the influence of vibrational degrees of freedom on the laser dynamics is considered for the first time.

Main text

The dynamics of a quantum dot (QD) which is incoherently pumped and interacts with a reservoir is considered. Among all levels of QDs we single out two: the ground

and excited states, thus passing to a two-level system (TLS). The Hamiltonian of such an QD has the following form:

$$\hat{H}_{\text{mol},j} = \hbar\omega_\sigma \hat{\sigma}_j^\dagger \hat{\sigma}_j + \hbar\omega_\text{v} \hat{b}_j^\dagger \hat{b}_j + \hbar g \hat{\sigma}_j^\dagger \hat{\sigma}_j \left(\hat{b}_j^\dagger + \hat{b}_j\right), \tag{1}$$

where $\hat{\sigma} = |g\rangle\langle e|$, $\hat{\sigma}^\dagger = |e\rangle\langle g|$ - operators of transitions from the excited state of QD $|e\rangle$ to the ground state $|g\rangle$ and vice versa, $\hat{b}^\dagger$ and $\hat{b}$ are vibron creation and annihilation operators (vibrons are the vibrational degrees of freedom of QD), g is the interaction constant of the electronic and vibronic subsystems of the QD, ω_σ is the QD exciton transition frequency, ω_v - vibron frequency.

The resonator's Hamiltonian has the form:

$$\hat{H}_\text{cav} = \hbar\omega_\text{a} \hat{a}^\dagger \hat{a}, \tag{2}$$

The interaction Hamiltonian of the QD and the reservoir has the form of the Jaynes-Cramings Hamiltonian [1, 2]:

$$\hat{H}_{\text{mol-cav},j} = \frac{\hbar\Omega_{\text{R},j}}{2} \left(\hat{a}\hat{\sigma}_j^\dagger + \hat{a}^\dagger \hat{\sigma}_j\right), \tag{3}$$

where $\Omega_{\text{R},j}$ is the Rabi frequency [1, 2], interaction constant between the TLS and the resonator.

To describe the relaxation processes, we use the Lindblad master equation for the density matrix. It looks like [2, 3, 4]:

$$\dot{\hat{\rho}} = \frac{i}{\hbar}[\hat{H}, \hat{\rho}] + L_\text{diss}[\hat{\rho}] + L_\text{pump}[\hat{\rho}] + L_\text{deph}[\hat{\rho}] + L_\text{v}[\hat{\rho}] + L_\text{a}[\hat{\rho}], \tag{4}$$

where $L_\text{diss}[\hat{\rho}]$ is the Lindblad superoperator describing nonradiative exciton relaxation, $L_\text{pump}[\hat{\rho}]$ - Lindblad superoperator describing incoherent exciton pumping, $L_\text{deph}[\hat{\rho}]$ - Lindblad superoperator describing exciton phase failure, $L_\text{v}[\hat{\rho}]$ is the Lindblad superoperator describing the vibron relaxation, $L_\text{v}[\hat{\rho}]$ - the Lindblad superoperator describing the relaxation of the resonator.

Having written the Heisenberg equation for all operators we obtain the following system of equations:

$$\dot{a} = \left(-i\omega_a - {}^{\gamma_a}/_2\right) a - i\Omega_{\text{R},j}\sigma_j \tag{5}$$

$$\dot{\sigma}_j = \left(-i\omega_\sigma - {}^{\gamma_\sigma}/_2\right) \sigma_j - ig\left(b_j + b_j^\dagger\right)\sigma_j + i\Omega_{\text{R},j} a D_j \tag{6}$$

$$\dot{b}_j = \left(-i\omega_\text{v} - {}^{\gamma_\text{v}}/_2\right) b_j - ig\frac{D_j + 1}{2} \tag{7}$$

$$\dot{D}_j = -\left(\gamma_\text{p} + \gamma_\text{D}\right)\left(D_j - D_o\right) + 2i\Omega_{\text{R},j}\left(a^\dagger\sigma_j - \sigma_j^\dagger a\right) \tag{8}$$

This system is non-linear, so it has several solutions. The main solutions are: the zero trivial solution ($a_{\mathrm{st},0} = 0$, $\sigma_{\mathrm{st},0,j} = 0$, $D_{\mathrm{st},0,j} = D_o$, $b_{\mathrm{st},0,j} = \mathrm{const}$), single-frequency solution, multi-frequency solution, and chaotic solution. Depending on the parameters of the system one or another solution is stable and this solution will be observed.

References

1. Mandel, L., Wolf, E. Optical coherence and quantum optics, Cambridge University Press, 1995, p. 1166.

2. M.O. Scully, M.S. Zubairy, Quantum optics, Cambridge University Press, 1997, p. 630

3. H.-P. Breuer, F. Petruccione, et al., The theory of open quantum systems, Oxford University Press on Demand, 2002, p. 625.

4. H.J. Carmichael, Statistical methods in quantum optics 1: master equations and Fokker-Planck equations, Springer Science & Business Media, 1999, p. 365.

Universality of the spectra of multiterminal $SNS-$junctions

A. F. Posadskii[1] and A. G. Semenov[2]

[1]P.N.Lebedev Physical Institute, 119991, Moscow, Russia

[2]Moscow Institute of Physics and Technology, 141701, Moscow region, Dolgoprudny

[3]National Research University "Higher School of Economics", 101000, Moscow, Russia

[1]posadskij.af@phystech.edu, [2]semenov.ag@mipt.ru

In 1962, B. Josephson [1] predicted the effect of nondissipative current flow through a weak bond between two superconductors in the absence of voltage. This phenomenon is still the basis for many theoretical and experimental studies. Recently, Josephson junctions with a large number of ($M > 2$) terminals based on normal metals, semiconductors, and superconductors have attracted great interest [2, 3, 4].

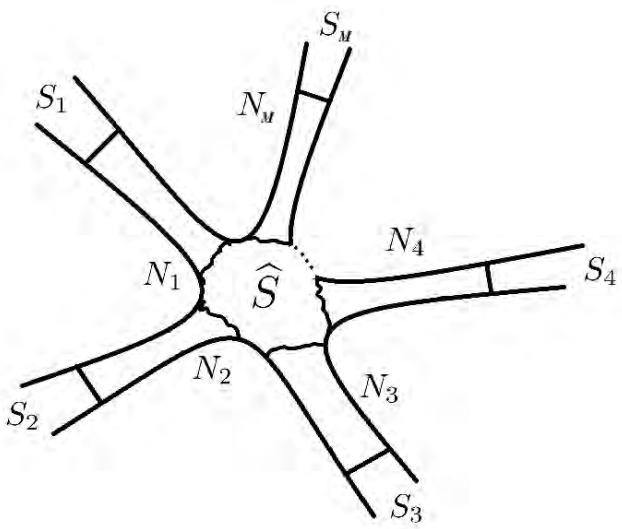

Figure 1: Schematic representation of the $M-$terminal junction. N_i-normal regions, S_i-superconducting regions. An impurity is located in the center, which is described by some scattering matrix $\widehat{S}$.

In our talk we consider $M-$terminal Josephson junction and discuss universality of Andreev bound state (ABS) spectra. Is it possible to calculate ABS if one knows

transmission probabilities? This question is actual since according to Landauer formula the last quantities can be reconstructed from the conductance measurements of the system in the normal state. We demonstrate that under some conditions the answer to this question is positive and spectra of ABS posess universality. It means that junctions with different reflection and transmition phases may have the same spectra.

References

1. B. D. Josephson, Possible new effects in superconductive tunnelling, Phys. Lett., **1**, 251-253 (1962),

2. Hong-Yi Xie, Maxim G. Vavilov, and Alex Levchenko, Topological Andreev bands in three-terminal Josephson junctions, Phys. Rev. B, **96**, 161406(R) (2017),

3. N. Pankratova, H. Lee, R. Kuzmin, K. Wickramasinghe, W. Mayer, J. Yuan, M. Vavilov, J. Shabani, and V. Manucharyan, The multi-terminal Josephson effect, Phys. Rev. X, **10**, 031051 (2018),

4. B. Doucot, R. Danneau, Kang Yang, Jean-Guy Caputo and R. Melin, Berry phase in superconducting multiterminal quantum dots, Phys. Rev. B, **101**, 035411 (2020).

Inertial dynamics and relaxation of the magnetization of ferromagnetic nanoparticles in a strong magnetic field.

A.S. Titov[1], V.A. Shchelkonogov[2], S.V. Titov[2]
[1]The Moscow Institute of Physics and Technology (State University), Dolgoprudny, Moscow reg. 141701, Russia
[2]Kotel'nikov Institute of Radioengineering and Electronics of the Russian Academy of Science, Fryazino, Moscow reg. 141190, Russia
[1]titov.as@phystech.edu, [2]vasiliy9999@yandex.ru, pashkin1212@yandex.ru

Abstract

Analytic solutions of the undamped limit of the inertial Landau-Lifshitz-Gilbert (ILLG) equation are presented for the longitudinal and transverse components of the magnetization of a single-domain ferromagnetic nanoparticle in a strong uniform external field. Analytical expressions for the longitudinal and transverse correlation functions pertaining to inertial magnetic relaxation are obtained by averaging the magnetization trajectories over all possible initial conditions applying the stationary Boltzmann distribution function. The components of the magnetic susceptibility tensor are calculated for a system of macrospins in a strong uniform external field. All the results originate from the analogy of the ILLG equation to a symmetric top with an electric dipole as used to model inertial (high-frequency) effects in the theory of dielectric relaxation. The obtained equations simultaneously describe the nutation resonance in THz frequency range as well as the ferromagnetic one associated with the usual precessional motion.

Key words: Magnetic nanoparticles, Magnetic relaxation, Inertial Landau-Lifshitz-Gilbert equation; Inertial magnetization dynamics, Magnetic susceptibility tensor, Nutation resonance.

Introduction

Until recently, the resonant in magnetic media have been studied based on the assumption of precession magnetization dynamics prevailing over nutation. However, the experimental detection of the nutation resonance [1] at terahertz (THz) frequencies makes it necessary to reconsider the conventional approach. It should be noted that the experimental investigation was preceded by the theoretical studies in which the inertial magnetization motion was compared with the kinematics of a symmetrical top [2]. As was shown in theoretical studies, nutation is caused by the inertia of the magnetization. The experimental observation of the nutation resonance gave a boost to the comprehensive study of the inertial dynamics of the magnetization. It is noteworthy that these investigations are important not only for fundamental research, but also for applications related to the development of THz technologies.

In the framework of the studies of the inertial dynamics of the magnetization, the inertialess Landau-Lifshitz-Gilbert equation for the magnetization **M** was generalized to the inertial case [2]. The generalized equation is conventionally called the ILLG equation and has the form

$$\frac{d\mathbf{M}}{dt} = \mathbf{M} \times \left(-\gamma \mathbf{H}_{eff} + \frac{\alpha}{M_S} \frac{d\mathbf{M}}{dt} + \frac{\tau}{M_S} \frac{d^2\mathbf{M}}{dt^2} \right), \qquad (1)$$

where $\gamma = 2.2 \times 10^5$ rad $\cdot$ m $\cdot$ A^{-1} $\cdot$ s^{-1} is the gyromagnetic ratio, M_S is the saturation magnetization, $\mathbf{H}_{eff}$ is the effective magnetic field, α is the precession damping parameter and

τ is the inertial parameter. The general solution of the ILLG equation is a rather complicated problem due to the need to take into account the magnetocrystalline anisotropy of ferromagnetic particles [3]. The problem significantly simplifies and becomes universal (the magnetocrystalline anisotropy is no longer important) if the contribution of the internal anisotropic field can be neglected in comparison with a strong external magnetic field **H**. Some other spin systems with no magnetocrystalline anisotropy can be considered in the same way.

Inertial magnetization dynamics, equilibrium correlations functions and magnetic susceptibility

The method used for solving Eq. (1) is based on simplifying this equation using the first integrals. The needed two integrals can easily be obtained using the analogy between the inertial motion of the magnetization and the mechanical rotation of a solid [4]. In the latter case, the total energy of the rotating body and the projection of the angular momentum onto the laboratory coordinate axis are conserved, namely $l = \eta\Omega_Z = \text{const}$ and $E = (\eta\Omega)^2 - \xi u_\parallel = \text{const}$, where $\mathbf{u} = \mathbf{M}/M_S$ is the unit vector directed along **M**, $\mathbf{\Omega} = \left(\Omega_X, \Omega_Y, \Omega_Z\right) = \left[\dot{\mathbf{u}} \times \mathbf{u}\right] + \tau^{-1}\mathbf{u}$, $\xi = 2\gamma H\eta^2/\tau$, $\eta = (v\mu_0 M_S \tau / 2\gamma kT)^{1/2}$, v is the particle volume, kT is the heat energy, and $\mu_0 = 4\pi \cdot 10^{-7}\,\mathrm{JA^{-2}m^{-1}}$ in the SI system. The solution of the simplified differential equation for the longitudinal component (along field) of the vector **u** can be expressed in terms of the doubly periodic Jacobi elliptic function

$$u_\parallel(t) = e_1 - (e_1 - e_2)\,\mathrm{sn}^2\left(t\sqrt{\xi(e_1 - e_3)}/(2\eta) + \delta \middle| m\right), \quad m = \frac{e_1 - e_2}{e_1 - e_3}, \tag{2}$$

where δ is determined by the initial conditions and e_i are the roots of the equation $(\xi u_\parallel + E)(1 - u_\parallel^2) + 2lu_\parallel\eta/\tau - l^2 - (\eta/\tau)^2 = 0$. The transverse component $u_\perp(t)$ of **u** is calculated by analogy. The solutions for $u_\parallel(t)$ and $u_\perp(t)$ allow us to calculate the nutation motion of the magnetization in the *XZ* plane (Fig. 1(a)). The nutation amplitude can be estimated as an oscillation amplitude of the *Z* component of the vector **u**: $u_{\parallel\max}(t) - u_{\parallel\min}(t)$. Figure 1(b) shows the dependence of this amplitude on the field ξ at different values of η/τ. It can be seen that an increase in the field leads to an increase in the nutation amplitude and the nutation amplitude decreases with the inertia and vanishes in the inertialess case ($u_\parallel(t) = \text{const}$).

Having determined $u_{\parallel,\perp}(t)$ we can calculate the transverse $C_\perp^{un}(t) = \left\langle u_\perp(0)u_\perp(t)\right\rangle$ and longitudinal $C_\parallel^{un}(t) = \left\langle u_\parallel(0)u_\parallel(t)\right\rangle - \left\langle u_\parallel(0)\right\rangle^2$ equilibrium correlation functions of the *undamped* rotation of magnetization. The equilibrium ensemble averages in the phase space of polar angles $\vartheta_0 = \vartheta(0)$ and $\varphi_0 = \varphi(0)$ and corresponding velocities $\omega_x^0 = \dot{\vartheta}(0)$ and $\omega_y^0 = \dot{\varphi}(0)\sin\vartheta(0)$ are [4]

$$\left\langle(\cdot)\right\rangle = Z^{-1}\int_0^\pi\int_0^{2\pi}\int_{-\infty}^{\infty}\int_{-\infty}^{\infty}(\cdot)\,e^{-\left(\eta\omega_x^0\right)^2 - \left(\eta\omega_y^0\right)^2 + \xi\cos\vartheta_0}\sin\vartheta_0\,d\omega_x^0\,d\omega_y^0\,d\varphi_0\,d\vartheta_0, \tag{3}$$

where Z is the partition function.

The values of microscopic variables separated by large timescales should be uncorrelated. This concept is reflected in the Lorentz diffusion model, in which the longitudinal and transverse correlation functions are expressed as $\dot{C}_{\parallel,\perp}(t) = \dot{C}_{\parallel,\perp}^{un}(t)e^{-t/T_{\parallel,\perp}}$ ($T_{\parallel,\perp}$ are relaxation

time constants) [5]. The components $\chi_{||,\perp}(\omega)$ of the magnetic susceptibility tensor can be expressed in terms of the appropriate equilibrium correlation functions (see Fig.2):

$$\chi_{||,\perp}(\omega) = C_{||,\perp}(0) + i\omega \int_0^\infty C_{||,\perp}(t) e^{i\omega t} . \qquad (4)$$

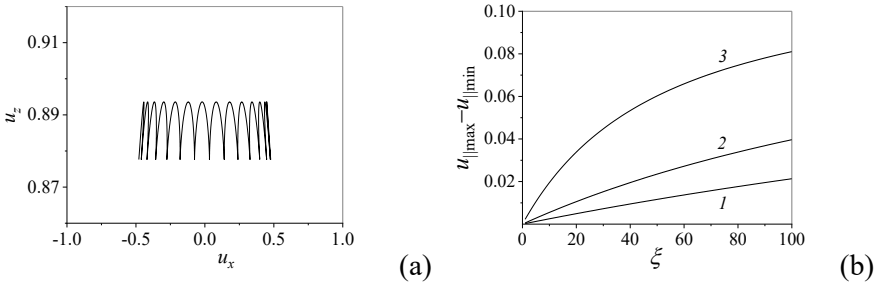

Figure 1: (a) Nutation motion of the magnetization $\boldsymbol{M}$ *(*$u_{X,Z} = M_{X,Z} / M_S$*) in the XZ plane calculated at* $\eta/\tau = 20$, $\xi = 50$; *(b) Nutation amplitude vs.* ξ *at* $\eta/\tau =$ *(1) 30, (2) 20, and (3) 10. The initial conditions are* $\vartheta(0) = 0.5$ *and* $\dot{\vartheta}(0) = \dot{\varphi}(0) = 0$.

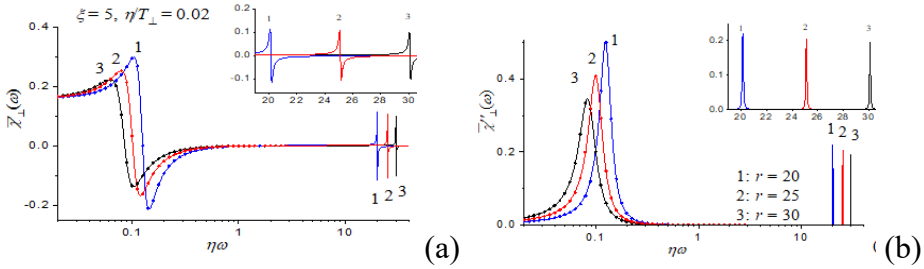

Figure 2: Real (a) and imaginary (b) parts of the transverse component of the susceptibility tensor $\chi_\perp(\omega) = C_\perp^{un}(0)\chi_\perp(\omega) / \chi_\perp$ *vs.* $\eta\omega$ *for* $\xi = 5$, $\eta / T_\perp = 0.02$ *and various values of inverse inertia parameter* $r = \eta / \tau$. *Solid lines: rigorous solution; symbols: approximate with Lorentz type curve.*

References

1. K. Neeraj *et al*, Inertial spin dynamics in ferromagnets, Nature Physics, **17**, 245, (2020).
2. J.-E. Wegrowe and M.-C. Ciornei, Magnetization dynamics, gyromagnetic relation, and inertial effects, Am. J. Phys. **80**, 607, (2012).
3. S.V. Titov, Yu.P. Kalmykov, K.D. Kazarinov, M.A. Cherkasskii, A.S. Titov, Inertial magnetization dynamics of ferromagnetic nanoparticles near saturation, Journal of Communication Technology and Electronics, **68**(5), 559 (2023).
4. S.V. Titov, W. T. Coffey, Yu. P. Kalmykov, M. Zarifakis, and A. S. Titov, Inertial magnetization dynamics of ferromagnetic nanoparticles including thermal agitation, Phys. Rev. B **103**, 144433 (2021).
5. S.V. Titov, W.J. Dowling, V.A. Shchelkonogov, and A.S. Titov, Inertial rotational diffusion and magnetic relaxation of the spin system in a strong magnetic field, Phys. Rev. B **107**, 174426 (2023).

Transport regimes for exciton-polaritons in disordered microcavities

A.N. Osipov[1], I.V. Iorsh[2], A.V. Yulin[3], I.A. Shelykh[4]

[1−4]Department of Physics, ITMO University, Saint Petersburg 197101, Russia

[3,4]Science Institute, University of Iceland, Dunhagi 3, IS-107, Reykjavik, Iceland

[2,4]Abrikosov Center for Theoretical Physics, MIPT, Dolgoprudnyi, Moscow Region 141701, Russia

[1]aleksey.osipov@metalab.ifmo.ru

Abstract

Coupling to the photonic mode in a planar optical microcavity significantly modifies transport regimes in the systems with excitonic disorder. We derived Master equations in Born-Markov approximation for density matrix of resonantly coupled exciton-photon system. It has been demonstrated that system has two transport regimes ballistic and diffusive in a limit of weak and strong disorder respectfully. The effective scattering efficiency and transport properties drastically depends on light-matter coupling parameters. The transition from diffusive to ballistic transport regimes due to the tuning of photonic portion in polariton's mode compound was demonstrated. The presented theory matches well the recent experimental results on transport in disordered microcavities.

Our paper preprint: `https://arxiv.org/abs/2305.16112`

Key words: Transport phenomena, Polaritons, Density matrix methods.

Introduction

Bright excitons are perspective particles for various optoelectronic applications [1]. However, excitons usually have small characteristic propagation distances, which becomes a major problem in such fields as photovoltaics [2]. Recently, the significant modification of the transport regimes of polaritons compared to bare excitons has been observed in organic [3], and inorganic [4] microcavities. It appeared that polariton's with high photonic portion are tends to have ballistic transport regime when increasing of excitonic fraction results in crossover to diffusive transport regime which was demonstrated in [3]. Scattering on randomly located impurities which gives the major contribution to the low temperature transport, affect only excitonic part of polariton's when photonic part stay coherent which provides the intuition about the effect. However, the derivation of the microscopic theory of exciton-polariton's

transport is still open question which is actual in perspective of recent experiments [3, 4].

In the present work we derived the transport theory for the polaritons using Born-Markov approximation to derive Master equations for polariton's density matrix in microcavities with randomly located impurities. We show that our model describes both diffusive [6], and ballistic propagation [7] in the limits of strong and weak disorder respectfully. The increasing of photonic fraction in mode compound drastically reduce scattering efficiency and enhance group velocities of polaritons leading to transition from diffusive to ballistic propagation.

Polariton's transport

We considered a 2D planar microcavity consisting excitonic quantum wells between two Bragg mirrors in the regime of strong light-matter coupling described by following Hamiltonian:

$$H = \sum_k \left[\varepsilon_x(\boldsymbol{k}) b^\dagger_{\boldsymbol{k}} b_{\boldsymbol{k}} + \varepsilon_c(\boldsymbol{k}) a^\dagger_{\boldsymbol{k}} a_{\boldsymbol{k}} + + \hbar\Omega_R (b^\dagger_{\boldsymbol{k}} a_{\boldsymbol{k}} + a^\dagger_{\boldsymbol{k}} b_{\boldsymbol{k}})\right] + \sum_{\boldsymbol{k}\boldsymbol{k'}} V_{\boldsymbol{k}\boldsymbol{k'}} b^\dagger_{\boldsymbol{k'}} b_{\boldsymbol{k}}, \tag{1}$$

where b_k, a_k are excitonic and photonic annihilation operators, $\varepsilon_x(\boldsymbol{k})$, $\varepsilon_c(\boldsymbol{k})$ - the corresponding dispersions. Ω_R is the Rabi coupling corresponding to light-matter coupling strenght, $V_{kk'}$ is the matrix element of the excitonic disorder potential.

The part of the Hamiltonian without random potential H_0 can be diagonalized by moving to the polaritonic basis $c_\pm$. Following to the well known procedure [5] the Master equation in Born-Markov approximation for polariton's density matrix ρ was derived

$$\partial_t \rho = -\frac{i}{\hbar}[H_0, \rho(t)] - \langle M_0 \frac{1}{\hbar^2}[H^I_V(t), \int_0^t dt'[H^I_V(t'), \rho^I(t)]] M_0^\dagger \rangle_c, \tag{2}$$

where $M_0 = \exp(-\frac{i}{\hbar} H_0 t)$ describes transition to interaction representation, index I denotes interaction representation. $\langle\rangle_c$ denotes taking average over random impurities positions.

The dynamics of the system is given by correlators $\rho_{\zeta_1,\zeta_2}(\boldsymbol{k}, \boldsymbol{k'}, t) = \mathrm{Tr}(\rho c^\dagger_{\boldsymbol{k}\zeta_1} c_{\boldsymbol{k'}\zeta_2})$ where $\rho^{\pm,\pm}(\boldsymbol{k}, \boldsymbol{k'})$, $\rho^{--}(\boldsymbol{k}, \boldsymbol{k'})$ define the distributions of upper and lower polaritons in the reversal space, $\rho^{\pm,\mp}(\boldsymbol{k}, \boldsymbol{k'})$ describe the correlations between polariton's branches. It occurs that in the limit of relatively weak disorder potential strength (compare to Ω_R) the correlations between branches can be adiabatically eliminated [8]. The final equations:

$$\partial_t \rho_{\pm,\pm}(\boldsymbol{k}, \boldsymbol{k'}, t) = \frac{i}{\hbar}(E_{\zeta_1}(\boldsymbol{k}) - E_{\zeta_2}(\boldsymbol{k'}))\rho_{\pm,\pm}(\boldsymbol{k}, \boldsymbol{k'}, t) - \frac{1}{\hbar^2} S(\rho_\pm), \tag{3}$$

where S is the term responsible for the scattering on impurites. The equations above has two well known limits. In the first limit of $V \to 0$ equations take form of

Shrodinger equation leading to the ballistic propagation of polaritons. In the second limit Boltzmann kinetic equations can be derived using Wigner representation. In this case S plays the role of scattering integral. The diffusive propagation of excitations can be derived in the second limit [9].

One of the major peculiarities of polariton's master equations is the appearance of Hopfield coefficients in $S \sim |\alpha_{ex}|^4$ representing weight of excitonic components. Therefore, for highly photonic polaritons the scattering efficiency is significantly suppressed. The another important factor is mush lower polariton's effective mass compared to the excitons which also leads to transport properties enhacement. As a result, it has been shown that transport of polariton's drastically depends on the weight photonic fraction in the mode compound. It has been demonstrated that highly photonic polaritons tend to have ballistic propogation (simular to Shrodinger equation case) when highly excitonic excitations tend have diffusive propogation(simular to Boltzman equation case). The results predicted by presented theory are in a good agreement with recent experiments [3, 4].

References

1. D. Sanvitto, F. Pulizzi, et al., Interlayer exciton optoelectronics in a 2d heterostructure p–n junction, Science **294**, 837 (2001).

2. A. J. Gillett, A. Privitera, et al., The role of charge recombination to triplet excitons in organic solar cells, Nature **597**, 7878, (2021).

3. M. Balasubrahmaniyam, A. Simkhovich, et al., From enhanced diffusion to ultrafast ballistic motion of hybrid light–matter excitations, Nature Materials 1-7 (2023).

4. M. Wurdack, E. Estrecho, et al., Motional narrowing, ballistic transport, and trapping of room temperature exciton polaritons in an atomically-thin semiconductor, Nature communications **12**, 5366 (2021).

5. H. Carmichael, Statistical Methods in Quantum Optics 1: Master Equations and Fokker-Planck Equations, Theoretical and Mathematical Physics (Springer Berlin Heidelberg, 2013).

6. M. Kulig, J. Zipfel, et al., Exciton diffusion and halo effects in monolayer semiconductors, Physical review letters **120**, 207401 (2018).

7. V. M. Agranovich and Y. N. Gartstein, Nature and dynamics of low-energy exciton polaritons in semiconductor microcavities, Physical Review B **75**, 075302 (2007).

8. E. Brion, L. H. Pedersen, and K. Molmer, Adiabatic elimination in a lambda system, Journal of Physics A: Mathematical and Theoretical **40**, 1033 (2007).

9. E. Lifschitz and L. Pitajewski, Physical kinetics, in Textbook of theoretical physics. 10 (1983).

Electromagnetically Induced Transparency in Cells of Finite Longitudinal Sizes with Antirelaxation Wall Coating

G. Voloshin[1], I. Sokolov[1], H. Meng[1], A. Kuraptsev[1], A. Litvinov[1], K. Barantsev[1]

[1]Peter the Great St.Petersburg Polytechnic University (SPbPU)

[1]office@spbstu.ru

Abstract

The phenomenon of electromagnetically induced transparency is widely used in problems of quantum memory and precision spectroscopy. In this work, electromagnetically induced transparency resonances excited in a cell filled with alkali atom vapors are studied theoretically in the presence of various types of anti-relaxation wall coatings: specular-incoherent, specular, and diffuse. An approach is proposed that makes it possible to obtain an analytical expression for the absorption spectrum of signal radiation. As a result, the change in the shape of the resonance of electromagnetically induced transparency is analyzed upon varying the parameters of the medium and laser pumping for various types of coatings. On the basis of the Autler-Townes splitting effect, a physical explanation is proposed for the difference between the spectra for the Stokes and anti-Stokes scattering channels of probe radiation.

Key words: Electromagnetically induced transparency, alkali vapor, anti-relaxation coating

Introduction

It is known that quantum interference during the interaction of two-frequency laser radiation with resonant atomic media under certain conditions leads to the appearance of a narrow transparency line in the absorption spectrum of one of the frequency components of the laser field, which is called the effect of electromagnetically induced transparency (EIT) [1, 2]. The width of such a line can be made much smaller than the width of a natural absorption line, which leads to the application of the EIT effect in such areas as magnetometry, lasing without inversion, recording and processing of quantum information, quantum frequency standards, etc.

Collisions of atoms with each other and with the walls of the cell are a negative factor, since they destroy the atomic coherence induced by the field and degrade the quality of the EIT resonance. One way to deal with collisions is the use of special antirelaxation coatings. When colliding with them, atoms can exhibit different behaviors depending on the type of coating. In this work, three limiting cases of such behaviors are studied: specular, specular-incoherent, and diffuse reflection [3]. While

in many works only collisions with the side walls of a cell are studied, in the formation of the EIT resonance by wide laser beams, an important role is played by collisions with walls in the direction longitudinal to the laser beam, the influence of which is studied in this work.

Mathematical model and results

The basis of the mathematical model of the interaction of bichromatic radiation with the medium of moving atoms is the method of a single-particle density matrix in the Wigner representation in translational degrees of freedom of atoms. In this case, a four-level Λ-scheme is used, which takes into account the hyperfine splitting of the excited states. Wall collisions are taken into account by introducing various types of boundary conditions. Using the approximation of a strong control field and a slow decay rate of low-frequency coherence, it is possible to reduce the expression for the absorption spectrum of the scanning field to a closed analytical form.

It is shown that the obtained analytical expressions agree with the corresponding numerical calculation. Based on the analysis of these expressions, a physical explanation, different from that given in [4], was proposed for the difference between the Stokes and anti-Stokes scattering channels of probe radiation during EIT detection in terms of dressed states. Transparency effects detected in cells with specular and diffuse reflections of atoms from walls were compared with each other in terms of the shape of the resonances and in terms of the spatial distribution of low-frequency coherence. It is shown that a significant difference in the shape of the resonances is observed only for cells that have longitudinal dimensions that are small compared to the ground state splitting wavelength. It is found that in a number of practically significant cases, diffuse reflection exhibits the properties of a mirror-incoherent one. It has been shown that the presence of an additional fourth level leads not only to the appearance of additional resonances, but also to a distortion of the shape of the main one, the greater the higher the amplitude of the binding field [5].

This work was financially supported by by the Foundation for the Development of Theoretical Physics and Mathematics "BASIS" (grant "Leader" № 21-1-1-36-1) and the Russian Science Foundation (grant no. 21-72-10004).

References

1. S.E. Harris, J.E. Field, A. Imamoglu, Phys. Rev. Lett. **64**, 1107 (1990).
2. K.-J. Boller, A. Imamoğlu, S. E. Harris, Phys. Rev. Lett. **66**, 2593 (1991).
3. B. D. Agapyev, M. B. Gorny, B. G. Matissov. ZhTF **58**, 12 (1988). (in Russian)
4. Ya.A. Fofanov, I.M. Sokolov, JETPh **135**(3), 255 (2022).
5. G.V. Voloshin, H. Meng, A.S. Kuraptsev, I. M. Sokolov, JETPh **135**(3), 269 (2022).

Electromagnetically Induced Transparency in Finite Longitudinal Size Cells with Antirelaxation Wall Coating

G. Voloshin[1], H. Meng[1], I. Sokolov[1], A. Kuraptsev[1], A. Litvinov[1], K. Barantsev[1]

[1]Peter the Great St.Petersburg Polytechnic University (SPbPU)

[1]office@spbstu.ru

Abstract

The phenomenon of electromagnetically induced transparency is widely used in problems of quantum memory and precision spectroscopy. In this work, electromagnetically induced transparency resonances excited in a cell filled with alkali atom vapors are studied theoretically in the presence of various types of anti-relaxation wall coatings: specular-incoherent, specular, and diffuse. An approach is proposed that makes it possible to obtain an analytical expression for the absorption spectrum of signal radiation. As a result, the change in the shape of the resonance of electromagnetically induced transparency is analyzed upon varying the parameters of the medium and laser pumping for various types of coatings. On the basis of the Autler-Townes splitting effect, a physical explanation is proposed for the difference between the spectra for the Stokes and anti-Stokes scattering channels of probe radiation.

Key words: Electromagnetically induced transparency, alkali vapor, anti-relaxation coating

Introduction

It is known that quantum interference during the interaction of two-frequency laser radiation with resonant atomic media under certain conditions leads to the appearance of a narrow transparency line in the absorption spectrum of one of the frequency components of the laser field, which is called the effect of electromagnetically induced transparency (EIT) [1, 2]. The width of such a line can be made much smaller than the width of a natural absorption line, which leads to the application of the EIT effect in such areas as magnetometry, lasing without inversion, recording and processing of quantum information, quantum frequency standards, etc.

Collisions of atoms with each other and with the walls of the cell are a negative factor, since they destroy the atomic coherence induced by the field and degrade the quality of the EIT resonance. One way to deal with collisions is the use of special antirelaxation coatings. When colliding with them, atoms can exhibit different behaviors depending on the type of coating. In this work, three limiting cases of such behaviors are studied: specular, specular-incoherent, and diffuse reflection [3]. While

in many works only collisions with the side walls of a cell are studied, in the formation of the EIT resonance by wide laser beams, an important role is played by collisions with walls in the direction longitudinal to the laser beam, the influence of which is studied in this work.

Mathematical model and results

The basis of the mathematical model of the interaction of bichromatic radiation with the medium of moving atoms is the method of a single-particle density matrix in the Wigner representation in translational degrees of freedom of atoms. In this case, a four-level Λ-scheme is used, which takes into account the hyperfine splitting of the excited states. Wall collisions are taken into account by introducing various types of boundary conditions. Using the approximation of a strong control field and a slow decay rate of low-frequency coherence, it is possible to reduce the expression for the absorption spectrum of the scanning field to a closed analytical form.

It is shown that the obtained analytical expressions agree with the corresponding numerical calculation. Based on the analysis of these expressions, a physical explanation, different from that given in [4], was proposed for the difference between the Stokes and anti-Stokes scattering channels of probe radiation during EIT detection in terms of dressed states. Transparency effects detected in cells with specular and diffuse reflections of atoms from walls were compared with each other in terms of the shape of the resonances and in terms of the spatial distribution of low-frequency coherence. It is shown that a significant difference in the shape of the resonances is observed only for cells that have longitudinal dimensions that are small compared to the ground state splitting wavelength. It is found that in a number of practically significant cases, diffuse reflection exhibits the properties of a mirror-incoherent one. It has been shown that the presence of an additional fourth level leads not only to the appearance of additional resonances, but also to a distortion of the shape of the main one, the greater the higher the amplitude of the binding field [5].

This work was financially supported by by the Foundation for the Development of Theoretical Physics and Mathematics "BASIS" (grant "Leader" № 21-1-1-36-1) and the Russian Science Foundation (grant no. 21-72-10004).

References

1. S.E. Harris, J.E. Field, A. Imamoglu, Phys. Rev. Lett. **64**, 1107 (1990).
2. K.-J. Boller, A. Imamoğlu, S. E. Harris, Phys. Rev. Lett. **66**, 2593 (1991).
3. B. D. Agapyev, M. B. Gorny, B. G. Matissov. ZhTF **58**, 12 (1988). (in Russian)
4. Ya.A. Fofanov, I.M. Sokolov, JETPh **135**(3), 255 (2022).
5. G.V. Voloshin, H. Meng, A.S. Kuraptsev, I. M. Sokolov, JETPh **135**(3), 269 (2022).

Combined two-loop self-energy corrections at finite and zero temperatures

T. Zalialiutdinov [1,2] and D. Solovyev [1,2]

[1]Department of Physics, St. Petersburg State University, Petrodvorets, Oulianovskaya 1, 198504, St. Petersburg, Russia

[2]Petersburg Nuclear Physics Institute named by B.P. Konstantinov of National Research Centre 'Kurchatov Institut', St. Petersburg, Gatchina 188300, Russia

[1]t.zalialiutdinov@spbu.ru, [2]d.solovyev@spbu.ru

Abstract

In this work, we investigate higher-order corrections to the energies of bound states in hydrogen under the influence of an external blackbody radiation field. Specifically, we analyze combined type of two-loop self-energy corrections that involve one zero and one finite temperature loops, within the framework of thermal quantum electrodynamics and S-matrix approach. By utilizing the method of dimensional regularization, we derive closed analytical expressions for the energy shifts of atomic levels. Our numerical calculations demonstrate that even at room temperature they can be significant for excited states, reaching the magnitude of the thermally induced Stark contribution.

Key words: Theoretical physics, Finite temperature quantum electrodynamics

In this study, we extend the application of quantum electrodynamics to the calculation of combined two-loop self-energy radiative corrections with one ordinary and one thermal loop to the energy level of a hydrogen-like atom, see Fig. 1. Our approach for evaluating the relevant equations incorporates the bound-state S-matrix, finite-temperature quantum field theory, and non-relativistic quantum electrodynamics (NRQED), together with a technique known as dimensional regularization. The incorporation of these higher-order corrections can be essential for achieving more accurate determinations of the blackbody radiation (BBR) shift in various physical systems. Our numerical calculations demonstrate that even at room temperature they can be significant for excited states, reaching the magnitude of the thermally induced Stark contribution Obtained results pave the way for further progress in this field.

The interaction between blackbody radiation (BBR) and atomic systems has been a subject of interest for many years [1]. Recent advancements in atomic physics have revealed the significance of BBR-stimulated effects in both fundamental and applied sciences [2]. In the pursuit of greater precision in the measurement of atomic transition energies and the development of frequency standards, the impact of uncertainty caused by BBR cannot be ignored, as evidenced by the most accurate clock experiments [3]

and transition frequencies measurements [2]. This challenge has prompted extensive research on the calculation of BBR-induced shift in clock systems [4], with the potential to revolutionize the field of high-precision metrology [5].

While early research on BBR-induced effects focused primarily on Rydberg atoms, the emergence of high-precision spectroscopy and frequency metrology has expanded the study of thermal induced effects to low-lying energy levels. This development offers a promising path towards understanding fundamental physical constants, including the Rydberg constant R_∞ and fine-structure constant α. However, the consideration of finite temperature effects in atomic systems is typically limited by the lower order of quantum mechanical (QM) perturbation theory.

Previously, we developed a method for calculating higher-order corrections in the framework of the S-matrix line profile approach and quantum electrodynamics of bound states at finite temperatures (TQED), which makes it possible to carry out calculations in complete analogy with ordinary quantum electrodynamics at zero temperature. In particular, thermal one-loop corrections to hyperfine splitting, g-factor, recombination cross sections, and probabilities of one- and two-photon transitions were calculated in [6, 7].

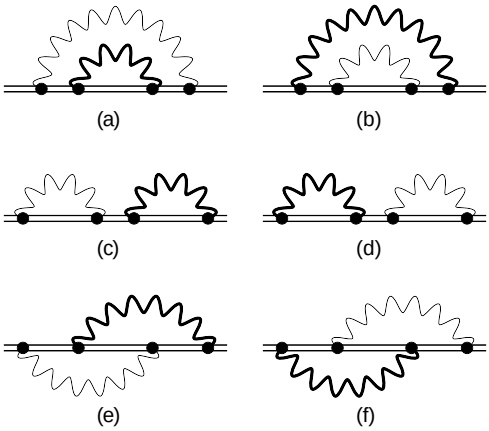

Figure 1: The Feynman graphs representing the combined two-loop self-energy QED corrections to the atomic energy level. Various contributions are indicated using the following notations: (a) - vacuum loop over thermal loop (VoT), (b) - vacuum loop inside thermal loop (ViT), (c) and (d) - loop-after-loop (LaL), (e) and (f) - crossed loops (CL). The double solid line denotes the electron in the external Coulomb potential V (the Furry picture), the tiny wavy line denotes the zero-temperature virtual photon, while the bold one corresponds to the finite temperatures.

References

1. Farley, J., Wing, W. (1981). Accurate calculation of dynamic Stark shifts and depopulation rates of Rydberg energy levels induced by blackbody radiation. Hydrogen, helium, and alkali-metal atoms. Phys. Rev. A, 23, 2397.

2. Brandt, A., Cooper, S., Rasor, C., Burkley, Z., Matveev, A., Yost, D. (2022). Measurement of the $2S_{1/2} - 8D_{5/2}$ Transition in Hydrogen. Phys. Rev. Lett., 128, 023001.

3. Kozlov, M., Safronova, M., Crespo Lopez-Urrutia, J., Schmidt, P. (2018). Highly charged ions: Optical clocks and applications in fundamental physics. Rev. Mod. Phys., 90, 045005.

4. S. G. Porsev, A. Derevianko (2006). Multipolar theory of blackbody radiation shift of atomic energy levels and its implications for optical lattice clocks. Phys. Rev. A, 74, 020502(R).

5. Riehle, F. (2006). Frequency standards: basics and applications. John Wiley and Sons.

6. Zalialiutdinov, T., Glazov, D., Solovyev, D. (2022). Thermal corrections to the bound-electron g-factor. Phys. Rev. A, 105, 012804.

7. Zalialiutdinov, T., Glazov, D., Solovyev, D. (2022). Thermal radiative corrections to hyperfine structure of light hydrogen-like systems. Phys. Rev. A, 106, 062808.

g factor of the ground and excited states of highly charged ions

D. V. Zinenko[1], V. A. Agababaev[2], E. A. Eshengulova[1], D. A. Glazov[1,3], A. D. Moshkin[1], V. M. Shabaev[1], E. V. Tryapitsyna[1,3], A. V. Volotka[3]

[1]Department of Physics, Saint-Petersburg State University, Saint-Petersburg, Russia
[2]Saint-Petersburg State Electrotechnical University "LETI", Saint-Petersburg, Russia
[3]School of Physics and Engineering, ITMO University, Saint-Petersburg, Russia

[1]dmitrii.zinenko@gmail.com,

Abstract

We present an overview of the current situation regarding the g factor of lithium- and boron-like ions. Ground and excited states are considered. First results for excited states of lithium-like and boron-like argon are presented.

Key words: highly charged ions, quantum electrodynamics, relativistic atomic theory, g factor

Research into the g factor of highly charged ions has significantly advanced in recent years. The most accurate value of electron mass to date has been achieved through the combined theoretical and experimental results for hydrogen-like ions [1]. Looking ahead, enhancements in theory and experiments are expected to allow the independent determination of the fine structure constant, α [2, 3]. Additionally, these improvements will allow us to validate the quantum electrodynamics (QED) beyond the Furry picture within the strong coupling region [4, 5], and ascertain the magnetic moments and radii of nuclei [6, 7]. Recently, it has been demonstrated that by measuring the g factor of the ground state of hydrogen-like and lithium-like thorium-229 ions, we can estimate the lifetime of the isomeric state of this isotope [8].

The calculations performed so far for lithium-like ions have achieved an accuracy of $10^{-6} - 10^{-9}$ [9−13]. The theoretical results of [9−11] are consistent with accurate g-factor measurements of lithium-like silicon [14] and calcium [15], providing a rigorous test of many-electron QED effects in the presence of magnetic fields. However, in [12, 13], despite a significant improvement in theoretical accuracy, a discrepancy between theoretical and experimental values is claimed. To solve this problem, our group has performed new independent calculations of second and higher order many-electronic contributions [16, 17]. First and second order corrections were calculated within the framework of a rigorous QED calculation. The third and higher-order corrections to the interelectronic interactions have been calculated from the Dirac-Coulomb-Breit Hamiltonian using a relatively new method, the recursive perturbation

theory [18]. Nuclear recoil effect is also taken into account [19, 20]. In searching for a solution, we also investigated the gauge invariance of many-electron self-energy diagrams. Finally, we realised that the contradiction with previous results was an underestimation of the uncertainty of the higher-order contributions in [12, 13].

The theoretical calculations for boron-like ions have an accuracy of about 10^{-6} because of their more complex electronic structure, in contrast to hydrogen-like and lithium-like ions. The results of different groups [21−24] showed significant discrepancies, motivating new calculations and experiments. Our group calculated the g factor values for boron-like ions in the range $Z = 10 - 20$ for the ground $2P_{1/2}$ state [25]. Meanwhile, the ALPHATRAP project at the Max Planck Institute has obtained highly accurate experimental values for the $2P_{1/2}$ state of boron-like argon [26]. The experimental data obtained are in excellent agreement with our group results and independent calculations [27, 28].

We also performed similar calculations of the g factor for the first excited state of boron-like ions [21, 23, 29]. The first measurement was reported in [30], albeit with a modest accuracy of around 10^{-3}. Subsequently, the ALPHATRAP project achieved a new value with an improved accuracy of 10^{-4} [31]. Following this, a superior level of accuracy was attained for the $2P_{3/2}$ state of the same boron-like argon using the quantum logic method [32]. This result corroborates our theoretical value and paves the way for measuring the Zeeman splitting of excited states of highly charged ions, extending beyond merely boron-like ions. We anticipate that new experiments for the g factor of excited states of highly charged ions, together with theory, will provide promising scenarios for the determination of fundamental constants, nuclear parameters and the search for new physics.

In response to these advancements, we have embarked on calculations of the g factor for the excited states of highly charged ions. More specifically, we are considering the $2P_{3/2}$ state for boron-like ions and the $2P_{1/2}$ and $2P_{3/2}$ states for lithium-like ions. We present the preliminary results of the g factor of the excited states of lithium- and boron-like argon.

The work was supported by the Russian Science Foundation (Grant No. 22-12-00258) and by the Foundation for the Advancement of Theoretical Physics and Mathematics "BASIS".

References

1. S. Sturm *et al.*, Nature **506**, 467 (2014).

2. V. M. Shabaev *et al.*, Phys. Rev. Lett. **96**, 253002 (2006).

3. V.A. Yerokhin *et al.*, Phys. Rev. Lett. **116**, 100801 (2016).

4. V. M. Shabaev *et al.*, Phys. Rev. Lett. **119**, 263001 (2017).

5. A. V. Malyshev *et al.*, JETP Letters **106**, 765 (2017).

6. W. Quint *et al.*, Phys. Rev. A **78**, 032517 (2008).
7. V. A. Yerokhin *et al.*, Phys. Rev. Lett. **107**, 043004 (2011).
8. V.M. Shabaev *et al.*, Phys. Rev. Lett. **128**, 043001 (2022).
9. A.V. Volotka *et al.*, Phys. Rev. Lett. **112**, 253004 (2014).
10. V. A. Yerokhin *et al.*, Phys. Rev. A **95**, 062511 (2017).
11. D.A. Glazov *et al.*, Phys. Rev. Lett. **123**, 173001 (2019).
12. V. A. Yerokhin *et al.*, Phys. Rev. A **102**, 022815 (2020).
13. V. A. Yerokhin *et al.*, Phys. Rev. A **104**, 022814 (2021).
14. A. Wagner *et al.*, Phys. Rev. Lett. **110**, 033003 (2013).
15. F. Köhler *et al.*, Nat. Commun. **7**, 10246 (2016).
16. V.P. Kosheleva *et al.*, Phys. Rev. Lett. **128**, 103001 (2022).
17. D. V. Zinenko *et al.*, Phys. Rev. A **107**, 032815, (2023).
18. D. A. Glazov *et al.*, Nucl. Instr. Methods Phys. Res. B **408**, 46 (2017).
19. V. M. Shabaev *et al.*, Phys. Rev. Lett. **119**, 263001 (2017).
20. V. M. Shabaev *et al.*, Phys. Rev. A **98**, 032512 (2018).
21. D. A. Glazov *et al.*, Phys. Scr. **T156**, 014014 (2013).
22. S. Verdebout *et al.*, ADNDT **100**, 1111 (2014).
23. A. A. Shchepetnov *et al.*, J. Phys. Conf. Ser. **583**, 012001 (2015).
24. J. P. Marques *et al.*, Phys. Rev. A **94**, 042504 (2016).
25. V. A. Agababaev *et al.*, J. Phys. Conf. Ser. **1138**, 012003 (2018).
26. I. Arapoglou *et al.*, Phys. Rev. Lett. **122**, 253001 (2019).
27. D. E. Maison *et al.*, Phys. Rev. A **99**, 042506 (2019).
28. H. Cakir *et al.*, Phys. Rev. A **101**, 062513 (2020).
29. V. A. Agababaev *et al.*, X-Ray Spectrometry **49**, 143 (2020).
30. R. Soria Orts *et al.*, Phys. Rev. A **76**, 052501 (2007).
31. A. Egl *et al.*, Phys. Rev. Lett. **123**, 123001 (2019).
32. P. Micke *et al.*, Nature **578**, 60 (2020).